THE UNIVERSITY
of EDINBURGH

Chronic impact of reduced cerebral blood flow on synaptic structure and glial responses.

Jemma Pilcher BSc (Hons) MSc

Doctor of Philosophy

2019

Table of Contents

Acknowledgements

Firstly, I would like to acknowledge the guidance and mentorship I received from my supervisors, Prof. Karen Horsburgh, Dr Jill Fowler and Dr Noboru Komiyama. I also would like to thank my colleagues who performed or assisted with certain experiments needed for my research. Thank you to Karen Horsburgh, Jill Fowler and Juraj Koudelka for performing the surgeries required for these studies. Thanks to Juraj for the multiphoton microscopy; Yasmina Manso for doing the radial arm maze experiment; Edel Hennessy for teaching me how to western blot and Jessica Duncombe for assisting me with the rose bengal optimisation experiment. Also, thanks to the rest of Horsburgh group; Emma, Mosi, Josh, Stefan, Sanny, Martina, Akihiro and Alessio for their support and encourage throughout this process. And a massive merci beaucoup to my dear friend, colleague and former flat-mate, Margaux Aimable, for her kindness and eagerness to cheer me up when things weren't going well. My grateful thanks are also extended to Cathy McLaughlin and members of Seth Grant's lab for their synapse and western blot expertise. I would like to express my appreciation for the work of the LF2 animal unit staff, who are so incredibly helpful. I would also like to thank Dr Paddy Hadoke and Prof Megan Holmes for their advice and support. Lastly, I wish to thank Prof Catherine Mitchell, from University of Exeter, for her kindness and for inspiring me to complete this thesis.

I feel tremendously grateful to my boyfriend, Dr Simon Fokt, who has given me so much support over the last 3 years. Thank you being so patient and putting future plans on hold while I completed this. And thank you for proof-reading my thesis! Also, thank you to my wonderful parents, Jane and Bruce, who have always reminded me to put my health and happiness first. I also want to express my appreciation for Beltane Fire

Society, especially for the Reds and the Wild Hunt, for keeping my life interesting and enabling me to have a creative outlet during my PhD. Finally, I would like to thank all my friends for the great parties and bringing so much joy to my life over the last 4 years.

Funding

I would like to thank my funders for their contributions to my research. The Centre for Cognitive Ageing and Cognitive Epidemiology (CCACE), who are a Medical Research Council (MRC) funded centre, provided me with a studentship stipend for my MSc and PhD. Furthermore, the funding for the laboratory work was covered by grants from Alzheimer's Research UK (ARUK) and the Alzheimer's Society.

Declaration

I declare that this thesis has been composed solely by myself, that it has not been submitted for any previous degree or qualification, and that the work described within this thesis comprises my own original work except where stated otherwise in the text.

Signed:

Date: 6/11/19

List of figures

List of tables

Abbreviations

AD	Alzheimer's disease
AMPAR	α-amino-3-hydroxy-5-methyl-4-isoxazolepropionic acid receptor
ATP	Adenosine triphosphate
Aβ	β-amyloid
BA	Basilar artery
BBB	Blood brain barrier
BCAS	Bilateral common carotid artery stenosis
BDNF	Brain-derived neurotrophic factor
CAA	Cerebral amyloid angiopathy
CCA	Common carotid artery
CFS1R	Colony stimulating factor 1 receptor
CNS	Central nervous system
CSF	Cerebrospinal fluid
DTI	Diffusion tensor imaging
ECA	External carotid artery
eGFP	Enhanced green fluorescent protein
GABA	γ-aminobutyric acid
GFAP	Glial fibrillary acid protein
GluR1	Glutamate receptor 1
Iba1	Ionized calcium binding adapter molecule 1
ICA	Internal carotid artery
ISF	Interstitial fluid
LTD	Long term depression
LTP	Long term potentiation
MAP2	Microtubule-associated protein 2
MCA	Middle cerebral artery
MRI	Magnetic resonance imaging
NFT	Neurofibrillary tangle
NMDAR	N-methyl-D-aspartate receptor
PCA	Posterior cerebral artery
PSD95	Postsynaptic density 95
PT	Photothrombosis
ROI	Region of interest

ROS	Reactive oxygen species
SAH	Subarachnoid haemorrhage
SNR	Substantia nigra pars reticulata
VaD	Vascular dementia
VCI	Vascular cognitive impairment
VGCC	Voltage-gated calcium channels
VGLUT1	Vesicular glutamate transporter 1
VSMC	Vascular smooth muscle cells
WT	Wild type

Abstract

Vascular cognitive impairment (VCI) results from a heterogeneous range of cerebrovascular injuries, such as stroke, cerebral large and small vessel disease, or cerebral amyloid angiopathy, which reduce cerebral blood flow and starve brain cells of oxygen and nutrients needed for normal function. Blood flow reductions are central to VCI and can range from mild chronic hypoperfusion to severe issues such as focal ischemic stroke. Cerebrovascular pathology and blood flow reductions are also a feature of Alzheimer's disease, which has considerable overlap with VCI. There are few therapeutic options to treat VCI, and they are limited by mechanistic insight.

Synapse loss is considered to be the pathological feature that underpins cognitive decline in Alzheimer's disease and dementia. In Alzheimer's disease (AD), synaptic dysfunction is known to occur early in the disease progression and it is thought to be the result of synaptotoxicity caused by oligomeric forms of soluble β-amyloid, a central pathogenic feature of AD. Previous studies have found that severe reductions in cerebral blood flow (ischaemia) cause immediate synaptic and neuronal degeneration. However, there is limited understanding of the longer-term impact of ischaemia on synapses, and even less knowledge of whether more modest reductions of blood flow also cause alterations in synapses. Gaining a better understanding of those issues is important in determining how synaptic changes contribute to the spectrum of VCI, and whether there are common changes that may be targeted therapeutically.

Glutamate is the main excitatory neurotransmitter in the brain. There is evidence that glutamatergic neurons and synapses are particularly vulnerable in a number of neurodegenerative conditions, including stroke and AD. Dendrites and axons, the

neuronal processes that pre- and postsynaptic terminals project from, have also been found to be susceptible to degeneration in pathological conditions. The studies in this thesis, therefore, investigate the overarching hypothesis that a range of cerebral blood flow reductions causes a long-term loss of glutamatergic pre- and postsynaptic terminals culminating in VCI, and that the additional comorbidity of β-amyloid pathology will lead to worsened synapse loss and functional impairment.

At the outset, the first aim was to assess the long-term effects of modest cerebral hypoperfusion on dendrites and glutamatergic pre- and postsynaptic terminals. Modest cerebral blood flow reductions were surgically induced in mice, by bilateral common carotid stenosis (BCAS). The densities of dendrites and glutamatergic pre- and postsynaptic terminals were measured with histological and immunohistochemical approaches in wild-type (WT) mice, 1 and 3 months after BCAS. Spatial working memory was assessed using an 8-arm radial arm maze at 3 months, although there was no significant difference between sham and BCAS animals. In the BCAS group, there were no overall significant alterations in dendrites and glutamatergic pre- and postsynaptic terminals compared to sham at either 1 month or 3 months. In the majority of mice (12 out of 16) there was no evidence of ischaemic neuronal damage at either 1 month or 3 months. However, in a subset of mice (4 out of 16), global hypoperfusion resulted in ischaemic neuronal damage in the CA1 region of the hippocampus (in 3 mice from the 1 month cohort and 1 mouse from the 3 month cohort). These mice exhibited focal dendritic loss in the same regions showing ischaemic neuronal damage, without changes in the synapse density. Overall, this study demonstrated that modest chronic cerebral hypoperfusion does not induce degeneration of dendrites and glutamatergic pre- and

postsynaptic terminals in the CA1, apart from in the few animals with ischaemic neuronal pathology in this region, which coincided with a significant loss of dendrites.

The second study focused on the long-term changes to glutamatergic pre- and postsynaptic terminals and axons in a model of focal ischaemia. Previous publications have shown that synaptic terminals are vulnerable within hours to days after ischaemic stroke, however, little is known about chronic synaptic changes. Focal ischaemia was induced with 15 minutes of middle cerebral artery occlusion (MCAO), followed by 3 months of recovery. This model results in a diffuse ischaemic lesion in the ipsilateral striatum. The transgenic line used for this study was generated by crossing TgSwDI mice, which produce progressive β-amyloid pathology, with mice expressing enhanced green fluorescent protein (eGFP) tagged onto the postsynaptic protein PSD95 (PSD95:eGFP). TgSwDI x PSD95:eGFP mice and their WT x PSD95:eGFP littermates, underwent MCAO surgery to determine if focal ischaemia resulted in long-term synaptic degeneration and whether these changes are exacerbated by concurrent β-amyloid pathology. Histological techniques were used to determine the volumes of ischaemic neuronal pathology and axonal pathology for each brain. These measurements were compared between WT and TgSwDI mice, and showed that there was no genotype effect on total volume of ischaemic neuronal pathology or axonal pathology. The densities of glutamatergic pre- and postsynaptic terminals were analysed with immunohistochemistry and expression of PSD95:eGFP, within the striatal ischaemic lesion and surrounding peri-lesion. There was a significant loss of glutamatergic pre- and postsynaptic terminals within the ischaemic lesion in both WT and TgSwDI mice, but there were no significant differences between these groups. Glial responses are a feature of vascular pathology and may be involved in synapse degeneration. In this study the levels of microglia/macrophages and astrocytes

were increased in the lesion 3 months after MCAO, with evidence that microglia/macrophages levels were inversely correlated with the density of postsynaptic terminals. Overall, the results from this study demonstrated that brief focal ischaemia leads to long-term neuron and axon damage, loss of glutamatergic pre- and postsynaptic terminals, and glial responses within the ischemia lesion, however, the concurrent expression of TgSwDIAPP transgene did not exaggerate these changes.

Finally, the third study investigated the impact of secondary neurodegeneration following focal ischaemia, and whether it is exacerbated by β-amyloid pathology. In patients with focal ischaemic damage or stroke, pathological changes have been found in remote brain regions that are connected to the ischaemic territory. In the current study, after 15 minutes of MCAO in mice there was long-term axon degeneration in the ipsilateral internal capsule, as well as axon degeneration and postsynaptic loss in the ipsilateral substantia nigra pars reticulata (SN_R). In addition, microglia/macrophage and astrocyte levels were increased in the ipsilateral internal capsule and SN_R. Interestingly, there was a larger increase in these glial markers in the internal capsule in the TgSwDI mice compared to the WT mice, although there were no signs of exaggerated axon degeneration in these mice. The results may indicate that white matter tracts are sensitive to glial responses and were exacerbated by concurrent TgSwDIAPP expression. Additionally, there was a small long-term increase in glutamatergic post-synaptic terminals in the ipsilateral thalamus of WT and TgSwDI mice, which may suggest that there is some synaptic rewiring in brain regions to compensate for synapse loss in other brain regions. The levels of glial cells were increased in the TgSwDI ipsilateral thalamus compared to the WT mice, which coincided with areas of β-amyloid immunostaining. Taken together, the results of this study indicate that focal ischaemia can stimulate long-

term secondary synaptic and axon degeneration, as well as small increases in synapse terminal density, in brain regions that are connected to the lesion site. There were no genotype effects on synaptic and axon degeneration; however, the presence of β-amyloid did result in an even greater level of glial cells in the ipsilateral internal capsule and thalamus of TgSwDI mice after MCAO surgery, which may impact the integrity and function of this white matter tract.

As part of the studies within the thesis, an alternative approach for inducing focal ischaemia was developed using Rose Bengal photothrombosis to generate a lesion in the cortex. This technique has been used for capturing real-time changes in the brain with multiphoton microscopy. Experiments were performed to optimise this method with the aim to measure dynamic synaptic changes in the presence of an ischaemic lesion and β-amyloid with multiphoton microscopy. This study found that Rose Bengal photothrombosis caused large ischaemic lesions in the cortex, and in some cases the underlying subcortical structures, with variation and a lack of reproducibility between cases. Because of the challenges with using photothrombosis and multiphoton microscopy, the study design was changed to using MCAO and histological methods to measure synaptic changes, as described above.

Overall, the studies in this thesis further support the hypothesis that the degree and type of cerebral blood flow reduction has an impact on the extent of synaptic and neuron degeneration. The results showed that modest global cerebral hypoperfusion was insufficient to cause reductions in synaptic and dendritic densities, indicating that in this model cognitive impairment occurs independently of synaptic loss. Focal ischaemia, however, did cause chronic synaptic loss within the lesion and remote brain regions, coinciding with glial responses and with evidence that postsynaptic loss in the lesion

relates to the density of microglia/macrophages. Interestingly, the concurrent TgSwDIAPP expression did not exacerbate synapse and neuron degeneration, whereas it did increase the levels of glial cells in the ipsilateral internal capsule and thalamus. The data implies that in cases of chronic cerebral hypoperfusion, cognitive decline is not a result of glutamatergic synaptic degeneration. In patients with 'mixed' ischaemic and Alzheimer's pathology, degeneration of glutamatergic synaptic terminals is driven by mechanisms related to cerebral blood flow changes, rather than β-amyloid. However, concurrent β-amyloid can result in exaggerated glial responses in brain regions distal from the lesion site.

These studies demonstrate the long-term impact of brief or modest cerebral blood flow reductions on synapses and brain function. The results imply the need for adequate recognition, prevention and treatment measures which could help patients avoid the development of vascular cognitive impairment and dementia. Furthermore, this work suggests that while the presence of β-amyloid might contribute in some extent to glial responses, it has little impact on synaptic and neuronal damage. Therefore, the implications are that therapeutic intervention targeted at processes relating to ischaemia, rather than β-amyloid, would be more effective at alleviating synaptic and neuronal degeneration in cases of mixed pathology. Moreover, the studies indicated that glial changes are persistent features of cerebrovascular injury and can be exaggerated with multiple disease comorbidities. Future developments should focus on gaining a better understanding of this long-term immune response and how it influences brain function.

Lay summary

The human brain requires a constant blood supply, for delivering oxygen and nutrients to support the function of the cells. Neurons are a major type of brain cell; they form complex networks throughout the brain and communicate between one another through protrusions known as synapses. Synapses are essential for brain function, enabling our brains to perform tasks such as thinking, memorising and problem solving. They require high levels of oxygen and nutrients to function properly; therefore, if the brain blood flow is interrupted it may have a negative impact on the synapses. Loss of synapses is proposed to underpin the decline in brain function experienced by people with dementia causing impairment in their memory and problem solving abilities, as well as other brain functions. Reductions in brain blood flow have been shown to be associated with the development of dementia, however, it is not clear whether this occurs from damage to the synapses.

A number of different risk factors (such as high blood pressure, high fat diet) can cause disease in the brain blood vessels which results in reduced blood flow. These can result in a range of different blood flow changes, with some causing an overall decrease in blood flow throughout the brain, whilst in other cases the blood flow may be completely halted in a small area of the brain, leading to damage in this area. There is evidence linking the various types of blood flow reduction to the development of dementia, therefore, it is important to understand how a range of blood flow reductions can impact on the synapses. The studies in this thesis sought to investigate the long-term effect of (1) a modest and sustained reduction in blood flow throughout the brain, and (2) briefly halting blood flow in a small part of the brain, has on the synapses. The latter of these studies also investigated whether the addition of a protein, called β-amyloid, which is

thought to be damaging to synapses, results in worsened changes to the synapses. These studies used surgical mouse models to modulate brain blood flow. The first study revealed that a reduction in the entire brain blood flow did not result in memory decline in the mice, nor did it result in a loss of synapses. In the latter studies, halting blood flow in a small part of the brain caused long-term loss of synapses in that brain region and in other regions, as the damage spread along the networks of connected neurons. There was no difference in the synapses between mice with and without β-amyloid present, therefore, we concluded that this did not cause further synapse damage. The results imply that in humans if there is a reduction in brain blood flow and a build-up of β-amyloid protein simultaneously, it is the changes in blood flow that drives the mechanisms causing damage to the synapses, and dysfunction to the brain.

Chapter 1: Introduction

1.1 Overview

Synapses are neurochemically complex structures that facilitate the transfer of information between neurons within networks, and are totally essential for brain function. There are different types of synapses, which are normally categorised by the type of neurotransmitter they release (O'Rourke et al. 2013). Glutamate is the main excitatory neurotransmitter in the brain. In healthy conditions, glutamate is released from excited presynaptic neurons into the synaptic cleft, binding to receptors on the postsynaptic terminals, and stimulating depolarisation in the next neurons. Energy-dependent ion pumps and uptake of excess glutamate by nearby astrocytes is needed to reset the system (Mahmoud et al. 2019; Attwell & Laughlin 2001). The function of synapses and neurons is extremely metabolically demanding (Attwell & Laughlin 2001), so the brain requires a continuous blood supply to provide the cells with glucose and oxygen. This means that reductions in cerebral blood flow (CBF) and depletion of oxygen and glucose levels may cause dysfunction and degeneration of synaptic terminals. Ischaemia occurs when cerebral blood flow is reduced by 70% of its baseline (Heiss & Rosner 1983). The sudden lack of oxygen and glucose initiates the ischaemic cascade, causing impairment in ion balance and extracellular glutamate overload, leading to excitotoxicity, and synaptic and neurodegeneration (Dirnagl et al. 1999; Lai et al. 2014). While severe ischemia is well-understood, it is unclear whether more modest reductions in cerebral blood flow can also cause mechanisms leading to glutamatergic synaptic loss.

Synaptic degeneration is considered to underpin cognitive impairment and dementia, a condition extremely prevalent in our ageing population, affecting 40-50 million people

worldwide – a number which is expected to rise to 115 million people by 2050 (Wortmann 2012; Nichols et al. 2019). Although widely studied, the mechanisms which drive synaptic degeneration are still not fully understood. Robert Terry and colleagues were among the first to demonstrate that synapse loss occurs in Alzheimer's disease and correlates with cognitive decline (Terry et al. 1991). Less attention has been given to synaptic degeneration in vascular dementia, with a limited number of papers showing a decrease in synaptic protein levels (Sinclair et al. 2015; Kirvell et al. 2010). But as Alzheimer's disease and vascular dementia are overlapping conditions, with the most common forms of dementia having mixed pathology associated with both diseases (Hachinski & Bowler 1993; Gorelick et al. 2011), degeneration of synapses and neurons may occur through pathways related to both Alzheimer's and vascular pathology.

Reductions in cerebral blood flow (CBF) are prevalent features of Alzheimer's disease and vascular dementia. Modest, sustained CBF reduction or 'hypoperfusion' is a predictor for the development of cognitive decline and dementia (Alsop et al. 2010; Chao et al. 2010; Ruitenberg et al. 2005; Huang et al. 2002). Additionally, rapid and severe CBF decreases in the form of a stroke or transient ischaemic attack increases the risk of future dementia (Kalaria et al. 2016). There are a limited number of preclinical studies investigating the impact of CBF changes on synaptic density, and most of them have used models of severe global ischaemia or only analysed short-term changes after focal ischaemia. This has left gaps in the literature regarding long-term consequences of either chronic cerebral hypoperfusion or focal ischaemia on synapses. Furthermore, it has been predicted that dementia is the consequence of a number of disease comorbidities. The Nun Study showed that patients with Alzheimer's and vascular pathology had worsened cognitive outcomes than patients with just vascular pathology (Snowdon et al. 1997),

however, there have been very few preclinical studies published that were focused on uncovering these mechanisms.

A pathological hallmark of Alzheimer's disease is the deposition of plaques in the parenchyma and cerebral vasculature. The main component of these plaques is β-amyloid. There is a large body of evidence from rodent studies indicating that β-amyloid can cause toxicity for synapses and neurons, particularly in its soluble oligomeric form (Selkoe 2002; Walsh et al. 2002). Clinical trials targeting β-amyloid, however, have not been successful (Mehta et al. 2017), which may suggest that other disease factors are key contributors for synapse degeneration.

The studies presented in this thesis were conducted to address these gaps in our knowledge. They were designed to investigate the long-term impact of chronic cerebral hypoperfusion and focal ischaemia on synapses, and to establish whether concurrent β-amyloid pathology further exaggerates synapse degeneration.

1.2 Cerebrovascular architecture and blood flow regulation

The brain has low endogenous energy reserves, yet it has high metabolic activity. To support its function a continuous blood supply, at a rate of ~50ml/100g/min, is required to provide the brain with oxygen and nutrients, and for the removal of toxic waste (Cipolla 2009). The volume of blood which passes through the brain is disproportionately high for its mass; as 20% of cardiac output is received by the brain, although its mass

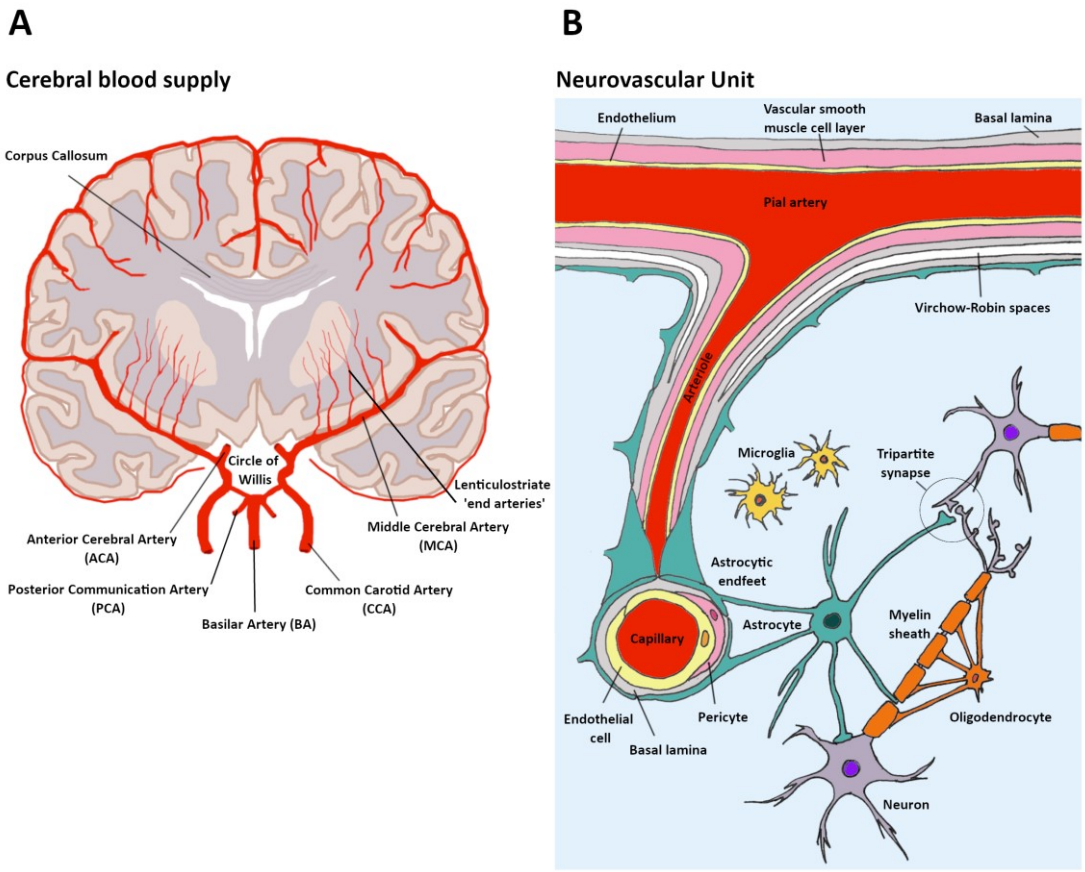

Figure 1.1 Schematic of cerebrovascular architecture and the neurovascular unit. (A) Blood is supplied to the brain via arteries connected at the circle of Willis. The arteries divide into small arteries and arterioles that penetrate into the brain. (B) Cerebral blood flow is regulated by a 'unit' of cells, the Neurovascular Unit. Figure based on figures from Jessen et al. 2015; Wardlaw et al. 2019 .

constitutes only 2% of the total body mass. Furthermore, the brain uses ~20% and ~25% of the body's oxygen and glucose intake, respectively (Zlokovic 2008).

Oxygenated blood is supplied to the brain via the left and right common carotid arteries, which arise from the aortic arch. The common carotid arteries (CCA) branch into the internal (ICA) and external carotid arteries (ECA), which supply the brain and scalp respectively. The internal carotid arteries meet with the basilar artery (BA) (which

supplies the back of the brain) to form an anastomotic ring at the base of the brain, known as the circle of Willis. This structure gives rise to three sets of cerebral arteries, anterior (ACA), middle (MCA), and posterior (PCA), which track along the surface of the brain (see Figure 1.1A). The cerebral vasculature in the grey matter is organised in a hierarchical manner, as the vessels on the surface are large, and branch into smaller arteries and arterioles, which penetrate into the brain (Cipolla 2016). The penetrating arteries divide into the parenchymal arterioles, which then supply the capillary beds, deep within the brain. The grey matter capillary beds are densely organised to support the high metabolic demand, whilst the density of the white matter capillaries is 10% of the grey matter (Klein et al. 1986).

1.2.1 The Neurovascular Unit

Cerebrovascular function is closely linked to neuronal activity through the neurovascular unit (NVU), which is a 'unit' of cells composed of neurons, endothelial cells, mural cells (pericytes and vascular smooth muscle cells (VSMCs)) and glial cells (astrocytes and microglia) (see Figure 1.1B) (Iadecola 2004). Bi-directional communication between these cells enables for the diameters of blood vessels to be mediated, as a response to neuronal activity or changes in the blood pressure (autoregulation). Endothelial cells line the lumen of blood vessels and are packed together connected by tight junction proteins, forming part of the blood brain barrier (BBB) and restricting the movement of cells and molecules into the brain (Anderson & Van Itallie 2009). Mural cells cover the abluminal side of the endothelium; for arteries and arterioles these cells are vascular smooth muscle cells (VSMCs), whilst they are pericytes at the capillary level (Hill et al. 2015; Haseloff et al. 2015). Structural integrity is provided to the endothelium by an abluminal basement membrane and functions as part of the blood brain barrier (Zlokovic

2008). Astrocytes form extensive connections with the endothelium through their specialised 'endfeet' processes. They also interact with neurons at nodes of Ranvier, and synapses in the 'tripartite synapse' (Araque et al. 1999), which have vital roles in synapse dynamics, modulating transmission, stability and plasticity (Liu et al. 2018). This physical interaction between the blood vessels and neurons through astrocytes is a key component for the NVU and regulating blood flow according to neuronal activity (Iadecola & Nedergaard 2007). Moreover, it is estimated that almost every neuron is linked to its own capillary (Zlokovic 2005). Inflammatory cells can also play a part in the NVU, as the release of cytokines and chemokines by resident microglia can modify the expression of tight junction proteins in the endothelium and allow the BBB to become permeable to other immune cells (Hudson et al. 2005).

1.2.2 Blood Brain Barrier

The BBB is the barrier formed by tight junctions in the endothelial cell layer, to restrict the movement of molecules and cells into the brain (Anderson & Van Itallie 2009). The endothelium is specialised to prevent easy movement between the cells and through the cells. An important role of the BBB is to protect the brain from peripheral infection and the movement of peripheral inflammatory cells from the blood stream.

1.2.3 Neurovascular coupling

Neuronal activity influences CBF through neurovascular coupling. Action potentials are generated through depolarisation of the neurons, whereby sodium ions diffuse into the cells through voltage-gated channels, then ATP-dependent ion channel transporters are required to restore the resting potential of the neuron, before another action potential can be generated. Continuous blood flow is required to supply oxygen and glucose for

ATP production to maintain the ion balance in neurons. If CBF is greatly reduced and ATP production is limited, neurons cannot restore their ion balance and return to their resting membrane potential, which can lead to hyperexcitability and excitotoxic cell death (Section 1.4.1.1) (Dirnagl et al. 1999). Under physiological conditions, neuronal activity can mediate CBF by the release of vasoactive neurotransmitters, such as serotonin, acetylcholine and norepinephrine, which bind to receptors on the endothelium and VSMCs of arteries and arterioles (Hamel 2006). These signals stimulate VSMCs to adjust vascular tone by vasodilation or vasoconstriction. Another approach by which neuronal activity is communicated to the vasculature is through the connections with astrocytes. Neuronal activity stimulates an increase in calcium ions in astrocytes, either through direct contact with astrocytic processes or induced by neurotransmitter release, which in turn induces the release of vasoactive molecules that modulate vascular tone (Bazargani & Attwell 2016).

1.2.4 Autoregulation of Cerebral Blood Flow

Constant CBF is critical to support brain function, therefore, the rate of CBF is autoregulated by adjusting the vascular tone of large surface arteries and arterioles, to counter any fluctuations in blood pressure (Fog 1938; Cipolla 2009). The mechanisms for autoregulation are unclear, however, it may be stimulated by the release of vasoactive substances during states of reduced CBF, such a H^+, K^+, O_2 and adenosine (Cipolla 2009). As previously mentioned, healthy CBF is maintained at ~50mL per 100g of brain tissue per minute, if the cerebral perfusion pressure is within a range of ~60 to 160 mmHg. Autoregulation cannot be maintained if the pressure is above or below this range; when it is decreased below this limit the result is cerebral ischaemia (Cipolla 2009; Phillips & Whisnant 1992). Maintaining a healthy CBF is essential for supporting brain function, as

persistent reductions in CBF are associated with the development of cerebrovascular disease (CVD) and vascular cognitive impairment (VCI).

1.3 Vascular cognitive impairment

Vascular cognitive impairment (VCI) is a broad term describing any degree of cognitive decline, from mild cognitive impairment to dementia, that develops following any form of cerebrovascular disease (CVD) (Dichgans & Leys 2017). Dementia refers to a collection of conditions characterised by severe decline in memory and executive functions, with the most common forms being Alzheimer's disease and vascular dementia (Gorelick et al. 2011). Historically, these diseases were viewed as distinct from each other, however, it is now accepted that these conditions overlap significantly, and in fact the most common form of dementia is 'mixed dementia'; which combines both vascular and Alzheimer related pathology (Hachinski & Bowler 1993; Gorelick et al. 2011).

CVD is caused by a combination of vascular risk factors, such as age, stroke, hypertension, diabetes mellitus, atrial fibrillation and atherosclerosis (Abraham et al. 2016; Hofman et al. 1997; Knopman et al. 2001). These risk factors are associated with the development of a wide range of vascular pathologies, including reduced CBF, impaired vasodilation, vessel stiffening, dysfunctional interstitial fluid drainage, BBB dysfunction, large and small vessel disease, white matter rarefaction, myelin damage, ischaemic injury, secondary neurodegeneration and neuroinflammation (Wardlaw et al. 2019). Vascular dysfunction is thought to contribute to 50% of all dementia (Wardlaw et al. 2019). It has been hypothesised that changes leading to VCI and dementia begin to occur during mid-life, and over years and decades there is an accumulation of vascular

risk factors and subclinical brain lesion, culminating in symptomatic impairment (Knopman et al. 2001).

Reduced CBF is associated with cognitive decline. These reductions in perfusion can vary in degree: chronic cerebral hypoperfusion describes a sustained reduction in CBF, whilst cerebral ischaemia occurs when CBF is reduced by 70% of the baseline (Heiss & Rosner 1983). Different severities of CBF reductions may induce varying downstream mechanisms, culminating in VCI and dementia.

1.3.1 Chronic cerebral hypoperfusion and dementia

Cerebral hypoperfusion can result from large or small vessel diseases, cardiac arrest, severe cardiac failure, arrhythmias and severe hypotension (Stefansdottir et al. 2013; Qiu et al. 2006; Alosco et al. 2013; Justin et al. 2013; Dichgans & Leys 2017). The main causes of cerebral vessel disease are processes related to ageing and hypertension, as well as aggregation of β-amyloid in the vessel walls in cerebral amyloid angiopathy (CAA) (Pantoni 2010). These conditions are associated with the development of cognitive decline, therefore, it has been proposed that cerebral hypoperfusion also is associated with cognitive decline. Evidence to support this has been presented by neuroimaging studies indicating that reduced cerebral perfusion is a predictor for the progression from normal cognition to cognitive impairment (Ruitenberg et al. 2005), and the conversion of mild cognitive impairment (MCI) to dementia; with the degree of CBF reduction correlating with the severity of dementia (Alsop et al. 2010; Chao et al. 2010; Huang et al. 2002).

White matter changes are pathological hallmarks of cerebrovascular disease, which are observed in neuroimaging studies of patients as white matter hyperintensities (WMH) using T2-weighted magnetic resonance imaging (MRI). There is evidence that low CBF

relates to the severity of WMH burden, leading to the hypothesis that cerebral hypoperfusion leads to the development of WMH, culminating in cognitive impairment (Duncombe et al. 2017). Evidence published by our group and others have supported this theory, as they found that surgically inducing cerebral hypoperfusion in rats and mice results in white matter pathology and cognitive impairment (Kitamura et al. 2017; Manso et al. 2018; Coltman et al. 2011; Farkas et al. 2007).

An alternative theory is that reduced CBF, as measured in patient neuroimaging studies, may result from a loss of viable tissue from cerebrovascular pathology, rather than being the causative factor of cerebrovascular pathology and VCI (Wardlaw et al. 2019). This is supported by evidence indicating that the baseline burden of WMHs in patients is a predictor for reductions in CBF, but not the vice versa (Wardlaw et al. 2019; Shi et al. 2016). It has been proposed that analysis of resting CBF is not a reliable measurement for lesion-related vascular changes, as CBF fluctuates considerably from minute to minute, and varies between brain regions (Promjunyakul et al. 2018; Wardlaw et al. 2019). Moreover, resting CBF is not necessarily an indicator of the amount of oxygen extracted and used by the tissue, as oxygen extraction is less efficient with high capillary flow velocities (Østergaard et al. 2016). It has been proposed a better indicator of cerebrovascular pathology is to measure changes in neurovascular coupling; the ability of arterioles and capillaries to dilate with increased neuronal activity (Thrippleton et al. 2018; Wardlaw et al. 2019). This is consistent with a study of patients with the genetic form of SVD called CADASIL (Cerebral Autosomal Dominant Arteriopathy with Subcortical Infarcts and Leukoencephalopathy); which found no difference in resting CBF compared with controls, but did find them to have impaired neurovascular coupling (Huneau et al. 2018). A decline in neurovascular coupling was reported in a previous study by our group, demonstrating

that while resting CBF was unchanged between young and aged mice, aged mice had reduced vascular reactivity to neuronal stimulation (Duncombe et al. 2017). Impaired cerebrovascular reactivity has been associated with aging and higher WMH burden (Sam et al. 2016; Blair et al. 2016). Furthermore, increased systolic blood pressure, pulse pressure and intracranial vascular pulsatility have been linked to reduced cerebrovascular reactivity, whereas there is a lack of association with reduced resting CBF (Shi et al. 2020; Wardlaw et al. 2019; Blair et al. 2019). Taken together, these studies indicate that it is still uncertain whether cerebral hypoperfusion is a causative factor in VCI or a result of reduced demand for a high blood supply to damaged tissue.

1.3.2 Stroke, focal ischaemia and dementia

Stroke is a sudden cerebral attack that cuts off blood supply in a focal part of the brain, which can manifest through ischaemia or a haemorrhage. Ischaemic stroke is the common type, accounting for about 80% of strokes (Kalaria et al. 2016). They are usually caused by vessel occlusion from an embolism or thrombosis, halting blood supply with nutrients and oxygen to the parenchyma. In *Time Is Brain-Quantified,* Saver estimates that every minute of an untreated ischaemic stroke leads to on average a loss of 1.9 billion neurons, 14 million synapses and 12km of myelinated fibres (Saver 2006). Rapid treatment with intravenous recombinant tissue-type plasminogen activator (r-tPA) is used to break down the clot and restore blood flow. This treatment will be effective only within a small window of about 4.5 hours (Powers et al. 2015). Improved treatment has increased the survival rate, however, even with the best treatments patients can still experience long-term motor and cognitive disabilities. Around 30% of stroke survivors

will experience some cognitive decline within 3 years of the attack, and stroke more than doubles the risk of developing dementia (Kalaria etal. 2016).

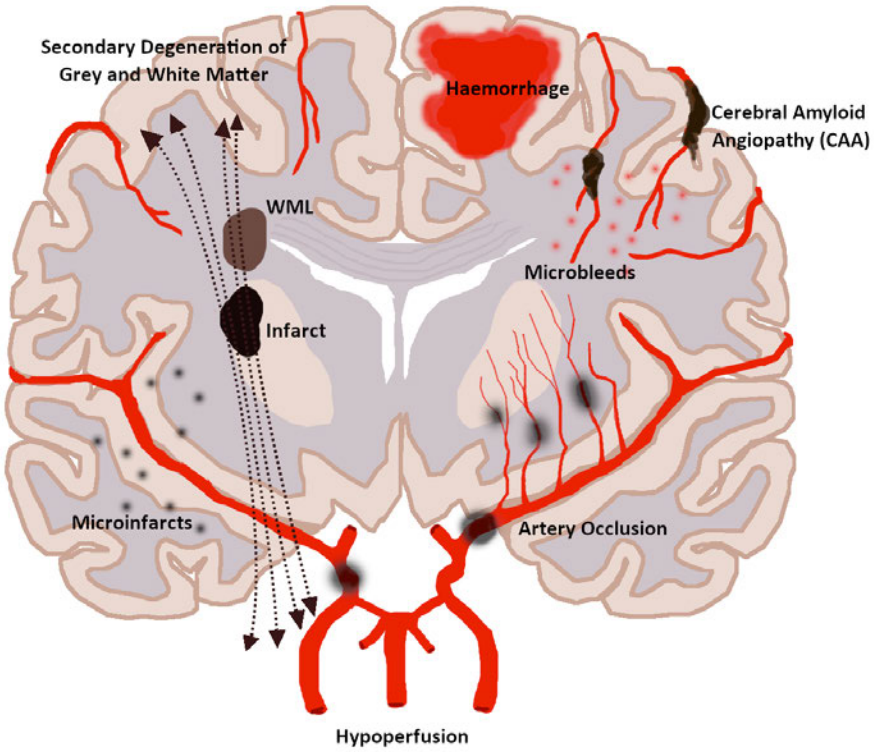

Figure 1.2 Neuropathology of VCI. Vascular causes and cerebrovascular injuries: hypoperfusion, artery occlusion, CAA, infarct, microinfarcts, microbleeds, haemorrhage, white matter lesion, and secondary degeneration. Figure based on a figure from Dichgans & Leys 2017.

1.4 Neuropathology of VCI

Cerebrovascular pathology is extremely heterogeneous in VCI given that cerebral blood flow can be reduced by varying degrees of severity; globally or focally; transient or permanent; and occurs in different brain regions. This wide range of different types of vascular pathology associated with VCI, is shown in Figure 1.2 (Dichgans & Leys 2017). It

is important, therefore, to gain insight into the long-term degenerative processes following global and focal cerebral blood flow changes, and of varying severities.

1.4.1 Ischaemic Damage

Ischaemic neuron damage occurs when blood flow is reduced to 30% of the normal level (Heiss & Rosner 1983). The drop in blood flow diminishes the supply of oxygen and nutrients to the cells, setting in motion processes that result in ischaemic damage, known as the ischaemic cascade.

1.4.1.1 The Ischaemic Cascade

Ischemic stroke or global ischaemia causes an immediate lack of blood and supply of oxygen and glucose resulting in an energy imbalance. Neurons and glia become unable to maintain their ionic gradients, which are ATP dependent, causing a build up of intracellular Na^+ ions and for the cells to depolarise. Presynaptic Ca^{2+} concentrations increase with the activation of voltage-gated Ca^{2+} channels (VGCCs) and reverse Na^+/Ca^{2+} exchange, leading to the release excitatory neurotransmitters into the synaptic cleft and extracellular space. Glutamate is the main excitatory neurotransmitter for the brain. Furthermore, energy-dependent reuptake of glutamate and other neurotransmitters by synaptic vesicle recycling and by astrocytes is impaired, which leads to extracellular glutamate overload. This in turn activates postsynaptic and extrasynaptic AMPA- and NMDA-receptors, resulting in spreading depolarisation to neighbouring neurons. Excessive influx of Na^+ ions into the postsynaptic terminal unblocks Mg^{2+} from NMDARs, leading to large cation influxes. For both the pre- and postsynaptic neurons, the lack of ATP impairs their ability to restore the ion balance, causing an osmotic gradient and

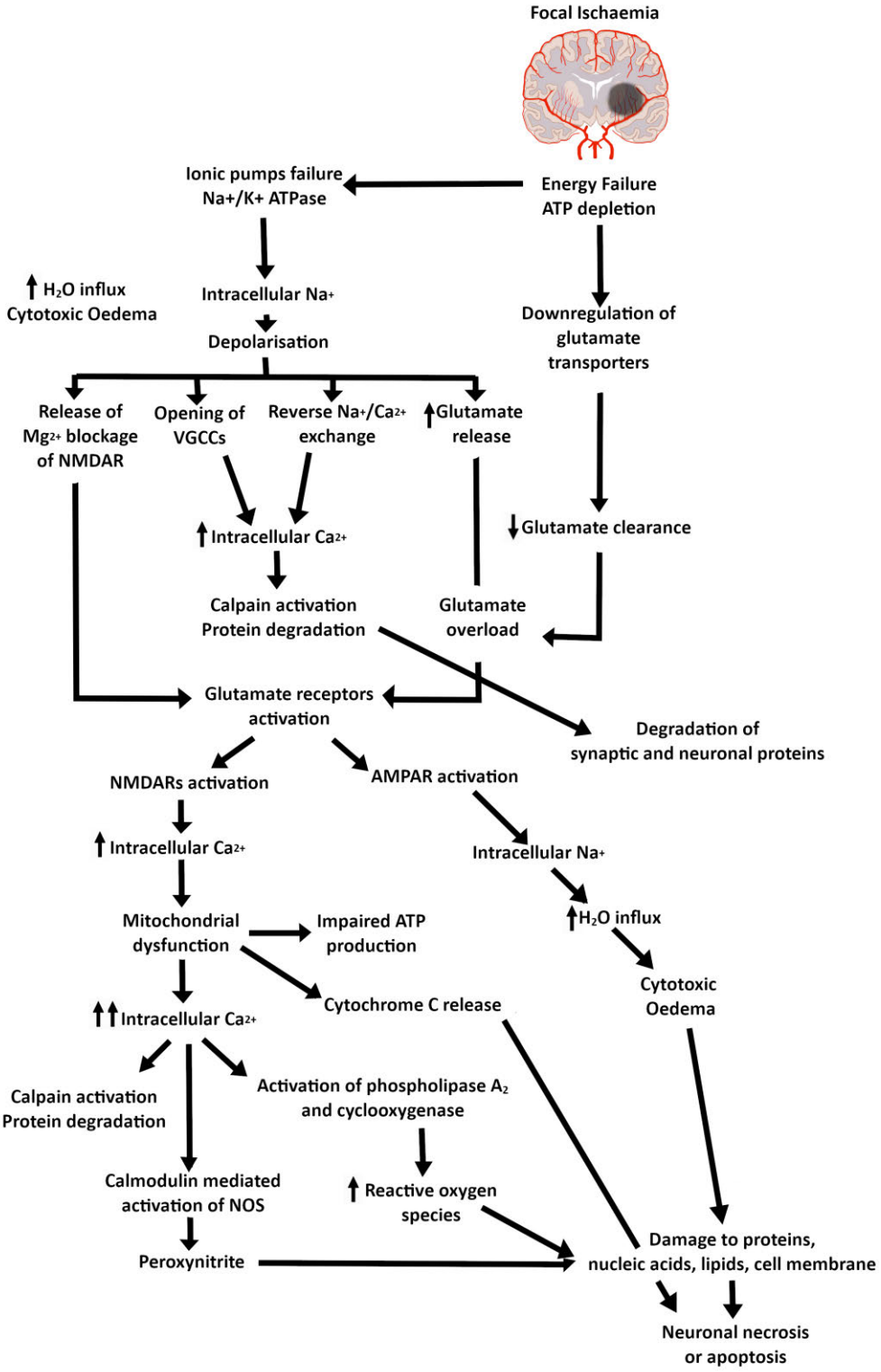

Figure 1.3 The Ischaemic Cascade. Adapted from (Mayor & Tymianski 2017).

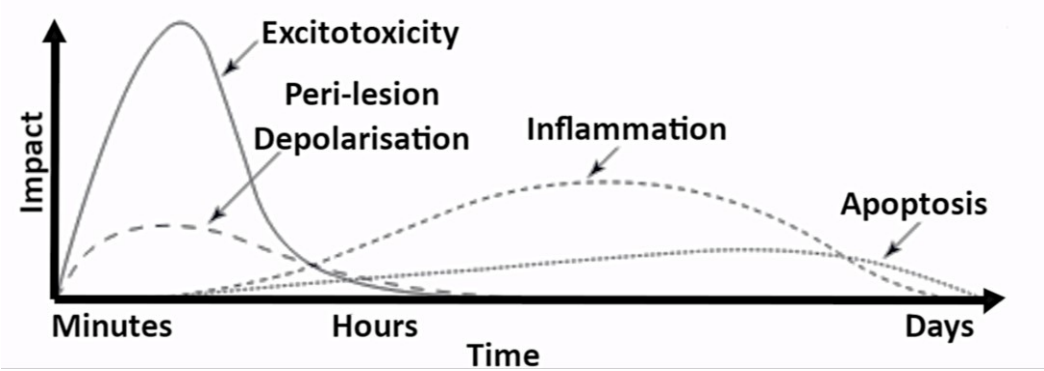

Figure 1.4 Damaging events in focal cerebral ischaemia at acute and sub-acute timeframe. Ischaemia results in early excitotoxicity within minutes, followed by peri-lesion depolarisation. Neuron damage stimulates inflammation and apoptosis over the following hours and days. Adapted from (Dirnagl et al. 1999).

water flows into the cells, leading to oedema. Brain oedema is one of the earliest markers for focal ischaemic damage, which can be studied with MRI and computed tomography neuroimaging (Dirnagl et al. 1999; Lai et al. 2014; Mayor & Tymianski 2017) (Figure 1.3).

Activation of glutamate receptors leads to an overload of intracellular Ca^{2+} ions, which initiates downstream mechanisms that can cause delayed cell damage to the cells in the peri-lesion, the area around the ischaemic core. This includes the activation of proteolytic enzymes, such as calpains, that degrade the neuronal and synaptic proteins causing them to become dysfunctional and lose structural integrity (Lai et al. 2014). Furthermore, calcium-dependent activation of phospholipase A_2 and cyclooxygenase leads to the cells becoming overwhelmed with the generation reactive oxygen species (ROS), which damage lipids, proteins and DNA, as well as stimulating neuroinflammation and apoptosis (Dirnagl et al. 1999). Calcium-dependent neuronal nitric oxide synthase

(nNOS) is activated by Ca^{2+} influx particularly in postsynaptic terminals, due to this enzyme being tethered to NMDA-receptors by scaffold protein PSD95, producing peroxynitrite which is highly reactive and damaging (Lai et al. 2014). Injury to neuronal mitochondrial further impairs the production of ATP and causes greater energy deprivation; whilst perforations in the membrane causes cytochrome C release and stimulates apoptosis.

Focal ischaemia leads to rapid lesion formation due to this bioenergetics failure, surrounded by a region of tissue of constrained blood flow with partially preserved metabolism, known as the peri-lesion or penumbra. In the absence of treatment or reperfusion, this surrounding area may also become part of the lesion, through delayed spreading depolarisation and apoptotic cell death (Dirnagl et al. 1999). There is evidence that focal ischaemic damage can also lead to delayed secondary neurodegeneration, in brain regions that connect with the injured region (Zhang et al. 2012) (see Figure 1.4).

Injured neurons release factors known as damage-associated molecular patterns (DAMPs), which elicit local inflammation (Liesz et al. 2015). Resident microglia and astrocytes become activated, and the release of chemokines and cytokines promotes infiltration of circulating neutrophils and macrophages into the parenchyma (see Figure 1.4). There is evidence that neuroinflammatory cells can be elevated in ischaemic lesions for months after the injury has occurred (Mena et al. 2004), however, it is unclear whether this is protective or detrimental to the brain tissue (see Section 1.4.4).

1.4.1.2 Ischaemic pathology and infarction

Ischaemic lesions can vary hugely in location, size and severity of tissue damage, ranging from areas of diffuse selective neuronal loss with intact extracellular matrix, to large

infarcts with pannecrosis – necrosis of all cell types within the NVU (Baron et al. 2014). The resulting lesion will depend on the location and type of vessel occlusion and whether there is reperfusion. This may also depend on the presence of other disease comorbidities, such as β-amyloid. Large infarcts (strokes) or multiple small subcortical infarcts or ischaemic lesions are linked to cognitive decline and high risk of dementia (Hachinski et al. 1974; Schneider et al. 2003). Infarcts can have a severe impact on cognition if they are present in strategic brain regions, such as the basal ganglia, caudate nucleus and globus pallidus, thalamus and angular gyrus (Jellinger 2008; Szirmai et al. 2002). The CA1 region of the hippocampus is particularly vulnerable to global ischaemia, and its damage is thought to contribute to spatial working memory deficits (Tsien et al. 1996; Stackman et al. 2016). Sudden reperfusion to an ischaemic area can cause 'reperfusion injury', associated with the generation of reactive oxygen species (ROS) initiating cell death sequences, and causing more tissue injury (Wu et al. 2018). Furthermore, focal ischaemic injury can spread through spreading depolarisation and secondary neurodegeneration, resulting in progressive neurodegeneration of more extensive tissue damage than the primary lesion site (Hartings et al. 2003; Zhang et al. 2012).

1.4.2 White Matter Pathology

White matter is particularly vulnerable to blood flow disruption, as its collateral supply is limited. Cerebral white matter tracts are composed of myelinated and unmyelinated axons, oligodendrocytes which ensheath the myelinated axons, astrocytes and microglia, and blood vessels. As the white matter tracts enable neuronal circuits and different brain regions to communicate, white matter injury can have detrimental effects on brain function. White matter pathology is present to different degrees in normal aging, stroke,

vascular dementia and Alzheimer's disease (de Leeuw et al. 2006; Brun & Englund 1986). The presence of white matter infarcts increases the risk of mortality (Conijin et al 2011). In dementia patients, the extent of white matter damage is related to a decline in cognitive processing speed (Mungas et al. 2001) and impairment in executive function (Cohen et al. 2002). Loss of white matter integrity is thought to be an early stage of pathological progression to dementia, as it has been seen in patients with mild cognitive impairment. There is a relationship between the global volume of white matter lesions and cognitive impairment in these patients (Garde et al. 2000). Disruption in white matter tracts is also a feature of Alzheimer's disease, and is associated with neurofibrillary tangles, one of the classical pathological hallmarks of the disease (Kantarci et al. 2017).

White matter pathology is predicted to have a vascular origin. It is present in 64-86% of all stroke patients (Fu et al 2005; Li et al 2013). Low cerebral blood flow in the intact white matter of stroke/transient ischaemic attack patients predicts the appearance of white matter hyperintensities on follow-up MR imaging (Bernbaum et al. 2015). Previous findings from our lab have demonstrated that surgically induced modest cerebral hypoperfusion in mice is sufficient to cause long term white matter disruption, predominantly in the corpus callosum, internal capsule and optic tract (Coltman et al. 2011; Holland et al. 2011; Kitamura et al. 2017). The extent of white matter pathology has an impact on the functional outcome, as the decrease of white matter integrity in the corpus callosum correlates with impaired spatial working memory, and reduced action potential conduction across this structure (Kitamura et al. 2017).

1.4.3 Alzheimer's pathology

Alzheimer's disease (AD) and vascular dementia (VaD) are overlapping conditions, with the majority of dementia cases have mixed Alzheimer's and vascular pathology (Hachinski & Bowler 1993; Gorelick et al. 2011). There is a growing body of evidence indicating that these different pathologies interact and may exacerbate each other. Furthermore, there is evidence that the presence of both Alzheimer's and vascular pathology may worsen the cognitive outcome, compared to dementia patients with just vascular pathology (Snowdon et al. 1997).

Histologically, Alzheimer's pathology was classified by the presence of extracellular amyloid plaques (also known as senile plaques) that are predominantly composed of β-amyloid protein, and intracellular neurofibrillary tangles containing hyperphosphorylated tau. β-amyloid proteins can exist in different forms, with the molecules aggregated together in insoluble deposits, as well as being present in soluble monomers and oligomers. Soluble oligomeric β-amyloid has been shown to induce a reduction in synaptic activity and is considered to be the main driver for synaptic loss in AD (Section 1.7.1-2). In addition, β-amyloid has many negative implications for the vasculature. It is a potent vasoconstrictor and has been shown to reduce neurotransmitter-mediated vasodilation (Thomas et al. 1996). This may contribute to the cerebral hypoperfusion in the early stages of AD (Huang et al. 2002). Furthermore, administration of $A\beta_{40}$, the main β-amyloid species in the vasculature, to mouse brains lead to a reduction of their CBF (Niwa et al. 2001). β-amyloid proteins can become aggregated within the basement membrane of vessels, particularly in the leptomeningeal arteries and cortical arterioles, known as cerebral amyloid angiopathy (CAA) (Pimentel-coelho et al. 2013; Love & Miners 2016). This can be very damaging to

blood vessels, as it is associated with the development of small vessel disease, white matter injury and arteriolosclerosis (Thal et al. 2003; Gurol et al. 2006; Charidimou et al. 2016). β-amyloid deposition in the vasculature can cause the vessels to become rigid and loose vascular tone (Kimbrough et al. 2015). Moreover, β-amyloid and neuroinflammation induced by it, can exert degenerating effects on smooth muscle cells and pericytes (Brown & Thore 2011; Reijmer et al. 2016; Sengillo et al. 2013). This can lead to BBB break down, resulting in microbleeds or haemorrhages, and promoting further immune responses (Dierksen et al. 2010; Gurol et al. 2012).

The increased burden in β-amyloid may result from impairment in its clearance pathways, which normally prevents it from aggregating. In normal conditions, β-amyloid and other waste substances are cleared from the brain through the two main drainage pathways: perivascular drainage of interstitial fluid (ISF), and glymphatic drainage through cerebrospinal fluid (CSF) (Hawkes et al. 2014; Iliff et al. 2012). In perivascular drainage, waste solutes move with ISF bulk-flow through the basement membrane of capillaries and drain along the arterioles and arteries, towards the leptomeningeal arteries at the brain's surface and eventually reaching the cervical lymph nodes at the exterior of the skull. Alternatively, in glymphatic drainage CSF is pumped from the Virchow-Robin spaces (see Figure 1.1) into para-arterial spaces around penetrating arteries, then into the parenchyma where CSF/ISF solute exchange occurs, and exits through para-venous spaces into subarachnoid compartments. The CSF-ISF fluid dynamics through the parenchyma rely of the aquaporin water channels expressed at the astrocytic endfeet that ensheath the vasculature in the NVU (Sun et al. 2018). Arterial pulsation is thought to be a main driver for both types of drainage. There is evidence that aggregation of β-amyloid in the vasculature can obstruct drainage

pathways, which would in turn prevent the clearance of β-amyloid through these pathways, and result in further accumulation leading to CAA (Hawkes et al. 2011; Hawkes et al. 2014). Drainage pathways can become impaired after ischaemic and haemorrhagic stroke. A study of different focal ischaemia in mouse models showed that glymphatic drainage was impaired during ischaemia, but was restored with spontaneous arterial recanalization (Gaberel et al. 2014). If ischaemic or haemorrhagic damage impairs cerebral drainage, this may at least partially account for β-amyloid burden in patients with VCI.

Another mechanism by which β-amyloid is removed from the brain is by transportation across the BBB via low density lipoprotein receptor-related protein (LRP1), expressed by endothelial cells and astrocytes (Liu et al. 2017; Storck & Pietrzik 2017). There is evidence from a mouse model that reduced CBF results in decreased protein levels of LRP1 whilst protein levels of $A\beta_{1-42}$ and $A\beta_{1-40}$ were increased (Ashok et al. 2016). This indicates that cerebrovascular injuries leading to reduced perfusion may impair β-amyloid clearance through the BBB into the bloodstream, and contribute to an increase in β-amyloid burden in the brain. Alternatively, the production of β-amyloid may be enhanced by cerebrovascular injuries. BACE1 is one of the enzymes that process amyloid precursor protein (APP) into β-amyloid and its expression has been shown to be increased with hypoxia (Salminen et al. 2017). The exposure to hypoxia following CBF reduction, therefore, can stimulate the expression of BACE1 and enhance β-amyloid production. Taken together, the evidence indicates that β-amyloid can exacerbate vascular pathology, whilst vascular pathology can stimulate more β-amyloid production and decrease its clearance.

1.4.4 Neuroinflammation

Neuroinflammation is the brain's immune response to pathological changes, such as cellular injury, build-up of debris and invading pathogens. As with all neurological and neurodegenerative conditions, it is clear that neuroinflammation plays key roles in CVD and Alzheimer's diseases, and may have both detrimental and protective roles. Glial cells, microglia and astrocytes, are the resident cells that can detect even subtle changes in the brain environment, and can propagate an immune response depending on the stimulation (Sims & Yew 2017; Salter & Stevens 2017; Liddelow & Barres 2017; Hammond et al. 2019). Noxious stimuli in the brain activate microglia and astrocytes, causing morphological and phenotypic changes, and proliferate. Microglia are transformed from ramified cells with small somas and long processes, to an 'amoeboid' morphology (Schilling et al. 2003). Astrocytes also undergo a similar morphology change, as their somas become bigger and the processes become shorter and thicker. Activation of astrocytes includes an upregulation of intermediate filament proteins, such as glial fibrillary acidic protein (GFAP), which is often used as a marker for immunohistochemical detection of reactive astrocytes (Eng et al. 1971). As previously mentioned, activated microglia and astrocytes can have both detrimental and beneficial roles in brain injuries. This has lead to the classification of their activation states being shoe-horned into either pro-inflammatory (M1 and A1) or anti-inflammatory (M2 and A2). However, there is now a greater understanding of different transcriptomic, proteomic and epigenomic characteristics of activated microglia and astrocytes, revealing that their activation states are much more complex and context-dependent (Sims & Yew 2017; Salter & Stevens 2017; Liddelow & Barres 2017; Hammond et al. 2019).

Stroke and focal ischaemic lesions trigger a robust neuroinflammatory response, as damaged neurons release DAMPs (Liesz et al. 2015). Resident microglia are the first to respond, increasing their cell numbers within hours of injury and maintaining high levels over the following days, as found in rodent models (Wattananit et al. 2016; Zarruk et al. 2017; Yoon et al. 2018; Rajan et al. 2018). Astrocytes are also activated in the acute phase, potentially by pro-inflammatory signals released from activated microglia (Liddelow et al. 2017). They further contribute to the pro-inflammatory environment by releasing cytokines, which recruit peripheral immune response to the lesion site (Li et al. 2017). Focal ischaemia causes endothelial activation, upregulation of adhesion molecules and infliltration of myeloid cells and lymphocytes (Gauberti et al. 2013; Neumann et al. 2015; De Meyer et al. 2016; Shi et al. 2019). Release of pro-inflammatory signals, including cytokines, chemokines, ROS and matrix metallopeptidases (MMPs), contributes to neurotoxic cell death and compromises BBB function, as well as further promoting immune responses by the infiltration of leukocytes (Giraud et al. 2015; Neumann et al. 2015).

Microglia and astrocytes have protective and restorative roles following focal ischaemia, through the release of anti-inflammatory cytokines, such as IL-10 and TGF-β, and neuroprotective factors, glial cell line-derived neurotrophic factor (GDNF) and brain-derived neurotrophic factor (BDNF) (Sandvig et al. 2018; Gordon 2003; Neumann et al. 2006; Liu & Chopp 2016a). There is evidence that depletion of microglia with colony-stimulating factor-1 receptor (CFS1R) inhibitor in a mouse model of transient focal ischaemia, results in a larger lesion and exacerbated the levels of pro-inflammatory cytokines and lymphocyte levels at 1 and 3 days after surgery, indicating that microglia do provide some neuroprotection and anti-inflammatory functions (Jin et al. 2017).

Recently, the use of single-cell RNA sequencing has enabled better characterisation of the activation states of microglia and astrocytes in brain injures. Rajan et al. found that microglia are the predominant immune cell at day 3 after focal ischaemia and express pro-inflammatory signals, such as the gene for TNFα (Rajan et al. 2019). Interestingly, their study revealed that macrophage levels increased at day 3 and expressed genes for anti-inflammatory and wound healing signals. They proposed, therefore, that microglia may have a predominately deleterious effect at the early stages after a focal ischaemic injury, and macrophages infiltrate into the lesion to counteract microglial activity.

Astrocytes are also very sensitive to ischaemia, causing them to change to their activated morphology. They also lose their ability for glutamate uptake from the synaptic cleft, thereby contributing to glutamate overload and excitotoxicity (Ouyang et al. 2007). An important function of astrocytes in a focal injury is that they bundle to form a glial scar, which encapsulates the lesion, seals the damaged BBB and protects the surrounding tissue from exposure to neurotoxic molecules and invading immune cells (Sofroniew 2009). Although this scar may act as a barrier to prevent damage to healthy tissue, the astrocytes in the scar express a number of molecules that prevent axon regeneration in this region (Gris et al. 2007). Astrocytes also have neuroprotective roles by providing metabolic support to neurons during ischaemia (Rossi et al. 2007). There is evidence that astrocytes partake in a number of reparative processes, including regulating neurogenesis, promoting synaptogenesis, and enhancing BBB repair and angiogenesis (Liu & Chopp 2016).

Post-ischaemic neuroinflammation is not confined to the primary injury site, but is elevated throughout the brain and can persist for weeks/months/year afterwards (Mena et al. 2004; Shi et al. 2019; Linck et al. 2019). As previously described, focal ischaemic

injury can lead to diaschisis and secondary neurodegeneration in distal brain regions (Hartings et al. 2003; Zhang et al. 2012). Studies conducted in human stroke patients and rodent models indicate that chronic neuroinflammation coincided with these changes (Morris et al. 2018; Linck et al. 2019; Weishaupt et al. 2016; Rodriguez-Grande et al. 2013). The mechanisms underlying global neuroinflammation following ischaemic injury are unknown, yet it may result from the spread of pro-inflammatory mediators and cytokines through the cerebrospinal fluid (CSF) and extracellular space (Shi et al. 2019). Furthermore, there is evidence that sustained inflammation worsens the outcome of focal ischaemia, as elevated levels of inflammatory components, is associated post-stroke cognitive decline and recurrence of stroke (Boehme et al. 2016; Elkind et al. 2014; Narasimhalu et al. 2015; Shi et al. 2019). Activated microglia and astrocytes have been found in regions of white matter pathology, and may be stimulated for clearance of myelin debris (Johnson 2013; Lloyd et al. 2017). There is evidence that more modest CBF changes can induce neuroinflammation. Previous research from our group and others have demonstrated that chronic cerebral hypoperfusion causes an increase in microglia/macrophages and astrocyte densities, particularly in the white matter tracts (Shibata et al. 2004; McQueen et al. 2014; Reimer et al. 2011; Holland et al. 2011). Moreover, white matter neuroinflammation in this model appears to impact the function of the white matter, as increased level of microglia/macrophages correlated with the slowing conduction velocity in the corpus callosum; which was alleviated by treatment with anti-inflammatory drugs (Fowler et al. 2018; Manso et al. 2018). There is also evidence that hypoperfusion stimulates a release of pro-inflammatory cytokines and chemokines in the white matter, which may cause axon-glial integrity and conduction velocity (Reimer et al. 2011). Collectively, these studies demonstrate that reductions in

CBF can lead to chronic neuroinflammation, which may contribute to degenerative changes and worsened functional outcome.

Neuroinflammation is also a prominent feature of AD and is associated with β-amyloid pathology. Microglia express a number of cell-surface receptors that bind to soluble β-amyloid oligomers and insoluble fibrils (Stewart et al. 2010; Bamberger et al. 2003; Paresce et al. 1996); activating them for β-amyloid clearance by phagocytosis or the release of degradation enzymes (Lee & Landreth 2010; Paresce et al. 1996). Astrocytes may also have roles in internalising and degrading β-amyloid (Wyss-Coray et al. 2003; Jiang et al. 2008). Activation of these cells, however, results in increase levels of pro-inflammatory cytokines, which can have downstream neurotoxic effects (Heneka et al. 2015), as previously discussed. Moreover, impairment in β-amyloid clearance may be a major contributor to disease progression. Advancements have been made in understanding genetic variants linked with AD, and revealed that the majority of the identified loci are expressed in microglia or myeloid cells (Villegas-Llerena et al. 2016; Efthymiou & Goate 2017). This includes a variant of TREM2, which has functions in inflammatory and phagocytic signalling, and could reduce β-amyloid clearance (Hsieh et al. 2009; Colonna & Wang 2016). Another proposed mechanism by which microglia may contribute to AD pathogenesis and cognitive decline is by aberrant synaptic stripping (Hong et al. 2016). This is the theory that microglia physically engulf and remove synaptic terminals during neurodegenerative disease (Rajendran & Paolicelli 2018). β-amyloid may also 'prime' or 'sensitise' glial cells, leading to an exaggerated immune response with subsequent stimulation. Glial priming has been found in ME7 neurodegeneration prion disease mice and Tg2576 mice, as LPS-induced systemic inflammation resulted in even higher levels of neuroinflammatory cells compared to WT mice (Cunningham et al. 2005; Sly et al. 2001).

These studies imply that multiple disease comorbidities can exacerbate neuroinflammation, which may result in worsened neurotoxicity and degeneration.

Taken together, there is a large body of evidence indicating that neuroinflammatory responses to CBF reductions and β-amyloid pathology can contribute to degenerative changes in the brain. The mechanisms behind the pathobiology of VCI and AD are not fully elucidated, however, the use of rodent models to mimic aspects of these diseases are enabling greater understanding of the underlying processes.

1.5 Models of reduced CBF

Advancements in our understanding of the mechanisms underlying CVD and VCI have been made through the use of rodent models, which mimic the breadth of human cerebrovascular injuries. Surgical models have been established to investigate the impact of reduced CBF on the brain and whether it is causative for the development of CVD and VCI.

1.5.1 Global ischaemia and hypoperfusion models

Surgical procedures have been established to reduce global CBF in rodents. Common approaches for this is to permanently or transiently block or restrict flow through one or both common carotid arteries (Jessica Duncombe et al. 2017).

1.5.1.1 Chronic cerebral hypoperfusion rodent models

A number of rodent models have been developed to mimic the chronic reductions of cerebral perfusion that occur in aging and early stages of dementia, without inducing overt ischaemic damage, usually by restricting the flow through one or both of the common carotid arteries. In one of these mouse models, bilateral common carotid

stenosis (BCAS), CBF in the forebrain is decreased through application of microcoils to both common carotid arteries (Shibata et al. 2004). This model usually uses C57Bl/6J mice, as 90% mice of this strain have an incomplete circle of Willis (McColl et al. 2004). CBF measurements with laser speckle imaging show that the initial reduction after BCAS is ~30-40% of the baseline, with recovery to ~20% over the following month, in 3-4 month-old mice (McQueen et al. 2014).

A number of groups, including ours, have found that BCAS surgery in mice leads to cognitive impairment, particularly in tasks assessing spatial working memory deficits, such as the 8-arm Radial Arm Maze (RAM). The RAM was first designed by Olton and Samuelson in 1976 for rats and has since been adapted for mice (Olton & Samuelson 1976). The apparatus consists of a maze with 8 identical arms that radiate from a central platform and are equidistant from each other. Prior to starting the experiment the rodents are food restricted, providing an incentive for them to explore the maze which is baited with a food pellet at the end of each arm. The task requires the rodents to use external visual cues on the surrounding walls to remember which arms they have been in and to go into novel arms to collect their food reward. Visiting an arm more than once is known as a 'revisiting error' and the number of revisiting errors is used as a measure of spatial working memory deficit. A previous study from our group found that after one month of BCAS surgery, the mice had a small impairment in spatial learning memory, but the spatial learning and memory abilities were unchanged compared to sham animals (Coltman et al. 2011). Spatial learning and memory was assessed with the Morris Water Maze (Morris et al. 1982). This is a widely used method, designed by Richard Morris, which requires the rodents to swim within a tank of cloudy water, and use external visual cues to learn and remember where a hidden platform is, enabling them to escape. Escape latency is measured as an assessment

of memory. The task usually has a second stage when the hidden platform is removed and the time the rodent spends in the correct quadrant is measured. Another previous study by our group found that spatial working memory deficits were present 3 month after BCAS surgery (Kitamura et al. 2017), whilst our collaborates used a 3D 9-arm radial arm maze to show BCAS induces cognitive decline at 4 months after BCAS surgery (Hase et al. 2017). At 6 months after BCAS surgery, cognitive deficits were evident from both RAM and WMW tasks, indicating that longer term hypoperfusion impacts more cognitive functions (Holland et al. 2015).

Studies from our group and others have demonstrated that BCAS has acute and chronic effects predominately in the white matter. At 3 days, microarray analysis indicated that genes related to angiogenesis and neuroinflammation were altered in the white matter (Reimer et al. 2011). White matter tracts are shown to be vulnerable to this surgery, as shown by histological analysis and MRI/DTI, 1 months and 6months after surgery (Holland et al. 2011; Holland et al. 2015; Shibata et al. 2004; Coltman et al. 2011). Other pathological features present at this time-point are activation of astrocytes and microglia, axon-glial breakdown and disruption in the blood brain barrier. To date, most studies have focussed on the impact of BCAS on the evolving diffuse white matter pathology, but limited studies have also shown degenerative effects. At 6 months, BCAS results in multiple subcortical microinfarcts and microbleeds (Holland et al. 2015), and at 8 months BCAS lead to hippocampal atrophy (Nishio et al. 2010). This model was used in the work presented in Chapter 3 of this thesis, to investigate the impact of chronic CBF reductions on glutamatergic synapses.

A disadvantage of the BCAS model is that the mice experience an initial large reduction in CBF followed by gradual recovery. This is unlike the human condition where the restriction of the blood vessels causes progressive reduction in CBF. An alternative model could be gradual common carotid artery stenosis (GCAS), which uses ameroid restrictors on the carotid arteries instead of microcoils. The restrictors absorb water and swell over time, gradually restricting CBF over 28 days (Hattori, Kitamura, Nagatsuka, et al. 2014). This procedure results in multiple infarcts in the cortex, corpus callosum, hippocampal fimbria and caudoputamen.

1.5.1.2 Global ischaemia rodents models

Many previous studies have used vessel occlusion models to induce hypoperfusion with ischemic damage. Although these models were not used in the present research, other groups used the to investigate the impact of CBF reduction on synapses. Bilateral common carotid artery occlusion (BCCAO or 2VO) is frequently used in rats and mice. Permanent BCCAO in rats has been shown to result in an acute CBF reduction of ~55-65% in the cortex and white matter, and ~20-40% reduction in the hippocampus, with recovery to baseline level over the following 2-6 months (Otori et al. 2003; Choy et al. 2006).

A number of studies have published evidence that BCCAO surgery results in cognitive decline (Farkas et al. 2007). The MWM and RAM tests have been the most widely used to show that BCCAO surgery results in hippocampal-dependent memory impairment in rats, as early as 7 days after surgery (Farkas & Luiten 2001; Murakami et al. 2000; Sopala et al. 2000; Liu et al. 2005). BCCAO surgery has also been found to impact other non-spatial forms of memory, such as impairment in an object recognition test at 60 and 90 days after surgery (Sarti et al. 2002).

Histological analysis has revealed that hippocampal CA1 neurons are damaged 2 weeks after surgery, and their condition worsens over time (Ohtaki et al. 2006; J. Liu et al. 2006). BCCAO also induces white matter disruption and neuroinflammation in the corpus callosum, optic tract and internal capsule (Cho et al. 2006). Ligation of both common carotid arteries in mice resulted in progressive spatial memory impairment, and neuron loss in the hippocampus and cortex (Wang et al. 2016).

1.5.2 Focal ischaemia models

The majority (~70%) of human strokes occur within the MCA and its branches (Koizumi et al. 1986). Models of middle cerebral artery occlusion (MCAO), therefore, resemble the majority of human ischaemic strokes (Tamura & Teasdale 1981). There are a number of different approaches to achieve MCAO through the use of an intraluminal suture, electrocoagulation, microaneruysn clip, micro embolism, vasoconstriction or photothrombosis (Fluri 2015). The results of these different methods are differing severity and locations of ischaemia damage. The majority of these procedures have MCAO performed in mice and rats; however, some studies using higher organisms such as gerbils and non-human primates have been used for these studies.

1.5.2.1 Intraluminal suture MCAO

Intraluminal suture MCAO is a widely-used method for induced focal ischaemia in rats and mice, and was used in the studies presented in Chapters 5 and 6 of this thesis. This method involves ligating the CCA and ECA, then introducing a silicone-coated monofilament through a small incision in the ECA and moving it up to occlude the entrance of the MCA. This approach can be used for transient and permanent occlusion. The maximum occlusion time for transient MCAO in mice is 60 minutes, whilst longer

occlusion times of 60, 90 and 120 minutes occlusion are most commonly used for rats. This surgery has a high success rate of 88-100% (Tsuchiya et al. 2003; Liu et al. 2009). An advantage of intraluminal suture MCAO is that is does not require a craniotomy, making the procedure less invasive compared to other MCAO methods.

The type of intraluminal suture MCAO surgery used in the present study was previously described by Hata et al. (Hata et al. 1998). In this model, ischaemic cell injury first occurs within the striatum, with delayed damage expanding to the overlying frontoparietal and temporal cortices, which will often result from longer occlusion times. The striatum is vulnerable to ischaemia following MCAO, as the end arteries branching from the MCA are end-arteries and do not form collaterals (see Figure 1.1A). This is supported by observations that the striatal CBF remains reduced, whilst cortical CBF recovers to its baseline value 2 hours after reperfusion in rat MCAO (Takagi et al. 1995; Fluri 2015). The cell damage that occurs in the striatum is mostly rapid, necrotic and irreversible, and reaches its maximum volume by 24 hours post-occlusion. In the cortex, however, the changes tend to be delayed and apoptotic, making up the penumbra or peri-lesion. The extent of damage is largely dependent on the duration of the occlusion. A study by Pedrono et al. demonstrated that there was a fivefold increase in lesion volume between mice after 15 minutes and 30 minutes of MCAO. The smallest duration of MCAO that will result in ischaemic damage is 15 minutes, while 10 minutes or less result in no detectable lesion (Pedrono et al. 2010).

Alongside the advantages previously mentioned about the physiological relevance of the model, the surgical procedure is also relatively quick and easy to perform with good reproducibility. It success rate is high, although sometimes premature reperfusion can occur. Moreover, there can be variations in the pathological outcome, such as

inadequate MCAO leading to no evidence of ischaemia damage, or excessive injury. An adverse side effect of the surgery can be subarchnoid haemorrhage (SAH), although this can be improved by the use of silicone-coated filaments, which adhere better to the endothelium (Bouley et al. 2007). In addition, Laser Doppler imaging can be used to guide the placement of the filament (Schmid-Elsaesser et al. 1998). Another early adverse effect of the surgery can be difficulty with eating and weight loss, as ischaemia can occur in the muscles that control mastication and swallowing (Dittmar et al. 2003). There are a number of different types of MCAO surgery, which are described below, as these models were used in publications discussed later in this thesis.

1.5.2.2 Distal MCAO

There are two main models of distal MCAO, which involve exposing the MCA via a narrow craniectomy and an incision into the dura mater. The first method permanently occluded the MCA by electrocoagulation, application of a microaneurysm clip, vessel ligation or photothromobosis using Rose Bengal (Fluri 2015). The main regions of damage are in the striatum, subcortical white matter and ipsilateral cortex. The second approach is known as the three-vessel model (3VO), which involves the first method plus bilateral common carotid artery occlusion. Permanently or transiently occluding the MCA or CCA is a common method for inducing focal ischaemia (Yanamoto et al. 2003). This model results in injury predominately in the cortex and underlying white matter, with limited damage in the striatum (Desk et al. 1992). Although these techniques are much more invasive than the intraluminal suture model, they enable much better targeting of the occlusion site leading to more restricted regions of damage. The main disadvantage of this model is that it requires a craniectomy, which could be damaging for the brain and induce a neuroinflammatory response. Application of the

vasoconstrictor endothelin-1 is another method used to induce distal MCAO or injected into specific brain regions (Fluri 2015).

Kristian Doyle and colleagues use a modified version of distal MCAO; after dMCAO surgery the mice are placed in a hypoxic chamber for an hour. They call this model Distal Hypoxia Stroke model (DH stroke). They found that the addition of hypoxia created a lesion that is larger than the usual dMCAO lesion, and has better reproducibility (Doyle et al. 2012). The model also resulted in acute motor and neurological deficits, with impaired hippocampal long-term potentiation and cognitive decline appearing at 7 weeks after surgery (Doyle et al. 2015). The authors propose that this is an appropriate model for studying post-stroke dementia.

1.5.2.3 Cognitive Impairment following MCAO

A number of studies have investigated whether MCAO surgery in rats induces spatial learning and working memory impairment, assessed with the RAM or MWM tests. Although some studies did find a significant impairment (Okada et al. 1995; Yonemori et al. 1996; Markgraf et al. 1992), the results may be confounded as there is an abundance of evidence indicating that MCAO surgery impacts motor ability which could affect their performance in the MWM and RAM tests. Bingham et al. adapted the analysis for their MWM experiment, by which they compared the 'accuracy in crossing the platform location' between sham and MCAO animals (Bingham et al. 2012). This is calculated by the number of times the rats cross the platform in the target quadrant, minus the number of crossings in equivalent locations in the other three quadrants, thus the result is not dependent on escape latency. This study found that one month after permanent MCAO, the rats only had a minimal deficit in spatial memory compared to sham and un-operated animals (Bingham et al. 2012). Novel object recognition (NOR) task has also been used to

assess non-spatial memory impairment after MCAO surgery. Fréchou et al. found that 60 days of permanent MCAO in mice resulted in impairment in recognition memory, in the novel object recognition test (Fréchou et al. 2019). Whereas, Nguyen et al. using the DH stroke mouse model discovered that young mice experienced memory impairment in the NOR task at 7 weeks after surgery, whilst older mice experienced memory impairment earlier at 4 weeks (Nguyen et al. 2018).

1.5.2.4 Photothrombosis

Another popular model for inducing focal ischemic lesions is photothrombosis. Light-sensitive Rose Bengal is injected intravenously injected in rodents and illuminated through the skull, to cause the generation of singlet oxygen, focal endothelial damage, platelet activation and focal clotting (Dietrich et al. 1986). The result is the formation of a focal ischaemic lesion in the cortex at the location of illumination. This method enables the researcher to have high control over where the lesion forms, however, the lesions are restricted to the cortex. Moreover, the pathological process of the lesion formation is different to that in human stroke, which is characterised by cyotoxic edema. In this model the lesion forms rapidly from cytotoxic (intracellular) and vasogenic (extracellular) edema from endothelial injury (Lee et al. 1996). Experiments were undertaken to optimise an approach for Rose Bengal photothrombosis, as described in Chapter 4.

Photothrombosis in rats and mice has been shown to induce motor impairment, however, far fewer studies have investigated the impact this has on cognition. Sadigh-Eteghad et al. showed that a photothrombotic lesion in the medial prefrontal cortex leads to longer escape latencies in the Barnes maze (Sadigh-Eteghad et al. 2018). The Barnes maze is a land version of the MWM, with the maze being an open circular surface

with holes around the perimeter, and one hole leading to a plastic box enabling the mice to escape the maze (Barnes 1979). Similarly to the MWM, the Barnes maze requires the mice to use external visual cues to learn and remember which hole leads to the escape box and the longer escape latency is an indication of worsened spatial memory. Sadigh-Eteghad et al. also demonstrated that the locomotion activity was unchanged between the ischaemic mice and the sham mice, suggesting that the Barnes maze experiment was not confounded by motor deficits (Sadigh-Eteghad et al. 2018). Another study using Rose Bengal photothrombosis to induce a large unilateral cortical lesion found that these mice had longer escape latencies and fewer crossings of the hidden platform in the MWM compared to sham animals, whilst ischaemic animals that had environmental enrichment in their cages had shorter escape latencies and more platform crossings, indicating improved spatial memory (Wang et al. 2016).

1.5.3 Mouse strains

There are a number of mouse strains used in basic research, and the genetic variations between them can result in differing success of surgery to reduce CBF. C57Bl/6J are frequently used in models of VCI, as they have poor posterior communicating arteries and the majority of them have an incomplete circle of Willis, so their collateral blood supply is reduced (McColl et al. 2004). When compared to Sv129 mice, following permanent MCAO, C57Bl/6J mice have been found to have larger lesions (Doyle et al. 2012; Maeda et al. 1999). The present studies used C57Bl/6J mice for BCAS and MCAO surgeries. As well as differences in the cerebral vascular architecture between strains, the weight and age of the animals will influence the outcome of the surgery, as older and heavier animals tend to have more fat around vessels (Hata et al. 1998; Spratt et al. 2006; Fluri 2015).

1.6 Models of β-amyloid pathology

As previously discussed, there is a large body of evidence indicating that β-amyloid pathology and vascular pathology interact and exacerbate each other. Advancements in understanding this interaction have largely resulted from the use of transgenic mouse models that mimic aspects of Alzheimer's disease.

Numerous transgenic mouse lines have been generated to express elements of Alzheimer's pathology, although none of them exhibit all of the pathological features of the disease. The most widely used types of Alzheimer mouse models are ones that express mutated versions of human amyloid precursor protein (APP), which were identified in patients with familial forms of Alzheimer's disease. The different APP mutations lead to variations in the resulting pathology. One of the first transgenic lines developed is the PDAPP mice, which overexpress APP harbouring the Indiana mutation V717F, leading to early cognitive impairment and synaptic depression (Games et al. 1995; Larson et al. 1999). The Swedish double mutation (K670N/M671L) is the most common mutation in APP transgenic mouse lines, which increases β-amyloid production by changing the β-secretase cleavage site (Sasaguri et al. 2017). This mutation can be expressed alone in some APP models, such as Tg2576 (Hsiao et al. 1996), whilst others combine it with another mutation. J20 mice express the Swedish double mutation and the Indiana mutation (Mucke et al. 2000) and Thy1-hAPP$^{Lond/Swe}$ combines the Swedish mutation with the London mutation (Rockenstein et al. 2001). The human mutated APP mouse model used for the studies in this thesis expressed the Swedish, Dutch (E22Q) and Iowa (D23N) mutations (TgSwDI) (Davis et al. 2004). Some transgenic mouse lines also include mutations in presenilin-1 (PSEN 1), a subunit of γ-secretase, an enzyme complex that processes APP into β-amyloid. These transgenic lines include APP-PS1,

which harbours the Swedish mutations plus PSEN1 L166P (Radde et al. 2006); and PS/APP, which harbours Swedish APP mutation and PSEN1 M146L (A>C) (Holcomb et al. 1998). Whilst PS/APP induces early (3 months old) cognitive decline, with delayed β-amyloid deposition and gliosis (Gordon et al. 2002); APP-PS1 has very early β-amyloid deposition and gliosis (1 month old), with delayed cognitive decline (Radde et al. 2006; Bittner et al. 2012).

Research described in the present thesis used TgSwDI mice. The Dutch and Iowa mutations causes CAA in humans, therefore, expression of these in mice results in vascular β-amyloid accumulation (Davis et al. 2004). TgSwDI tend to have diffuse β-amyloid deposition in the parenchyma with some more compact aggregation around the vessels (Davis et al. 2004; Xu et al. 2007; Duncombe et al. 2017). The TgSwDIAPP transgene is under the control of the thymocyte differentiation antigen 1 (Thy-1) promoter, which drives neuron-specific expression. The benefits of this type of promoter are that it does not switch on expression until around postnatal day 7, avoiding development complications (Hall & Roberson 2012). Moreover, the expression of the transgene is around the level of endogenous mouse APP (Davis et al. 2004). Many studies in the field have used over-expression APP mouse models with transgenes controlled by the prion protein (PrP) promoter, such as Tg2576. The PrP promoter causes a 15-fold human APP expression level increase compared to the endogenous level, and induces this expression in both neurons and glia, culminating in severe pathological changes that may not be relevant to the human disease (Hall & Roberson 2012).

TgSwDI is an appropriate mouse model to use to investigate changes related to CVD, as it develops β-amyloid deposition in the microvasculature. Previous work conducted by our lab demonstrated that chronic cerebral hypoperfusion, induced by BCAS surgery,

resulted in an increase in soluble and insoluble $A\beta_{40}$ pools at 1 month and 3 months, respectively (Salvadores et al. 2017). This study also found an increase in the burden of β-amyloid in the microvasculature after 3 months of hypoperfusion. To date, there is no evidence indicating whether focal ischaemia induces an increase in β-amyloid burden in this model. Moreover, it is unknown whether synaptic loss occurs in this model. There is evidence that homozygous TgSwDI have memory impairment starting at 3 months of age (Xu et al. 2007), however, it remains to be seen whether this is the result of synaptic degeneration.

1.7 Synaptic changes in Vascular Cognitive Impairment and Alzheimer's disease

1.7.1 Normal synaptic structure and function

Synapses are neurochemically complex structures that facilitate the transfer of information between neurons within networks. A synapse consists of a presynaptic terminal from one neuron apposing with a postsynaptic terminal on a dendrite from another neuron (see Figure 1.5). These structures are supported by a cytoskeleton that is predominately made of filamentous actin (F-actin). The gap between the pre- and postsynaptic terminals is ~20nm wide and is known as the synaptic cleft (Stewart et al. 2013). In chemical synapses, an action potential arriving at the presynaptic terminal stimulates the release of neurotransmitter from synaptic vesicles into the synaptic cleft, which diffuses to the postsynaptic terminal and binds to receptors, which stimulates the opening of ion channels for the next neuron to become activated.

Presynaptic terminals contain synaptic vesicles, which are packed full of neurotransmitter. The majority of CNS presynaptic terminals have an active zone (AZ) where vesicles fuse

with the presynaptic membrane and release neurotransmitter into the synaptic cleft (Landis et al. 1988). This region is rich with proteins specialised for facilitating vesicle docking, priming and fusing with the presynaptic membrane (Dresbach et al. 2001; Gundelfinger & Dieck 2000). Synaptic vesicles exist and move between different pools within the presynaptic terminal, mediated by the actin cytoskeleton and Ca^{2+}-dependent protein-protein interactions (Sankaranarayanan & Ryan 2000; Doussau & Augustine 2000; Ashery et al. 2014). At the presynaptic terminals, vesicles detach from the actin cytoskeleton and become docked at the AZ where they are then primed ready for fusion. Synapsins are a key family of presynaptic proteins that help cluster vesicles in the presynaptic terminal, whilst the SNARE family are essential for vesicle priming and fusion (Ashery et al. 2014; Söllner et al. 1993; Ferreira et al. 2000). Priming refers to the process of tethering the vesicles to the presynaptic membranes. The SNARE protein, synaptobrevin, is expressed on the surface of the vesicles, whilst other SNAREs, syntaxin and SNAP-25, are expressed on the presynaptic membrane, and interact with another key protein called Munc18 (de Wit et al. 2009; Sinha et al. 2011). The vesicular and presynaptic membranes SNARE proteins become tightly interwoven in a complex, pulling the vesicle to the presynaptic membrane and merging the membranes, priming the vesicle for fusion (Baumert et al. 1989; Hanson et al. 1997; Lin & Scheller 1997; Ashery et al. 2014). When an action potential arrives at the nerve terminal and the presynaptic membrane becomes depolarised, presynaptic voltage-gated calcium channels open enabling an influx of Ca^{2+} ions (Barnett & Larkman 2007; Catterall 2011; Mahapatra et al. 2012). The increase in presynaptic Ca^{2+} levels activates vesicular fusion, as another vesicular protein, synaptotagmin, joins the complex and the vesicle is opened into the synaptic cleft, and enabling the neurotransmitter to diffuse out and across to the postsynaptic terminal

(Ashery et al. 2014). Synaptic vesicles are recycling by clathrin-mediated endocytosis, to maintain the size of the presynaptic membrane (Ashery et al. 2014).

The released neurotransmitter diffuses across the synaptic cleft and binds to receptors on the postsynaptic membrane. This in turn causes either depolarisation or hyperpolarisation of the postsynaptic membrane, depending on the type of neurotransmitter, leading to excitatory (e.g. glutamate, epinephrine, acetylcholine) or inhibitory (e.g. GABA, norepinephrine) transmission, respectively. Excitatory postsynaptic terminals have a postsynaptic density (PSD), which is a ~30-40nm thick, protein-rich structure where various neurotransmitter receptors, transmembrane proteins, scaffold proteins, regulatory enzymes and signalling proteins. The complexes present in the PSD are specialised for signal transduction. Moreover, these proteins are modifiable by phosphorylation, local translation, ubiquidation, degradation and subcellular redistribution, enabling synaptic strengthening and weakening according the activity of the synapse (reviewed by Verpelli et al. 2013) .

The majority of excitatory synapses are glutamatergic synapses. Ionotrophic receptors for glutamate, NMDA-, AMPA- and kainate receptors, cluster within the PSD. An important protein for PSD function is postsynaptic density-95 (PSD95), which has roles in organising signal complexes, such as linking NMDA-receptor subunits to intracellular signalling proteins (Bresler 2004). PSD95 (also known as synapse-associated-protein-90, SAP90) comes from a larger family of membrane-associated guanylate kinases (MAGUKs), which also includes PSD93/chapsyn-110, SAP107 and SAP97 (Elias & Nicoll 2007; Sheng & Sala 2001). When glutamate binds to these receptors on the postsynaptic membrane, it causes the opening of cation channels and enabling the influx of calcium and sodium ions,

resulting in a wave of depolarisation and, if the threshold is reached, continuation of an action potential onto the next neuron (Michael-Titus et al. 2010; Kusano et al. 1975). In addition, increased intracellular calcium levels can activate enzymes within the PSD and modify intracellular signalling. An example of this is the tethering of neuronal nitric oxide synthase (nNOS) to NMDA-receptors via PSD95, which can then be more easily activated by the influx of Ca^{2+} ions, resulting in increased nitric oxide production; which has roles in neuronal signalling and excitotoxicity (Lai et al. 2014).

Once glutamate has been released from the presynaptic terminal and activated the postsynaptic receptors, it is important that the neurotransmitter is 'mopped-up' to prevent excessive cation influxes into the postsynaptic terminal. Astrocytic processes that closely appose the synaptic terminals in the 'tripartite synapse' have a key role here, as they take up glutamate with excitatory amino acid transports (EAATs) (Shigeri et al. 2004; Tzingounis & Wadiche 2007). When inside the astrocytes, glutamate is converted to non-signalling glutamine with glutamine synthetase, which is then transported to the presynaptic terminal where it is converted back to glutamate (Hertz & Zielke 2004). Vesicular glutamate transports (VGLUTs) are a family of proteins that package glutamate into synaptic vesicles in the presynaptic terminals, and exist in three isoforms (VGLUT1-3) (Montana 2004).

Historically, synapses are classified by the type of neurotransmitter they release, such as glutamatergic, GABAergic, dopaminergic, serotonergic, cholinergic and adrenergic. Glutamate is the main excitatory neurotransmitter, whilst GABA is the main inhibitory neurotransmitter. Proteomic studies in rodents have revealed that more than 3000 proteins are expressed in the synaptic terminals, with roles in scaffolding, vesicular

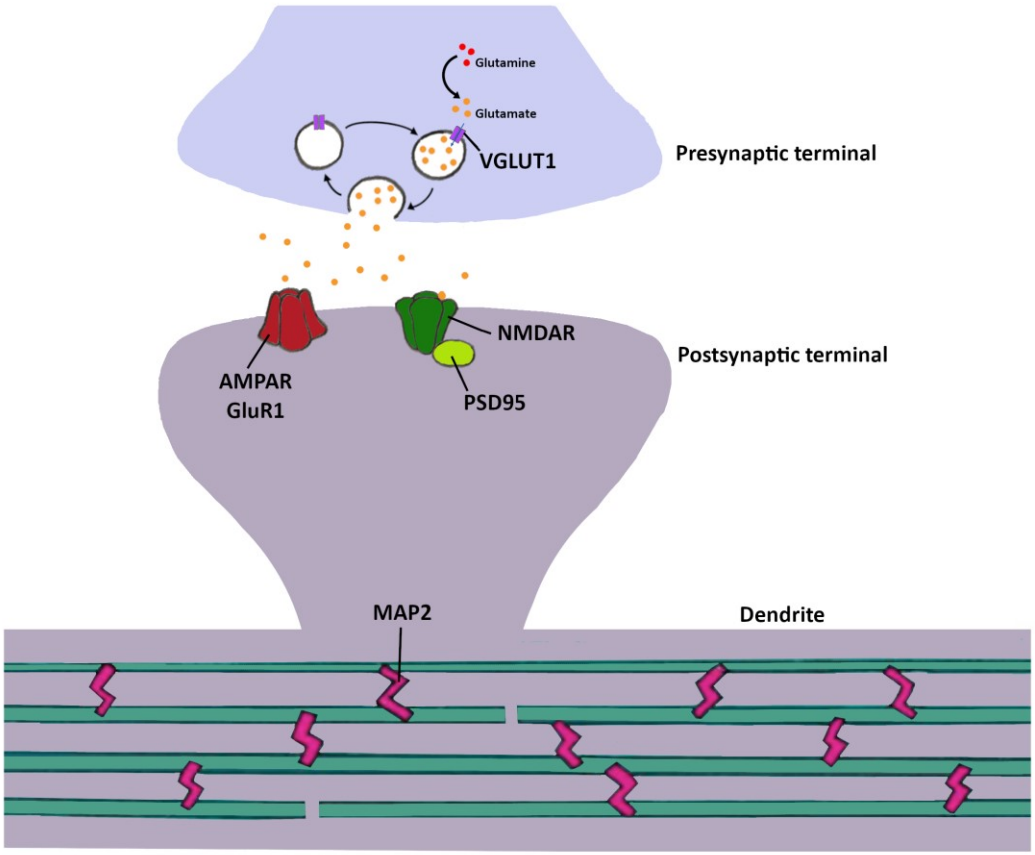

Figure 1.5 Schematic of glutamatergic synapse. VGLUT1 is a presynaptic protein that transports glutamate into synaptic vesicles. Glutamate binds to AMPA- and NMDA-receptors

transporters, adhesion proteins and receptor subunits (Filiou et al. 2010; Schrimpf et al. 2005; O'Rourke et al. 2013). Furthermore, there is now a greater understanding about the breadth of synaptic proteomic "intra-type" diversity within classes of synapses, and how it affects aspects of synaptic function, including strength, kinetics and plasticity (O'Rourke et al. 2013). Molecular diversity will partly result from multiple isoforms of synaptic proteins, which may be expressed in different parts of the brain or in different cell types (Gong et al. 2003; Lein et al. 2007). For example, this type of diversity occurs the three isoforms of VGLUTs (VGLUT1-3). These isoforms vary in their expression levels in different brain regions, and have distinct protein-protein interactions that affect the functionality of the

synapses (Vigneault et al. 2015; Zhang et al. 2018; De Gois et al. 2006). Another example of this is the diversity within the subunits for AMPA-receptors (GluR's) and NMDA-receptors (GluN's), as the assembly of subunits vary for different brain regions and cell types (Isaac et al. 2007; Cull-Candy & Leszkiewicz 2004).

Synaptic transmission is critical for cognitive function; and dysfunction or degeneration of synapses is a primary feature in many brain diseases, including forms of dementia (Clare et al. 2011; Bayés et al. 2011). The concept that synaptic degeneration underpins cognitive decline in dementia was first proposed by Santiago Ramon y Cajal:

"dementia could result when synapses between neurons are weakened as a result of more or less pathological condition, that is, when processes atrophy and no longer form contacts, when cortical mnemonic or association areas suffer partial disorganization" (Cajal 1928).

1.7.2 Synaptic loss in human post-mortem studies

There is considerable evidence that synapse loss occurs at an early stage of the pathological progression to dementia. This is based on the demonstration that synapse loss predates neuronal loss in post mortem brain tissue from elderly individuals, MCI and AD patients (Davies et al. 1987; Masliah et al. 1989; Terry et al. 1991; Scheff et al. 2006; DeKosky & Scheff 1990). In Alzheimer's post-mortem brain tissue, there is a significant reduction in synaptic terminals in cortical layer V whilst the neuron density remains unchanged compared to control samples (Davies et al. 1987). Additional studies have shown that in Alzheimer's brain tissue, the densities of presynaptic terminals are reduced in specific brain regions, including the parietal, temporal, midfrontal cortices (Masliah et al. 1989; Terry et al. 1991) and the hippocampus; whilst in the densities

remained unchanged in other brain regions (Perdahl et al. 1984). These findings indicate that there is a selective vulnerability of synapses in specific brain regions. Moreover, they demonstrate that the synaptic changes are not homologous between different types of dementia, as the reduction in presynaptic terminals the hippocampus found in AD brains was not present in the samples from multi-infarct dementia patients (Perdahl et al. 1984). Another important finding in these studies was that synapse loss correlated with cognitive decline, more strongly than any other pathological feature of AD (DeKosky & Scheff 1990; Scheff et al. 2006; Terry et al. 1991). Furthermore, they found that synapse loss occurs in MCI and proposed that progressive synapse loss converts a normal cognitive state to MCI, and MCI to AD (Scheff et al. 2006). The methods used for detecting synapses in these publications were immunohistochemistry of abundant presynaptic protein synaptophysin (Terry et al. 1991; Masliah et al. 1991), and electron microscopy (Scheff et al. 2006; DeKosky & Scheff 1990), which do not distinguish between different types of synapses.

Synapses have diverse neurochemical composition depending on the type of neurotransmitter they release, which can elicit selective vulnerability in pathological conditions. In AD, the networks most susceptible to damage include glutamatergic and cholinergic transmission (Bell & Claudio Cuello 2006). The glutamatergic presynaptic proteins vesicular glutamate transport (VGLUT) -1 and -2 were shown to be reduced in protein levels and terminal density in the prefrontal cortex of Alzheimer's patients (Kashani et al. 2008). This study also investigated the levels of these proteins in tissue from patients with MCI, which showed a smaller reduction in VGLUT2 levels and no change in VGLUT1 levels compared to controls; reinforcing the theory that mild cognitive impairment is a precursor state to AD, and progressive synapse loss is part of the

pathological process. Importantly, this paper indicates that VGLUT1 protein levels correlate with the clinical dementia rating score from the individual patients, highlighting that VGLUT1 in the prefrontal cortex is crucial for cognitive function. Postsynaptic density 95 (PSD95) is an abundant scaffolding protein in excitatory postsynaptic densities. There is conflicting evidence as to whether there are changes in PSD95 in AD, as reviewed in (Savioz et al. 2014). Taken together, there is substantive evidence that glutamatergic presynaptic terminals and proteins are reduced in AD, whilst conflicting evidence for postsynaptic changes may indicate resilience in these structures.

Less attention has been given to investigating synaptic changes in VCI and VaD (Clare et al. 2010). Synaptic protein levels were analysed in tissue from the superior temporal gyrus from vascular dementia patients, as infarcts have been shown to be prevalent in this region (Sinclair et al. 2015). The study found that levels of the presynaptic protein SNAP-25 were significantly reduced, whereas synaptophysin levels were unchanged. Conversely, the postsynaptic protein drebrin increased, whilst PSD95 was unchanged. This is an interesting result, as it indicates that vascular pathology may stimulate different mechanisms for pre- and postsynaptic structures, and the authors hypothesise that the increase in drebrin could be involved in a compensatory response following ischaemia. Reductions in levels of the glutamatergic presynaptic protein VGLUT1 have been found in the in the frontal and temporal cortices of VaD, AD, and mixed dementia brains (Kirvell et al. 2010). Interestingly, the protein levels of VGLUT1 correlated with the pre-mortem mental health and memory scores from these patients, further indicating that glutamatergic presynaptic loss results in cognitive decline. Overall, there is evidence that in VCI there is some selective vulnerability of some presynaptic proteins, whilst postsynaptic proteins appear to be more resilient.

Studies using post-mortem human brain tissue have enabled end-stage analysis of synapse density, however, it remains a challenge to investigate progressive synapses changes and the underlying mechanisms. Recently technological advancements have been made enabling synaptic density to be measured in the living human brain (Finnema et al. 2016), which could be applied to understand synaptic changes during the development of VCI and dementia. The use of rodent models, however, has enabled huge advancements to be made in understanding the mechanisms underlying synapse dysfunction and loss.

1.7.3 Synapse changes in models of Alzheimer's pathology

The amyloid cascade hypothesis of AD was proposed by John Hardy and Gerald Higgins in 1992, stating that β-amyloid is the causative agent of AD, leading to downstream NFTs, synaptic and neurodegeneration, vascular degeneration and dementia (Hardy & Higgins 1992). Previous to this, β-amyloid had been discovered as the main component of plaques in the human AD brain (Glenner & Wong 1984), which was later identified as a product of amyloid precursor protein (APP), the gene for which is localised on chromosome 21 (Tanzi et al. 1987). The link between β-amyloid and AD was further solidified by the discovery that mutations in the APP gene, or in genes encoding the enzymes that process APP to β-amyloid, were present in patients with early-onset familial AD. Furthermore, trisomy of chromosome 21 causes Down's syndrome and is associated with early-onset AD (Tanzi et al. 1987; St. George-Hyslop et al. 1987). In transgenic mouse lines expressing human mutated APP, there was evidence reduced densities of hippocampal dendrites and dendritic spines with age, and coinciding with an increase in β-amyloid burden (Lanz et al. 2003; Moolman et al. 2004). Furthermore, dendrites and axons become swollen within an area of ~15μm around fibrillar amyloid

plaques, indicating that β-amyloid exerts neurotoxicity only within nearby neurons (Tsai et al. 2004). However, the hypothesis that β-amyloid plaques drive synapse degeneration was further scrutinised, as studies failed to find a relationship between synaptic loss and β-amyloid plaque burden (Mucke et al. 2000).

The amyloid cascade hypothesis was then refined, as later research has indicated that soluble oligomers of β-amyloid is a driver for synaptic and neurodegeneration in Alzheimer's disease (Selkoe 2002). Seminal work conducted by Dominic Walsh showed that cerebral microinjections of soluble human β-amyloid oligomers and monomers into rats resulted in inhibited hippocampal long-term potentiation (Walsh et al. 2002). It was later shown by Koffie et al. that amyloid plaques have a 'halo' of oligomeric β-amyloid around dense core plaques, which is associated with synaptic degeneration immediately around the plaque (Koffie et al. 2009). They then went on to discover a similar finding in human post-mortem tissue (Koffie et al. 2012). These studies indicate that oligomeric β-amyloid is the main synaptotoxic form of β-amyloid, but it may be seeded from around dense plaques.

It is unclear by which mechanisms β-amyloid can induce synapse dysfunction and degeneration, however, there is evidence that it can inferere with a number of processes affecting both pre- and post-synaptic terminals. An increase of β-amyloid may result from clustering of BACE1 enzyme at presynaptic terminals, as observed in J20 mice (Ye et al. 2017). β-amyloid can disrupt presynaptic processes, such as axonal transport, synaptic vesicle cycling and neurotransmitter release (Chen et al. 2019). There is evidence that β-amyloid oligomers can induce calcium ion influxes into presynaptic terminals by co-localising with voltage gated calcium channels (VGCC), which can impair axonal transport (Gan & Silverman 2015). Furthermore, oligomeric β-amyloid-induced

presynaptic calcium influxes can promote release of glutamate into the synaptic cleft and enhance postsynaptic activity (Brito-Moreira et al. 2011). Another proposed mechanism came from a study by Fogel and colleagues, which indicated that $A\beta_{40}$ peptides can bind to APP dimers in the presynaptic membrane, stimulating intracellular signalling through APP/G_o-protein complex to cause calcium influxes and neurotransmitter release (Fogel et al. 2014). There is evidence that oligomeric β-amyloid can bind to distal axons and induce local synthesis of a number of proteins including transcription factor ATF4, which was shown to have roles in neurodegeneration (Baleriola et al. 2014).

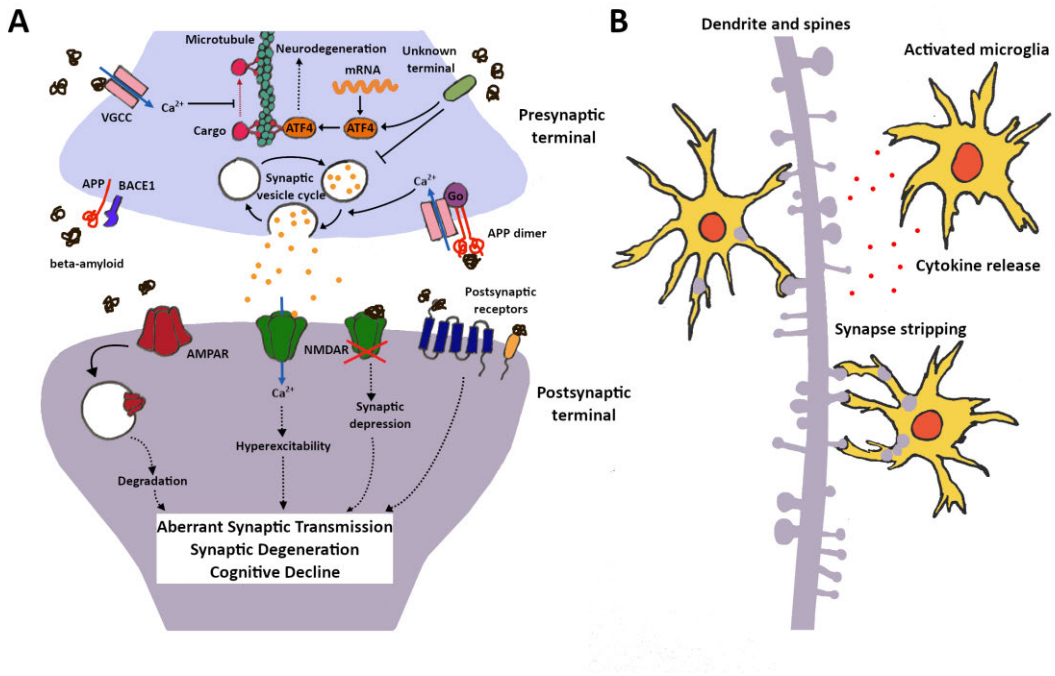

Figure 1.6 Mechanisms of β-amyloid – induced synaptic dysfunction and loss.
(A) Underlying mechanisms of synaptic dysfunction and degeneration by β-amyloid binding to synaptic receptors on presynaptic and postsynaptic terminals. (B) β-amyloid - activated microglia inducing synaptic dysfunction by releasing cytokines, and physically stripping and engulfing synaptic terminals. Based on figures from Chen et al. 2019; Rajendran & Paolicelli 2018.

There also is a growing body of evidence indicating that β-amyloid can cause dysfunction through mechanisms affecting the postsynaptic terminals. Publications by Shankar and colleagues have revealed that β-amyloid can induce postsynaptic dysfunction through NMDA-receptors. The application of naturally secreted β-amyloid dimers and trimers to rat organotypic slices lead to progressive loss of dendritic spines, and reduced the number and strength of active excitatory synapses in the hippocampus (Shankar et al. 2007). They found that β-amyloid oligomers diminished calcium influxes through NMDA-receptors, and later showed that they inhibited glutamate uptake, culminating in long-term depression (LTD) (Li et al. 2009). In another study they found that β-amyloid

oligomers extracted from human AD cortices enhanced LTD and caused spine loss in rat hippocampal slices, as well as resulting in learning deficits when injected into the lateral ventricles of normal rats (Shankar et al. 2008). Moreover, when β-amyloid peptides were administered with antibodies against them this prevented the activity deficits. There is evidence that increased levels of β-amyloid can lead to a removal of AMPA-receptors from postsynaptic terminals, particularly receptors containing GluR3 subunits, contributing to synaptic depression (Guntupalli et al. 2016; Chang et al. 2006; Hsieh et al. 2006; Reinders et al. 2016). A number of additional mechanisms have been proposed whereby β-amyloid induces synapse dysfunction by binding to other receptors on postsynaptic terminals, as reviewed by (Chen et al. 2019). Selective neuronal hyperactivity and seizures has emerged as an early pathological process in AD (Selkoe 2018; Zott et al. 2019; Palop & Mucke 2016; Busche et al. 2012). A recent study has found compelling evidence that β-amyloid induces hyperactivation by blocking glutamate reuptake, leading to synapse dysfunction and neurodegeneration (Selkoe 2018; Zott et al. 2019).

β-amyloid may also act indirectly to drive synaptic dysfunction, through activation of the immune system. As previously described, microglia and astrocytes are very sensitive to changes in the brain environment and stimulated by the build-up of β-amyloid, and activated glia are observed clustered around amyloid plaques in AD post-mortem tissue (Serrano-Pozo et al. 2011). There is evidence that pro-inflammatory cytokines released by neuroinflammatory cells, such as TNFα and IL-1β, can elicit excitotoxic effects on synapses (Wang et al. 2015). More recently it has been proposed that in neurodegenerative diseases microglia physically strip away synaptic terminals. Hong and colleagues found evidence that β-amyloid-activated microglia colocalise with synaptic

terminals which appear to be engulfed by the cells (Hong et al. 2016). Taken together, the evidence implies that β-amyloid oligomers drive can directly or indirectly cause synapse dysfunction and loss.

1.7.4 Synaptic changes in models of VCI

1.7.4.1 Global cerebral blood flow reduction and synapse changes

Compared to the vast body of literature that has focused on synaptic dysfunction and Alzheimer's pathology, there is limited evidence regarding synaptic changes in models of VCI. Of these few studies, the majority of them have investigated the effect of global ischaemia, with permanent BCCAO in rats. This model results in gradual decrease of presynaptic protein synaptophysin and dendritic protein MAP2 in the hippocampus, over 20 weeks after surgery (Liu et al. 2005). Reduced levels for both of these protein levels correlated with memory deficits probed by the Morris Water Maze, indicating that ischaemia-induced degeneration of dendrites and presynaptic terminals in the hippocampus directly relates to cognitive decline. There is evidence that dendrites and dendritic spines in layer 3 of the medial prefrontal cortex have selective vulnerability to ischaemia-induced degeneration as well (Jia et al. 2012). A similar finding was made in another study investigating the effect of transient global ischaemia, using a model of bilateral common carotid artery ligation (BCAL) on YFP mice. The researchers found that induction of BCAL caused blebbing of the dendrites and dendritic spines, however, when reperfusion was induced at 20 minutes or 1 hour after ligation, considerable restoration followed over the next three hours. For mice ligated for 3 or 6 hours, the dendrites remained blebbed and irreversibly damaged (Zhu et al. 2017).

Glutamatergic synapses are particularly vulnerable to ischaemia. Excessive glutamate levels are released from metabolically challenged neurons (Dawson et al. 2001; Drejer et al. 1985), whilst glutamate clearance systems are impaired (Rothstein et al. 1993); leading to glutamate spillover and over-activation of AMPA- and NMDA- receptors. This causes disruption to calcium homeostasis, which can initiate many pathological cascades, such as the breakdown of synaptic proteins from calpain activation (Lai et al. 2014). Proteins involved in excitatory transmission were found to more vulnerable than those with inhibitory functions; vesicular glutamate transporters, VGLUT1 and 3, were reduced in the hippocampus 3 days after BCCAO in rats, whilst their GABAergic counterpart, VGAT, remained unchanged (Cao et al. 2016). Whilst glutamatergic transmission has acute vulnerability, delayed deficits in GABAergic may contribute to excitotoxic degeneration (Schwartz-Bloom & Sah 2001). A recent study investigated the protein changes in synaptosome fractions from the cortex of BCCAO rats 7 weeks after surgery, and found that proteins involved in glutamatergic and GABAergic transmission were reduced (Völgyi et al. 2017). This is supported by the observation that a $GABA_B$ receptor agonist, baclofen, ameliorated cognitive impairment after BCCAO in rats (Li et al. 2014; Lu et al. 2016; Luo et al. 2016).

Global ischaemia also impacts post-synaptic terminals, largely as a result of glutamate spillover and overactivation of postsynaptic glutamate receptors. A study investigating the protein levels of different AMPAR and NMDAR subunits demonstrated that some subunits are more vulnerable than others in the CA1 in the sub-acute stage following transient global ischaemia (Han et al. 2016). In particular, AMPAR subunit GluR2 levels were decreased, while GluR1 levels remained unchanged; and while NMDAR subunits NR2A and NR2B were both reduced, the effect was more pronounced in the case of

NR2A. Interestingly, the researchers did not find any changes in AMPAR or NMDAR subunits in the CA3 compared to sham controls, indicating that this region is not susceptible to ischaemic damage, unlike the neighbouring CA1. Their interpretation was that the CA3 has greater inhibitory innervation than the CA1 (Yao et al., 1996), therefore it has greater resistance to excitotoxcity; there are higher levels of AMPAR and NMDAR subunits in the CA3 compared to the CA1 under normal conditions (Coultrap et al. 2005; Butler et al. 2010) and CA3 express hamartin an endogenous neuroprotective factor, which protect against ischaemic injury (Papadakis et al. 2013).

AMPAR and NMDAR are crucial for synaptic morphology and plasticity, thus changes in their expression will impact synapse function. A recent study showed that the density of GluR2-positive termials was reduced in the CA1 at 1-24 weeks post-BCCAO in rats, whilst NR1 density increased (Wang et al. 2016). They theorised that this was a result of converting functional AMPAR-rich postsynaptic terminals, into AMPAR-silent non-functional synapses, linking this to the fact that their rats showed evidence of impaired spatial and working memory. Other research indicates that the mechanism underlining this change in synapse functionality is due to internalization of GluR2 AMPA-receptor subunits during ischaemic conditions (Liu et al. 2006). In another study, however, BCCAO resulted in reductions of hippocampal PSD95 and NMDAR subunit NR2B protein levels, LTP deficits and spatial memory impairment, as found 4 weeks after surgery (Yang et al. 2017). Conversely, in a model using unilateral common carotid artery occlusion (UCCAO), PSD95 protein levels was slightly increased in the cortex at 2.5 months after surgery (Zhao et al. 2014). UCCAO surgery induces an acute CBF reduction, which is statistically indistinct at day 15 from the before-surgery recording (Guo et al. 2011). This model, therefore, has modest blood flow changes compared to BCCAO surgery, and instead of

inducing postsynaptic degeneration it may stimulate compensatory mechanisms resulting in a PSD95 increase.

Taken together, these papers indicate that dendritic, and glutamatergic pre- and postsynaptic loss occurs at acute and long-term stages after global ischaemia. To the best of my knowledge, to date there are no studies that have investigated whether modest, sustained, global hypoperfusion induced by carotid artery stenosis results in synaptic changes.

1.7.4.2 Focal ischaemia and synapse changes

A number of publications have investigated predominantly acute impact of focal ischaemia on synapses. Publications by Tim Murphy and colleagues have demonstrated, with in vivo multiphoton imaging through cranial windows, that cortical photothrombosis results in focal blebbing of dendrites and dendritic spines, which postsynaptic densities project from (Brown et al. 2007; Zhang et al. 2005; Zhang & Murphy 2007; Li & Murphy 2008; Enright et al. 2007). Their studies have shown that dendrites and spines are rapidly disrupted near the occlusion site, leading to a reduction in the activity of the forelimb response of the somatosensory cortex. An interesting finding was that if the clots broke up and reperfusion occurred between 20-50 minutes after activation, there is partial restoration of the dendrites and spines, whilst prolonged ischaemia resulted in irreversible damage (Zhang et al. 2005). In a focal ischaemic lesion, there is a lesion core of irreversible neuron death, whilst the tissue immediately surrounding the lesion is a region of delayed damage, known as the penumbra or peri-lesion. An additional study from Tim Murphy's group demonstrated that the ~50-100 µm surrounding the core had delayed dendrite and spine loss, which gradually occurred over 5-6 hours post-activation (Zhang & Murphy 2007). They further investigated the effect of

vessel occlusion on local dendritic structure by applying transient MCAO to the YFP mice. In this study they showed that 60 minutes of MCAO resulted in a lesion core of irreversible dendritic damage, however, the penumbra region experienced some recovery, 3 hours after reperfusion (Li & Murphy 2008). These studies demonstrated that dendrites and spines are vulnerable to focal ischaemia, but undergo some recovery if the blockage is removed or within the peri-lesion at the acute stages following ischaemia.

To date there have been few studies that have investigated the sub-acute and chronic stages of focal ischaemia on synapses. A study analysing the protein levels of VGLUT isoforms following transient MCAO in rats showed that VGLUT1 is increased above the control level at day 1 in the striatum and day 3 in the cortex, which then drops below the control level by day 7 (Sánchez-Mendoza et al. 2010). This result indicates that an increase in VGLUT1+ synaptic terminals could be an early response to focal ischaemic damage, with delayed synaptic degeneration occurring at sub-acute and chronic stages. This finding is contradicted by another study which found gradually increasing levels of synaptophysin from 8 days to 30 days in the lesion and peri-lesion cortex using the photothrombotic model in mice (Madinier et al. 2013). The discrepancy between these papers may result from the differences in the model, as others have reported that photothrombosis stimulates synapse reorganisation in the peri-lesional cortex. Among these studies is a recent paper by Stokowska et al, who found a long-term increase of synapsin I+ and VGLUT1+ terminals in the peri-lesional cortex, compared to the contralateral hemisphere, 21 days after photothrombosis (Stokowska et al. 2016). Cooperrider et al. demonstrated that the protein levels of PSD95 and synaptophysin were increased in the peri-lesion, 5 weeks after inducing a small ischaemic lesion in the

motor cortex with ET-1 (Cooperrider et al. 2014). They also found that these protein levels were increased with deep cerebellar stimulation, indicating that electrical activity can stimulate synaptogenesis in the peri-lesion. Furthermore, multiphoton imaging captured the reorganisation of dendrites and blood vessels in the peri-lesion of a photothrombotically-induced lesion (Brown et al. 2007). Overall, these studies demonstrate that whilst focal ischaemia induces synaptic degeneration within the lesion site, it can also stimulate recovery processes that include a delayed increase in synaptic terminal densities in the peri-lesions.

Focal ischaemia can induce neurodegeneration in distal brain regions, connected to the occlusion territory, by secondary neurodegeneration. This is based on evidence from animal models that demonstrated that activity dysfunction and cell damage occurs in brain regions connect to the lesion site, known as diaschisis (Carrera & Tononi 2014). MCAO surgery causes ischaemic lesions to occur within the striatum, which is connected to the substantia nigra, thalamus and cortex (see Figure 1.7), therefore, pathological changes have been identified in these regions in this model. MCAO surgery in rats induced a decrease in synaptic activity in the ipsilateral substantia nigra (Nakanishi et al. 1997). Distal MCAO or Rose Bengal photothrombosis induce ischaemic lesion predominantly in the cortex, therefore, leads to secondary pathological changes in the thalamus (Doyle et al. 2015; Kluge et al. 2018; Jones et al. 2018)and hippocampus (Sopala et al. 2000). Interestingly, there is also evidence of focal ischaemia stimulating recovery processes in diaschisis sites, as it induced a delayed increase in hippocampal synaptophysin levels (Madinier et al. 2013) and activate neurogenesis in the dendate gyrus subgranular zone (Lichtenwalner & Parent 2006). Taken together, these studies

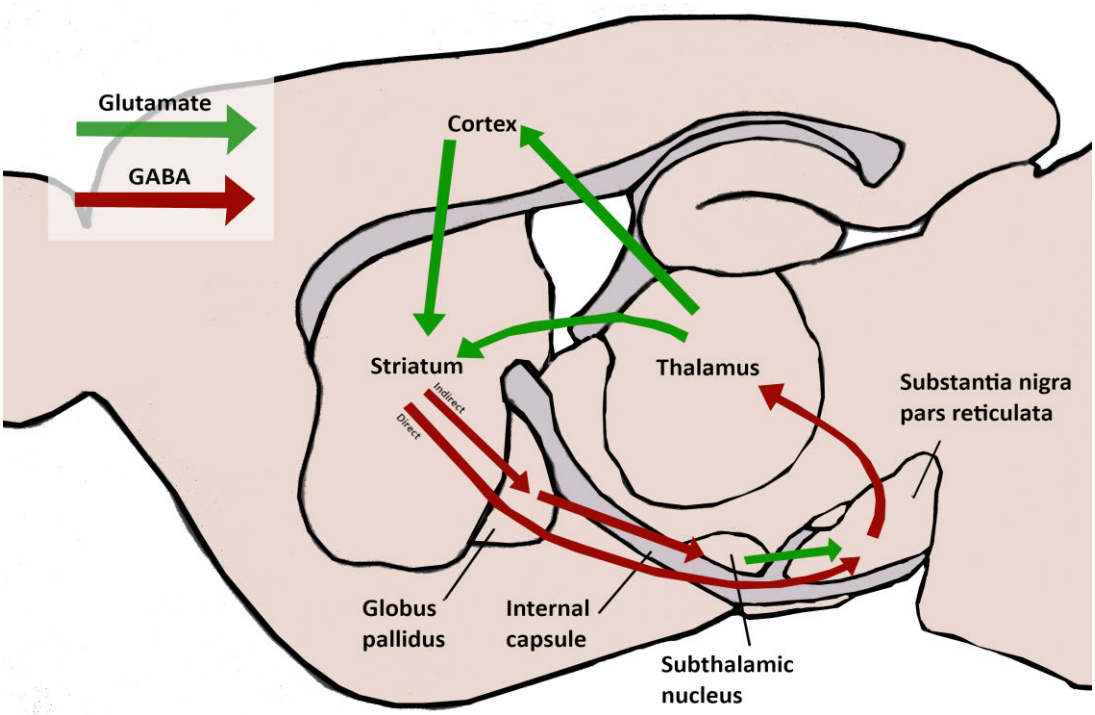

Figure 1.7 Neuronal network connecting the striatum to the internal capsule, substantia nigra pars reticulate and thalamus; regions that are vulnerable to primary and secondary neurodegeneration in rodent MCAO model. The striatum receives glutamatergic projections from the thalamus and cortex. Inhibitory neurons project from the striatum to the substantia nigra pars reticulata (SN_R) in the direct pathway, whilst in the indirect pathway, inhibitory and excitatory projections connect the striatum, globus pallidus (GPe) and subthalamic nucleus (STN) and SN_R (Benarroch 2016). These projections run through the internal capsule white matter tract (Reinius et al. 2015).

demonstrate that focal ischaemia can induce secondary neurodegenerative changes in connected brain regions, as well as stimulating some recovery changes.

Most studies of experimental models of hypoperfusion/ischaemia have not taken into consideration the heterogeneity of the human condition where multiple comorbidities in addition are normally present. There is a gap in our knowledge as to whether multiple comorbidities have an exaggerated impact on synapses. There is evidence that the comorbidities of focal ischaemia and age resulted in significant synapse protein loss in the thalamus, compared to the young mice (Kluge et al. 2018). As previously mentioned,

the Nun study showed that the presence of Alzheimer's pathology and vascular pathology result in worsened functional outcome, compared to patients with only vascular pathology (Snowdon et al. 1997). A recent publication, demonstrated that DH stroke model induced more exacerbated cholinergic degenerated in the cortex of APP-SL transgenic mice (Nguyen et al. 2018). There is also evidence that focal ischaemia in Tg2576 results in larger infarcts than in WT mice (Milner et al. 2014). Moreover, previous work from our group demonstrated that hypoperfusion induced more microinfarcts in TgSwDI mice than in WT mice (Salvadores et al. 2017). These studies imply that comorbidities of hypoperfusion/ischaemia and β-amyloid induce worsened pathology when present together, and remains to be seen whether they exacerbate synaptic degeneration.

1.8 Hypothesis

The over-arching hypothesis of this thesis is the chronic impact of reduced CBF is the degeneration of glutamatergic pre- and post-synaptic terminals in specific brain regions. Second to this, these changes are exacerbated when concurrent β-amyloid pathology is also present. To address this, the impact of different models of CBF reductions, BCAS and MCAO, were studied in WT and TgSwDI mice with the following aims.

1.9 Aims

1. To establish whether chronic cerebral hypoperfusion (induced by BCAS surgery) results in degeneration of dendrites and glutamatergic pre- and postsynaptic terminals, in brain regions that are associated with spatial working memory.

2. To elucidate whether transient focal ischaemia (induced by MCAO surgery) causes long-term focal degeneration of glutamatergic pre- and post-synaptic terminals in the ischaemic territory in WT mice, related to impaired motor function. And whether these changes are exacerbated in TgSwDI mice.

3. To determine whether transient MCAO causes long-term degeneration of glutamatergic pre- and post-synaptic terminals in remote brain regions that connect with the primary lesion site and to elucidate whether these changes are exaggerated in TgSwDI mice.

Chapter 2: Materials and Methods

2.1 Animals

All procedures were authorised under the project licence number 60/4350 held by Prof. Horsburgh, approved by the UK Home Office and the University of Edinburgh's Ethical Review Committee and adhered to regulations specified in the Animals (Scientific Procedures) Act (1986).

All mice used in the studies were male. In the studies of wild-type mice, the strain used was C57BL/6J mice purchased from Charles River. Transgenic mice used were all on a C57Bl/6J background. This strain is appropriate to use for our investigations, as unlike other strains, they mostly have an incomplete circle of Willis and poor collateral supply, which increases the chances of successful surgically induced CBF reductions.

The mice were housed in groups of up to 6, on a 12-hour light/dark cycle, with a constant temperature and free access to food and water. The ages and the 'n' numbers for the mice are stated in the methods section for each results chapter.

2.1.1 TgSwDI mice

TgSwDI mice express human neuronal amyloid precursor protein (APP), harbouring the Swedish (K670N/M671L), Dutch (E22Q) and Iowa (D23N) mutations, under the control of the Thy1.2 promoter (Figure 2.1). The Swedish mutation causes increased burden of $A\beta_{40}$ and $A\beta_{42}$ peptides (Kalaria & Hedera 1996), whereas the Dutch and Iowa mutations lead to increased $A\beta_{40}$ deposition in the vasculature (Levy et al. 1990; Grabowski et al. 2001).

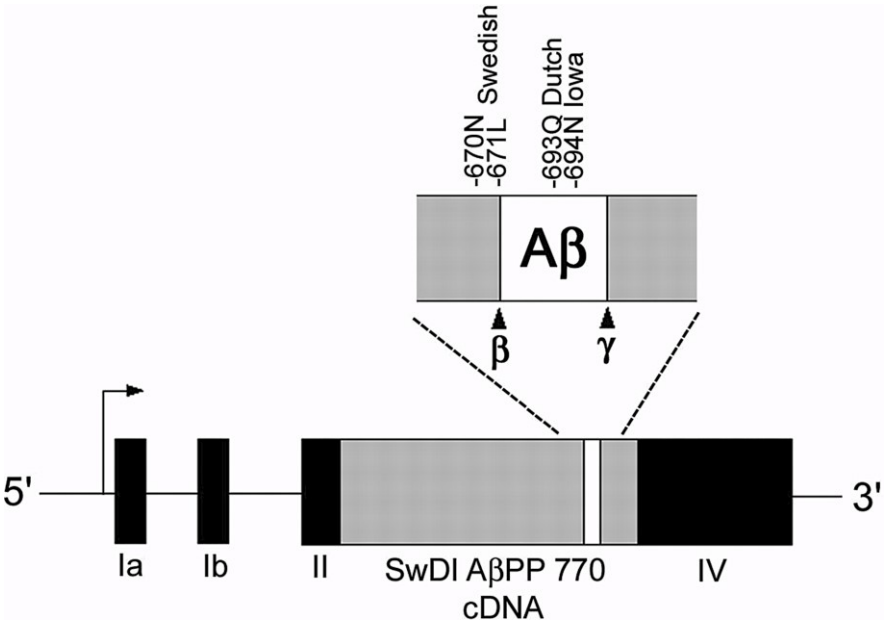

Figure 2.1 Schematic of the TgSwDI mutant human APP construct, expressed by the mice. TgSwDI contains the Swedish (K670N/M671L), Dutch (E693Q) and Iowa (D694N) mutations under the Thy1.2 promoter. Taken from (Davis et al. 2004).

TgSwDI is not an overexpression model, as the expression of human APP is about 50% less than that of the endogenous mouse APP (Davis et al. 2004). Heterozygous TgSwDI transgene causes progressive β-amyloid deposition in the parenchyma and microvasculature, starting at approximately six months of age. The brain regions which exhibit β-amyloid burden in older mice are the thalamus and cortex (Miao et al. 2005).

2.1.2 PSD95:eGFP x TgSwDI

Male homozygous PSD95:eGFP mice on a C57BL/6J background were supplied by our collaborator Prof. Seth Grant, Edinburgh. PSD95 is a stable scaffold protein involved in the assembly of receptors and signalling proteins in the postsynaptic densities (Zhu et al. 2018). This model has enhanced green fluorescent protein (eGFP) fused onto endogenous PSD95 (Figure 2.2). The male homozygous PSD95:eGFP mice were bred in house with

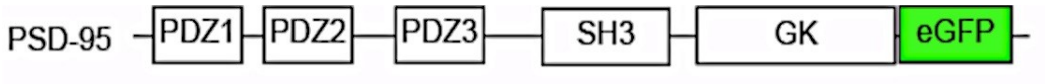

Figure 2.2 Schematic of PSD95:eGFP transgene. Image provided by Noboru Komiyama.

homozygous TgSwDI females on C57BL/6J background, to result in PSD95:eGFP$^{+/-}$ x TgSwDI$^{+/-}$ and PSD95:eGFP$^{+/-}$ x TgSwDI$^{-/-}$ (referred to as WT littermates) offspring.

2.1.3 Arc-Venus

Arc-Venus mice on a C57BL/6J background were also supplied by Prof. Seth Grant. Arc is localised in postsynaptic sites and its mRNA is rapidly transcribed following synaptic activity (Link et al. 1995). Tagging endogenous Arc with Venus fluorescent protein enables the detection of synaptic activity (Fernández et al. 2017).

2.2 Surgery

2.2.1 Bilateral common carotid artery stenosis

Chronic cerebral hypoperfusion was induced surgically by bilateral common carotid artery stenosis (BCAS). This model has been well-characterised by our group (Coltman et al. 2011; Reimer et al. 2011; Kitamura et al. 2017; Holland et al. 2011; McQueen et al. 2014). Mice were anaesthetised initially with 5% isofluorane, then with 1.5% isofluorane during surgery. A midline cervical incision was made and the common carotid arteries were exposed. Microcoils with an internal diameter of 0.18 mm or 0.16mm (Sawane Spring Co. Japan) were permanently fitted onto both common carotid arteries, with a 30 minute interval between application of each microcoil (Figure 2.3). The wound was sutured up and the mice were placed in an incubator (30° C) until fully recovered from the anaesthesia. The same surgical procedure was performed on the sham animals, but without the

application of the microcoils. Following surgery, the weight and general health of the mice were closely monitored. The surgery was performed by Prof. Karen Horsburgh.

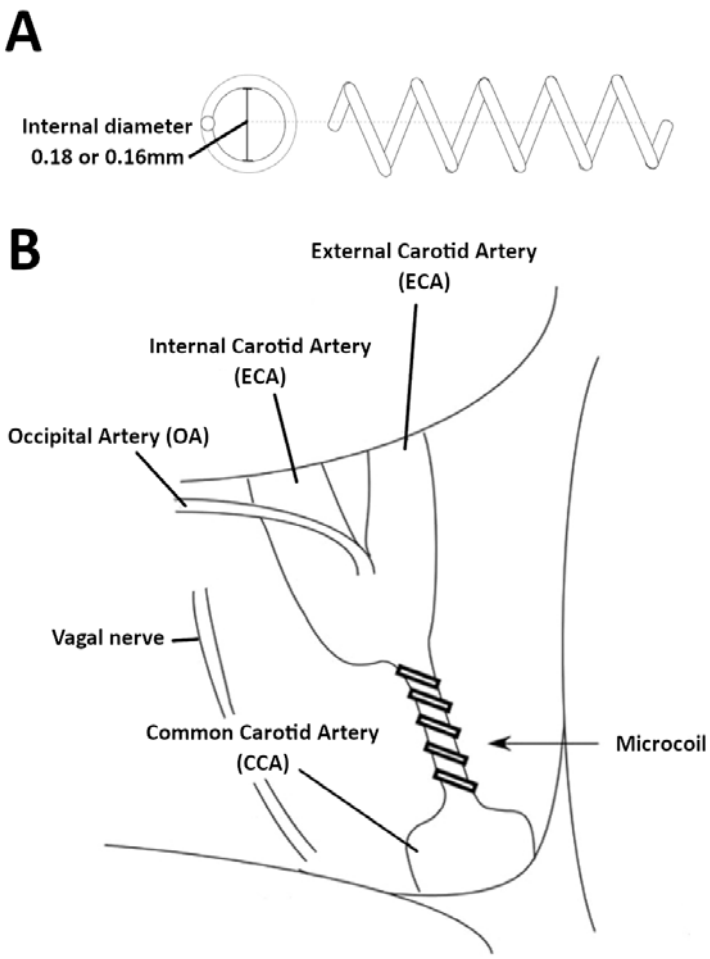

Figure 2.3 Schematic representation of bilateral common carotid artery stenosis (BCAS) surgery used to induce cerebral hypoperfusion. (A) Microcoil schematic with internal diameter of 0.18mm or 0.16mm, for modest or severe hypoperfusion, respectively. (B) Microcoil application onto both common carotid arteries. Adapted from (Shibata et al. 2004).

2.2.2 Middle cerebral artery occlusion

Focal ischaemia was induced by 15 minutes of middle cerebral artery occlusion (MCAO). The mice were anaesthetised, initially with 5% isofluorane, then with 1.5% isofluorane during surgery. A midline cervical incision was made to expose the left common carotid (CCA), external carotid (ECA) and internal carotid (ICA) arteries and their branches. A 6-0 silk suture was tied around the CCA proximal to the bifurcation of the ECA and ICA, then a second suture was tied around the ECA distal to the superior thyroid artery (STA). The STA and occipital artery (OA) was closed by electrocoagulation. A silicone-coated

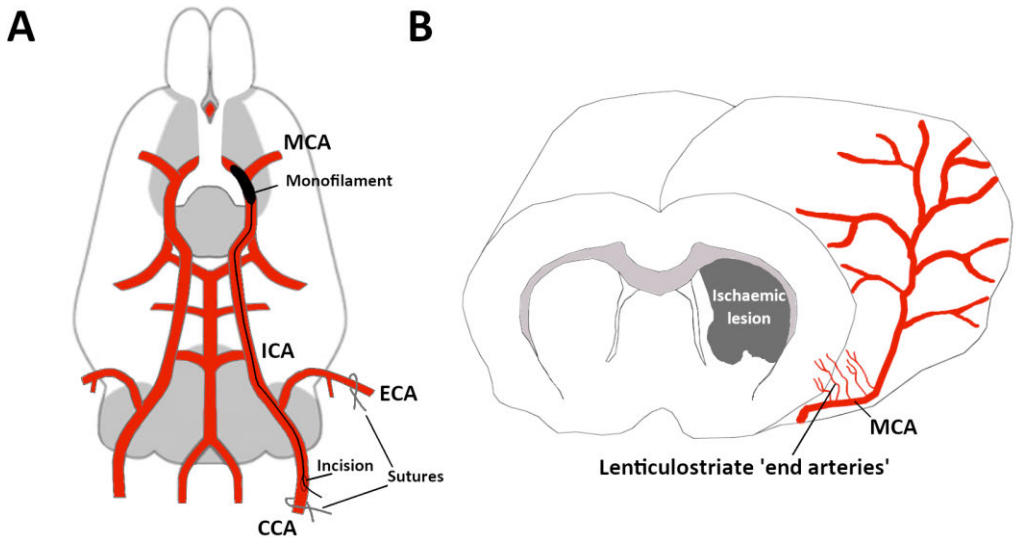

Figure 2.4 Schematic presentation of middle cerebral artery occlusion (MCAO) surgery used to induce focal ischaemia. (A) The common carotid artery (CCA) and external carotid artery (ECA) are permanently ligated with sutures and a monofilament is inserted into an incision in the internal carotid artery (ICA) and advanced to occlude the entrance of the middle cerebral artery (MCA). (B) Schematic showing the anatomical location of the MCA on a mouse brain and the lenticulostriate 'end arteries' that supply the striatum, plus the location of a striatal ischaemic lesion caused by MCAO surgery. Adapted from (Morris et al. 2016).

monofilament (diameter 220 μm) was introduced into the CCA via a small incision and advanced 10 mm distal to the carotid bifurcation, to occlude the MCA. The wound was then closed with one suture. The mice were placed in an incubator (30° C) for the duration of occlusion time (15 minutes) and recovered from anaesthesia during this period. Following this, the mice were re-anaesthetised with isofluorane; the suture was removed to reopen the wound and the monofilament was withdrawn. The ECA remained permanently ligated. The wound was closed and the mice were placed in an incubator for 2 hours to recover. The mice were monitored 2-3 times a day for the first week, and regularly monitored thereafter.

2.2.3 Rose Bengal photothrombosis

Experiments were performed to optimise an approach that induces the formation of a cortical ischaemic lesion with Rose Bengal photothrombosis. See experiment details in Chapter 4.

2.3 Laser speckle imaging

Laser speckle imaging was used to assess the cortical cerebral blood flow following Rose Bengal photothrombosis and MCAO surgery. The mice were anaesthetised with 5% isofluorane. Once fully anaesthetised, the mice were placed on a stereotaxic frame, with the head secured with ear and tooth bars, and ventilated through a nose cone with 1.5% isofluorane and 100% oxygen, at a rate of 150 breaths per minute. A midline incision was made and the scalp was held open by clips to expose the skull. The skull was cleaned from fur using ultrasound gel and sterile cotton buds, then a layer of gel was spread over it to prevent the skull from drying. The cortical cerebral blood flow was recorded for 3 minutes using a Laser Speckle Contrast Imager (Moor FLPI2 Speckle Contrast Imager, Moor

Instruments, UK). The wound was then sutured and the mice were recovered in an incubator. The laser speckle images were analysed using MoorFLPI-2 Review software.

2.4 Behaviour

2.4.1 Radial arm maze

To determine whether mild chronic cerebral hypoperfusion affected the spatial working memory, the animals underwent behavioural experiments in an eight-arm radial arm maze (RAM), as previously described (Coltman et al. 2011). One week prior to starting the RAM experiment (eight weeks after surgery), animal food consumption was restricted to reduce the animals by 10-15% of their initial weight. A former member of the group, Dr Yasmina Manso Sanz, carried out the RAM experiment, and I did the statistical analysis and interpretation of the data.

The RAM procedure commenced with two days of pre-training, in which the mice were allowed to freely explore the maze and collect food pellets from the ends of the maze arms, to become habituated to the apparatus and the task. Following this, the spatial working memory of the mice was probed. The eight arms of the RAM were baited with food pellets. Each mouse was placed in the central platform of the maze and allowed to choose an arm to receive the food pellet at the distal end and return to the centre, ready to choose again. The task was completed when the mouse had visited all eight different arms to retrieve the food pellet, or after 25 minutes of the test. Each mouse received 1 trial per day for 16 consecutive days. The number of revisiting errors was recorded for each trial; higher errors indicated a greater deficit in spatial working memory. The data was expressed as averages for each block: Block A is averaged data from day 1-4; Block B, day 5-8; Block C, day 9-10; Block D, day 11-12; Block E, day 13-14; and Block F, day 15-16. The

data was analysed by comparing the average revisiting errors between sham and BCAS mice over-time, with repeated measures two-way ANOVA.

2.4.2 Ladder-rung test and neurological score

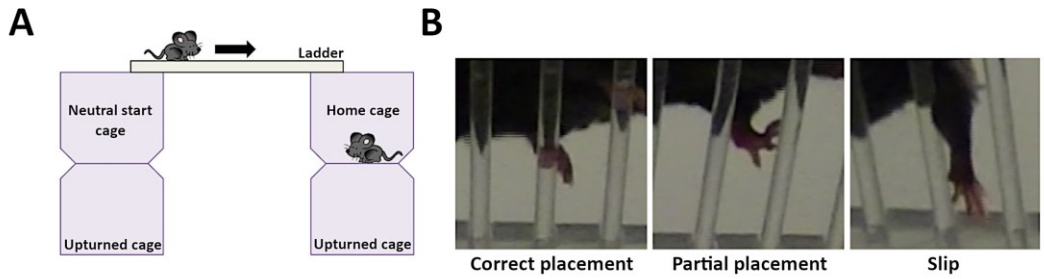

Figure 2.5 Schematic of the ladder-rung test. (A) Apparatus set up for the ladder-rung test. (B) Types of limb placement recorded.

A modified version of the ladder-rung test was used to probe for motor deficits following MCAO (Farr et al. 2006). A clear Perspex ladder (35cm long, 8cm wide, with 1.5cm gap between rungs) was suspended between two stacks of cages on a flat tabletop. The ladder started on the lid of a neutral cage containing only clean bedding, and ended on the lid of the mice's homecage. Both cage were stacked on top of upturned cages so there was enough space for a camcorder to be placed underneath. The mice were placed on the start cage and had to walk across the ladder to their home cage, whilst their limb placements on the rungs were recorded with the camcorder below. On each day, they did one practice trial and three experimental trials. The contralateral limb placements were analysed by watching the recordings at half speed and counting how many times the mice made a correct limb placement, partial limb placement or slipped. Partial placement was when the mouse would place one or two digits on the rung. At each time point for each mouse, the sum of the number of partial placements and slips for all 3 trials was divided by the total

number of limb placements, and multiplied by 100 to get a limb placement % error (Figure 2.5).

2.5 Tissue harvesting and processing

2.5.1 For histology

2.5.1.1 Transcardial perfusion

Mice were placed in an anaesthetic chamber containing 5% isoflurane. Once deeply anesthetised, they were transferred to an operating table and maintained under 3% anaesthesia during the procedure. A midline incision was made and the diaphragm and ribcage were cut to expose the heart. A butterfly needle connected to a cannula was inserted into the left ventricle and clamped into place, followed by a small incision in the right atrium for blood to drain out. The mice were perfused by pumping 30 mL of 0.1% heparinised phosphate buffered saline (PBS) (pH 7.4) through the cannula, at a rate of 2 mL/minute.

2.5.1.2 Cryostat cutting

Brains were removed from the skull and immersion fixed in 4% paraformaldehyde (PFA) and stored at 4°C for 24 hours. The brains were then transferred to 30% sucrose (Sigma S9378) solution for 72 hours. Following this, the brains were frozen in isopentane at -42˚C and kept at -80˚C before cutting on a cryostat (Leica CM1950). The brains were cut into 30 µm coronal sections, and slide-mounted or placed in cryoprotective medium (30% glycerol, 30% ethylene glycol in PB) in 24 well plates, and stored in -20˚C freezer.

2.5.1.3 Vibratome cutting

As before, each brain was removed from the skull and immersion fixed in 4% paraformaldehyde (PFA) and stored at 4°C for 24 hours. The brains were then transferred into PBS and cut on a vibratome. The brains were cut into 30 µm coronal sections, using frequency of 70, amplitude of 0.9 and velocity of 18. The sections were stored at -20˚C in cryoprotective medium (30% glycerol, 30% ethylene glycol in PB) in 24 well plates.

2.5.2 For biochemistry

Mice were culled by schedule 1 cervical dislocation, followed by decapitation. The brains were removed and sectioned into 2 mm slices using a mouse brain matrix; the slices were taken from around 0.38mm to -1.62mm from bregma was identified. The slices were cut into hemibrains and frozen in liquid nitrogen and stored in the -80˚C freezer.

2.6 Histology

2.6.1 Haematoxylin and eosin staining

Before staining, the sections were washed in PBS pH 7.4 (3 x 15minutes) and TB pH 7.6 (2 x 15minutes) to remove the cryoprotective medium; mounted on superfrost plus slides (VWR International) and left to air-dry overnight. Sections were dehydrated starting from running tap water and taken through serial alcohols (70%, 90%, 100%) and then in xylene for 10 minutes; then rehydrated by the reverse. Sections were stained with filtered haematoxylin (Thermo Fisher, UK) for 3 minutes, rinsed in running water and placed in 1% Acid Alcohol for 10 minutes and rinsing in running water again for 2 minutes. The sections were then placed in Scott's tap water for 2 minutes, stained with EosinY Alcoholic (Thermo Fisher, UK) for 20 seconds, and rinsed in running water again. Finally, the sections were

dehydrated again via the same procedure and incubated in xylene for 15 minutes before mounting the cover-glass with DPX.

2.6.2 Cresyl violet staining

Sections were mounted on slides, dried, dehydrated and rehydrated as described in Section 2.6.1 for Haematoxylin and Eosin staining. After rinsing in running water for 5 minutes, the sections were stained with filtered cresyl violet solution for 20 minutes. The sections were then dipped into the serial alcohols (70%, 90%, 100%) and incubated in xylene for 15 minutes for mounting with DPX.

2.6.3 Immunohistochemistry

All primary and secondary antibodies used in immunohistochemistry are listed in Table 2.1**.** Optimisation experiments were undertaken to determine the primary antibody concentrations, retrieval types and whether to use direct or indirect secondary labelling in protocols. For each experiment there was a negative control of an additional section that did not receive primary antibody incubation.

2.6.3.1 Immunoperoxidase labelling

The sections were washed in PBS pH 7.4 (3 x 15minutes) and TB pH 7.6 (2 x 15minutes) to remove the cryoprotective medium; mounted on superfrost plus slides (VWR International) and left to air-dry overnight. Sections were dehydrated from running tap water, through serial alcohols (70%, 90%, 100%) and in xylene for 10 minutes.

The sections were then rehydrated in 100% ethanol and endogenous peroxidase was quenched using 3% hydrogen peroxide solution for 30 minutes. For Iba1 and GFAP detection, antigen retrieval was performed by incubating the slides in 10mM citric acid

(pH6) and heating to 95˚C for 10minutes, in Decloaking Chamber NxGen (Biocare Medical). For 6E10 detection, the sections were placed in 70% formic acid for 20 minutes. Following retrieval, the sections were washed in PBS and incubated in blocking solution (10% horse or goat normal serum, 0.5% bovine serum albumin (Sigma A7030) in PBS) for 2 hours at room temperature. The primary antibodies in blocking solution were incubated on the sections overnight at 4˚C. Following this, the sections were washed in PBS and incubated with the secondary biotinylated antibody for 1 hour at room temperature. Signal amplification was performed using a Vector ABC Elite Kit (Vector Labs, UK) for 1 hour at room temperature. The sections were washed with PBS and peroxidase activity was detected with 3 minute incubation with 3,3' diaminobenzadine tetrahydrochloride (DAB, Vector Labs, UK). The sections were rinsed in running water and dehydrated through serial alcohols (70%, 90%, 100%), then kept in xylene for 15 minutes before mounting with DPX.

Table 2.1 Primary and Secondary Antibodies used in immunohistochemistry

Primary antibody	Label	Dilution	Retrieval	Supplier	Secondary antibody	Dilution	Supplier
MAP2	Dendrites	1:250	-	Sigma M9942	Anti-mouse Alexa Fluor 546	1:500	Invitrogen A1103
VGLUT1	Glutamatergic presynapses	1:1000	-	Millipore Ab5905	Biotinylated anti-guinea pig Streptavidin Alexa Fluor 488	1:100 1:100	Vector BA7000 Invitrogen S32354
PSD95	Postsynaptic densities	1:200	Citric acid, 110°C	NeuroMab 75-028	Biotinylated anti-mouse Streptavidin Alexa Fluor 488	1:100 1:100	Vector BA2001 Invitrogen S32354
GluR1	Glutamatergic postsynapses	1:500	-	Abcam 31232	Biotinylated anti-rabbit Streptavidin Alexa Fluor 488	1:100 1:100	Vector BA1100 Invitrogen S32354
Iba1	Microglia	1:1000	Citric acid, 95°C	Menarini MP290	Biotinylated anti-rabbit	1:100	Vector BA1100
GFAP	Astrocytes	1:2000	Citric acid, 95°C	Life-tech 13-0300	Biotinylated anti-rat	1:100	Vector BA1100
APP	Axon bulbs	1:20,000	Citric acid, 95°C	Millipore MAB348	Biotinylated anti-mouse	1:100	Vector BA2000
TMEM119	Microglia	1:500	Citric acid	Abcam ab209064	Anti-rabbit Alexa Fluor 546	1:500	Invitrogen A11040
6E10	β-amyloid	1:10,000	70% Formic acid	Biolegend SIG-39320	Biotinylated anti-mouse	1:100	Vector BA2000

2.6.3.2 Immunofluorescent labelling, slide mounted method

The sections were washed, mounted on slides and dehydrated as described above in Section 2.6.3.1. Sections for PSD95 detection underwent citrate antigen retrieval, at 110°C for 10 minutes, then were rinsed in running water and washed with in PBS with 0.2% triton X for 15 minutes each. Sections for GluR1 detection did not require antigen retrieval. The sections were blocked in 10% horse or goat normal serum, 0.5% bovine serum albumin (Sigma A7030) in PBS with 0.2% triton-x for 2 hours at room temperature. The primary antibodies in blocking solution were incubated on the sections overnight at 4˚C. Following this, the sections were washed in PBS and incubated with the secondary biotinylated antibody in PBS (1:100) for 2 hours. This was followed by PBS washes and application of streptavidin alexa flour 488 in PBS (1:100) for 2 hours. Finally, the sections were washed twice in PBS, then once in TB for 10 minutes each, and air-dried in the dark. The cover-glasses were applied with vectashield hardset with DAPI (Vector H-1500), sealed with nail varnish and stored at 4˚C to await imaging.

2.6.3.3 Immunofluorescent labelling, free-floating method

The protocol was carried out on sections in 24 well plates placed on a shaker. The sections were washed in PBS (3 x 15minutes). For the sections immunostained for TMEM119, antigen retrieval was performed by microwaving a flask of citric acid (10mM, pH6) to boiling (5 minutes) and pouring it into the well plate for 30 minutes, before removing the solution and washing with PBS. In all protocols, the sections were wash in PBS with 0.1% triton-x (3 x 15 minutes) and then blocked for 2 hours with 10% horse or goat normal serum, 0.5% bovine serum albumin (Sigma A7030) in PBS. Next, the sections were incubated overnight at 4˚C with primary antibodies in blocking solution. The sections were returned to room temperature and washed in PBS. For direct staining (MAP2 and

TMEM119 IHC), the sections were incubated for 2 hours with fluorescent conjugated antibodies in PBS (1:500), then washed in PBS and TB, and mounted onto superfrost plus slides (Thermo Scientific). For indirect staining (VGLUT1 IHC), biotinylated secondary antibodies in PBS (1:100) were applied to the tissue for 1 hour, washed with PBS and incubated with streptavidin alexa fluor 488 in PBS (1:100) for 2 hours at room temperature. The sections were dried in the dark, cover glasses applied with vectashield hardset with dapi (Vector H-1500), sealed with nail varnish and stored at 4˚C.

2.6.4 Analysis of histology

2.6.4.1 Confocal imaging

Laser scanning confocal microscopy system used was LSM 710 (Carl Zeiss Microscopy, Cambridge, UK). Image analysis was performed with ImageJ software (v1.46, NIH Bethesda, MD, USA). See chapter methods for specific analysis details.

2.6.4.2 Slide scanner imaging

Zeiss Axio Scan.Z1 slide scanner was used to capture tiled images of entire tissue sections and the images were converted into tiff files with ZEN imaging software by Zeiss. Image analysis was performed with ImageJ software (v1.46, NIH Bethesda, MD, USA). See chapter methods for specific analysis details.

2.7 Biochemistry

2.7.1.1 Tissue homogenisation

After harvesting and freezing tissue (Section 2.5.2), the sections were removed from -80°C freezer. The sections were placed on a lid of a plastic petri dish in a tub of wet ice and allowed to thaw slightly. Using a scalpel, the striatum was cut away from each section and

weighed in fresh eppendorf tubes and put on wet ice. The tissue was homogenised in a buffer of: 20mM Tris Base; 1mM EDTA; 1mM EGTA; 250mM sucrose; 1:100 protease inhibitors (Calibiochem, 53913) and 1:50 phosphatase inhibitors (Merck, 524629). The volume of buffer used was 5x the weight of the tissue and added to the eppendorf tube. Fifteen strokes of a plastic plunger tip was used to homogenise the tissue, then a motorised homogeniser was used with same plunger tip for a count of 4. The homogenate was centrifuged at 3000 rpm for 5 minutes at 4°C and the supernatant was taken off and aliquoted for protein concentration analysis and western blotting.

2.7.1.2 Protein concentration

The protein concentrations were analysed with the Pierce BCA Protein Assay Kit (Thermo Scientific) and performed according to the manufacturer's instructions. The absorbances were measured at 562nm on a FilterMax microplate reader (Molecular Devices, CA, USA).

2.7.1.3 Western blot

Optimisation experiments were performed to determine the protein concentration, primary antibody concentration, and whether to use direct or indirect secondary labelling in these protocols.

NuPage western blot products were sourced from Invitrogen. Samples were prepared to 15µg in 10µl in NuPage LDS sample buffer (4x) and NuPage reducing agent (10x), and denatured at 90°C for 10 minutes. 12µl of the sample solutions were run on NuPage 4-12% Bis-Tris 1.0mm x 15 well gels, in with NuPage Mes SDS running buffer. The gels were run for 1.5 hours at 80V. Proteins were transferred onto PVDF membranes (Immobilon-FL, Millipore) in transfer buffer (192mM glycine; 25mM pH8.3 trizma base; 20% v/v methanol), at 70V for 2 hours. Afterwards, the membranes were blocked for an hour in Odyssey

blocking buffer (Licor, 927-40000), made up in PBS at 1:1. The membranes were then incubated overnight at 4°C with primary antibodies (see Table 2.2) in 1:1 Odyssey blocking buffer: PBS 0.1% Tween, on a shaker. The next day, the membranes were washed with PBS 0.1% Tween and then incubated secondary antibody dilutions (see Table 2.2) at room temperature for an hour, in a black box on a shaker. For targets that required signal amplification with indirect labelling, the membranes were washed again in PBS 0.1% Tween, and fluorescent streptavidin solution was applied for an hour. Following fluorescent labelling, the membranes were washed in PBS 0.1% Tween and imaged with Odyssey FC.

Table 2.2 Primary and Secondary Antibodies used for western blotting

Primary antibody	Label	Dilution	Supplier	Secondary antibody	Dilution	Supplier
VGLUT1	Glutamatergic presynapses	1:2000	Millipore Ab5905	Biotinylated anti-guinea pig Streptavidin IRDye 800	1:600 1:2500	Vector BA7000 Li-cor 925-32230
PSD95	Postsynaptic densities	1:1000	BD Bioscience 610495	Anti-Mouse IgG IRDye 800	1:10,000	Li-cor 926-32212
Iba1	Microglia	1:500	Menarini MP290	Anti-Rabbit IgG IRDye 800	1:10,000	Li-cor 926-32213
GFAP	Astrocytes	1:1000	Life-tech 13-0300	Anti-Rat IgG IRDye 800	1:10,000	Li-cor 926-32219
α-tubulin	Housekeeping	1:10,000	Sigma T6074	Anti-Mouse IgG IRDye 680	1:10,000	Li-cor 926-68073

2.8 Statistical analysis

All statistical analysis was performed on GraphPad Prism software (v5.01, GraphPad Software Inc., La Jolla, USA). Details for the specific statistical analysis details are stated in the chapter methods. All data is presented as mean ± standard deviation, and $p<0.05$ was considered to be statistically significant.

2.9 ARRIVE and IMPROVE guidelines

ARRIVE (Animal Research: Reporting of *In Vivo* Experiments) guidelines are designed to improve the reporting of studies that use animal models. The present studies were designed according to ARRIVE recommendations. The number of experimental and control groups for each study are stated in the methods section for each results chapter. To minimise experimental bias, the animals were randomly allocated to sham-operated or BCAS/MCAO-operated groups. The experiments and analysis were performed in a blinded-manner: the animals were randomly assigned a numerical code and the data was recorded under this code, without knowing the surgery or genotype status of the animals. After the data sets from all experiments had been finalised, the codes were broken and the data was statistically analysed between the experimental groups.

The MCAO studies followed IMPROVE (Ischaemic Models: Procedural Refinements Of in Vivo Experiments) guidelines, which promotes experimental design that improves animal welfare and reduces their suffering, while maintaining the value of the research (Percie du Sert et al. 2017). Firstly, the present studies followed the IMPROVE guidelines by the choice of MCAO model: 15 minutes of intraluminal filament MCA occlusion. As these

studies were investigating the chronic impact of focal ischaemia and required the animals to be recovered for 3 months after surgery, a relatively short occlusion time was chosen to reduce the animals' suffering and increase their chances of surviving for that long. Furthermore, the animals were closely monitored after surgery, by checking their body weight and condition every day for the first week and regularly thereafter.

The IMPROVE guidelines stipulate the importance of pre-surgery acclimatisation (Percie du Sert et al. 2017). The mice used in these studies were bred in-house and were acclimatised to the animal unit prior to surgery. The condition of the mice was observed before surgery, checking their body weight and coat condition; one mouse was culled before surgery as it was the runt of the litter. IMPROVE guidelines were followed in that the mice were housed with the same groups before and after surgery. The cages contained the same environmental enrichment as each other, consisting of two cardboard tunnels and nesting material; 'super-enrichment' was not used to prevent neurorestorative effects. As recommended by IMPROVE, the animals were randomised so each cage contained both sham- and MCAO-operated animals. The diet was kept the same for the animals before surgery and throughout the experimental period, and they had a plentiful supply.

All surgical procedures were performed with aseptic techniques. Sham-operated animals received the same anaesthetic and surgical treatment as MCAO-operated animals, apart from insertion of the intraluminal filament. The mice were checked to be deeply anaesthetised prior to surgical incisions being made. The animals' body temperatures were regulated throughout surgery with a rectal thermometer and heated mat. The animals' respiratory rates were also regulated throughout surgery. Immediately after surgery, the

mice were pre-emptively given a 500mL subcutaneous injection of sterile saline solution to help prevent dehydration.

The animals were closely monitored after surgery and the vet was consulted about animals that were losing too much weight or appeared to be in pain. The animals were checked three times a day for 48 hours after surgery, then 2 times a day for the rest of the week. These checks included observing whether the mice were eating and drinking, their coat quality and movement abilities. Their body weight was recorded every morning for the first week after surgery, and then once a week thereafter. For the first week after surgery the animals were given 'mash', which was their diet pellets soaked in drinking water. Animals that lost 18% of their pre-surgery body weight were given a 500mL subcutaneous injection of sterile saline solution to help them become rehydrated and improve their condition. If the animals' weight decreased by 20% of their pre-surgery body weight, they would be culled to prevent suffering. Thanks to rigorous animal monitoring only 3 mice out of a total of 80 that underwent MCAO (or sham) surgery had to be culled due to significant weight loss. None of the animals were found dead. Notes were taken to record the conditions of the mice throughout their recovery period.

Chapter 3: The impact of chronic cerebral hypoperfusion on dendrites and glutamatergic synapses

3.1 Introduction

Chronic cerebral hypoperfusion has been proposed as a central common mechanism, contributing to cognitive decline and degenerative processes leading to dementia. This is based on evidence that global reductions in blood flow are associated with increased risk of progression from mild cognitive impairment to dementia, with the degree of CBF reduction correlating with the severity of cognitive impairment (Alsop et al. 2010; Chao et al. 2010; Huang et al. 2002; Ruitenberg et al. 2005). Moreover, investigations in rodent models have shown that hypoperfusion can induce pathological changes relevant to VCI and dementia. Previous studies from our group and others have shown that surgically induced hypoperfusion leads to long-term deficits in spatial working memory (Coltman et al. 2011; Kitamura et al. 2017; Shibata et al. 2004; Holland et al. 2015). A number of mechanisms have been proposed that link hypoperfusion to cognitive decline, however, it is unclear whether these include synaptic dysfunction and loss. Synaptic loss is the strongest correlating factor with cognitive decline in Alzheimer's disease (Terry et al. 1991). It may also underpin cognitive decline in VCI, however, there have only been a few studies investigating changes in synaptic protein levels in this disease (Sinclair et al. 2015; Kirvell et al. 2010). A number of studies have shown that global ischaemia models in rodents results in synapse and dendritic loss, with selective vulnerability to excitatory, glutamatergic terminals in the CA1 of the hippocampus (Jia et al. 2012; Wang et al. 2016). It is unknown,

however, whether modest chronic cerebral hypoperfusion, indicative of early stages of VCI and dementia, contributes to synaptic degeneration. This study was designed to investigate whether chronic cerebral hypoperfusion (induced by BCAS surgery) would lead to progressive dendritic and glutamatergic synaptic degeneration, culminating in impaired spatial working memory.

3.1.1 Hypothesis

Chronic cerebral hypoperfusion leads to progressive degeneration of dendrites and glutamatergic pre- and postsynaptic terminals, culminating in cognitive decline and dementia.

3.1.2 Aims

The aim of this study was to establish whether chronic cerebral hypoperfusion (induced by BCAS surgery) results in degeneration of dendrites and glutamatergic pre- and postsynaptic terminals, in brain regions that are associated with spatial working memory.

3.2 Methods

3.2.1 Animals

Male C57Bl/6J mice (4-5 months old) were used for a chronic cerebral hypoperfusion study. The mice were maintained on a 12:12 hour light/dark cycle, with *ad libitum* food and water access. All experiments were conducted in accordance with the Animals (Scientific Procedures) Act 1986 and local ethical approval at the University of Edinburgh and were performed under personal and project licenses granted by the Home Office. The data was collected and analysed in a blinded manner.

3.2.2 Bilateral common carotid artery stenosis (BCAS)

Cerebral hypoperfusion was induced with BCAS surgery, according to Section 2.2.1. The microcoils of 0.18mm diameter were used. This study had two cohorts; one with 1 month recovery from sham or BCAS surgery, and the other had 3 months recovery from sham or BCAS surgery.

The animal cohorts used for this study had been previously processed before I started in the lab. The tissue from the 1 month BCAS cohort was from an unpublished study, and the tissue 3 month cohort came from animals used in this published study (Kitamura et al. 2017). Kitamura et al. were investigating whether the drug cilostazol alleviates white matter pathology after 3 months of BCAS surgery. Therefore, both 3-month sham and BCAS groups used in the present study were actually vehicle-treated controls.

The present study did not use all of the animals in the 1 and 3 months cohorts; instead 8 mice per group were randomly selected. This group size was chosen to make the experimental procedure more manageable, enabling all the tissue from all selected animals to be immunostained at once and for all the slides to be imaged in one session. This approach was chosen to try to reduce experimental variation between animals. Power-calculations were not used to determine the group size. The animals had been given an experimental code. To select the 8 mice per group to use for the study, the total list of animal codes for each group were copied and pasted into an online randomiser (www.random.org), which then randomised the list of animal codes and the top 8 codes from each list were selected for the study.

3.2.3 Radial arm maze (RAM)

Eight-arm RAM was used to probe for spatial working memory deficit in the 3-month cohort, see Section 2.4.1. The mice were trialled for 16 consecutive days. Number of revisiting errors were averaged and blocked, as previously described. Former lab member Dr Yasmina Manso conducted the RAM experiment.

3.2.4 Tissue harvesting and processing

Mice were transcardially perfused, as described in Section 2.5.1.1, and the tissue was processed, cut and stored according to Section 2.5.1.2. The tissue was cut into 30µm coronal sections, taken from throughout the striatal and hippocampal levels, and stored at -20˚C as free-floating sections in cryoprotective medium (30% glycerol, 30% ethylene glycol in PB) in 24 well plates.

3.2.5 Detection of ischaemic neuronal pathology

Tissue sections from level 0.14mm and -1.70mm from bregma were stained with haematoxylin and eosin (Section 2.6.1). The stained sections were viewed with a brightfield microscope, and areas of ischaemic neuronal pathology were imaged and measured with ImageJ.

3.2.6 Detection of dendrites and synaptic terminals with immunohistochemistry

For each mouse in both 1- and 3-month cohorts, a section was taken from level 0.14mm and -1.70mm from bregma. Dendrites, glutamatergic pre- and postsynaptic terminals were detected with immunofluorescent labelling for MAP2, VGLUT1, PSD95 and GluR1, as stated in Section 2.6.3.2-3 and Table 2.1.

3.2.7 Confocal microscopy and Image analysis

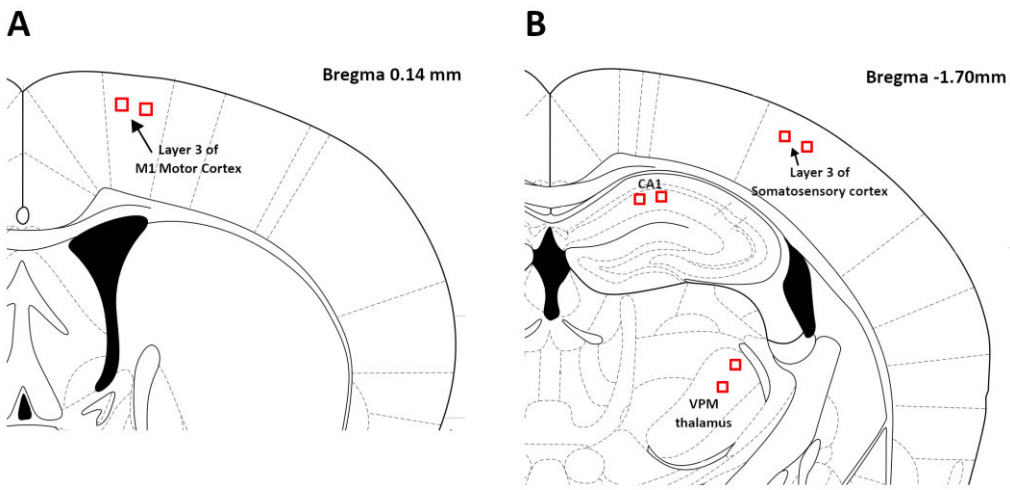

Figure 3.1 Brain regions where the densities of MAP2, VGLUT1, PSSD95 and GluR1 were imaged and analysed.

Laser scanning confocal microscopy system used was LSM 710 (Carl Zeiss Microscopy, Cambridge, UK), to capture immunofluorescent detection of MAP2, VGLUT1, PSD95 and GluR1. The brain regions imaged were the CA1 hippocampus, VPM thalamus, and layer 3 of the somatosensory cortex (at level -1.70mm) and layer 3 of the motor cortex (at level 0.14mm) (see Figure 3.1).

In each brain regions of interest, two z-stacks were captured. The z-stacks were captured 2 µm from the tissue surface and were 1.04 µm deep. The images were taken with 63x objective (1.4 NA) resulting in each slice having the dimensions of 43.53 x 43.53µm. Framesize was 1024 x 1024 pixels and the interval between each image was 0.13 µm. The two stacks were taken 50 µm apart from each other. Stereotactic maps and DAPI staining were used to locate the regions of interest. The images were taken and analysed in a blinded manner, as each animal was given a code to conceal which experimental group they were from.

Image analysis was performed with ImageJ software (v1.46, NIH Bethesda, MD, USA). An autothreshold to cover the area of positive staining was used to measure the %density of MAP2, VGLUT1, PSD95 and GluR1 at each plane in the image stacks. The %density of each marker was averaged for each stack and then an average from the two stacks were calculated, to result in one %density value for each marker for each brain regions, per mouse.

3.2.8 Statistical analysis

The RAM data was analysed by comparing the average revisiting errors between sham and BCAS mice over-time, with repeated measures two-way ANOVA. Plus, the average of Blocks E and F was compared between sham and BCAS mice with Mann-Whitney test. The %densities of MAP2, VGLUT1, PSD95 and GluR1 were compared between sham and BCAS mice at 1 month and 3 months post-surgery, with Mann-Whitney test. A significance level of $p<0.05$ was considered to be statistically significant.

3.3 Results

3.3.1 BCAS did not result in long-term spatial memory working deficits.

Previous results from our group and others have demonstrated that chronic cerebral hypoperfusion leads to an impairment in spatial working memory (Coltman et al. 2011; Holland et al. 2015; Shibata et al. 2007). In the current study, spatial working memory was probed by the 8-arm radial arm maze. The mice were trialled for 16 consecutive days before being culled, 3 months after BCAS surgery. The average revisiting errors from each block was compared between sham and BCAS mice over-time, with repeated two-way ANOVA (Figure 3.2). Statistical analysis showed a significant effect of time ($F(5,70) = 17.37$, $p <0.0001$), as the average revisiting errors have decreased over time as the mice learnt

the task. However, there was no significant effect on surgery ($F(1,14) = 0.600$, $p = 0.452$, with no factor interaction ($F(5,70) = 1.171$, $p = 0.332$). This result contradicted previous

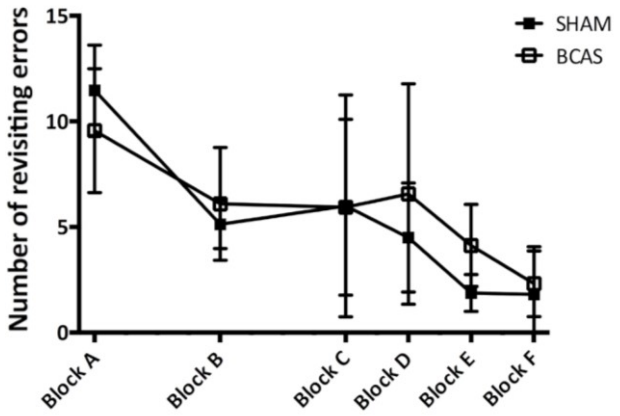

Figure 3.2 BCAS surgery did not result in significant spatial working memory impairment. There was no significant difference in the average number of revisiting errors over blocks A-F between sham and BCAS mice. Repeated two-way ANOVA. Data presented as mean ± SD, n = 8 per group.

findings from our group. The next stage was to investigate whether BCAS surgery induced pathological changes related to spatial working memory impairment.

3.3.2 CA1 dendrites and glutamatergic synaptic structures were resilient to the effects of BCAS surgery. Dendrites were vulnerable to ischaemic damage.

Following the finding that BCAS surgery causes a trend of spatial memory impairment, the underlying pathological alterations were investigated with a focus on the hippocampus, which is important in memory processes and is also vulnerable to global cerebral blood flow reductions (Cassel et al. 1998; Kril et al. 2002; Ordy et al. 1993; Hatakeyama et al. 1988; Nishio et al. 2010). Haematoxylin and eosin staining was used to identify whether BCAS surgery induced ischaemic neuronal pathology in the CA1. There was no evidence of ischemic neuronal damage in any of the 16 sham mice and the majority of BCAS mice did not show evidence of ischemic neuronal damage (12 out of 16). However, a subset of

hypoperfused animals had ischaemic damage in the CA1 (4 out of 16), which included 3 animals in the 1 month hypoperfused group had CA1 ischaemic damage of the following

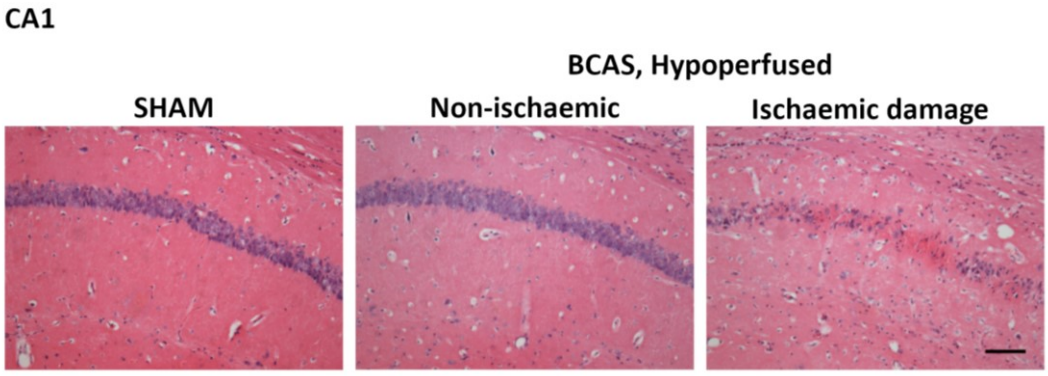

Figure 3.3 BCAS surgery with 0.18mm microcoil resulted in no ischaemic neuronal damage in the CA1 of sham mice and in the majority (12/16) of BCAS mice. Only a subset of BCAS mice (4 out of 16) had ischaemic neuronal damage in the CA1. Scale bar = 100µm.

areas: 0.030 mm^2, 0.036 mm^2 and 0.026 mm^2; whilst 1 animal in the 3 month hypoperfused group had CA1 ischaemic damage of 0.056 mm^2 (Figure 3.3). This provided evidence that BCAS surgery can lead to heterogeneity in neuronal pathology.

The next aim of the study was to address whether chronic cerebral hypoperfusion resulted in the degeneration of dendrites and glutamatergic pre- and postsynaptic terminals. Since BCAS surgery resulted in heterogeneous pathology, the subset of animals with CA1 ischaemic neuronal pathology were highlighted on the graphs in red (Figures 3.4 and 3.5). The dendrites and synaptic densities in the CA1 were compared between sham and BCAS mice, at 1 and 3 months post-surgery, with Mann-Whitney test. MAP2 immunohistochemistry was used to visualise dendrites in the CA1 after sham or BCAS surgery (Figure 3.4). In the 1 month cohort, there was no significant difference in the MAP2 %density CA1 in the between the sham and BCAS ($p = 0.104$) (Figure 3.4B). Although there was no overall effect of BCAS surgery, there was a trend for a decrease in the BCAS group, with the lowest dendritic densities occurring in the animals with CA1 ischaemic damage

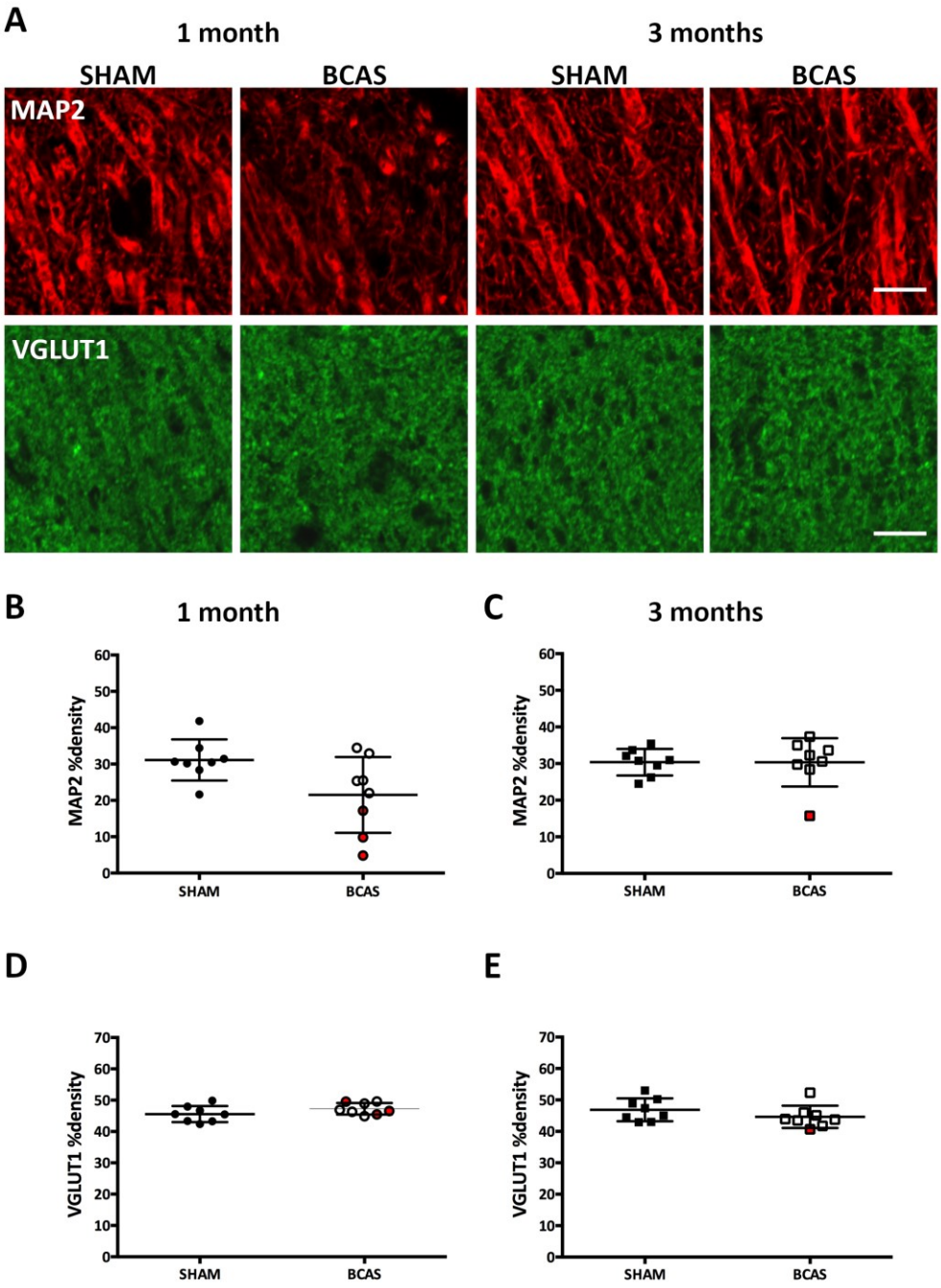

Figure 3.4 Dendrites and glutamatergic presynaptic terminals in the CA1 were resilient to BCAS surgery, although there was indication that dendrites were vulnerable to ischaemic damage. (A) MAP2 and VGLUT1 immunohistochmistry to detect dendrites and glutamatergic presynaptic terminals in the CA1. (B) At 1 month and (C) 3 months after surgery, there was no significant different in MAP2 %densities between sham and BCAS mice. The mice with CA1 ischaemic damage (red points) had the lowest MAP2 %densities, indicating that dendrites were vulnerable to ischaemic damage. (D) At 1 month and (F) 3 months after surgery, there was no significant different in VGLUT1 %densities between sham and BCAS mice. Data presented as mean ± SD, n = 8 per group. Scale bar = 10 µm. Mann-Whitney test.

(marked red). In the 3 month cohort, there was no significant effect of BCAS surgery on CA1 MAP2 density ($p = 0.777$) (Figure 3.4C), however, the dendritic density in the animal with CA1 ischaemic damage had the lowest value. Taken together, this data showed that BCAS induced hypoperfusion does not cause significant loss of dendrites in the CA1 at 1 or 3 months post-surgery, however, there was indication the CA1 ischaemic damage does cause some degeneration of dendrites.

Glutamatergic transmission is known to be vulnerable in cognitive decline and dementia; therefore, the densities of glutamatergic pre- and postsynaptic terminals were measured in the CA1 after hypoperfusion. VGLUT1, an abundant marker of glutamatergic presynaptic terminals was analysed (Figure 3.5). The CA1 VGLUT1 %densities were compared between the sham and BCAS mice, 1 month after surgery, and found no significant difference ($p = 0.232$) (Figure 3.5D). For the 3 month cohort, there was also no significant difference in CA1 VGLUT1 %densities between sham and BCAS mice ($p = 0.275$) (Figure 3.5E). Unlike the MAP2 %densities, the VGLUT1 %densities from the BCAS mice with CA1 ischaemic damage were not obviously lower than the values from mice without ischaemic damage. Overall, the results showed that hypoperfusion from BCAS surgery did not cause a loss of glutamatergic presynaptic terminals in the CA1.

Next, the impact of BCAS surgery of glutamatergic post-synaptic densities was investigated, by immunostaining for PSD95 and GluR1 (Figure 3.5A). PSD95 is an abundant protein in the postsynaptic densities of excitatory synapses. PSD95 %densities in the CA1 were unchanged between the sham and BCAS mice at both 1 month ($p = 0.275$) (Figure 3.5B) and 3 month ($p = 0.275$) (Figure 3.5C) post-surgery. GluR1 is a subunit of AMPA-receptors. Similarly, the %densities of GluR1 in the CA1 were unchanged between sham and BCAS, at 1 month ($p = 0.130$) (Figure 3.5D) and 3 months ($p = 0.560$) (Figure 3.5E) after surgery.

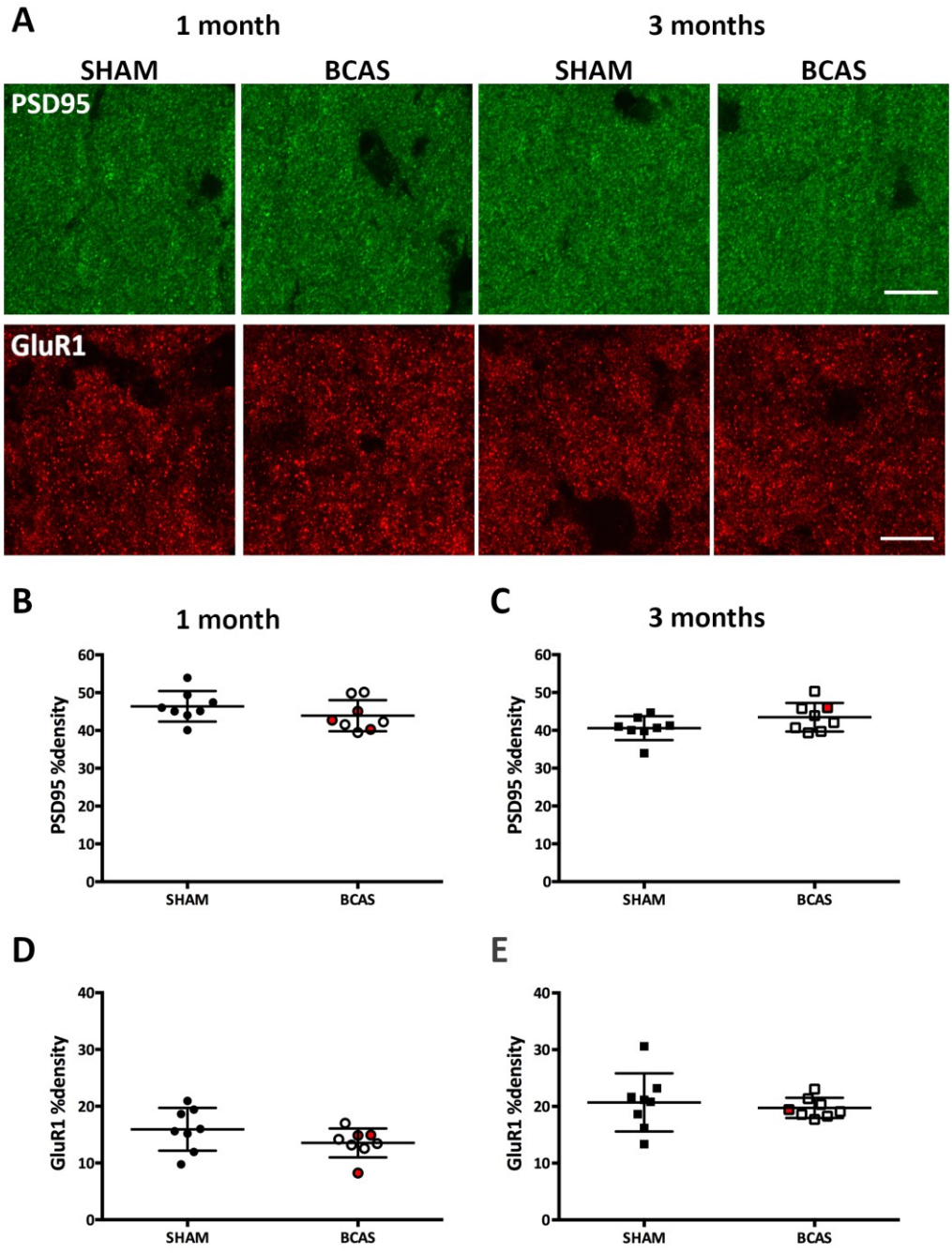

Figure 3.5 Glutamatergic postsynaptic terminals in the CA1 were unchanged with BCAS surgery. (A) PSD95 and GluR1 immunohistochemistry to detect dendrites and glutamatergic presynaptic terminals in the CA1. There were no differences in the %density of PSD95 at (B) 1 month and (C) 3 months after BCAS surgery. There were no differences in the %density of GluR1 at (D) 1 month and (E) 3 months after BCAs surgery. Data presented as mean ± SD, n = 8 per group. Scale bar = 10 µm. Mann-Whitney test.

There was also no indication that ischaemic damage in the CA1 lead to lower values of glutamatergic post-synaptic densities, apart from in one mouse in the 1 month cohort. Taken together, the data showed no effect of chronic cerebral hypoperfusion on the densities of glutamatergic postsynaptic terminals in the CA1.

Overall, the data indicated that dendrites and glutamatergic pre- and postsynaptic terminals in the CA1 were resilient to the effects of chronic cerebral hypoperfusion; and although there was indication that CA1 dendrites were vulnerable to ischaemic damage, there was no evidence of it causing synapse loss.

3.3.3 Dendritic and synaptic structures in the thalamus were resilient to BCAS surgery.

The thalamus is another brain region that has been found to be vulnerable following chronic cerebral hypoperfusion and subcortical microinfarcts have been identified at 6months post-BCAS (Holland et al. 2015). In the present study, however, there was no

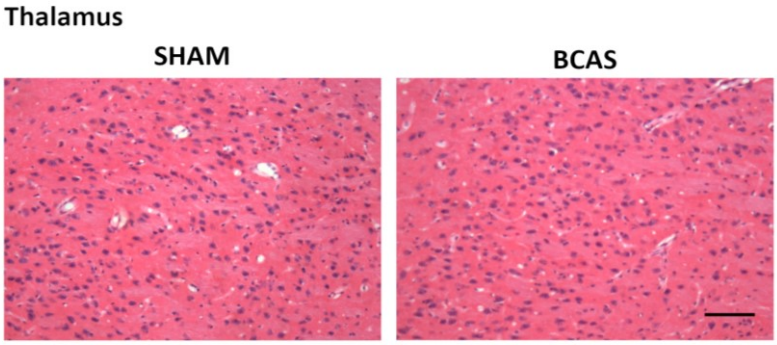

Figure 3.6 There was no ischaemic neuronal damage in the thalamus after sham or BCAS surgery. Scale bar = 100 µm.

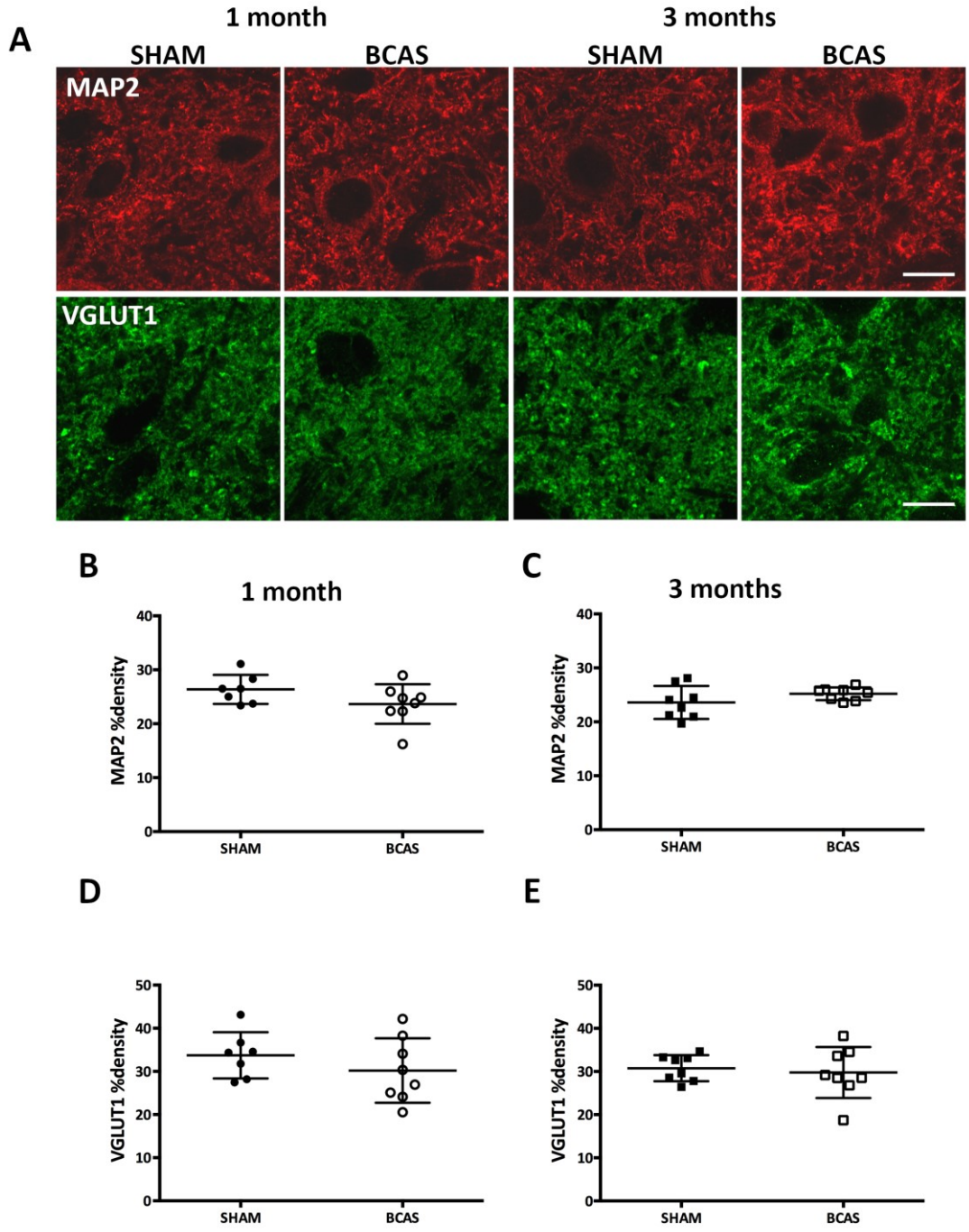

Figure 3.7 Dendrites and glutamatergic presynaptic terminals were unchanged with BCAS surgery in the thalamus. (A) MAP2 and VGLUT1 immunohistochemistry to detect dendrites and glutamatergic presynaptic terminals in the thalamus. There were no differences in the %density of MAP2 at (B) 1 month and (C) 3 months after BCAS surgery. There were no differences in the %density of VGLU1 at (D) 1 month and (E) 3 months after BCAS surgery. Data presented as mean ± SD, n = 8 per group. Scale bar = 10 µm. Mann-Whitney test.

evidence of ischaemic neuronal damage in the thalamus at 1 and 3 months post-BCAS (Figure 3.6). Next, the densities of dendrites and glutamatergic presynaptic and postsynaptic terminals were investigated in the VPM thalamic nuclei (Figure 3.7A). The %densities of MAP2 in the thalamus were unchanged between the sham and BCAS mice, at 1 month ($p = 0.151$) (Figure 3.7B) and 3 month ($p = 0.275$) (Figure 3.7C) after surgery. Similarly, there were no differences in the VGLUT1 %densities between the sham and BCAS mice, at 1 month ($p = 0.230$) (Figure 3.7D) and 3 months ($p = 0.854$) (Figure 3.7E) after surgery.

The densities of PSD95 and GluR1 were also measured in the thalamus at 1 month and 3 months after BCAS surgery (Figure 3.8). Interestingly, there was a small but significant increase in PSD95 %density in the BCAS mice at 1 month after surgery ($p = 0.0379$) (Figure 3.8B). In the 3 month cohort, however, there was no significant difference in PSD95 %densities between sham and BCAS mice, ($p = 0.932$) (Figure 3.8C). GluR1 %densities in the thalamus were unchanged between sham and BCAS mice at 1 month ($p = 0.854$) (Figure 3.8D) and 3 months ($p = 0.160$) (Figure 3.8E) after surgery. Overall, BCAS surgery did not impact the densities of dendrites and glutamatergic pre- and post-synaptic terminals in the thalamus, apart from causing a small increase in PSD95+ terminals after 1 month.

The %densities of MAP2, VGLUT1, PSD95 and GluR1 were also measured in the motor and somatosensory cortex, as these are other brain regions associated with spatial working memory function and VCI. The densities of the dendritic and synaptic markers were unchanged between sham and BCAS mice, at 1 and 3 months after surgery; apart from a small significant increase in MAP2 %density in the motor cortex after 3 months of BCAS (see Supplementary Figure S3.1 and S3.2).

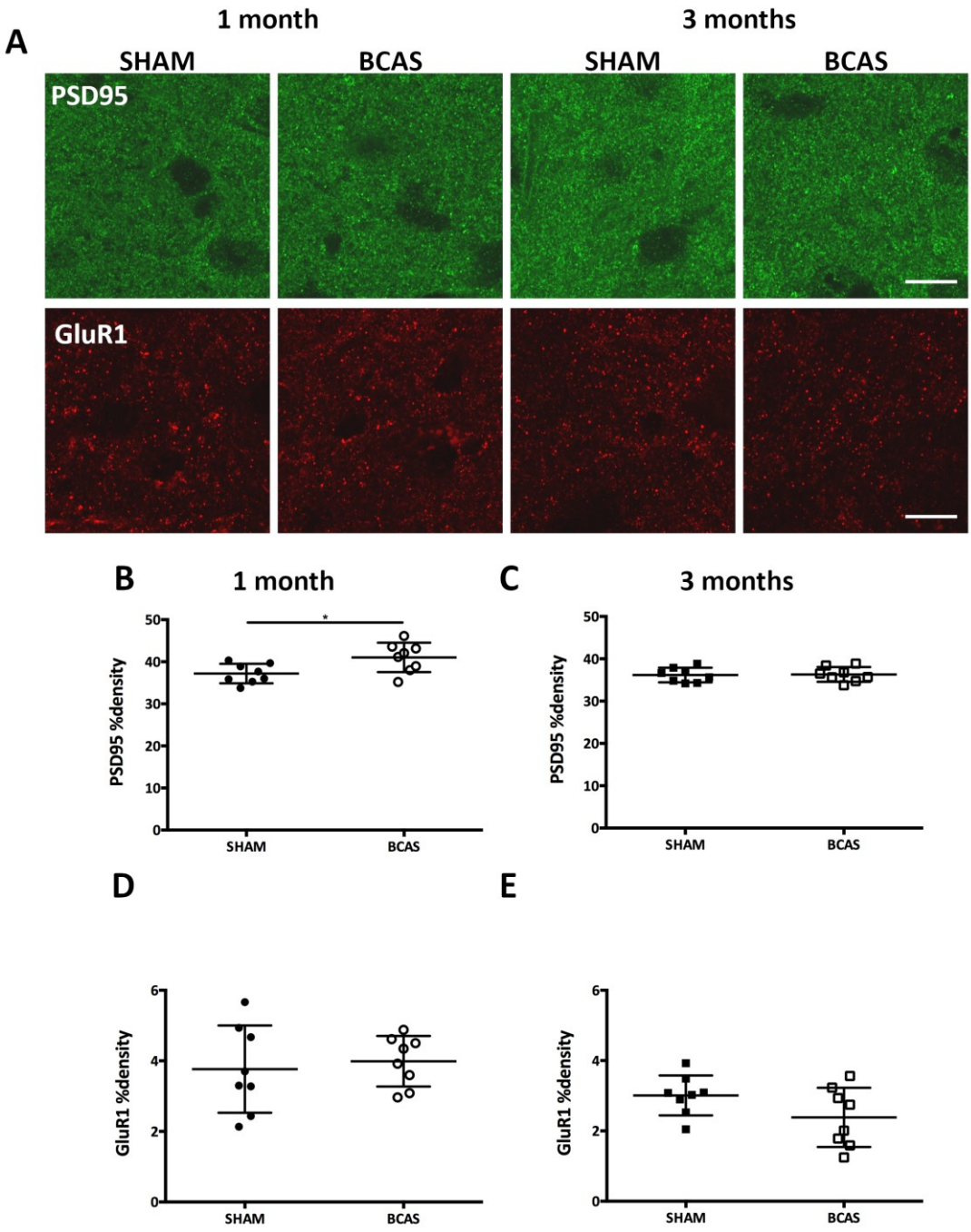

Figure 3.8 Glutamatergic postsynaptic terminals in the thalamus were unchanged with BCAS surgery, apart from a small increase in PSD95 %density. (A) PSD95 and GluR1 immunohistochemistry to detect dendrites and glutamatergic presynaptic terminals in the thalamus. (B) There was a small increase in PSD95 %density, 1 month after BCAS surgery compared to sham mice. (C) PSD95 %densities were unchanged between sham and BCAS mice at 3 months. There were no differences in the %density of GluR1 at (D) 1 month and (E) 3 months after hypoperfusion. Data presented as mean ± SD, n = 8 per group. Scale bar = 10 µm. Mann-Whitney, *p<0.05.

Overall, this study demonstrated that glutamatergic pre- and postsynaptic terminals were robust and were largely unchanged after 1 and 3 months of BCAS-induced hypoperfusion. The dendrites were also largely resilient to change, although there was some implication that ischaemic neuronal pathology in the CA1 caused some degeneration of dendrites.

3.4 Discussion

The purpose of this investigation was to determine whether chronic cerebral hypoperfusion, which is a key feature of cerebral vascular disease and a predictor for dementia, causes a loss of dendrites and glutamatergic synaptic terminals in the hippocampus and thalamus, culminating in a decline in spatial working memory. In this study, there was no significant difference in the spatial working memory abilities of mice at 3 months after sham or BCAS surgery. Furthermore, there was no evidence of synaptic loss with hypoperfusion, and instead dendritic loss was only evident in cases with ischaemic damage in the CA1. Taken together, this data rejects the original hypothesis that chronic cerebral hypoperfusion leads to progressive degeneration of dendrites and glutamatergic pre- and postsynaptic terminals, culminating in cognitive decline and dementia.

3.4.1 Chronic cerebral hypoperfusion caused a trend towards spatial working memory impairment.

Vascular cognitive impairment is diagnosed based on the presence of vascular pathology and decline in four cognitive domains: executive/attention, memory, language and visuospatial functions (Gorelick et al. 2011). Clinical studies have revealed that mild cognitive impairment, related to subcortical vascular pathology, is characterised by deficits in executive function (Breteler et al. 1994; O'Brien et al. 2003). Key aspects of executive function include working memory and problem solving (Chan et al. 2008). In preclinical

studies, chronic cerebral hypoperfusion (induced by BCAS surgery) results in impairment in spatial working memory (Shibata et al. 2007; Holland et al. 2015; Coltman et al. 2011; Saggu et al. 2016), as well as in other hypoperfusion rodent models (Hattori et al. 2015; Hattori et al. 2014; Kitamura et al. 2012). The radial arm maze test is designed to probe for spatial working memory deficits in rodents (Olton et al. 1980) and was used in the current study and previous hypoperfusion studies (Holland et al. 2015; Coltman et al. 2011; Shibata et al. 2007). In this test the mice are required to enter each arm of the maze to obtain a food pellet and use visuospatial clues to work out which arms they have yet to enter. The number of errors they make by revisiting an arm is recorded, and the higher number of revisiting errors is a sign of impaired spatial working memory.

In the present study, both sham and BCAS mice initially made many errors as they were learning the task, which is consistent with previous publications. However, unlike our previous findings, there was no overall surgery effect on the average number of revisiting errors over the trial. In the 3-month cohort, there was only one mouse with any ischaemic neuronal damage in the brain regions analysed, and this only occurred in the CA1 of the hippocampus. There is a large body of evidence from preclinical studies showing that the CA1 of the hippocampus is particularly vulnerable to global reductions in CBF, resulting in ischaemic neuronal damage and atrophy in this region (Ordy et al. 1993; Hatakeyama et al. 1988; Farkas et al. 2007a; Keiko Nishio et al. 2010), as will be discussed in more detail in the following section. Moreover, it is widely accepted that the hippocampus is a key brain region in memory formation processes. The hippocampus has been shown to have a role in spatial working memory, as animals with lesions in the hippocampus or fimbria-fornix (output nerve bundles from the hippocampus) resulted in worsened scores for the RAM test (Cassel et al. 1998; Warburton et al. 2000). Moreover, a number of studies have shown

that BCCAO in rats leads to ischaemic neuronal damage in the CA1 of the hippocampus. As reviewed by Farkas et al., at 2 weeks post-BCCAO, 6-29% of animals have CA1 ischaemic neuronal injury; at 4 weeks, this has been exhibited by 55% of animals; and at 8-13 weeks, 67% of BCCAO rats had total hippocampal destruction (Farkas et al. 2007a; Farkas et al. 2006; Ohtaki et al. 2006; Schmidt-Kastner et al. 2001; Liu 2006). There is evidence of hippocampal ischaemic injury occurring in animals with spatial working memory deficits, as shown in BCCAO rat models (Bennett et al. 1998; Ni et al. 1994) and BCAS mouse models (Nishio et al. 2010). Taken together, this may indicate that hypoperfusion-induced ischaemic injury contributes to spatial working memory deficits and may explain why the present study did not find spatial working memory deficits, as only one animal in the 3-month BCAS group had CA1 ischaemic pathology. This would suggest that pathological changes as a result of ischaemia leads to cognitive impariment, rather than hypoperfusion directly.

3.4.2 Chronic cerebral hypoperfusion resulted in heterogeneous hippocampal pathology.

The present study found evidence of ischaemic neuronal pathology in the CA1 hippocampus of only a subset of hypoperfused mice. Hippocampal atrophy and CA1 neuronal loss has been shown to be a feature of human vascular dementia (Kril et al. 2002; Du et al. 2002). This is consistent with observations of selective ischaemic damage and atrophy in rodent models of chronic global ischaemia (Ordy et al. 1993; Hatakeyama et al. 1988) and hypoperfusion (Nishio et al. 2010). Transient global ischaemia in monkeys also resulted in loss of CA1 and CA2 neurons (Zola-Morgan et al. 1992).

In the present study, a subset of the hypoperfused animals showed evidence of ischaemic neuronal damage in the CA1. This finding is consistent with previous results from our

group, which has found varying degrees of ischaemic neuronal damage post-BCAS. For example, in one particular study Coltman et al. found that in different cohorts post-BCAS there was evidence of ischaemic neuron damage in 2 out of 17 hypoperfused animals in cohort 1 one month after surgery; 4 out of 14 hypoperfused animals in cohort 2 and 17 out of 24 hypoperfused animals in cohort 3, both 2 months after surgery (Coltman et al. 2011). Another group reported that the CA1 neurons remained intact 30 days after BCAS surgery (Shibata et al. 2007). Furthermore, Nishio et al. showed that there was significant hippocampal atrophy and frequent signs of ischaemic damage in mice 8 months after BCAS (Nishio et al. 2010). Taken together, our results and these publications indicate that chronic cerebral hypoperfusion can result in long-term ischaemic damage in the CA1. Ischaemic neuron damage occurs when cerebral blood flow drops to 30% that of baseline levels (Heiss & Rosner 1983; Baron 2001), whereas previous work from our group has shown that the acute cortical blood flow in the BCAS is only 60-70% of the baseline, and then recovers to ~80% over a month after surgery (McQueen, et al. 2014). Although these studies refer to cortical CBF measurements, and CBF reductions have been shown to be less severe in the cortex (Hattori et al. 2016), it may be that for the majority of mice post-BCAS the subcortical CBF is not reduced enough to induce CA1 ischaemic damage. CBF was not measured in the present study, however, an improvement to this study would be to use Arterial Spin Labelling (ASL) to measure CBF in subcortical regions and to determine whether hippocampal CBF related to the extent of ischaemic neuronal pathology in these animals.

In the present study, ischaemic neuronal pathology was present in the CA1 of a subset of mice post-BCAS, whilst the other hippocampal regions remained intact. Previous studies have found selective vulnerability of CA1 neurons compared to other CA hippocampal

regions, as shown in a range of neurological disorders (Bartsch et al. 2015), including Alzheimer's disease (Hyman et al. 1984; Braak & Braak 1991; Terry et al. 1991). It has been proposed that selective vulnerability of CA1 neurons is a consequence of genomic differences increasing the sensitivity to oxidative stress and excitotoxicity (Wang & Michaelis 2010). The sensitivity of CA1 neurons to oxidative stress was shown in an experiment where superoxide-generating compound, duroquinone, was applied to organotypic hippocampal slice cultures, resulting in extensive CA1 cell death whilst sparing the CA3 neurons (Wang et al. 2005). Furthermore, they found that cortical neurons were also resilient to oxidative stress (Wang et al. 2009), which is consistent with the present study as there was a lack of cortical ischaemic damage whilst some mice had ischaemic CA1 damage. The selective vulnerability of CA1 may result from higher endogenous levels of reactive oxygen species in these neurons compared to CA3 (Mattiasson et al. 2003); and genes related to ROS-generation, anti-oxidants and cellular stress are more highly expressed in CA1 neurons (Wang et al. 2005; Wang et al. 2007). CA1 neurons may have higher reactive oxygen species as it is required for long-term potentiation in this region (Klann et al. 1998). The increased levels of reactive oxygen species in the CA1 neurons may predispose this region to neurodegeneration through oxidative stress (Wang et al. 2007). Selective CA1 neuronal vulnerability may be linked to the activation of glutamate receptors. In oxygen-glucose deprived hippocampal sections, the CA1 neurons more rapidly released glutamate and in greater quantities than CA3 (Uchino et al. 2001). Excessive glutamate release and glutamate receptor activation can cause downstream excitotoxicity via the ischaemic cascade, Section 1.4.1.1. This pathway generates reactive oxygen species, as activation of NMDA-receptors by glutamate can induce activation of neuronal nitric oxide synthase (Lai et al. 2014). The greater release of glutamate and

increased oxidative stress, therefore, may underpin the selective CA1 damage seen in the current study.

3.4.3 CA1 dendrites and glutamatergic pre- and postsynaptic terminals were resilient to chronic cerebral hypoperfusion.

The next task in this study was to investigate whether hypoperfusion resulted in degeneration of dendrites and glutamatergic pre- and postsynaptic terminals in the CA1. Dendrites were detected with immunohistochemistry for microtubule-associated protein-2 (MAP2), an abundant cytoskeletal phosphoprotein associated with dendritic microtubules (Friedrich & Aszódi 1991). The analysis showed that dendritic density in the CA1 was unchanged with hypoperfusion, however, there was indication that dendrites were vulnerable in animals with CA1 ischaemic neuropathology. This is also supported by reports that MAP2 loss is a sensitive marker for ischaemic lesions (Dawson & Hallenbeck 1996). Previous studies of global ischaemia found a loss of hippocampal dendrites. In a model of permanent global ischaemia in rats, MAP2 protein and mRNA levels were gradually reduced in the hippocampus over 4 weeks after surgery (Liu et al. 2005). This study also reported that the loss of MAP2 correlated with deficits in spatial memory of the rats, which suggest that hippocampal dendrite degeneration is a cause of cognitive impairment after global ischaemia. Another study demonstrated that dendritic branching in the CA1 is progressively reduced from 2 to 16 weeks after BCCAO in rats (Jia et al. 2012).

The mechanism by which dendrite degeneration occurs in the CA1 after cerebral hypoperfusion is unclear. It may occur as a result of progressive ATP depletion and oxidative stress, which could cause downstream blockage of dendritic and axonal trafficking by binding of cofilin-1 to ADP-actin (Won et al. 2018). This mechanism may exist to save energy in metabolically challenged neurons, yet it inhibits the processes needed for

dendrites to function and dendritic degeneration may ensue. Another proposed mechanism could be the dysregulation of autophagy in dendrites, which is the cell's method of removing dysfunctional or redundant proteins and organelles. Excessive autophagy could be stimulated by deficits in dendritic transport and accumulation of proteins and organelles. Oxidative stress and energy deprivation has been shown to increase autophagy (Filomeni et al. 2015), and global ischaemia causes autophagosomes to become concentrated in CA1 synaptic terminals and dendrites, 48 hours after surgery (Ruan et al. 2012). The increase in autophagy may be a self-destructive mechanism, as in *Drosophila* heterozygous for Nmnat, blocking autophagy prevented hypoxia-induced dendritic degeneration (Wen et al. 2013). These studies may suggest that ischaemia in the CA1 results in dendritic degeneration by over-activation of autophagy (Yang et al. 2013).

In the current study, the density of glutamatergic presynaptic protein, VGLUT1, and postsynaptic proteins, PSD95 and GluR1, were also measured in the CA1 to identify whether chronic cerebral hypoperfusion causes degeneration of these structures. However, the data did not find significant differences in the densities of any of these markers, showing that 1 and 3 months of hypoperfusion does not cause degeneration of glutamatergic pre- or postsynaptic terminals in the CA1. To the best of our knowledge, this is the first study that has investigated whether modest chronic cerebral hypoperfusion causes synaptic loss. Previous studies have shown hippocampal synaptic degeneration occurs with global ischaemia, most commonly with bilateral common carotid artery occlusion (BCCAO) in rats. There are reports that BCCAO in rats causes a progressive loss of CA1 dendritic spines between 2 and 16 weeks post-surgery (Jia et al. 2012), and gradual reductions of hippocampal synaptophysin protein levels, over 20 weeks post-surgery (Liu

et al. 2005). The functional impact of these changes have been measured as reduction in CA1 synaptic plasticity, 3 weeks after BCCAO in rats (Xu et al. 2012).

VGLUT1 was used as a marker for glutamatergic presynaptic terminals, as it is a transporter for packaging glutamate into synaptic vesicles in presynaptic terminals (Fujiyama et al. 2001). VGLUT1 appears to have a important roles in cognition, as there was a significant reduction in its protein levels in the cortex from vascular dementia patients, compared to cortices from stroke patients who had not experienced dementia (Kirvell et al. 2010). Furthermore, VGLUT1 protein levels positively correlated with a pre-mortem cognitive score, further indicating that decreased VGLUT1 is associated with cognitive decline. In another study, CA1 levels of VGLUT1 and its isoform VGLUT2, were reduced 7 days after transient BCCAO in mice (Khan et al. 2018). The data presented in Section 5.3.3 demonstrates that focal ischaemia induced by transient MCAO leads to loss of VGLUT1+ terminals within the ischaemic lesion. Taken together, the results indicate that VGLUT1 is resilient to modest hypoperfusion and more vulnerable to ischaemic damage. In the present study, however, there was no evidence of VGLUT1+ terminal loss in the animals with ischaemic CA1 damage, even though there was evidence of dendritic damage. This was a recurrent theme with the other synaptic markers, PSD95 and GluR1. For a discussion on mechanisms of ischaemia-induced VGLUT1 loss see Section 5.4.2.

PSD95 is commonly used as a marker for excitatory postsynaptic terminals, as it is an abundant scaffolding protein expressed in postsynaptic densities (Migaud et al. 1998). The present study did not show any changes in the densities of PSD95+ terminals in CA1 after 1 or 3 months of cerebral hypoperfusion. Previous work has shown that PSD95 protein levels in the hippocampus are significantly reduced long-term in rats after BCCAO (Nie et al. 2016; Hu et al. 2019). In a study of unilateral common carotid artery occlusion (UCCAO),

PSD95 protein levels were unchanged in the ipsilateral hippocampus and actually increased in the ipsilateral cortex (Zhao et al. 2014). This latter result is consistent with the data in the present study and indicates that PSD95 can be resilient to hypoperfusion.

GluR1 is a subunit of AMPA-receptors, abundantly expressed in the postsynaptic densities of glutamatergic synaptic terminals (Angulo et al. 1997). The present study did not find a difference in the densities of GluR1+ terminals between sham and BCAS mice, at 1 and 3 months after surgery. A previous study showed that the densities of terminals positive for another AMPA-receptor subunit, GluR2, were significantly reduced in the hippocampus, 1-24 weeks after BCCAO in rats (Wang et al. 2016). They also reported that the density of terminals positive for NMDA-receptor subunit NR1 and colocalised NR1-synaptophsyin terminals increased, which they theorise is to show an increase in the number of non-functional, 'AMPAR-silent' synapses, which do not respond to presynaptic stimulation (Hanse et al. 2013). GluR1 was used in the present study, as this is the dominant AMPA-receptor subunit in activity-dependent subunit recruitment and long-term potentiation induction. Protein levels of both GluR1 and GluR2 were reduced in the CA1, CA3 and dentate gyrus, 2 days after transient global ischaemia (Dos-anjos et al. 2009), indicating that both subunits are acutely vulnerable to ischaemia. In another study, however, they found that whilst immunoreactivity of GluR2 was reduced in the CA1 after 6-48 hours after transient four vessel occlusion, GluR1 levels remained stable (Han et al. 2016). This may suggest that GluR2 subunits are more vulnerable than GluR1. 80% of synaptic AMPARs in the CA1 are composed of GluR1-GluR2 heteromers (Lu et al. 2009), yet these can be replaced with GluR2-GluR3 heteromers especially in the absence of activity (Shi et al. 2001). The current study could be developed to detect whether chronic cerebral hypoperfusion has an impact on GluR2, to determine whether this subunit is more

vulnerable than GluR1. Taken together, the results showed that modest chronic cerebral hypoperfusion does not cause loss of glutamatergic pre- and postsynaptic terminals in the CA1, even in cases with some ischaemic neuronal pathology in this region.

A surprising finding in this study was the significant loss of MAP2 dendrites occurred in mice with CA1 ischaemia neuronal, whilst there was no significant differences in the pre- and postsynaptic markers in the same regions. Previous studies have shown that ischaemia-induced dendritic blebbing includes loss of dendritic spines, which post-synaptic densities project from (Zhang et al. 2005; Brown et al. 2007; Zhu et al. 2017). Therefore, the expectation was that that synaptic degeneration would occur in regions of dendritic degeneration. The lack of synaptic changes in these animals could be the result of different mechanisms governing dendritic and synaptic degeneration, or due to a lack in sensitivity in the methods used for their detection, as discussed below. It has been reported that dendrites contain particularly high densities of reactive mitochondria compared to axons and spines (Kageyama & Wong-Riley 1982), which could make dendrites even more vulnerable to ischaemia and energy depletion than these other structures.

As previously discussed, PSD95 has been shown to be resilient to hypoperfusion, 2.5 months after UCCAO (Zhao et al. 2014). This study also investigated the density of degenerating neurons in the CA1, CA3 and dentate gyrus with fluoro-jade staining. In the ipsilateral CA1 and CA3, there was a small but non-significant increase in neurodegeneration, whilst there was a significant increase in the dentate gyrus. Although the hippocampal protein levels of PSD95 were significantly indistinct between the contralateral and sham hippocampi, there was a trend towards a small increase in ipsilateral PSD95 (Zhao et al. 2014). Although these changes were small, the data may indicate that whilst neurodegeneration occurs in the hippocampus, the synapses may be

stable or may even increase in density. There is a growing body of evidence focused on neuronal plasticity and rewiring after ischaemic injury (Carmichael et al. 2017). Increased expression of VGLUT1 has also been found in ischaemia-induced synaptogenesis in a focal ischaemia model (Stokowska et al. 2017). In animals with ischaemic damage in the present study, ischaemia may have promoted synaptogenesis in the CA1, which may have resulted in synaptic densities that were indistinct from sham animals. Immunostaining of GAP43 could be used to detect whether there has been CA1 synaptogenesis following BCAS (Stokowska et al. 2017; Carmichael 2003).

As previously mentioned, the methods used for the analysis of synaptic density may lack sufficient specificity and sensitivity for detecting small changes. All of the structures were analysed with immunohistochemistry, which can be susceptible to cross-reactivity of antibodies with other proteins especially if there are isoforms of the target proteins. The specificity of the VGLUT1 antibody used in the present study had previously been checked by other groups, as discussed in Section 5.4.2. The antibody used to detect PSD95 was recommended to us by members of Seth Grant's lab, as they had previously checked the specificity by immunostaining tissue from PSD95 KO mice and found no signal. We did not check the specificity of the GluR1 antibody. A concern may be that GluR1 is also expressed by astrocytes, as some AMPA-receptors are, however, the evidence indicates that GluR2 is the predominant subunit of astrocytic AMPA-receptors (Zhang et al. 2014; Mölders et al. 2018; Rusnakova et al. 2013). Taken together these results suggest that the antibodies used for this study are specific to the proteins of interest.

Insufficient sensitivity in the microscopy and image analysis approaches used may also result in the inability to detect small differences in synaptic density in this study. Confocal microscopy was used to capture stacks of planar images through the tissue, as described in

Section 3.2.7. The images were taken with a 63x objective and 3.1 zoom, so punctate immunostaining was visible. The original plan for this study was to use a new analysis method developed by the Grant lab, which uses a machine learning algorithm to count the number of synaptic terminals in the confocal images (Zhu et al. 2018). This method requires the images to be of high resolution and in stacks, in order to count the synaptic terminals within 3D space. In the present study, the images were taken as z-stacks of 1.04µm, with an interval of 0.13µm. On attempting the analysis with the method, it became obvious that this method needed images of even higher resolution. We tried to deconvolve the images using Hugyens software, however, this raised concerns that it would create artefacts that looked like synaptic terminals (Sibarita 2005; Monici 2005). Furthermore, it became clear that the machine learning algorithm takes a long time to process the images, which would have impacted on the 'n' numbers of the study, as it would not have been possible to analyse n = 8/group using this method. Instead, the decision was made to analyse the images as %density of positive signal, with an autothreshold on ImageJ. This approach, however, may lack sensitivity and is still liable to issues caused by suboptimal resolution. As %density measurement does not need z-stacks to terminals number in 3D, it may have been more beneficial to image multiple regions on one plane or making a tiled image to cover the whole of the CA1. The current method may be under-sampling as it is captured from a small area in the CA1. An improvement of this method was to use a Zeiss Axio Scan.Z1 slide scanner microscope in the studies for Chapter 5 & 6, which takes tiled images of entire coronal brain sections.

The present study focused on whether chronic cerebral hypoperfusion resulted in structural changes of synapses and dendrites, however, it does not provide any insight into the functional state. As hypoperfusion leads to impairment in spatial working memory,

there may have been dysfunction of the synapses in the hippocampus and cortex, even though there was no sign of synaptic loss. Previous work has demonstrated that BCCAO surgery in rats leads to deficits in spatial learning and memory processes and impaired long-term potentiation in the CA1 from 4-12 weeks after surgery (Luo et al. 2015). The present study could be developed to investigate the changes to long-term potentiation in hippocampal slices taken from mice 1 and 3 months after BCAS surgery, to identify whether there are changes in the synaptic function in the absence of synaptic loss.

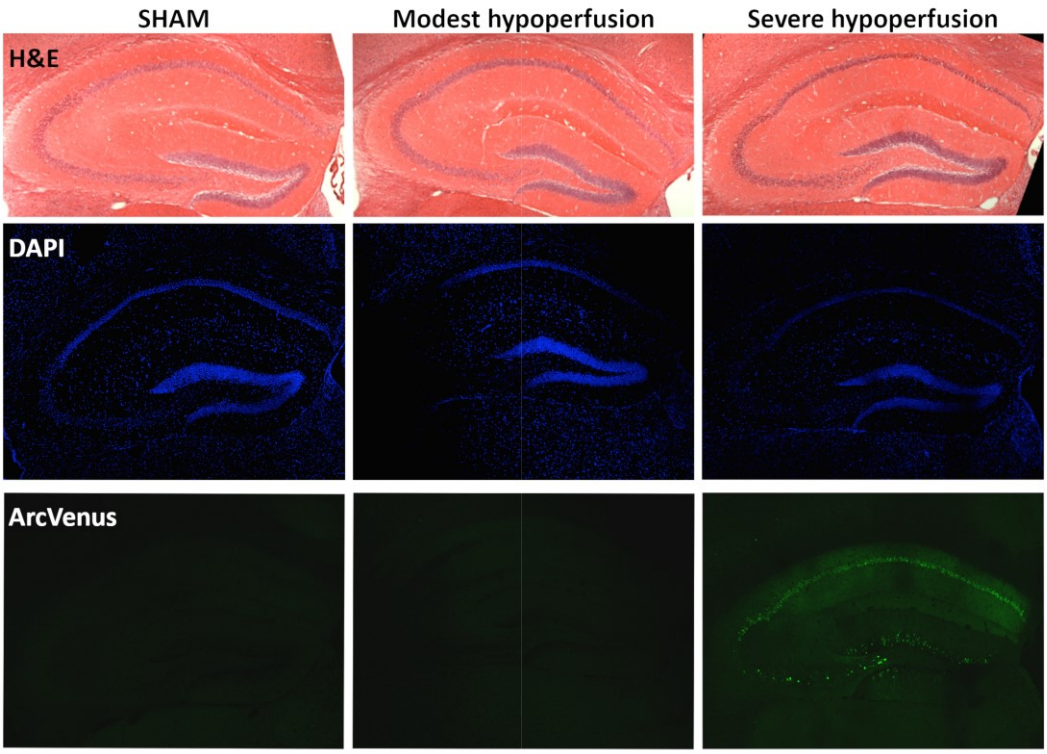

Figure 3.9 Severe hypoperfusion surgery (BCAS, 0.16mm) resulted in activation of Arc-Venus after 24 hours. Arc-Venus mice underwent sham, modest (0.18mm microcoil) and severe (0.16mm microcoil) BCAS surgery. Arc-Venus signal was greatly increased after severe hypoperfusion, compared to after sham or modest hypoperfusion surgery.

An alternative approach would be to use transgenic mice that express fluorescent signals when their neurons are active. Arc-Venus and Arc-dVenus mice would be appropriate for

such an experiment. Arc is a postsynaptic protein that interacts with PSD95 and is upregulated during excitatory synaptic activity (Fernández et al. 2017). Venus and the destabilised version (dVenus) are fluorescent yellow proteins that have been tagged onto Arc to track its expression; with dVenus signal fading quicker than Venus (Eguchi & Yamaguchi 2009). Rudinskiy et al. used the Arc-dVenus model to show that neuronal activity was reduced around amyloid plaques in the cortex of APP/PS1 mice (Rudinskiy et al. 2012). Arc-Venus or dVenus mice could be used to develop on the work of the current study to determine whether chronic cerebral hypoperfusion causes a reduction in neuronal activity in the CA1. Before culling the mice, the specific brain region would need to be stimulated, similar to Rudinskiy et al. using light to stimulate neurons in the visual cortex (Rudinskiy et al. 2012). For the current study, the radial arm maze task could be used to stimulate the brain regions relevant to spatial working memory and show where there is less activity in dysfunctional neurons. A pilot study, conducted by my colleagues Juraj Koudelka and Karen Horsburgh, investigated the acute effect of BCAS surgery on Arc-Venus mice, supplied by the Grant Lab. They compared the effect of using the normal 0.18mm microcoils and thinner 0.16mm microcoils, to result in modest and severe hypoperfusion, respectively. After 48 hours, there was no Arc-Venus signal in the modest hypoperfused mice, however, there was clear neuronal activation in the hippocampus and cortex in the severely hypoperfused mice (Figure 3.9). Histological analysis showed evidence of ischaemic neuronal damage in the hippocampus in severe hypoperfused animals but not in the modest hypoperfused animals. Severe hypoperfusion alone was sufficient to acutely activate neurons, most likely through ischaemia-induced hyperexcitability, whilst modest hypoperfusion did not. This method could be applied to a chronic study, although it would require a method for stimulating the CA1 neurons just before culling the animals, such as with a hippocampal-dependent behavioural task. This approach could be used to

determine whether chronic cerebral hypoperfusion results in long-term neuronal dysfunction in the hippocampus. Moreover, the findings in the Arc-Venus pilot study support the data in the present study, as there was no evidence of neurodegenerative changes in mice without CA1 ischaemic pathology, whilst severe hypoperfusion resulted in CA1 ischaemic damage and degenerative changes.

3.4.4 Dendrites and synapses in the thalamus were unaffected by chronic cerebral hypoperfusion.

The thalamus appears to be another key brain region involved in spatial working memory (Hallock et al. 2016). Previous work by our group showed that 6 months after BCAS surgery resulted in ischaemic and haemorrhagic lesions in the thalamus, whereas these were absent at 1 month after surgery (Holland et al. 2015). The present study also showed no evidence of ischaemic neuronal damage in the thalamus 1 month and 3 months after surgery. The expectation was that ischaemic damage would occur in the thalamus by 3 months, as the number of ischaemic lesions increased over time in the data by Holland et al. The lack of thalamic ischaemic neuropathology detected in the present study may result from the thickness of the tissue sections; they were quite thick at 30µm, which could affect the sensitivity of detecting small ischaemic lesions, whilst Holland et al. used sections of 6µm thick. Alternatively, other environmental factors may have reduced the extent of neuropathology in the 3 month cohort, such as inconsistencies in the animal unit and cold temperatures having neuroprotective affects (Talma et al. 2016).

The impact of chronic cerebral hypoperfusion on dendrites and glutamatergic pre- and postsynaptic terminals in the thalamus was investigated, at 1 and 3 months after surgery. There was no significant difference in any of the markers, apart from a small significant increase in PSD95 %density in the 1 month hypoperfused thalamus. This was a surprising

finding, as we would have expected to see synaptic degeneration induced by hypoperfusion. This result may indicate the new postsynaptic terminals have formed in the hypoperfused thalamus. There is evidence of thalamocortical circuits undergo rewiring after ischaemic stroke (Tennant et al. 2017), therefore, there may be small amounts of rewiring in the thalamus after chronic cerebral hypoperfusion. Interestingly, in the study presented in Chapter 6, there was a small significant increase in PSD95 %density also in the VPM thalamic nuclei. This data could indicate that there was a small increase in PSD95+ terminals in the hypoperfused thalamus to compensate for pathological changes elsewhere, however, this is a puzzlingly finding as there does not appear to be many neuropathological changes to stimulate restoration mechanisms. There is substantial evidence to support that synaptic rewiring occurs in the cortex following a brain injury, whilst less attention has been given to subcortical reorganisation. As previously stated, GAP43 can be used as a marker for axon sprouting and synaptic plasticity (Frey et al. 2000), therefore, increased immunostaining in the hypoperfused thalamus would indicate that restoration mechanisms had been activated.

There were no significant differences in the %densities of MAP+ dendrites, VGLUT1+ and GluR1+ terminals in the hypoperfused thalamus. As previously discussed, the data indicates that the modest cerebral blood flow changes in this BCAS model are insufficient to result in loss of glutamatergic pre and postsynaptic terminals. The expression of GluR1 is limited in the thalamus under normal conditions (Ibrahim et al. 2000).

The somatosensory and motor cortices are additional brains regions known to be vulnerable to vascular pathology. Dysfunction of the frontal lobe is linked to vascular multi-infarct lesions in humans (Wolfe et al. 1990). Furthermore, the somatosensory cortex is considered to be important for working memory processes (Linden 2007). MEG data

collected from VCI patients showed changes in somatosensory evoked magnetic fields that correlated with cognitive decline (Sun et al. 2013), indicating alterations in the somatosensory system in VCI. In the present study, however, there was no evidence of ischaemic neuronal pathology, dendrite degeneration or synaptic loss in either the motor or somatosensory cortices. Although there was an increase in dendritic density in the motor cortex after 3 months of BCAS, which may result from compensatory mechanisms. Völgyi et al. performed proteome analysis on synaptosomes fractions from the cortex of rats, 5 weeks after BCCAO and found significant reductions in proteins involved in presynaptic vesicle cycling and in postsynaptic assembly (Völgyi et al. 2017), although VGLUT1 and PSD95 were not among the list of specific proteins. The present study demonstrated that modest chronic cerebral hypoperfusion was insufficient to cause reductions in the densities of dendrites, and glutamatergic pre- and post-synaptic terminals in the motor and somatosensory cortices.

Overall, the results in this study, and others, have implicated that chronic cerebral hypoperfusion leads to impairment in spatial working memory; however, this is not related to a loss of glutamatergic synaptic terminals or dendrites. A number of studies by our group and others have identified alternative mechanisms that can lead to downstream functional impairment and cognitive decline. White matter tracts are very sensitive to cerebral blood flow changes, and BCAS surgery has been shown to cause diffuse myelin damage in the corpus callosum, fimbria, internal capsule and optic tract, by 1 month after surgery (Shibata et al. 2004; Reimer et al. 2011; Holland et al. 2015; Holland et al. 2011; Sigfridsson et al. 2018). The extent of white matter damage in dementia is related to the decline in cognitive processing speed and executive function (Cohen et al. 2002; Mungas et al. 2001), as white matter disruption prevents communication between different brain

regions. A number of studies published from our group have demonstrated that white matter pathology occurs by 2 months after BCAS surgery (Coltman et al. 2011), and loss of white matter integrity relates to impairment in spatial working memory (Kitamura et al. 2017; Manso et al. 2018). Furthermore, there is evidence that hypoperfusion reduces efficient conduction of white matter tracts by disrupting paranodal axon-glial junctions (Reimer et al. 2011).

Mechanisms related to hypoxia are also considered to be important in hypoperfusion-induced pathology. BCAS surgery has been shown to greatly reduce oxygen levels in the corpus callosum at 3 days, 1 and 6 weeks after surgery (Duncombe et al. 2017). Moreover, hypoxia-related genes were expressed in the white matter 3 days post-BCAS (Reimer et al. 2011). Another study by our group showed that densities of oligodendrocytes and their precursors are reduced in the corpus callosum at 3 days post-BCAS (McQueen et al. 2014). It may be that hypoperfusion induces hypoxic mechanisms in the white matter, causing the degeneration of oligodendrocytes and disruption in axon-glial integrity, leading to reduced signal conducted in the white matter tract (Duncombe et al. 2017). Neuroinflammation appears to be another key player in the pathological changes following hypoperfusion, based on evidence that BCAS stimulates increases in microglia/macrophage and astrocyte densities, particularly in the white matter (Shibata et al. 2004; McQueen et al. 2014; Reimer et al. 2011; Holland et al. 2011). There is evidence that the level of microglia/macrophages relates to the slowing of conduction velocity in the corpus callosum, and therapeutic intervention with anti-inflammatory drugs improved conduction velocity (Fowler et al. 2018; Manso et al. 2018). Furthermore, white matter neuroinflammation may cause impairment in axon-glial integrity and conduction velocity, by the release of pro-inflammatory cytokines and chemokines (Reimer et al. 2011). Pro-

inflammatory cells also release matrix metalloproteinases (MMPs), which can degrade the myelin sheath, as well as the proteins in the extracellular matrix and tight junction proteins between endothelial cells, which have been associated with BBB breakdown (Seo et al. 2013; Chandler et al. 1995). Moreover, the release of reactive oxygen species (ROS) from activated microglia may also contribute to endothelial dysfunction (Freeman & Keller 2012).

Neurovascular coupling may also be impacted by hypoperfusion. As described in Section 1.2.3., neurovascular coupling is the fine-tuning of CBF in response to neuronal activity, that is mediated through the NVU and vasoactive neurotransmitter release. There is evidence that hypoperfusion, induced by UCCAO, results in a loss of vascular response to neuronal activity (Nishino et al. 2016). Furthermore, previous analysis from our group also found a smaller increase in CBF upon neuronal activation (by whisker stimulation) in BCAS mice compared to shams (Duncombe et al. 2017). This may result from uncoupling of the NVU, based on evidence that chronic hypoperfusion caused activation of astrocytes and displacement of their end-feet; although this finding was associated with thalamic ischaemic injury (Holland et al. 2015). Collectively, these studies indicate that chronic cerebral hypoperfusion results in a number of mechanisms that can cause functional impairment and cognitive decline, without inducing glutamatergic synapse loss in the hippocampus, thalamus and cortex.

3.4.5 Conclusions

Chronic cerebral hypoperfusion by BCAS surgery did not result in long-term spatial working memory impairment. Hypoperfusion leads to heterogeneous ischaemic neuronal pathology, as only a small subset of animals had CA1 ischaemic neuronal damage. Dendrites are resilient to hypoperfusion, but there was implication of their vulnerability to

CA1 ischaemic injury. Glutamatergic pre- and postsynaptic terminals were resilient to hypoperfusion. The overall implications of the study were that hypoperfusion may not be the main driver of degeneration and decline in VCI; and that hypoperfusion does not cause glutamatergic synaptic loss in VCI and VaD. It may be that ischaemic injury, which can result from hypoperfusion, is the initiator for degenerative mechanisms leading to VCI and dementia.

3.5 Supplementary figures

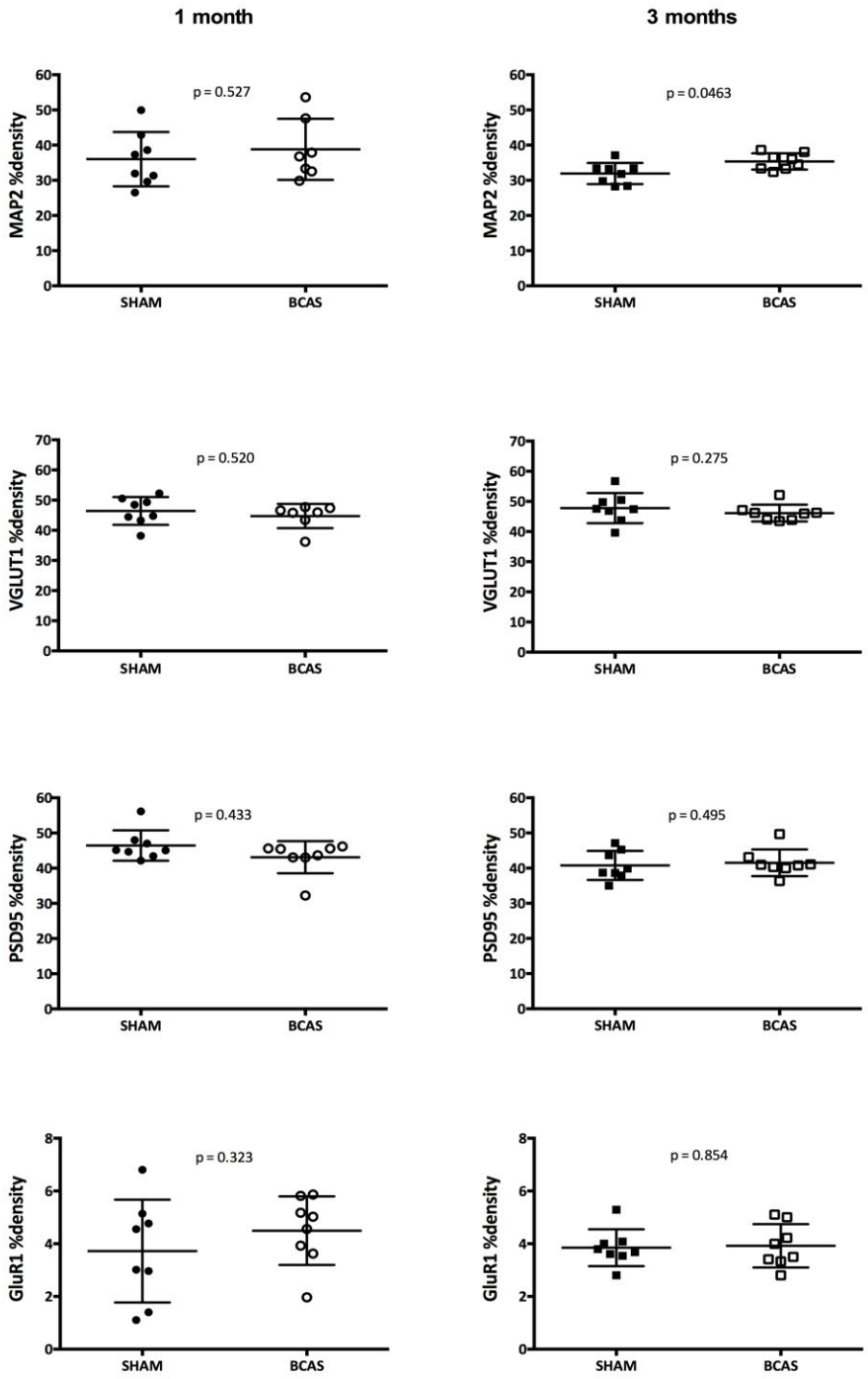

Figure S3.1 MAP2, VGLUT1, PSD95 and GluR1 %densities in the motor cortex were unchanged after 1 or 3 months of BCAS surgery, apart from a small increase in MAP2 %density at 3 months. Mann-Whitney test.

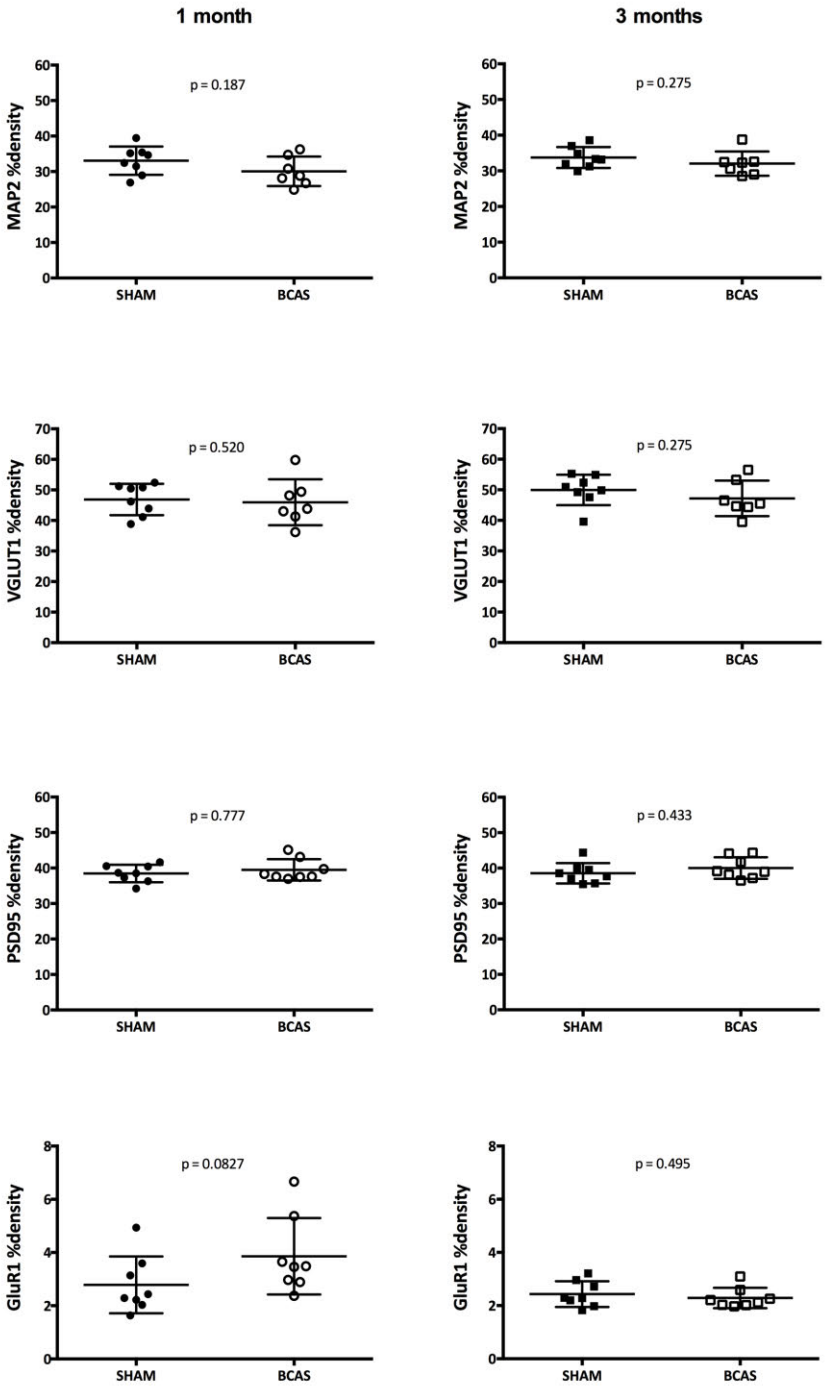

Figure S3.2 MAP2, VGLUT1, PSD95 and GluR1 %densities in the somatosensory cortex were unchanged after 1 or 3 months of BCAS surgery. Mann-Whitney test.

Chapter 4: Optimisation of photothrombosis and multiphoton microscopy

4.1 Introduction

The previous study demonstrated that glutamatergic pre- and postsynaptic terminals and dendrites are resilient to loss from chronic cerebral hypoperfusion, however, there was indication that dendrites were vulnerable to ischaemic damage. The development of this work, therefore, would be to investigate whether focal ischaemia leads to degeneration of glutamatergic pre- and postsynaptic terminals.

Publications by Tim Murphy, Shengxiang Zhang and colleagues have shown that cortical focal ischaemia caused by photothrombotic occlusion leads to rapid blebbing of dendrites and dendritic spines, the structures which excitatory postsynaptic terminals project from, within minutes (Zhang et al. 2005; Zhang & Murphy 2007). These studies used multiphoton *in vivo* microscopy and mice expressing YFP+ in layer VI cortical neurons, to capture dynamic changes. Furthermore, they found that these changes can be reversible, as timely reperfusion restored the dendrites and spines (Zhang et al. 2005). Furthermore, Zhu et al. demonstrated that global ischaemia also results in quick dendritic degeneration which can be reversed if reperfusion occurs 20 minutes later, whereas longer occlusion times lead to minimal or no recovery (Zhu et al. 2017). These studies focus on acute time-points and do not determine the chronic outcome of focal ischaemia on dendrites, spines or synapses.

There is a large body of literature supporting that β-amyloid has synaptotoxic effects, as described in Section 1.7.1. In cases with both vascular and Alzheimer's pathology, there is evidence of worsened cognitive outcome, compared to patients with just vascular

pathology (Snowdon et al. 1997), although the mechanism behind this is unclear. The current study sought to determine whether concurrent focal ischaemia and β-amyloid deposition would lead to worsened postsynaptic terminal loss, in comparison to focal ischaemia alone. To investigate this, mice harbouring APPTgSwDI transgene or WT controls were subject to focal ischaemia. These mice also expressed PSD95:eGFP to enable analyse of excitatory postsynaptic terminals to be analysed with multiphoton *in vivo* microscopy.

The photothrombotic occlusion model with Rose Bengal is a commonly used method for inducing a small focal ischaemic lesion in the cortex. Rose Bengal is activated when it is illuminated, leading to the generation of singlet oxygen, focal endothelial damage, platelet activation and focal clotting (Dietrich et al. 1986). It is also advantageous as it allows for targeting a specific area for occlusion. In the initial stages of my research, it was considered that this model may be beneficial to use to investigate the longitudinal effect of focal ischaemia and concurrent β-amyloid on postsynaptic terminals, as captured with multiphoton *in vivo* microscopy. This short chapter describes the optimisation experiments and preliminary results for Rose Bengal photothrombosis and multiphoton microscopy, how this informed the experimental plan for the following investigations.

4.2 Methods and Results

The experimental animals were all adult C57Bl/6J and PSD95:eGFP x TgSwDI. Both male and female mice were used for photothrombosis optimisation. The mice were housed on a 12-hour light/dark cycle, with a constant temperature and free access to food and water.

4.2.1 Optimisation of markers for multiphoton microscopy.

The aim was to optimise markers for multiphoton microscopy for detection of synaptic terminals, blood vessels and β-amyloid, with for the purpose of using this technique to

investigate the dynamic changes of postsynaptic terminals after an ischaemic lesion in the presence of β-amyloid.

4.2.1.1 Cranial window implantation

To enable dynamic changes in the brain to be visualised by *in vivo* imaging, the mice had cranial windows implanted and a head-plate fitted. This procedure was carried out by Dr Koudelka. The mice were anaesthetised in a chamber with 3% isoflurane, transferred to a stereotactic frame and maintained with 1.5-2.5% isoflurane. The fur from the top of the head was shaved off and eye ointment was applied. A cotton bud soaked in 70% ethanol was used to sterilise the exposed skin and a midline incision was made running from between the eyes to the top of the ears. Vetbond was applied to the edges of the skull, to seal the skin on the sides and prevent leakage underneath the head-plate. Once this has dried, Superglue Precision Max was applied to cover the Vetbond. The window was made in the skull by drilling as close to the midline as possible and just posterior to bregma, to expose the somatosensory cortex above the hippocampus: burr size 5 (0.5 mm) and drill speed of 2x1000 rpm. The part of the skull to be lifted was drilled more thinly, whilst the other side was left thicker and acted like a hinge. A sterile glass cover glass was cut to size, 3 x 3mm. A drop of saline was placed on the craniotomy and let soak into the skull for 10 minutes. Forceps were used to lift the skull fragment and with some saline on the back the cover glass was placed over the craniotomy and glued in place. Following this, the headplate was glued to the skull so it sits flat on the head, and the glue was allowed to dry for 20 minutes. Dental cement was applied to the outside of the headplate and covering the skull to make the craniotomy watertight. Finally, the animals were injected with 0.5mL of saline and allowed to recover in an incubator.

4.2.1.2 Multiphoton microscopy imaging

The first multiphoton imaging session took place at 24 hours after cranial window implantation, with follow up imaging up to 2 months afterwards. The mice were anaesthetised in a chamber and then transferred to a platform and maintained with 1.5-2.5% isofluorane with a mask. The dextran dye for vasculature detection was introduced through the tail vein (see below), before placing the mouse on its front on a moveable platform and securing its head-plate to it with screws. The success of the tail vein injections were checked under a fluorescent microscope before transporting the mice to the multiphoton microscope. Eye ointment was applied and the cover glass over the

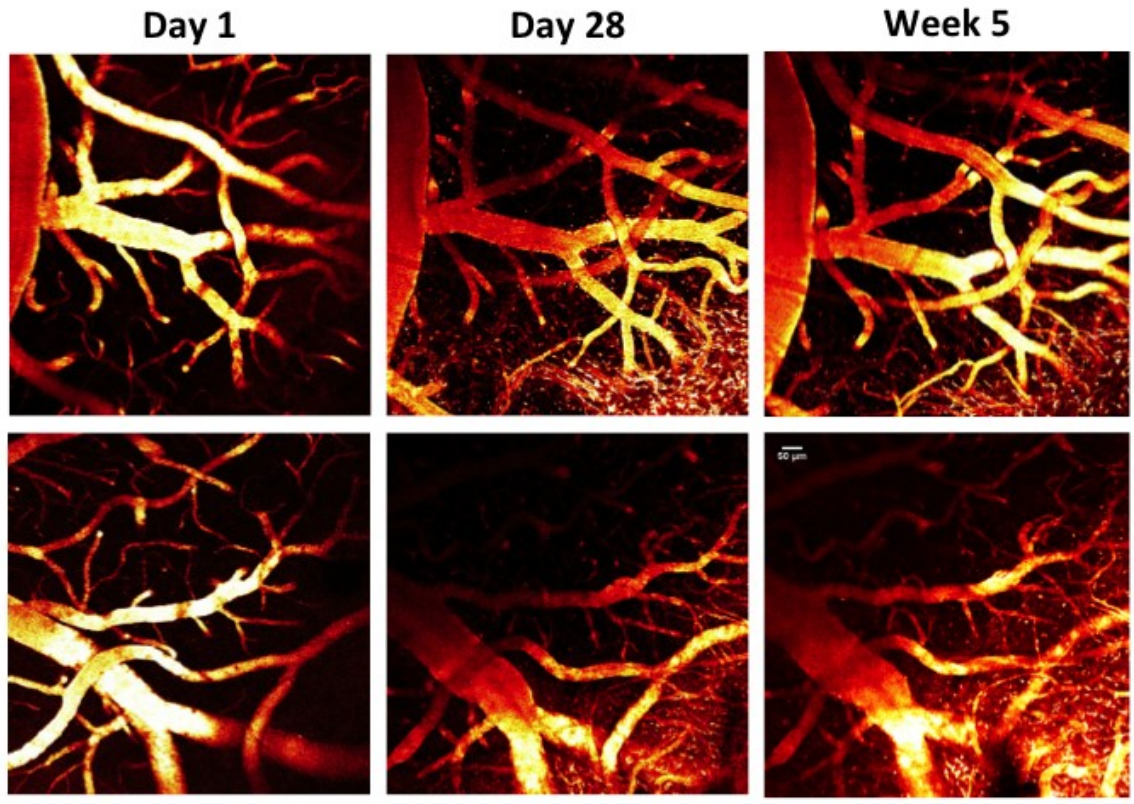

Figure 4.1 Multiphoton microscopy of the cerebrovasculature, with Texas Red detection. Multiphoton images from two mice, imaged at 1 day, 28 days and 5 weeks after cranial window implantation. Scale bar = 50µm.

craniotomy was cleaned with distilled water. The mouse's body temperature was monitored with a rectal thermometer and heated mat under its body, plus probes to monitor heart and breathing rates were used. The platform was placed in the chamber of the multiphoton and positioned with the objective above the cranial window for imaging.

4.2.1.3 Vasculature detection

Blood vessels were visualised with fluorescent dextran dyes, which were injected into the tail vein just before imaging. Initially, Texas Red dextran (Molecular probe, D1830) was used for this. Figure 4.1 shows the two examples of multiphoton imaging of the vasculature in mice 24 hours, 28 days and 5 weeks after cranial window implantation. At 24 hours after surgery, the vasculature was clearly detectable and could be imaged up to a depth of 400µm from the surface of the cortex. At the follow-up imaging sessions, many bright fluorescing cells were observed around the vasculature at 28 days and 5 weeks after cranial window surgery. We speculated that the cranial window surgery had caused a localised inflammatory response, and these cells were 'mopping up' any Texas Red dextran that had leaked from the vessels. This would be a major caveat for use in future studies, as local inflammation reduced the clarity of the images and the depth of successful imaging, plus could effect the outcome of focal ischaemia.

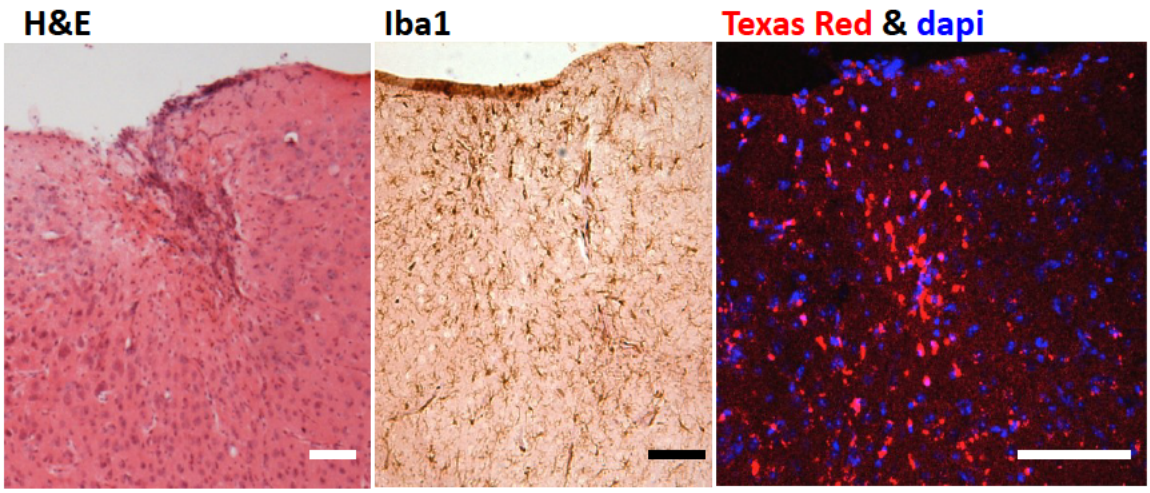

Figure 4.2 Histological analysis of brain tissue from mice with cranial window for 2 months. Haematoxylin and eosin showed tissue damaged in the region of the cranial window. There appears to be some clustering of Iba1+ cells within this area. Texas Red is retained in the cells in the sectioned tissue and also shows clustering in this region. Scale bar = 100µm.

Two months after cranial window surgery, the mice were transcardially perfused (Section 2.5.1.1) and the brains were processed and coronally sectioned with a cryostat (Section 2.4.1.2). Sections taken from the region where the cranial window sits and were stained with haematoxylin and eosin (Section 2.6.1). Figure 4.2 revealed that there was some tissue damage, with pallor and clustered nuclei, which may be inflammatory cells. Serial sections were immunostained for Iba1 (Section 2.6.3.1) to determine whether there was a microglia/macrophages response at the site of the cranial window. These sections were imaged with a brightfield microscope, a 10x objective. Another section was slide-mounted in vectashield hardset with DAPI (Vector H-1500) and imaged with confocal microscopy (Section 2.6.4.1), with 10x objective. There appeared to be some Iba1+ cells with activated morphology, with thicker processes and rounder bodies. Moreover, there was clear clustering of Texas Red+ cells in the fluorescent images. This analysis confirms that there is a local inflammatory response at the site of the cranial window, however, further

immunostaining and colocalisation of the Texas Red signal would be required to determine the type of inflammatory cells.

Texas Red dextran has a molecular weight of 70,000. Fluorescein isothiocynate (FITC) dextran (Sigma FD2000S) was tested as an alternative vascular marker, with a molecular weight of 2,000,000, as the larger size of the dye may prevent it from leaking from the vasculature. Figure 4.3 shows the vasculature with FITC dextran staining in C57Bl/6J mice. This dye, however, could not be used in PSD95:eGFP mice because of the overlapping wavelengths of the two markers.

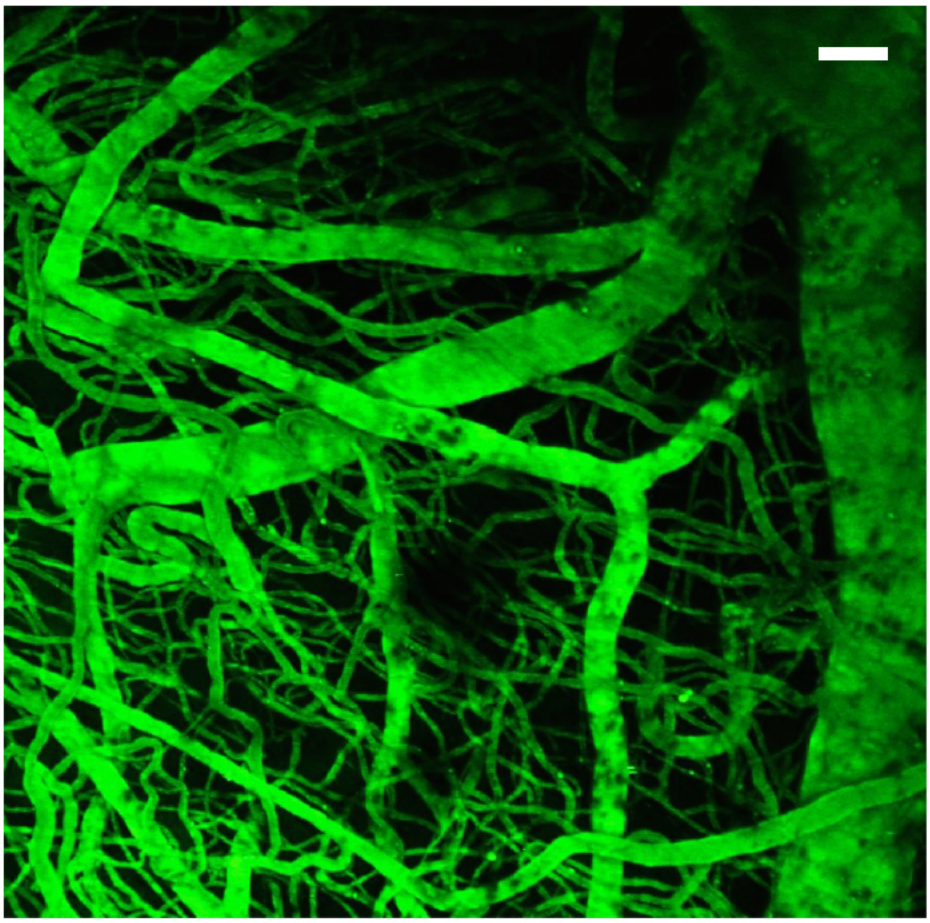

Figure 4.3 Vascular detection with FITC dextran, captured with multiphoton microscopy. Scale bar = 50μm.

4.2.1.4 PSD95:eGFP synaptic terminals

The multiphoton system used is LaVision TrimScope III with ImSpector for image acquisition. PSD95:eGFP mice were used to detect postsynaptic densities. The eGFP signal was imaged with 10x and 25x objectives, and could be imaged at a depth of around 200µm

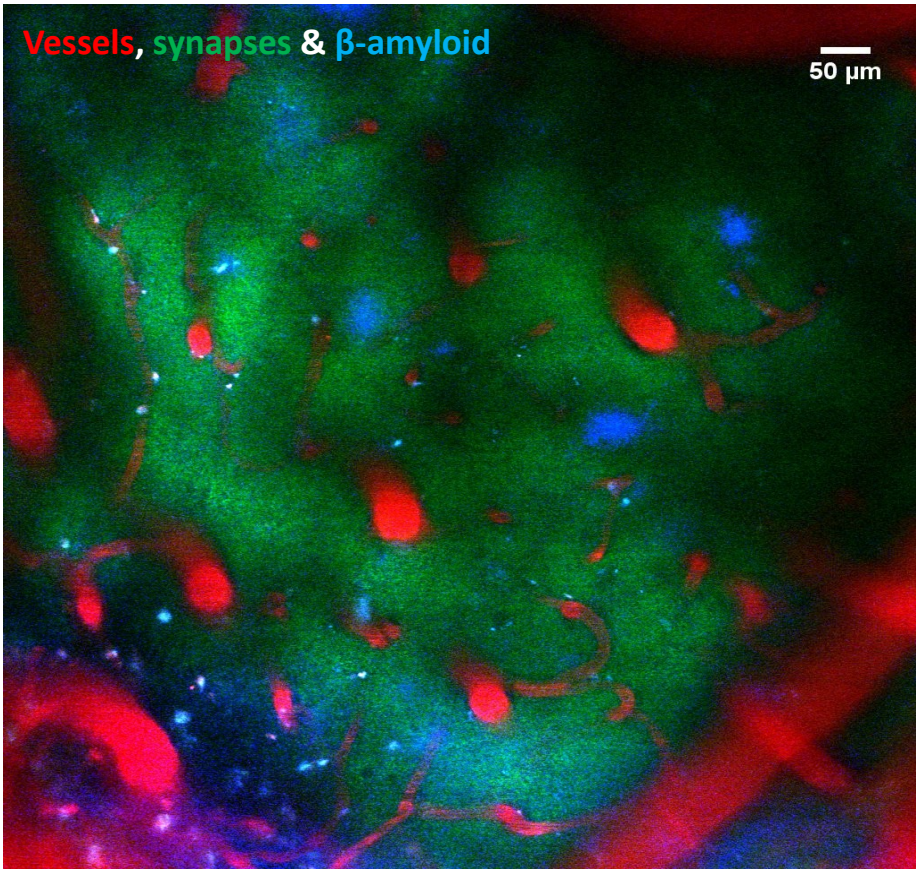

Figure 4.4 Detection of vessels, PSD95+ postsynaptic terminals and β-amyloid, captured by multiphoton microscopy. Scale bar = 50µm.

from the surface of the cortex. An issue we found with this approach was that large blood vessels on the cortex created shadows on the synaptic terminals, which would make it difficult to measure the density of synaptic terminals and determine whether they had changed between imaging sessions. Furthermore, the resolution of the eGFP signal was not good enough to see individual terminals or clusters (see Figure 4.4).

4.2.1.5 β-amyloid deposits

Methoxy-XO4 is a dye for detecting β-amyloid deposits. PSD95:eGFP x TgSwDI mice were injected with Methoxy-XO4 via intraperitoneal injection 24 hours before imaging. Figure 4.4 shows multiphoton image detecting Methoxy-XO4, Texas Red Dextran, and PSD95:eGFP in the somatosensory cortex, 120µm below the surface.

4.2.2 Optimisation of focal ischaemia by photothrombosis

4.2.2.1 LED light source

Experiments to optimise Rose Bengal photothrombotic occlusion were undertaken with the intention of using this approach to investigate the longitudinal effect of ischaemia and β-amyloid on postsynaptic terminals. Rose Bengal is activated by wavelength 532nm. Initially the approach was performed by illuminating the cortex with a LED/HBO fibre focused into the tissue with a 25x, 40x or 63x objective in the multiphoton microscope. Rose Bengal solution was prepared a day prior to injections (25 mg/mL in sterile PBS) and kept in the dark thereafter. As Rose Bengal dissipates quickly, there is only a window of 10-15 minutes between intravenous injection and illumination. Once the dextran dye was injected and the clarity of the window checked, the anaesthetic rig was moved to the multiphoton microscope and the mouse's headplate was attached to the platform. The platform was placed in the chamber, immediately putting the second anaesthetic mask over the mouse's nose, and arranging the position of the stand and mask with the 10x objective needed for imaging over the cranial window, and to check for the location of the vasculature. The mask was secured with tape and more tape was used to mark out the location of the platform. The platform was then removed back to the anaesthetic rig and the first mask used to maintain the aesthesia. Then 100µl of Rose Bengal solution was

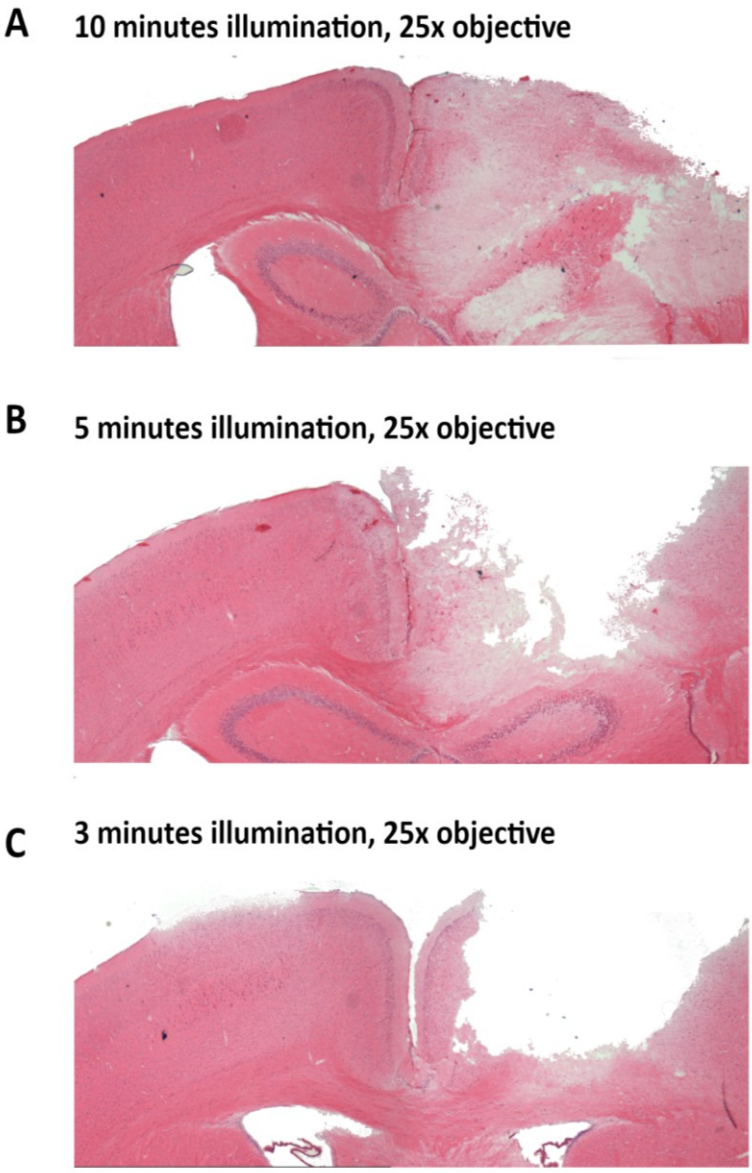

Figure 4.5 Lesions at 24 hours after Rose Bengal photothrombosis, using 25x objective lens for illumination, 100% strength and for different durations. Haematoxylin and eosin stained sections.

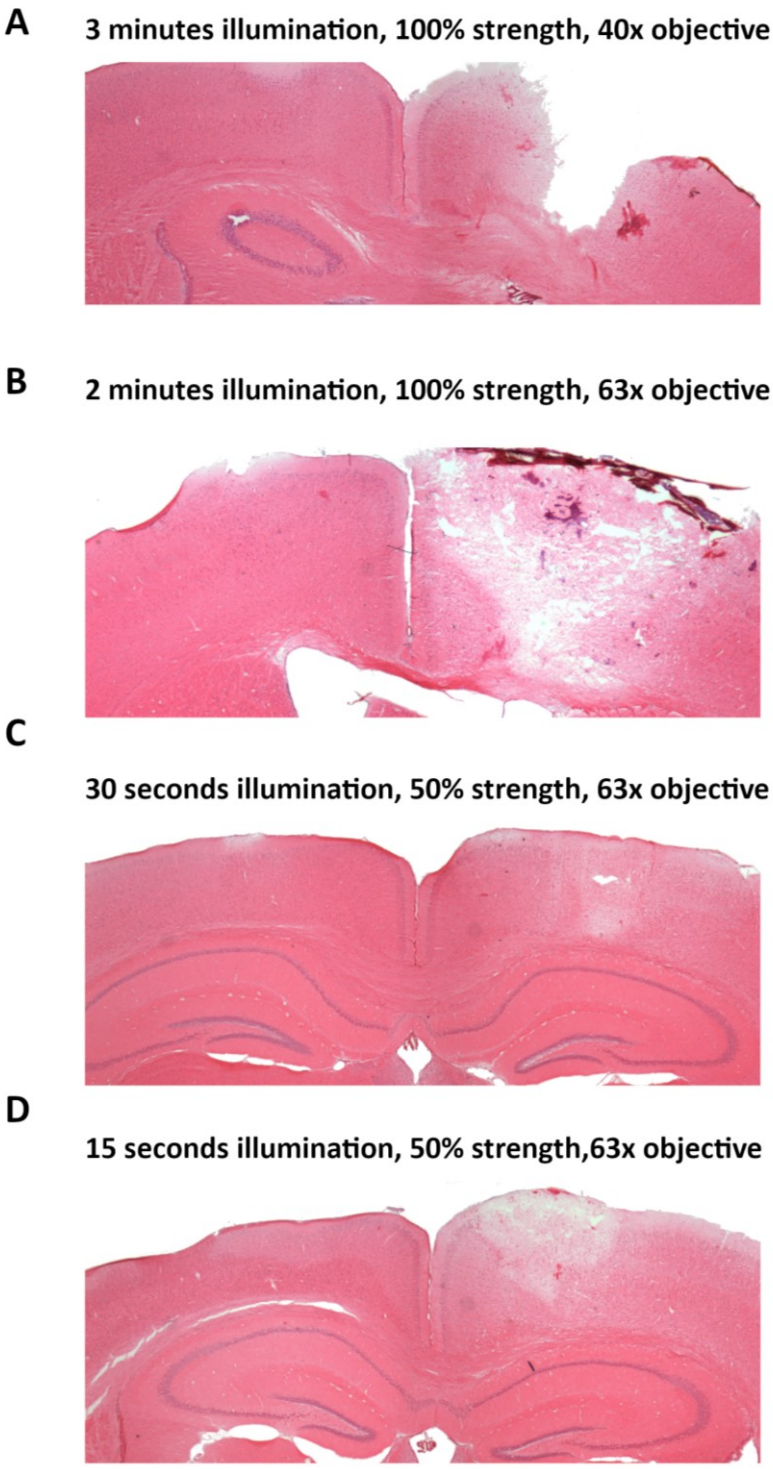

Figure 4.6 Lesions at 24 hours after Rose Bengal photothrombosis, using 40x and 63x objective lens for illumination, 100% and 50% strength and for different durations. Haematoxylin and eosin stained sections.

administered via the tail vein, and the 10x objective was replaced with 25x, 40x or 63x objective for illumination. Immediately after Rose Bengal injection, the platform was put back in the chamber, using the marks to find the right position quickly and the brain was illuminated through the LED/HBO fibre. The different objectives were tried with different LED strengths and illumination durations. The mice were perfused (Section 2.5.1.1) 24 hours later and the brains were processed and coronally sectioned with a cryostat (Section 2.4.1.2). Haematoxylin and eosin stain (Section 2.6.1) was used to access the extent of ischaemia damage. Figure 4.5 and 4.6 shows the resulting histology. Table 4.1 shows the

Table 4.1 Lesion areas and brain surface lengths resulting from different objectives, illumination duration, and LED strengths used for photothrombosis.

Animal code	Objective	Illumination time	LED strength	Lesion area (mm^2)	Surface lesion length (mm)
1	25x	10 mins	100%	11.004	4.524
2	25x	5 mins	100%	6.969	3.575
3	25x	3 mins	100%	3.247	2.654
4	40x	3 mins	100%	4.178	3.067
5	63x	2 mins	100%	5.422	1.961
6	63x	1 min	100%	2.281	2.727
7	63x	90 sec	100%	3.441	3.361
8	63x	90 sec	100%	3.405	3.209
9	63x	90 sec	80%	3.141	2.119
10	63x	90 sec	80%	3.685	2.470
11	63x	30 sec	50%	1.352	2.494
12	63x	12 sec	50%	1.287	1.443

area of lesion and the length of the lesion on the brain surface. As the cranial window was 3x3mm in size, the lesions had to be smaller to be able to capture the changes within the lesion and peri-lesion, however, the method here mostly resulted in lesions that were too large, this may have resulted from too much light scattering. The next stage was to modify this approach to get a more focal lesion, which was done using a fibre optic cable.

4.2.2.2 Fibre optic

A different approach was tried, using a fibre optic to target the region with stereotactic frame. This method was performed on C57Bl/6J without cranial windows, and laser speckle imaging was used to identifying regions of low cerebral blood flow. This procedure was conducted by myself with the assistance of Jessica Duncombe.

Rose Bengal solution was prepared as before (25 mg/mL in sterile PBS). The mice were anaesthetised in a chamber and then transferred to the stereotactic frame and maintained with 1.5-2.5% isofluorane with a mask. Their body temperature was monitored with a rectal thermometer and a heated mat. The skull was exposed and laser speckle imaging was used to record the baseline blood flow (Section 2.3). One end of a fibre optic cable (0.75mm diameter) was attached to the arm of the stereotactic frame and set to the coordinates of: 1.50mm right from the midline, and -1.70mm from Bregma; to target the somatosensory cortex above the CA1. The fibre optic was positioned so the end was touching the exposed skull, to reduce lateral light scattering. 100µl of Rose Bengal solution was injected via the tail vein, keeping the room as dark as possible to prevent its activation. Once the solution had been injected, a surgical lamp was turned on away from the mouse, with the other end of the optical fibre cable held to it to illuminate it and the skull in the targeted area. Illumination durations of 2 and 3 minutes were tried for different mice. Laser speckle imaging was performed immediately after to capture the acute blood flow

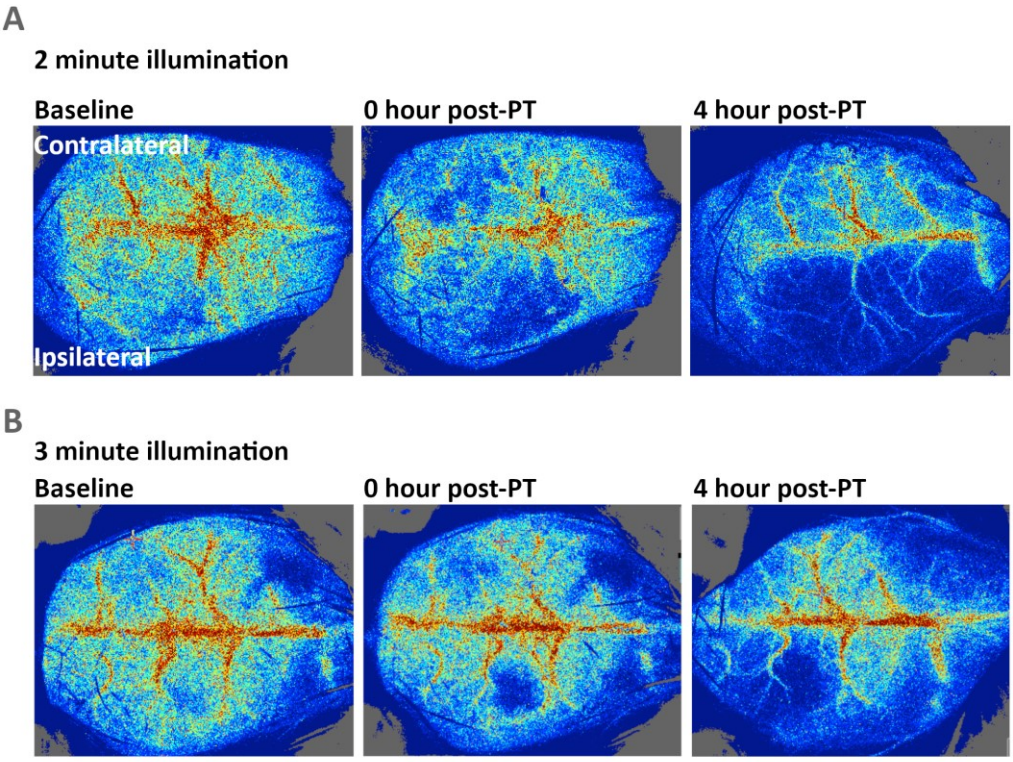

Figure 4.7 Laser speckle images showing in cortical cerebral blow flow changes at baseline, immediately after photothrombosis and 4 hours after photothrombosis.

change. The midline incision was closed up with a suture and the mice were recovered in an incubator. 4 hours later, laser speckle imaging procedure was repeated to measure blood flow changes. Mice were culled by schedule 1. Figure 4.7 shows the laser speckle images after 2 and 3 minute illumination. The laser speckle images at 0 hours already start to show a region of low CBF in the ipsilateral cortex, which increased in size by 4 hours post-photothrombosis. Although these images were not quantified and there was only 1 mouse for either 2 or 3 minute illumination, there was concern that the mouse that had received 2 minute illumination had a far larger region of low CBF than after 3 minute illumination. As longer illumination duration should increase the size of the ischaemic area,

this was indication that this approach may have poor reproducibility and an alternative model of focal ischaemia was chosen for future studies.

4.3 Discussion

4.3.1 Multiphoton microscopy

The use of multiphoton *in vivo* imaging through a cranial window in the skull is a beneficial approach for capturing dynamic real-time changes and to enable re-imaging of the same animals at different time-points. This could be particularly useful in the stroke field, as there is a disconnect in understanding how focal ischaemia can cause progressive damage, culminating in cognitive decline and dementia. The techniques described in this chapter were being optimised for a study to investigate the changes in density in excitatory postsynaptic terminals, at acute and chronic time points after a focal ischaemic lesion in the cortex of WT and TgSwDI mice. These procedures were very technically demanding and eventually we decided to change the approach to use the MCAO model, as presented in the following chapters.

The disadvantages of multiphoton imaging through a cranial window is that only a small area of the brain can be analysed, as the window size was 3x3mm, and the depth of imaging was 450µm, at best. These limitations could be overcome by adapting the cranial window techniques, such as using silicone-based polydimethylsiloxane (PDMS), which is flexible, transparent and allows better light penetration (Heo et al. 2016). This publication reported that their PDMS cranial windows for mice could be 18mm^2, and they could image to 550µm from the surface of the brain. Another benefit of PDMS window is that a micropipette can be used to inject through it, therefore, ion-sensitive dyes or pharmacological substances could be applied directly on to the brain. This would also allow

for measuring electrical activity with electrodes, to determine whether the synapses undergo functional changes.

The initial plan for this study was to use multiphoton *in vivo* microscopy to detect changes in PSD95:eGFP+ terminals, however, the resolution was too poor to see individual terminals or clusters of them. Studies by Tim Murphy and colleagues frequently used this technique to capture dendritic spines, however, they used a 60x objective and a mouse model with YFP expressing in cortical layer V neurons. The highest objective we had available for imaging was the 40x lens. Plus, the fluorescent labelling in heterozygous PSD95:eGFP is on half of the PSD95 proteins, rather than a specific population of neurons. These issues made it challenging to resolve individual terminals. An alterative approach could be to use a transgenic mouse model which produces a fluorescent signal for neuronal activity, such as Arc-Venus or Arc-dVenus (Fernández et al. 2017; Rudinskiy et al. 2012). As previously described (Section 3.4.3), Arc is an excitatory postsynaptic protein that is produced on activation, and tagging it with fluorescent Venus or dVenus signifies when the neurons are active. This approach of detecting a change in the fluorescent intensity of Arc-(d)Venus signal may be more sensitive than measuring the density of PSD95:eGFP+ terminals, which would require high microscopy resolution.

Another problem that was encountered was that the cranial window appeared to induce long-term elevation of inflammatory cells, and these cells were made visible by engulfing Texas Red. Heo et al. stated that there were no clear differences in the density of microglia/macrophages or astrocytes at 10 weeks in the ipsilateral hemisphere of a rat with PDMS window compared to a naïve rat (Heo et al. 2016). There was, however, a clear increase in microglial density at 1 week in $Cx3Cr^{GFP+/-}$ mice. It is likely that any cranial window surgery is going to cause some acute inflammatory response, and the best way

around it is to use the correct controls and to image at time points before and after the inflammation. In the present study, these cells were still present up to 2 months after window implantation. As these cells were not visible with use of the larger molecule weight dye, FITC dextran, it indicated that the smaller Texas Red dextran was leaking from the vessels and being taken up by these cells. FITC dextran is a green dye so it could not be used in mice expressed PSD95:eGFP, as the signals would be indistinguishable from each other. An alternative approach could be to use an even larger red fluorescent dextran, such as Tetramethylrhodamine, which can be imaged with PSD95:eGFP and would be too large to leak from the vessels and be engulfed by inflammatory cells. Taken together, we experienced a number of technical challenges with optimising multiple markers for multiphoton detection, and decided to instead use histological approaches for improved microscopy resolution in future studies (Chapters 5 and 6).

4.3.2 Rose Bengal photothrombosis

Previous publications have used Rose Bengal photothrombosis to induce a small cortical ischaemic lesions, in order to investigate the acute impact on dendrite and dendritic spines (Zhang et al. 2005; Zhang & Murphy 2007). In the present case, experiments were undertaken to optimise Rose Bengal photothrombosis for use in a future study, sought to determine whether focal ischaemia leads to long-term postsynaptic degeneration, and whether this would be exacerbated in TgSwDI mice. Initially, activation of Rose Bengal was trialled using a LED/HBO light source focussed through the 25x and 40x objectives, however, this resulted in large lesions that extended beyond the area exposed by the cranial window. This was improved somewhat by the use a 63x dipping objective, although this presented additional challenges as this objective could be used to focus the light for Rose Bengal activation, but it was not compatible for imaging with this microscope. As the

brain could not be imaged with this objective, it was very difficult to precisely illuminate the same area of the cortex between each mouse. The technique was made even more challenging by the speed required, as Rose Bengal dissipates after 10-15 minutes. The best method to overcome these issues would be to use a laser, at wavelength 561nm, to activate Rosen Bengal, as used by (Porritt et al. 2012; Stokowska et al. 2016). This should result in a small, precise cortical lesion. Plus, this approach would enable imaging to occur whilst the occlusion is being formed.

Further to this, a fibre optic cable was used to activate Rose Bengal by illuminating the skull as specific stereotactic coordinates, for either 2 or 3 minutes. As described, laser speckle imaging was used to capture the cortical CBF at the baseline, 0 hours and 4 hours after the procedure. Although this approach enabled a precise area of the skull to be targeted, there still appeared to be large areas of low CBF in the ipsilateral hemisphere. Histological analysis of the tissue was not performed, however, so we do not know how large the resulting lesion was. Moreover, as previously described, the mouse with shorter illumination duration had a larger area of low CBF, which implied that even with this approach there may be issues with reproducibility.

Overall, the results of these experiments indicated that this approach of Rose Bengal photothrombosis was too variable and presented too many challenges for a study. Moreover, there were concerns that the limited resolution of the multiphoton microscope would be insufficient to detect changes in the densities of synaptic terminals. It was decided, therefore, that an alterative model of focal ischaemia would be used, middle cerebral artery occlusion (MCAO), which was then established by Dr. Jill Fowler.

Chapter 5: The long-term impact of focal ischaemia and concurrent TgSwDIAPP expression on glutamatergic synapses and glial responses within the ischaemic territory

5.1 Introduction

The previous study determined that glutamatergic pre- and post-synaptic terminals and dendrites are resilient to modest hypoperfusion. There was implication that ischaemic injury caused some degeneration of dendrites, indicating that greater structural changes would occur in a model of focal ischaemia. As described in Section 1.7.3., there is evidence that focal ischaemia results in acute changes in glutamatergic synaptic protein levels and a loss of dendrites and dendritic spines. In remains unclear, however, what long-term impact focal ischaemia has on glutamatergic pre- and postsynaptic terminals.

There is a considerable body of literature indicating that an interplay between vascular and Alzheimer's pathology exists, and that patients with concurrent vascular and Alzheimer's pathology have worsened cognitive outcome compared with patients with just vascular pathology (Snowdon et al. 1997). The mechanisms underpinning this interaction, however, remain ill-defined. As well as the impact of ischaemia on glutamatergic transmission, there is evidence that β-amyloid causes downstream dysfunction and degeneration of glutamatergic pre- and postsynaptic terminals. Our prediction was, therefore, that in cases of mixed vascular and Alzheimer's pathology, there would be exaggerated synaptic dysfunction and degeneration, culminating in worsened cognitive decline. Furthermore, as both ischaemia and β-amyloid are known to trigger glial responses, we predicted that in

conditions of mixed pathology there would be an exacerbated glial response, which would contribute to degenerative processes. A limited number of studies have investigated the effect of focal ischaemia surgery on mice with β-amyloid pathology and found exaggerated tissue damage and glial responses (Milner et al. 2014; Amtul, Shawn N Whitehead, et al. 2015), however, the impact of these comorbidities on glutamatergic pre- and postsynaptic terminals is unknown.

The present study was designed to further elucidate the long-term outcome of focal ischaemia and concurrent β-amyloid pathology on neurons and glutamatergic synapses within the occlusion territory in relation to the glial response and functional outcome. Transient focal ischaemia was induced with 15 minutes of MCAO in TgSwDI mice and in WT littermates. Protein markers to of glutamatergic synapses were analysed. The mice used in the study expressed PSD95:eGFP so their postsynaptic densities could be readily imaged with fluorescent microscopy. Finally, glial cells, microglia/macrophages and astrocytes were investigated.

5.1.1 Hypothesis

Focal ischaemia leads to long-term degeneration of glutamatergic pre- and post-synaptic terminals and neuronal structures, plus chronic neuroinflammation, within the occlusion territory, culminating in functional impairment. In cases with concurrent focal ischaemia and β-amyloid this results in exaggerated long-term degeneration of these structures, exacerbated chronic neuroinflammation, and worsening functional impairment.

5.1.2 Aims

The aim of this study was to elucidate whether transient MCAO causes worsened outcome for neuronal and synaptic degeneration in the ischaemic territory in TgSwDI mice

compared to WT mice, and whether these changes are related to differences in chronic glial responses.

5.2 Materials and Methods

5.2.1 Animals

Male WT and heterozygous TgSwDI littermates (on a heterozygous PSD95:eGFP background, Section 2.1.2) underwent either 15 minutes of sham or MCAO surgery. The mice were 4-6 months old at the time of surgery. Three mice were culled in the first week after surgery as they had adverse side effects. Five mice were excluded from the study for not meeting the inclusion criteria of having a diffuse ischaemic lesion in the striatum; as three of these mice had large striatal and cortical infarcts, whereas the other two had no ischaemic pathology. The final group numbers were WTxPSD95:eGFP sham n = 6; TgSwDIxPSD95:eGFP sham n = 5; WTxPSD95:eGFP MCAO n = 7 and TgSwDIxPSD95:eGFP MCAO n = 6. These mice were recovered for 3 months after surgery before harvesting the tissue for histological analysis. An additional three cohorts were included for generating tissue for biochemical analysis. These cohorts were composed of C57Bl/6J and heterozygous TgSwDI mice on C57Bl/6J background. 15 minutes MCAO surgery was performed on these mice at ages 4-6 months. The brains were harvested at three time points: 24 hours (WT MCAO n = 9, TgSwDI MCAO n = 8), 1 month (WT MCAO n = 8, TgSwDI MCAO n = 8) and 3 months (WT MCAO n = 8, TgSwDI MCAO n = 10). The animal group numbers chosen for this study were based on the breeding constraints, rather than power calculations. For the histology cohort, the mice were assigned so the cages contained both sham- and MCAO-operated animals. The mice in the histology cohort are the same mice as used for the study in Chapter 6.

The mice were maintained on a 12:12hr light/dark cycle and had access to food and water ad libitum. All experiments were conducted in accordance with the Animals (Scientific Procedures) Act 1986 and local ethical approval at the University of Edinburgh and were performed under personal and project licenses granted by the Home Office. The experiments and data analysis were conducted in a blinded manner, so the genetic and surgical status of the mice were unknown until the data sets were finalized and statistically compared between groups.

5.2.2 Middle cerebral artery occlusion surgery

MCAO and sham surgery was performed when the mice were 4-6 months old. The details of the surgery are described in full in Section 2.2.2.

5.2.3 Laser speckle imaging

Cortical CBF was analysed with a Laser Speckle Contrast Imager (Moor FLPI2 Speckle Contrast Imager, Moor Instruments, UK), at 24 hours and 4 weeks after MCAO surgery, for the biochemistry cohorts (Section 2.3). CBF was recorded for 3 minutes. The recordings were analysed using MoorFLPI-2 Review software (version 4.0). Regions of interest were placed over the contralateral and ipsilateral cortices, in region supplied by the MCA (see Figure 5.2). Ipsilateral CBF was normalised to the contralateral CBF for each mouse, and compared between WT and TgSwDI mice.

5.2.4 Ladder rung test

At 3 days, 6 weeks and 11 weeks following sham or MCAO surgery, the mice underwent the ladder-rung test to probe motor function (Section 2.4.2).

5.2.5 Tissue collection and tissue processing

Mice for histological analysis were transcardially perfused with PBS according to Section 2.5.1.1, 3 months after surgery. The brains were sectioned using the vibratome (Section 2. 5.1.3); the sections were cut to 30µm thick and every section was taken between coronal levels +2.58 and -2.92 from bregma, and stored in a 24 well plate in cryoprotective medium.

Mice for biochemical analysis were culled at 24 hours, 1 month and 3 months after surgery, by schedule 1 cervical dislocation, followed by decapitation (Section 2.5.2). As previously stated, the brains were sectioned into 2mm slices, divided into hemispheres, and frozen in liquid nitrogen. The middle slice (~0.38mm to -1.62mm from bregma) was thawed and the striatum was dissected from each hemisphere and homogenised, as stated Section 2.7.1.1. Protein concentration analysed was performed (Section 2.7.1.2) and the samples were prepared for western blotting.

5.2.6 Detection of ischaemic neuronal pathology

For each mouse a section was taken from the following coronal levels: +2.58, +1.54, +0.98, +0.74, -0.10, -1.06, -2.06 and -2.92, and stained with cresyl violet (Section 2.6.2). The areas of ischaemic neuronal pathology were visible as regions with selective neuronal loss (absence of large neuronal somas). These areas were manually mapped out on line drawings of each coronal levels (Figure 5.3B) and the areas were scaled and measured using ImageJ. The areas of ischaemic neuronal pathology at each coronal level were compared between WT and TgSwDI mice. The volumes of ischaemic neuronal pathology were measured as the area under the curve and the volumes were compared between WT and TgSwDI mice.

5.2.7 Detection of APP+ axonal bulbs

Axonal bulbs were detected with APP immunostaining, according the method in Section 2.6.3.1, on sections taken from the same eight coronal levels. The areas of the brain that contain APP+ axon bulbs were manually mapped out on the line drawings of the coronal levels, as described above, and the areas and volumes of axonal pathology were measured and analysed using the same method.

5.2.8 Detection of glutamatergic pre- and postsynaptic terminals

Glutamatergic presynaptic terminals were detected with immunofluorescent labelling of VGLUT1, according to Section 2.6.3.3, whilst postsynaptic terminals were detect by expression of PSD95:eGFP transgene. The tissue for this analysis was taken from -0.10mm from bregma. The fluorescent markers were imaged with a Zeiss Axio Scan.Z1 slide scanner microscope, capturing tiled images of the entire tissue section with a 20x objective. The image acquisition parameters were as follows in Table 5.1. DAPI signal was imaged and used by the software for stitching together the image tiles. The resulting images were then converted to tiff files using Zeiss.

Table 5.1 Imaging parameters for fluorescent slide-scanner microscopy.

Label	Fluorescent signal	Illumination wavelength (nm)	Light source intensity (%)	Exposure time (ms)
VGLUT1	Alexa Fluor 546	545-565	50	180
PSD95	eGFP	460-480	100	180
Nuclei	DAPI	355-375	80	10

5.2.9 Detection of microglia/macrophages and astrocytes

Microglia/macrophages were detected with immunostaining for Iba1, whilst astrocytes were detected with immunostaining for GFAP, using the protocol described in Section 2.6.3.1. Neighbouring coronal sections were taken from -0.10mm from bregma coronal level. The entire sections were imaged with the Zeiss Axio Scan.Z1 slide scanner, using brightfield acquisition and 20x objective.

5.2.10 Analysis of %density within lesion and peri-lesion

5.2.10.1 Lesion and peri-lesion regions of interest

The %density of VGLUT1, PSD95, Iba1 and GFAP was measured in the lesion and peri-lesion. The lesion area was delineated using the cresyl violet stained sections. The cresyl violet stained sections from coronal level -0.10mm were imaged with the slide scanner, using brightfield acquisition and 20x objective.

VGLUT1 and PSD95 were detected with fluorescent microscopy and the resulting images had different pixel densities to the brightfield images taken of the cresyl violet stained sections. The brightfield images had to be scaled to fit the fluorescent images, so regions of interest delineated on the brightfield images could be superimposed on the fluorescent images. The scaling method used required the brightfield cresyl violet images and fluorescent PSD95:eGFP images from the same mouse to be opened together in ImageJ, and for a line to be drawn in the same place across a ventricle on both images. The plugin 'Align Image by line ROI' was then used to scale the brightfield image, so the lines drawn across the ventricles are the same size. In the new-scaled brightfield images, the ischaemic lesions were delineated by manually drawing around the region of ischaemic neuronal

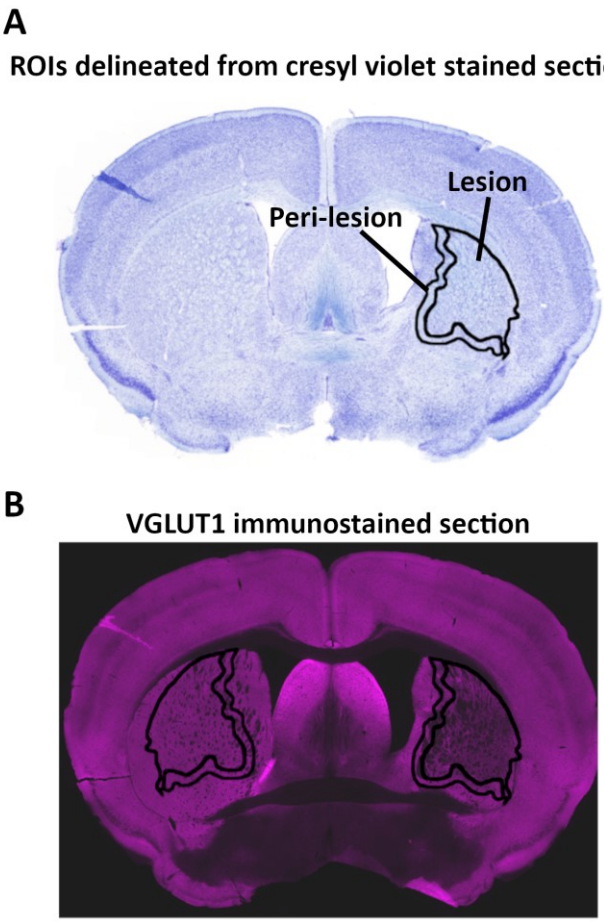

Figure 5.1 Lesion and peri-lesion ROI's delineated from cresyl violet stained sections. For each mouse, the lesion ROI was delineated from the ischaemic lesion from the image of cresyl violet stained section. The peri-lesion was constructed as a region of 100µm wide, surrounding the lesion. ROI's were superimposed onto the images to measure the %densities of VGLUT1, PSD95, Iba1 and GFAP for analysis. The images were flipped horizontally to measure the %densities of the markers on the contralateral hemisphere.

pathology in the striatum. These lesion regions of interest 'ROI' were then superimposed onto the fluorescent images of VGLUT1 and PSD95 detection for analysis within the area (Figure 5.1).

The peri-lesion ROI's were delineated as the region of 100µm wide around the outside of the lesion ROI within the striatum. These were constructed on ImageJ by using a

segmented line with the width set to 100µm, to draw around the lesion ROI. The 'Line to Area' function was then used to convert the line to an area with a width of 100µm to get the peri-lesion ROI (Figure 5.1). The lesion ROI and peri-lesion ROI for each mouse was superimposed onto the images with VGLUT1 staining and with PSD95:eGFP signal detection. The %density of VGLUT1 and PSD95 was measured with an autothreshold to cover the area of positive staining.

The same approach was used to measure the %densities of Iba1 and GFAP within the lesion and peri-lesion, however, as these were imaged using the brightfield the ROI's could be delineated from the images of creysl violet stained sections without scaling them first.

5.2.10.2 Sham analysis

The %densities of VGLUT1, PSD95, Iba1 and GFAP were also measured in the ipsilateral and contralateral striatum of the sham mice, and compared to the %densities in the contralateral striatum of the MCAO mice. This analysis was performed by measuring the %density of these markers within a square ROI of 19mm^3, which is the average area of the ischaemic lesion ROI's. The square ROI was consistently placed in the middle of the striatum on each hemisphere, to mirror the areas that are lesioned in the ipsilateral striatum of MCAO mice.

5.2.11 Colocalisation of microglia and PSD95:eGFP terminals

Sections from around – 0.10mm from bregma were taken from two WT and TgSwDI (x PSD95:eGFP), from the 3 month histology cohort. Microglia were detected with immunofluorescent detect of TMEM119, as described in Section 2.6.3.3. The tissue was imaged used confocal microscopy (Section 2.6.4.1), with 63x objective.

5.2.12 Western blot detection of VGLUT1, PSD95, Iba1 and GFAP

Western blot analysis was used to measure the protein levels of VGLUT1, PSD95, Iba1 and GFAP in enriched striatal tissue, taken from the ipsilateral and contralateral hemispheres of WT and TgSwDI mice, 24 hours, 1 month and 3 months after MCAO surgery. See Section 2.7.1.3 for method details.

5.2.13 Statistical analysis

Mann-Whitney test was used to statistically compare the normalised ipsilateral CBF between WT and TgSwDI mice, 24 hours and 4 weeks after MCAO surgery. Two-way ANOVA was used to statistical determine whether there was a surgery or genotype effect on limb placement %errors at 3 days, 6 weeks and 11 weeks after surgery. Bonferroni's multiple comparison test was used for post-hoc analysis. Two-way ANOVAs were used to compare the area of ischaemic neuronal pathology and axonal pathology at the different brain levels between WT and TgSwDI mice, whilst a Mann Whitney test was used to compare the total volume of ischaemic neuronal pathology and axonal pathology between the genotypes.

Two-way ANOVAs were used to compare between the %densities of VGLUT1, PSD95, Iba1 and GFAP in the ipsilateral and contralateral striatum of WT and TgSwDI sham mice. Two-way ANOVAs were also used for the comparison between the %densities of these markers in the contralateral striatum of WT and TgSwDI after either sham or MCAO surgery. Post-hoc analysis was performed using Bonferroni's multiple comparison test.

The %densities of VGLUT1, PSD95, Iba1 and GFAP immunostaining in the lesion and peri-lesion areas were statistically analysed with two-way ANOVA, to determine whether there were differences between the ipsilateral and contralateral hemispheres, and between WT

and TgSwDI mice. Plus, two-way ANOVAs were used to compare the %densities of these same markers from the contralateral striatum from WT and TgSwDI after sham and MCAO surgery. Post-hoc analysis was performed using Bonferroni's multiple comparison test. Spearman's rank correlation was used to establish whether %densities of VGLUT1 and PSD95 compared against %densities of Iba1 and GFAP.

Two-way ANOVA's were used to compare the protein levels between the hemispheres and genotypes, at 24 hours, 1 month and 3 months after MCAO, measured with western blotting. Bonferroni multiple comparisons was used as a post-hoc test.

For all analysis, $p<0.05$ was considered to be statistically significant.

5.3 Results

5.3.1 There were no differences in ipsilateral cortical CBF reduction between WT and TgSwDI mice at 24 hours and 4 weeks after MCAO surgery.

Cortical CBF was measured in the ipsilateral and contralateral cortex of WT and TgSwDI mice, 24 hours and 4 weeks after MCAO surgery, to determine whether there was a genotype effect on CBF reduction. Ipsilateral CBF, normalised to the contralateral hemisphere, was compared between WT and TgSwDI mice (Figure 5.2) Although at both time points CBF was reduced compared to the contralateral hemisphere (dotted line at 100%), there was no significant differences between WT and TgSwDI at 24 hours after MCAO ($p > 0.999$) and at 4 weeks ($p = 0.8541$). The values measured at 24 hours and 4 weeks were recorded from different cohorts of animals on different days, therefore, no

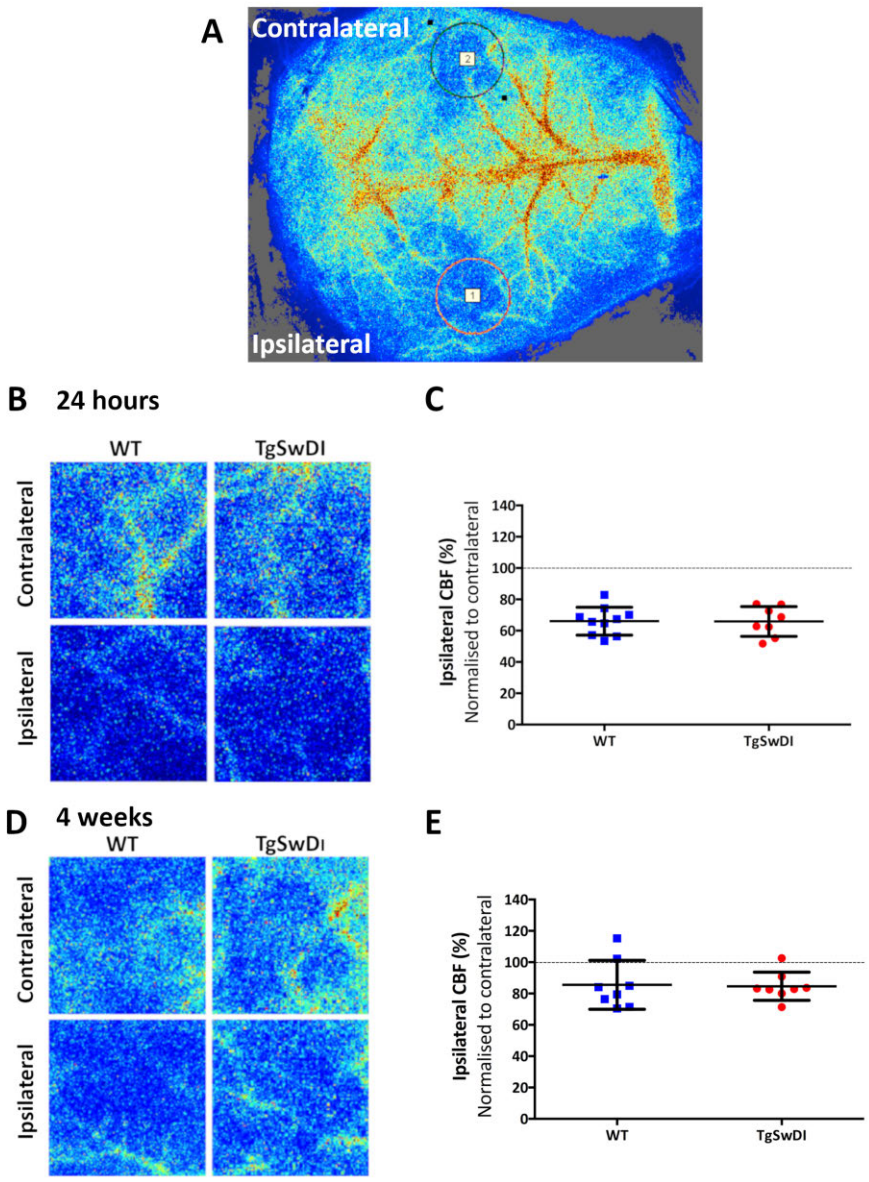

Figure 5.2 No difference in ipsilateral cortical blood flow between WT and TgSwDI mice at 24 hours and 4 weeks after surgery. (A) Laser speckle imaging used to measure cortical cerebral blood flow, ipsilateral normalised to contralateral. There were no differences in cortical blood flow reductions between WT and TgSwDI mice at (B,C) 24 hours and (D,E) 4 weeks after MCAO. Data presented as mean ± SD, n = 8-10 per group. Man-Whitney test.

statistical comparison was made between the two time points. However, the values from the two time-point do suggest that there may have been some restoration of blood flow between the acute and chronic time points post-MCAO. The result indicated that TgSwDIAPP expression does not worsen CBF reductions following MCAO surgery, and that any downstream effect of genotype on pathological changes is not a result of perfusion differences.

5.3.2 MCAO resulted in an acute motor deficit with long-term recovery, with no difference between WT and TgSwDI mice.

Movement problems in the contralesional limbs are common symptoms in patients with ischaemic damage/stroke in the middle cerebral artery territory, as injury to the striatum will cause motor impairment (Jorgensen et al. 1995; Cramer et al. 1997). A version of the ladder-rung test was used to determine whether 15 minutes of MCAO resulted in motor impairment, and whether there would be a worsened outcome in TgSwDI mice.

The apparatus set up for the ladder-rung test is shown in Figure 5.3A. A clear plastic ladder with regular rungs was suspended in a horizontal orientation, between a neutral start cage and the mice's home cage. These cages were stacked on top of empty upturned cages to raise them high enough for a camcorder to be placed underneath. The mice were given three trials of walking across the ladder and later their limb placements were analysed. For each mouse, the number of correct limb placements, partial limb placements and slips were recorded (Figure 5.3B) and the sum of partial placements and slips were divided by the total number of steps taken, to give a limb placement %error. This experiment was performed on groups of WT and TgSwDI mice 3 days, 6 weeks and 11 weeks after sham or MCAO surgery.

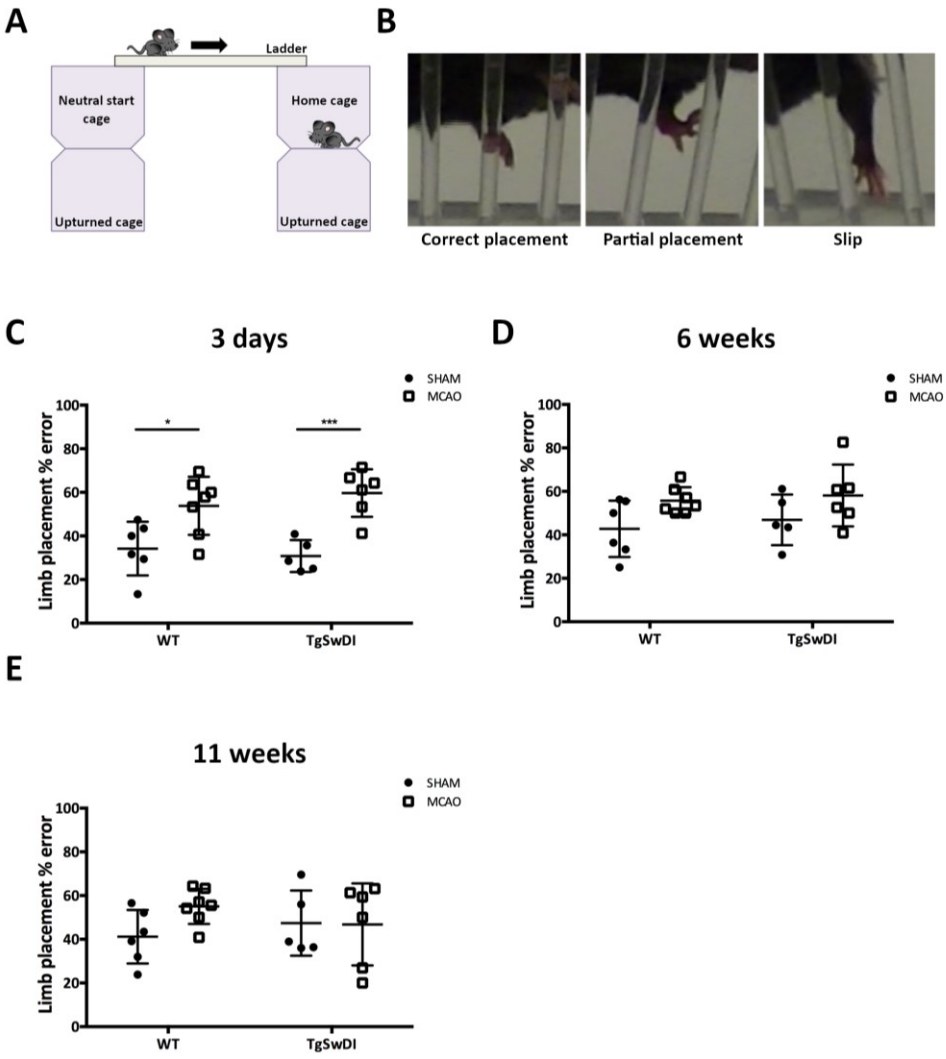

Figure 5.3 MCAO resulted in acute motor deficit. There were no deficits at later time-points. The ladder-rung test was used to probe for motor deficits. (A) Apparatus set up. (B) Type of limb placements. (C) At 3 days after surgery, there was a significant increase in limb placement % errors in MCAO mice compared to sham, in both WT and TgSwDI. At 6 weeks (D) and 11 weeks (E) there were no significant differences between the limb placement % errors in MCAO and sham mice, or with between WT and TgSwDI mice. Data presented as mean ± SD, n = 5-7 per group. Two-way ANOVA with Bonferroni's multiple comparison test. */***$p<0.05$.

At 3 days post-MCAO, there was an increase in the limb placement %error for MCAO mice in comparison to the shams ($F(1, 20) = 26.45$, $p < 0.0001$) (Figure 5.3C) and post-hoc analysis revealed that this increase occurred in both WT and TgSwDI mice. There was, however, no effect of genotype ($F(1, 20) = 0.0673$, $p = 0.798$) and no interaction between these factors ($F(1, 20) = 0.961$, $p = 0.339$). At 6 weeks, there was an overall effect of surgery ($F(1, 20) = 6.554$, $p = 0.0187$) (Figure 5.3D), however, Bonferroni multiple comparisons test did not show a significant surgery difference in either WT or TgSwDI mice. There was also no affect of genotype ($F(1, 20) = 0.485$, $p = 0.494$) or an interaction ($F(1, 20) = 0.0368$, $p = 0.850$) at 6 weeks. Finally, at 11 weeks there was no effect of surgery ($F(1, 20) = 1.379$, $p = 0.254$), genotype ($F(1, 20) = 0.0335$, $p = 0.857$) or an interaction ($F(1, 20) = 1.633$, $p = 0.216$) (Figure 5.3E).

These results indicate that at the acute stage there is an initial motor deficit caused by MCAO surgery, and the lack of statistical significance at later time-points suggests a possible restoration of motor ability. It also showed that there is no genotype effect, therefore, TgSwDIAPP expression does not cause greater motor deficit in these mice. The changes within ischaemic lesions at acute stages have been well characterised in many studies, however, the chronic changes are less well understood. Although the motor deficits are restored by 3 months post-MCAO, it is important to understand what damage is present in the brain at this time-point, and whether it is that affected by TgSwDIAPP expression. To answer those questions, the mice were culled the week after they had finished their last ladder-rung test, and their brains were harvested for histological analysis to address these questions.

5.3.3 MCAO caused long-term ischaemic neuronal and axon pathology, with no differential effect between WT and TgSwDI.

5.3.3.1 Ischaemic neuronal pathology

The next aim of the study was to determine whether transient MCAO causes long-term neuronal damage and whether these changes were exacerbated in TgSwDI mice. Cresyl violet stains cells bodies, and was used to analyse the regions of ischaemic neuronal pathology (Figure 5.4A). Fifteen minutes of MCAO resulted in diffuse ischaemic damage predominantly in the striatum. Two animals were excluded from the study as they showed no sign of ischaemic damage; whilst another three animals were excluded as their pathology was too severe and quite different from the other animals, with large infarcts and pan necrosis in the striatum and cortex.

Eight coronal sections were taken at specific levels throughout the brains and stained with cresyl violet. The images in Figure 5.4A are of cresyl violet stained sections at level -0.10mm from bregma, from WT and TgSwDI mice after either sham or MCAO surgery, imaged with 20x objective. The inserts show that in both hemispheres of the striatum in sham mice the neuron pathology looks normal in both genotypes, as many large neuronal cell bodies are present. The contralateral striatum of the MCAO mice for both genotypes appears to be indistinguishable from the shams, indicating that the surgery did not induce ischaemic neuron damage the contralateral hemisphere. In the ipsilateral hemispheres, however, there were diffuse regions with a clear absence of large neuron cell bodies. These regions of damage in the ipsilateral hemispheres were manually mapped out on line drawings of the coronal sections (Figure 5.4B), whilst observing the sections under the microscope. This is a standardised method for measuring tissue damage in stroke models (Osborne et al. 1987), to prevent under-estimation of the extent of tissue damage due to

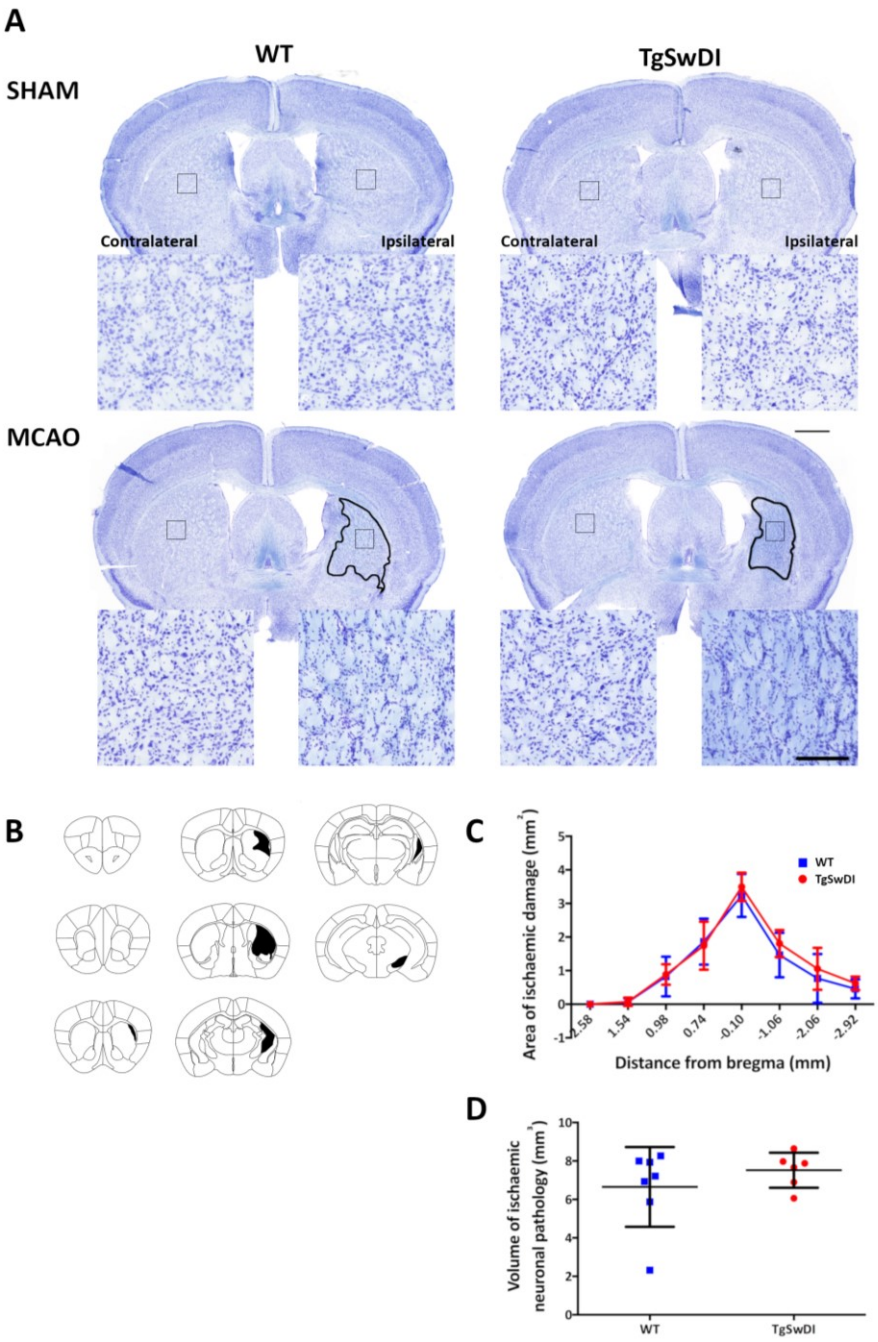

Figure 5.4 MCAO caused long-term ischaemic neuronal pathology, with no difference between WT and TgSwDI. (A) Cresyl violet stain was used to analyse ischaemia neuronal pathology, which was manually mapped out (B). (C) Areas of ischaemic neuronal pathology throughout the brain and (D) volume of ischaemic neuronal pathology were indistinguishable between WT and TgwDI. Data presented as mean ± SD, n = 6,7 per group. Two-way ANOVA and Mann-Whitney test. Scale bar = 1mm, 100µm insert. Grey boxes = inserts.

varying amounts of atrophy. The area of ischaemic neuron pathology and atrophy was measured from the line drawings, which were plotted against the distance from bregma. Statistical analysis showed that there was no significant difference in the area of ischaemic neuronal pathology between WT and TgSwDI mice at any of the coronal brain levels ($F(1,88) = 1.727$, $p = 0.192$) (Figure 5.4C). The volume of pathology for each brain was calculated as the area under the curve when pathology area is plotted against distance from bregma. There was no difference between the volume of ischaemic neuronal pathology between WT and TgSwDI mice ($p = 0.713$) (Figure 5.4D). These results showed that MCAO leads to long-term ischaemic neuronal pathology; however, TgSwDIAPP expression did not exacerbate the damage.

5.3.3.2 Axonal pathology

Axon damage has been shown to occur in regions of neurodegeneration in focal ischaemia models (Stephenson et al. 1992). To determine whether long-term axon pathology occurs following MCAO and whether there is a differential effect between WT and TgSwDI mice, axon bulbs were detected by immunohistochemistry for amyloid precursor protein (APP) (Figure 5.5A). APP is transported along axons under physiological conditions, however when axons become damaged, the protein accumulates into bulbs (Stephenson et al. 1992). The same method for measuring the volume of neuron pathology was applied to the analysis of axon pathology; regions containing axon bulbs on the ipsilateral hemisphere were manually mapped on the same line drawings of coronal levels (Figure 5.5B). As before, the areas of axonal pathology were plotted against the distance from bregma and the volumes were calculated. There were no significant differences in the areas of axonal pathology at each coronal level compared between WT and TgSwDI mice ($F(1,88) = 1.719$, $p = 0.193$) (Figure 5.5C). Furthermore, the volumes of axon pathology were indistinct

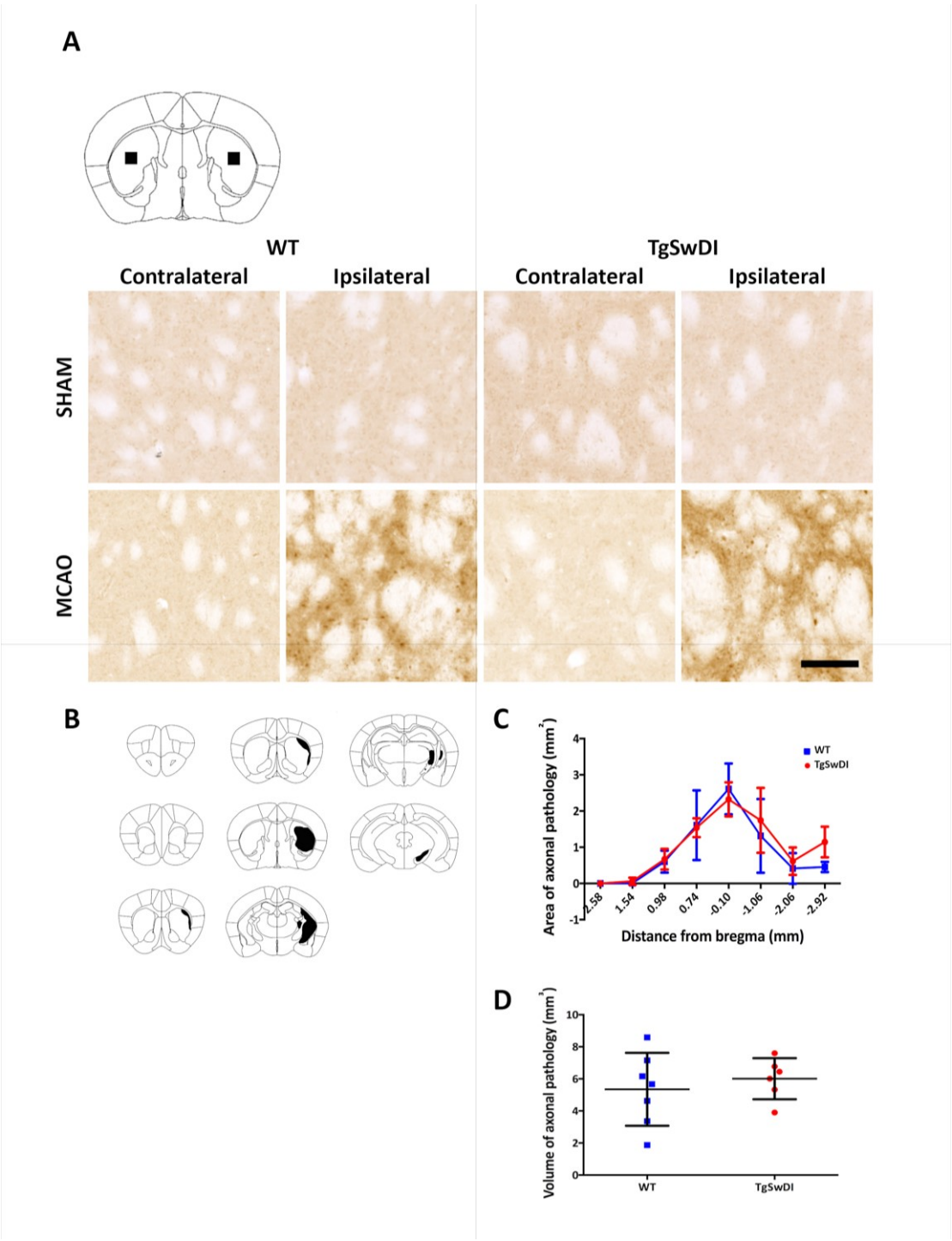

Figure 5.5 MCAO caused long-term axonal pathology, with no difference between WT and TgSwDI. (A) APP immunostaining was used to analyse axonal bulb pathology, which was manually mapped out (B). (C) Areas of axonal pathology throughout the brain and (D) volume of axonal pathology were indistinguishable between WT and TgSwDI. Data presented as mean ± SD, n = 6,7 per group. Two-way ANOVA and Mann-Whitney test. Scale bar = 100µm.

between WT and TgSwDI, (p = 0.615) (Figure 5.5D). This demonstrated that focal ischaemia causes axonal pathology throughout the brain, but this is not exacerbated by TgSwDIAPP expression.

5.3.4 MCAO lead to long-term loss of glutamatergic pre- and postsynaptic terminals within the lesion territory.

The previous study reported in Chapter 3 showed that glutamatergic pre- and postsynaptic terminals were resilient to modest global hypoperfusion, even in the CA1 where there were small areas of focal ischaemic damage in a subset of animals. We questioned whether a model using a more severe focal reduction in blood flow would cause synaptic changes, and whether another disease comorbidity, TgSwDIAPP expression, would exaggerate these changes. The next stage of the current study, therefore, was to determine whether MCAO results in long-term loss of pre- and post- glutamatergic synaptic terminals within the ischaemic territory, and whether there is a difference between WT and TgSwDI mice. The synaptic densities were analysed within the ischaemic lesion and the peri-lesion to determine whether synaptic terminals were vulnerable in regions with ischaemic neuron damage, and in the surrounding tissue with normal neuropathology.

5.3.4.1 Presynaptic terminal, VGLUT1

The densities of VGLUT1+ terminals were analysed with immunohistochemistry and image analysis. Before analysing the VGLUT1 %density in the ischaemic lesion, it was important to check that the VGLUT1 %density in the contralateral hemispheres could be used as the control measurements by comparing them to the sham mice. Immunofluorescent detection of VGLUT1 (in tissue from -0.10 mm from bregma level) and slidescanner imaging was undertaken for all animals at the same time. In the images, %density was measured a

square region of interest in the striatum from both hemispheres of sham animals and from contralateral hemisphere of MCAO animals (Figure 5.6A). Measurements from both hemispheres of WT and TgSwDI sham mice were compared to determine whether there was a genotype effect, and whether the sham surgery caused any synapse loss. These measurements were analysed with a two-way ANOVA, which found no differences between the striatal hemispheres ($F(1, 18) = 0.644$, $p = 0.433$), or between the genotypes ($F(1, 18) = 0.000596$, $p = 0.981$), and no interactions ($F(1, 18) = 0.410$, $p = 0.530$), confirming that in the sham mice VGLUT1 %densities were stable between both hemispheres and indistinguishable between the two genotypes (Figure 5.6B). The measurements for the contralateral hemispheres from the sham and MCAO mice were then compared to determine whether MCAO surgery affects synapses in the contralateral hemisphere. Two-way ANOVA analysis revealed that there was an overall significant surgery effect ($F(1, 20) = 4.600$, $p = 0.0444$), however, Bonferroni's multiple comparison test did not show a significant effect of surgery for either genotype. The data appears to show a slight increase in the VGLUT1 %density in the contralateral striatum of MCAO mice compared to the shams (Figure 5.6C). There was no genotype effect ($F(1, 20) = 0.572$, $p = 0.458$) and no interaction ($F(1, 20) = 0.000554$, $p = 0.982$) in these measurements. This result may indicate that MCAO surgery stimulates a small increase in the density of glutamatergic presynaptic terminals in the contralateral striatum. As these changes are small, the contralateral hemispheres of MCAO mice were used as the controls for the analysis of VGLUT1 changes in the ischaemic lesion.

Next, the VGLUT1 %density was measured from the lesion and peri-lesion in sections from MCAO mice. Specific regions of interest (ROI) for the lesion and peri-lesion were

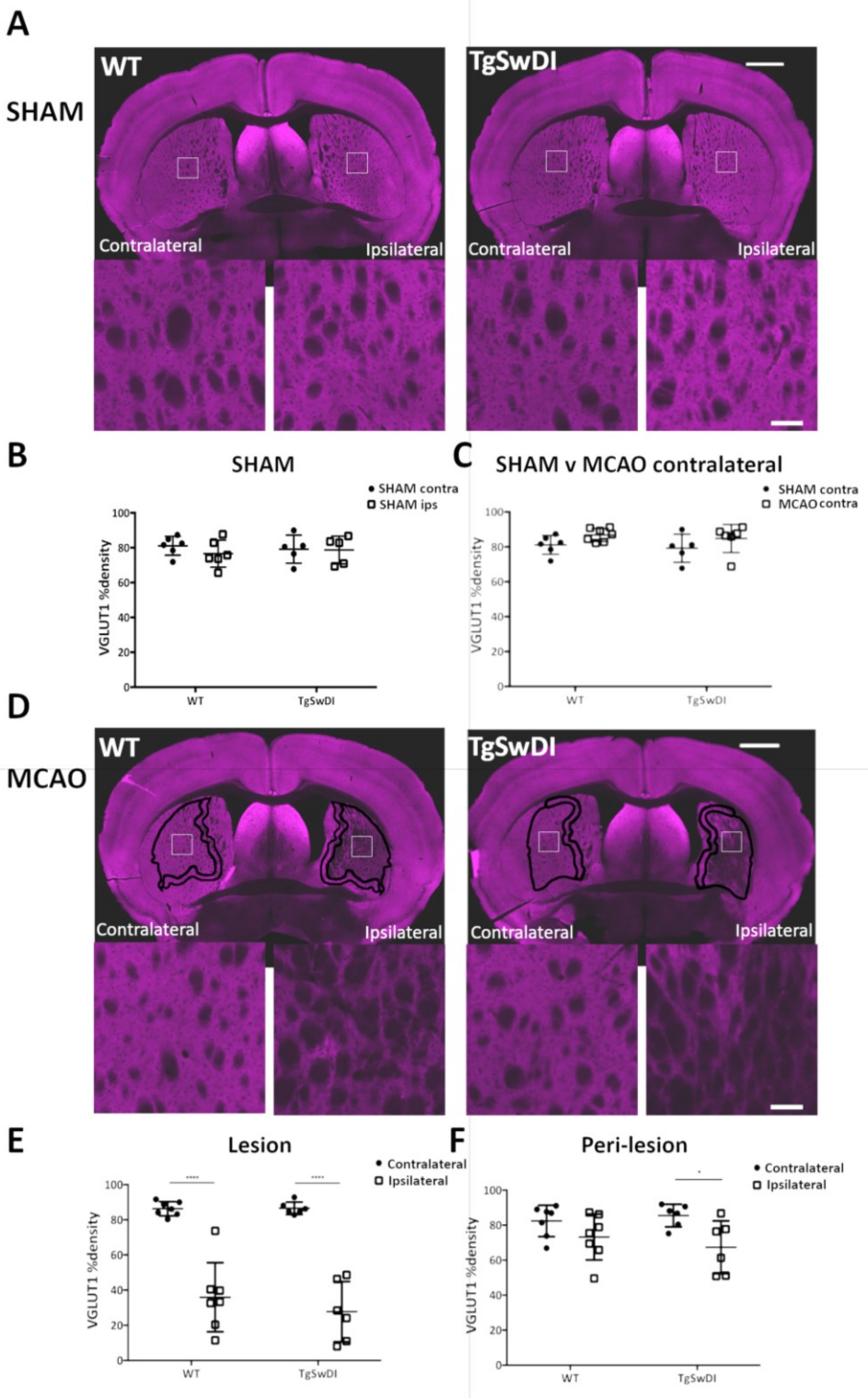

Figure 5.6 MCAO lead to long-term loss of glutamatergic presynaptic terminals within the lesion, and in the peri-lesion of TgSwDI mice. (A, D) Immunostaining for VGLUT1 used to detect glutamatergic presynaptic terminals. (B) VGLUT1 %density in sham mice was stable between the contralateral and ipsilateral striatum, with no difference between the

genotypes. (C) VGLUT1% comparison between the contralateral striatum of sham mice and MCAO mice of both genotypes showed an overall effect of surgery, but post-hoc analysis showed no significant differences between the groups, and no genotype effect. (E) VGLUT1 %density was reduced in the lesion in both WT and TgSwDI mice, no genotype effect. (F) VGLUT1 %density was reduced in the peri-lesion of only TgSwDI mice, although there was no overall genotype effect. Data presented as mean ± SD, n = 6,7 per group. Two-way ANOVA with Bonferroni's multiple comparison test. ***p<0.0001, *p<0.05. Scale bar = 1mm, 100µm insert. White boxes = inserts.

constructed from the cresyl violet stained section from each individual mouse (described in Section 5.2.10.1, and see Figure 5.1). These sections were from -0.10 mm bregma level, as at this level the area of ischaemic neuron damage is at its largest. The lesion ROI's were made by drawing around the area of ischaemic neuron pathology in the ipsilateral striatum with ImageJ, whilst the peri-lesion ROI was constructed by delineating an area of 100µm width around the lesion. To measure densities of markers on the contralateral hemispheres, the images were flipped horizontally.

The %density of VGLUT1+ presynaptic terminals were measured within the lesion and peri-lesion (Figure 5.6D), and compared between the hemispheres and genotypes to determine the long-term affect that MCAO and β-amyloid has on these structures. There was a significant surgery effect, reducing VGLUT1 %density in the striatal lesion in comparison to the contralateral hemisphere ($F(1, 22) = 107.3$, $p < 0.0001$), however, there was no difference between the genotypes ($F(1, 22) = 0.565$, $p = 0.460$) and no interaction ($F(1, 22) = 0.646$, $p = 0.430$) (Figure 5.6E). Post-hoc analysis revealed that the surgery effect was present in both WT and TgSwDI mice. There was a significant effect of surgery on the VGLUT1 %density in the peri-lesion ($F(1, 22) = 9.296$, $p = 0.0059$), although there was no effect of genotype ($F(1, 22) = 0.0946$, $p = 0.761$) and no interaction ($F(1, 22) = 1.002$, $p = 0.328$) (Figure 5.6F). Bonferroni's multiple comparison test showed that the surgery effect

causing a reduction VGLUT1 %density in the peri-lesion only reached significance in the TgSwDI mice. This result indicated that while presynaptic glutamatergic terminals are reduced in the focal ischaemic lesion, they are more resilient in the peri-lesion particularly in WT mice. Although there was no overall genotype effect, the significant reduction of VGLUT1 %densities in only TgSwDI mice may indicate that concurrent TgSwDIAPP expression does result in exaggerated degeneration of glutamatergic presynaptic terminals in the peri-lesion.

5.3.4.2 Postsynaptic terminals, PSD95

The next step was to determine whether MCAO surgery and TgSwDIAPP expression have an effect on the density of postsynaptic glutamatergic terminals. The mice used in this study express PSD95:eGFP, therefore, the density of PSD95+ postsynaptic terminals could be readily analysed in the same sections used to detect VGLUT1. As before, the %density of PSD95 was measured in contralateral striatum of the MCAO mice and in both hemispheres of the sham mice, and analysed to determine whether the PSD95 %density in the contralateral striatum remained stable after MCAO surgery. There were no significant differences in the PSD95 %density between the contralateral and ipsilateral striatum in the sham mice ($F(1,18) = 0.570$, $p = 0.460$), nor was there a genotype effect ($F(1,18) = 0.576$, $p = 0.458$) or an interaction ($F(1,18) = 0.891$, $p = 0.358$) (Figure 5.7B). This shows that the sham surgery does not cause a loss of postsynaptic terminals and there is no baseline genotype effect. When the PSD95 %density for contralateral striatum for the sham and MCAO mice were compared, similarly to VGLUT1, there was a significant surgery effect ($F(1,20) = 7.485$, $p = 0.0127$), but no effect of genotype ($F(1,20) = 0.554$, $p = 0.465$) and no interaction ($F(1,20) = 0.873$, $p = 0.361$) (Figure 5.7C). Post-hoc analysis revealed that there was a significant increase in PSD95 %density in the contralateral striatum of WT MCAO

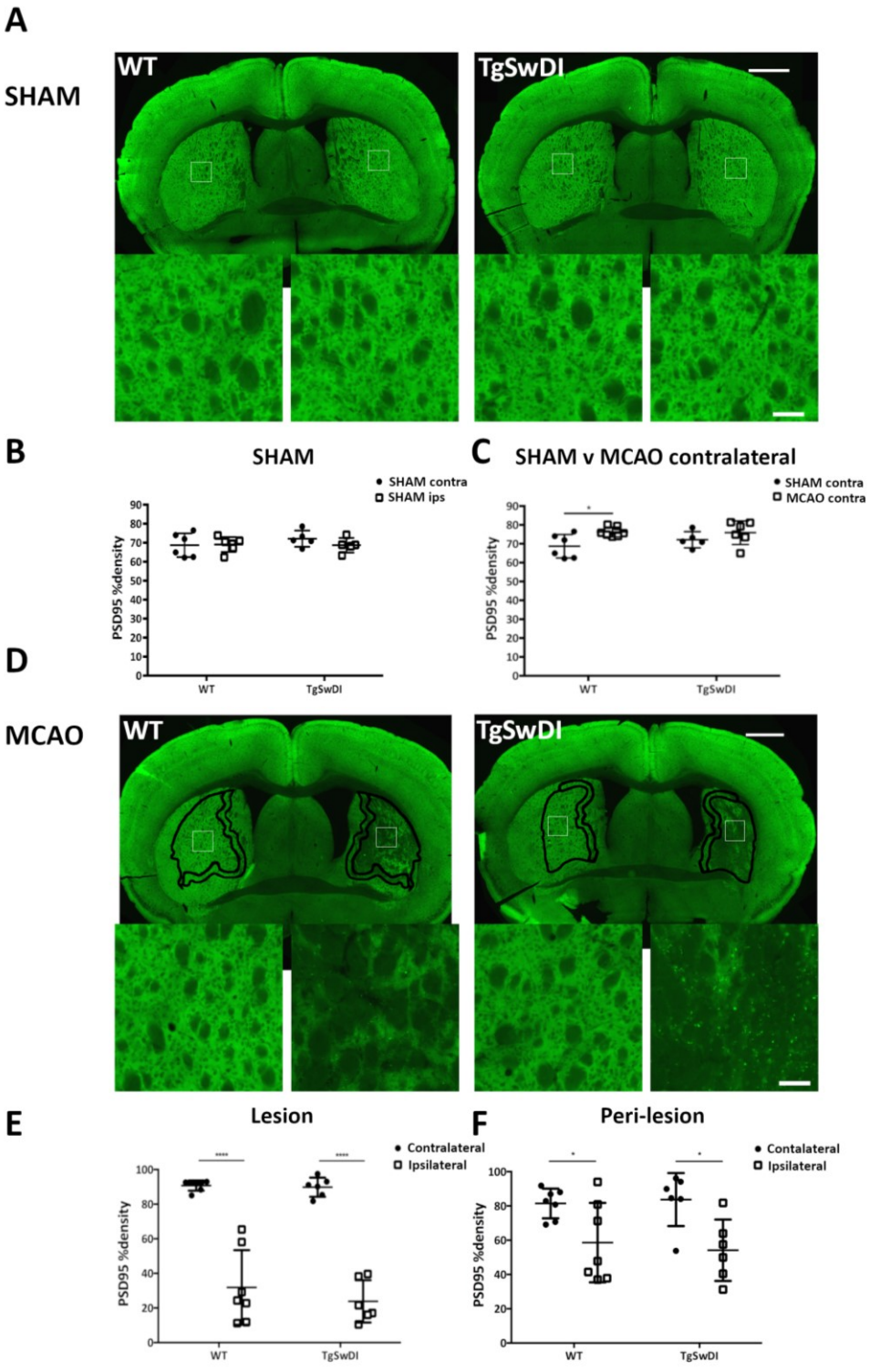

Figure 5.7 MCAO lead to long-term loss of glutamatergic postsynaptic terminals within the lesion and peri-lesion. (A, D) PSD95:eGFP to detect glutamatergic postsynaptic terminals. (B) PSD95 %density in sham mice was stable between the contralateral and ipsilateral striatum, with no difference between the genotypes.

(C) There was a small significant increase in PSD95 %density in the contralateral striatum of WT MCAO mice, compared to WT sham mice, with no differences in the TgSwDI mice. (E) PSD95 %density was reduced in the lesion of both WT and TgSwDI mice, compared to the contralateral hemisphere. (F) PSD95 %density was reduced in the peri-lesion of WT and TgSwDI, compared to the contralateral hemisphere. Data presented as mean ± SD, n = 6,7 per group. Two-way ANOVA with Bonferroni's multiple comparison test. ***p<0.0001, *p<0.05. Scale bar = 1mm, 100µm insert. White boxes = inserts.

mice compared to the shams, whereas there was no difference in TgSwDI mice. This analysis showed that there was a small increase of postsynaptic terminals in the contralateral striatum of WT animals following MCAO, however, as the difference was slight it was decided that the contralateral hemisphere would still be used as the control for analysing the effect of MCAO on postsynaptic terminals in the ipsilateral striatum.

The %density of PSD95 was measured in the same sections from MCAO mice as VGLUT1, using the same regions of interest (Figure 5.7D). The PSD95 %densities were significantly reduced in the striatal lesion in comparison to the contralateral hemisphere ($F(1,22) = 148.3$, $p < 0.0001$), although there was no effect of genotype ($F(1,22) = 0.760$, $p = 0.393$) and no interaction ($F(1,22) = 0.469$, $p = 0.501$) (Figure 5.7E). Post-hoc analysis showed that surgery effect on PSD95 %density occurred in the lesion of both WT and TgSwDI mice. PSD95 %densities were also significantly reduced in the ipsilateral peri-lesions compared to the contralateral hemispheres ($F(1, 22) = 15.10$, $p = 0.0008$), there was no effect of genotype ($F(1,22) = 0.0255$, $p = 0.875$) and no interaction ($F(1,22) = 0.250$, $p = 0.622$) (Figure 5.7F). Post-hoc analysis showed that surgery effect on PSD95 %density occurred in the peri-lesion of both WT and TgSwDI mice. These results showed that long-term loss of excitatory postsynaptic terminals occurs in the ischaemic lesion, as well as in the peri-lesion where there is no ischaemic neuronal damage. There was no difference between WT

and TgSwDI, showing that concurrent TgSwDIAPP expression did not worsen post-synaptic loss within the lesion or peri-lesion.

5.3.5 MCAO induced chronic glial responses within the lesion territory, with no differential effect between genotypes.

Chronic glial responses have been shown to be a feature of focal ischaemic injury, and are sensitive to β-amyloid pathology. There is also evidence that glial cells may have roles in synaptic loss and neurodegeneration. The next stage of the investigation, therefore, was to determine whether concurrent focal ischaemia and TgSwDIAPP expression would exacerbate the levels of glial cells, microglia/macrophages and astrocytes, and whether these related to synaptic loss. The densities of microglia/macrophages and astrocytes were analysed within the ischaemic lesion and the peri-lesion to determine whether chronic glial responses occurred in regions with ischaemic neuronal damage, and in the surrounding tissue with normal neuropathology.

5.3.5.1 Microglia/Macrophages, Iba1

Microglia/macrophage cells were detected using Iba1 immunohistochemistry and measured by image analysis, with similar methods to the synaptic analysis. As before, the levels were measured in the sham mice and compared with the contralateral hemisphere of MCAO mice (Figure 5.8). There were no significant differences in the Iba1 %densities between the contralateral and ipsilateral striatum of sham mice ($F(1,18) = 0.273$, $p = 0.607$), with no genotype effect ($F(1,18) = 1.725$, $p = 0.206$), and there was no interaction between these factors ($F(1,18) = 5.216$, $p = 0.0347$) (Figure 5.8B). This data showed that neither sham surgery or TgSwDIAPP expression lead to chronic elevation of

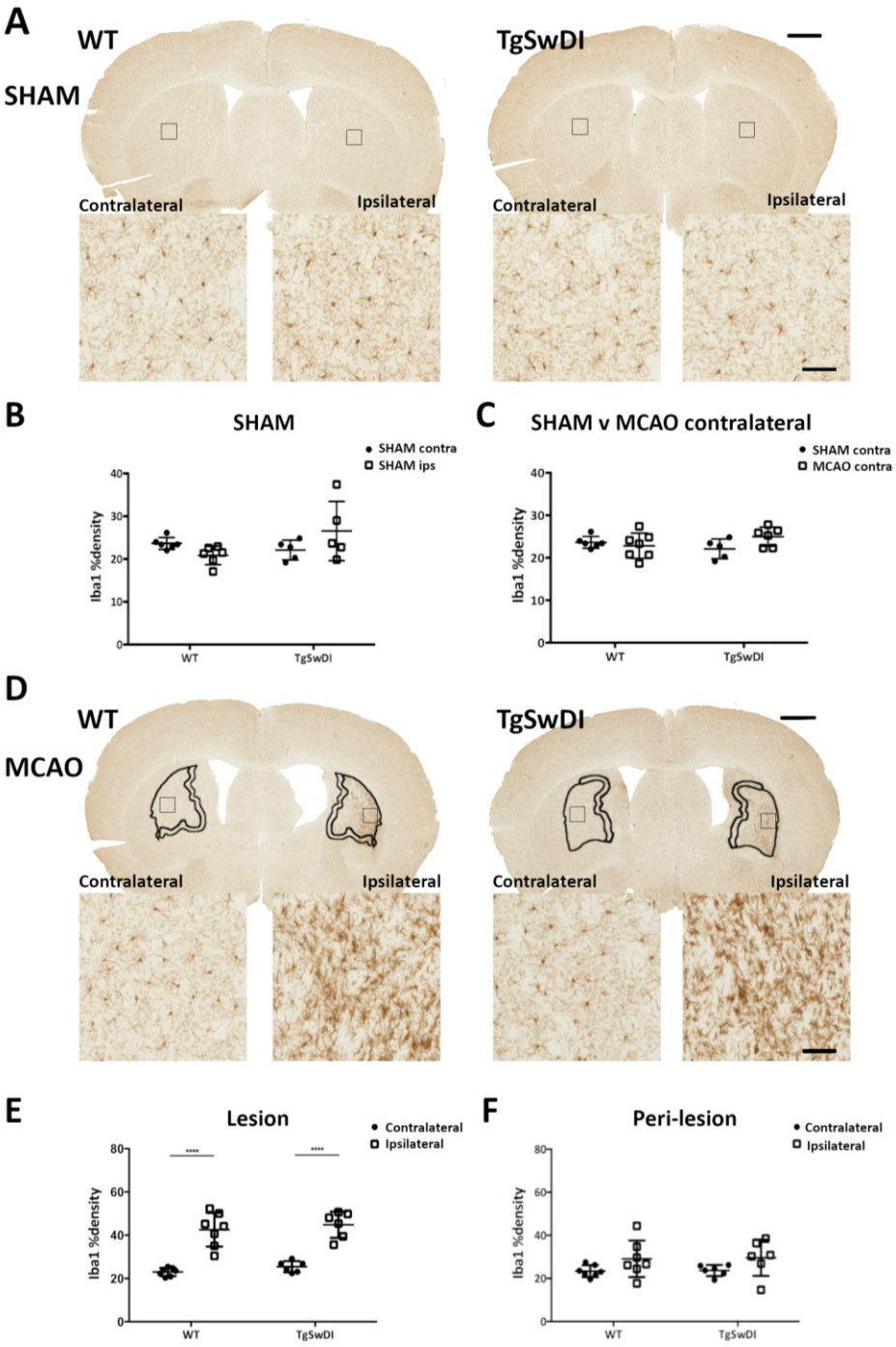

Figure 5.8 MCAO induced chronic microglia/macrophage elevation within the lesion. (A, D) Iba1 immunohistochemistry to detect microglia/macrophages. (B) Iba1 %density in sham mice was stable between the contralateral and ipsilateral striatum, with no difference between the genotypes. (C) Iba1 %density was unchanged between contralateral striatum of sham and MCAO mice, with no

effect of genotype. (E) Iba1 %density was elevated in the lesion, compared to the contralateral hemisphere, with no effect of genotype. (F) Iba1 %density was unchanged in the peri-lesion compared to the contralateral hemisphere, with no effect of genotype. Data presented as mean ± SD, n = 6,7 per group. Two-way ANOVA with Bonferroni's multiple comparison test. ***p<0.0001. Scale bar = 1mm, 100µm insert. Grey boxes = inserts.

microglia/macrophages in the striatum. Iba1 %density in the contralateral striatum of sham and MCAO mice, and found no effect of surgery ($F(1,20) = 1.166$, $p = 0.293$), no effect of genotype ($F(1,20) = 0.101$, $p = 0.754$), and no interaction ($F(1,20) = 3.673$, $p = 0.0697$) (Figure 5.8C). This showed that the levels of microglia/macrophages were stable between the contralateral striatum of sham and MCAO mice, therefore, the contralateral hemisphere was used as the control for analysing the effect of MCAO on microglia/macrophages in the ipsilateral striatum.

Iba1 %density was measured in the lesion and peri-lesion of each animal (Figure 5.8D), using the same ROIs as for the VGLUT1 and PSD95 measurements. There was a surgery effect increasing the Iba1 %density in the ipsilateral lesion ($F(1,22) = 88.94$, $p < 0.0001$), with no genotype effect ($F(1,22) = 1.322$, $p = 0.263$) and no interaction ($F(1,22) = 0.000137$, $p = 0.971$) (Figure 5.8E). Post-hoc analysis showed that Iba1 levels increased in the lesion of both genotypes. In the lesion the Iba1+ cells appear to have an activated morphology, as they have larger cells bodies with shorter and thicker processes, whereas they are smaller with thinner and longer processes in the contralateral striatum, as can be seen in the inserts in Figure 5.8D. In the peri-lesion, however, the Iba1 %densities were not increased compared to the contralateral hemisphere (Figure 5.8F). These results demonstrate that a focal ischaemic lesion leads to a chronic elevation of microglia/macrophages contained within the lesion, and not in the surrounding peri-lesion. The changes were not exaggerated by concurrent TgSwDIAPP expression.

5.3.5.2 Astrocytes, GFAP

Reactive astrogliosis is another key pathological feature found in chronic stroke tissue and Alzheimer's disease tissue. The next aim of the study was to determine whether MCAO resulted in long-term elevation of reactive astrocyte within the striatal lesion. Reactive astrocytes were analysed by immunohistochemical detection of GFAP. As with Iba1, the %densities of GFAP were first measured in both hemispheres of the sham animals and contralateral hemispheres of the MCAO animals (Figure 5.9A). The levels of astrocytes were very low in the sham animals and the contralateral striatum of MCAO animals. In sham mice, there were no significant differences in GFAP %densities between the striatal hemispheres ($F(1,18) = 1.345$, $p = 0.261$), plus no genotype effect ($F(1,18) = 0.743$, $p = 0.4002$) and no interaction ($F(1,18) = 0.163$, $p = 0.692$) (Figure 5.9B). Furthermore, the GFAP %densities from the contralateral hemispheres from sham and MCAO mice were indistinct ($F(1,20) = 0.118$, $p = 0.734$), with no genotype effect ($F(1,20) = 0.000766$, $p = 0.978$) and no interaction ($F(1,18) = 0.209$, $p = 0.653$) (Figure 5.9C), showing that there was no effect of surgery and genotype on these measures and that the MCAO contralateral hemispheres were suitable to use as controls measuring astrocytes in the ischaemic lesion.

GFAP was detected in the next serial sections taken as used for VGLUT1/PSD95 and Iba1, and the same ROIs were used for the image analysis (Figure 5.9D). The GFAP %density was significantly elevated in the lesion compared to the contralateral hemisphere ($F(1,22) = 553.1$, $p < 0.0001$), however, there was no genotype effect ($F(1,22) = 0.927$, $p = 0.346$) and no interaction ($F(1,22) = 0.892$, $p = 0.355$) (Figure 5.9E). Post-hoc analysis showed that the increase in reactive astrocytes was present in the lesion of both WT and TgSwDI mice. The astrocytes within the lesion and peri-lesion have an activated morphology, with overlapping processes so individual cells are difficult to distinguish, see inserts in

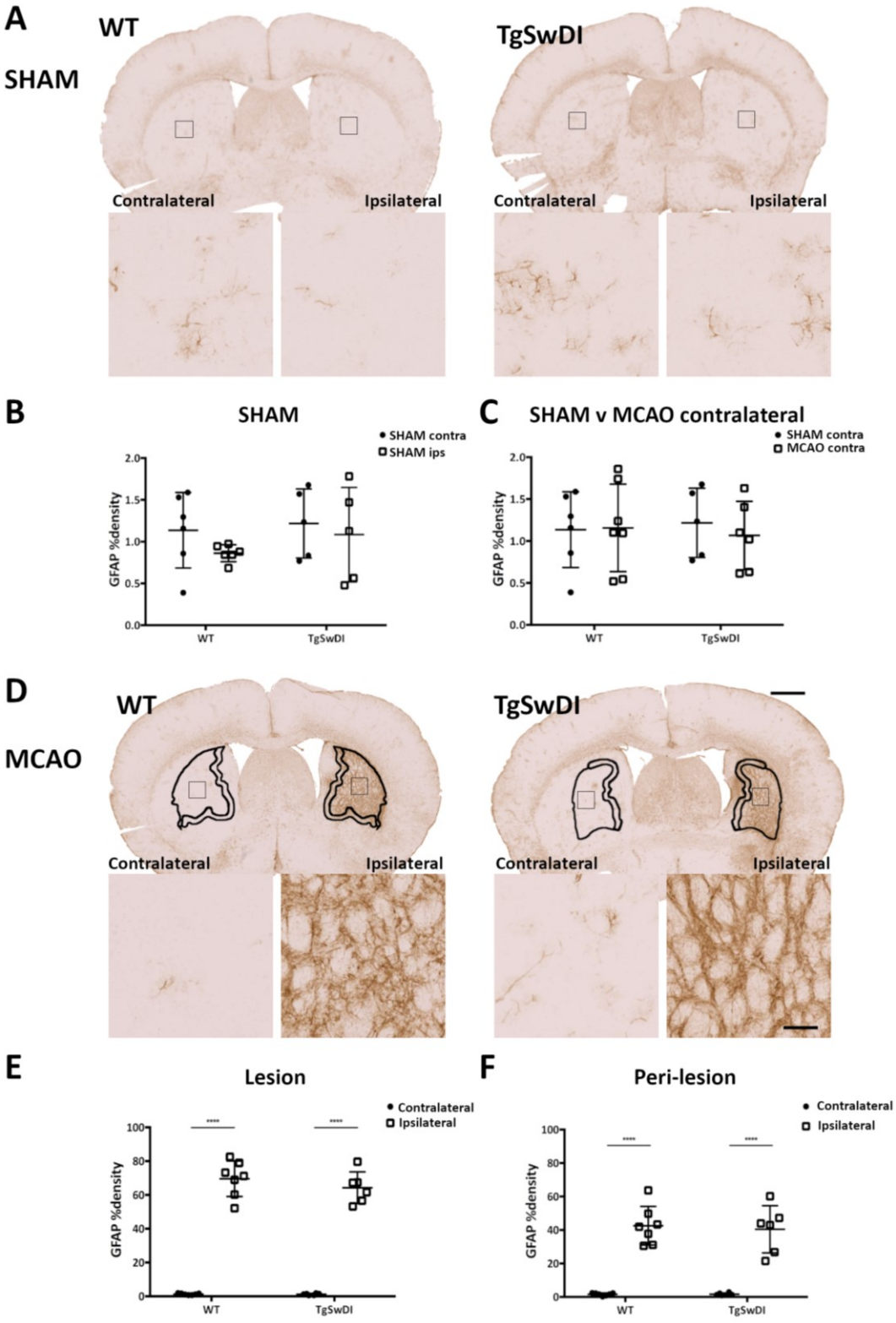

Figure 5.9 MCAO induced chronic astrocyte elevation within the lesion and peri-lesion. (A, D) GFAP immunohistochemistry used to detect reactive astrocytes. (B) GFAP %density in sham mice was stable between the contralateral and ipsilateral striatum, with no difference between the genotypes. (C) GFAP %density was unchanged between

contralateral striatum of sham and MCAO mice, with no effect of genotype. (E) GFAP %density was elevated in the lesion compared to the contralateral hemisphere, with no genotype effect. (F) GFAP %density was increased in the peri-lesion compared to the contralateral hemisphere, with no effect of genotype. Data presented as mean ± SD, n = 6,7 per group. Two-way ANOVA with Bonferroni's multiple comparison test. ***p<0.0001. Scale bar = 1mm, 100µm insert. Grey boxes = inserts.

Figure 5.9D. There was a surgery effect, increasing the GFAP %density in the peri-lesion in the ipsilateral hemisphere compared to the contralateral ($F(1,22) = 125.5$, $p < 0.0001$), however, there was no genotype effect ($F(1,22) = 0.0880$, $p = 0.770$) and no interaction ($F(1,22) = 0.0949$, $p = 0.761$) (Figure 5.9F). Post-hoc analysis showed that this occurred in both genotypes. This is an interesting finding, as it shows that within the striatum, the area of reactive astrogliosis extends beyond the borders of the ischaemic lesion and is more widespread than microgliosis.

These results demonstrate that a focal diffuse ischaemic lesion leads to a chronic elevation of astrocytes within the lesion and the peri-lesion. Surprisingly, there was no differential effect between WT and TgSwDI mice, suggesting that concurrent TgSwDIAPP expression did not exacerbate the neuroinflammatory response within the lesion or peri-lesion.

5.3.5.3 Microglia/macrophage density and not astrocyte density inversely related to PSD95 %density in the lesion.

There is evidence that microglia/macrophages and astrocytes may have a role in synapse dysfunction and degeneration in disease. The %density of Iba1 in the lesion was plotted against the %density of VGLUT1 (Figure 5.10A) and PSD95 %density (Figure 5.10B). Iba1 %density in the lesion did not significantly correlate with VGLUT1 %density (Spearman $r = -0.4011$, $p = 0.1759$), however, it did significantly inversely relate to the PSD95 %density in the striatal lesion (Spearman $r = -0.5714$, $p = 0.0449$). This is an interesting result, as it

shows that an increase in the density of microglia/macrophages directly relates to the loss of glutamatergic postsynaptic terminals within the ischaemic lesion. The %density of GFAP was then plotted against %densities of VGLUT1 (Figure 5.10C) and PSD95 (Figure 5.10D). GFAP %density did not significantly correlate with either VGLUT1 (Spearman r = -0.3462, p = 0.2471) or PSD95 %densities (Spearman r = -0.1703, p = 0.5786) in the lesion. The peri-lesion %densities of VGLUT1 and PSD95 were plotted against Iba1 and GFAP, however, there was no evidence of correlation indicating that the levels of glutamatergic pre- and post-synaptic terminals do not relate to the levels of microglia/macrophages or astrocytes

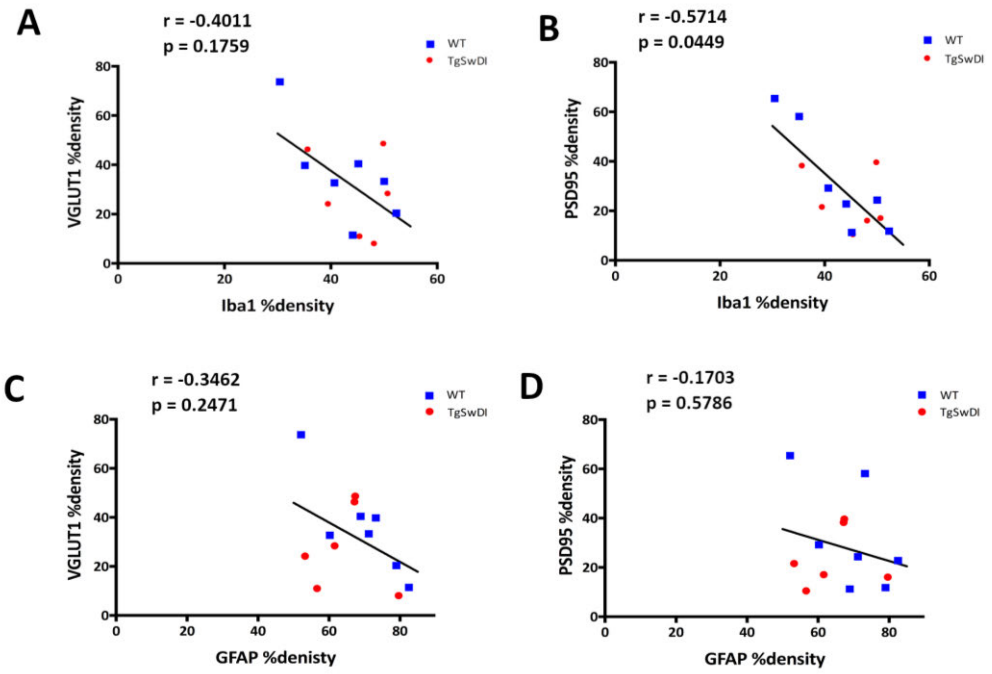

Figure 5.10 Microglia/macrophages density inversely related to the levels of glutamatergic postsynaptic terminals in the lesion. (A) Iba1 %density did not relate to the VGLUT1 %density in the lesion, however, (B) it did significantly inversely relate to the PSD95 %density in the lesion. (C) GFAP %density did not relate to the VGLUT1 %density and (D) it did not relate to PSD95 %density. Spearman's rank.

in the peri-lesion (data not shown). Recently there has been a growing body of literature proposing that microglia strip synaptic terminals during brain injuries and diseases. A preliminary study was undertaken to investigate whether synapses co-localised with microglia post-MCAO. Sections from WT and TgSwDI mice x PSD95:eGFP, 3 months after MCAO were immunostained for microglia-specific TMEM119 and imaged with high power confocal microscopy to assess the potential co-localisation of microglia with PSD95 terminals. In support of this within the ischaemic lesion in the striatum, microglial cells appeared to co-localise with PSD95+ clusters in the ischaemic striatum, whilst there is minimal colocalisation in the contralateral striatum (Figure 5.11).

Overall, these results demonstrated that 15 minutes of MCAO resulted in chronic elevation of microglia/macrophages and astrocytes within the lesion, as well as an increase of astrocytes in the peri-lesion. Surprisingly, there was no effect of genotype, indicating the concurrent TgSwDIAPP expression did not exaggerate the levels of microglia/macrophages and astrocytes in the ischaemic lesion or peri-leison. The study found evidence that in the ischaemic lesion the levels of microglia/macrophages inversely related to the density of PSD95+ synaptic terminals. Furthermore, a preliminary study with confocal microscopy appeared to show physical interaction between microglia and PSD95+ terminals in the lesion.

5.3.6 Western blot analysis: temporal synaptic profile

The results to date have shown that a diffuse ischemic lesion following transient MCAO leads to long-term loss of glutamatergic pre- and post- synaptic terminals and chronic neuroinflammation. This analysis, however, does not establish at what time-point post-MCAO these changes occurred. The next stage of the investigation, therefore, was to determine the temporal profile of glutamatergic pre- and post-synaptic proteins levels and

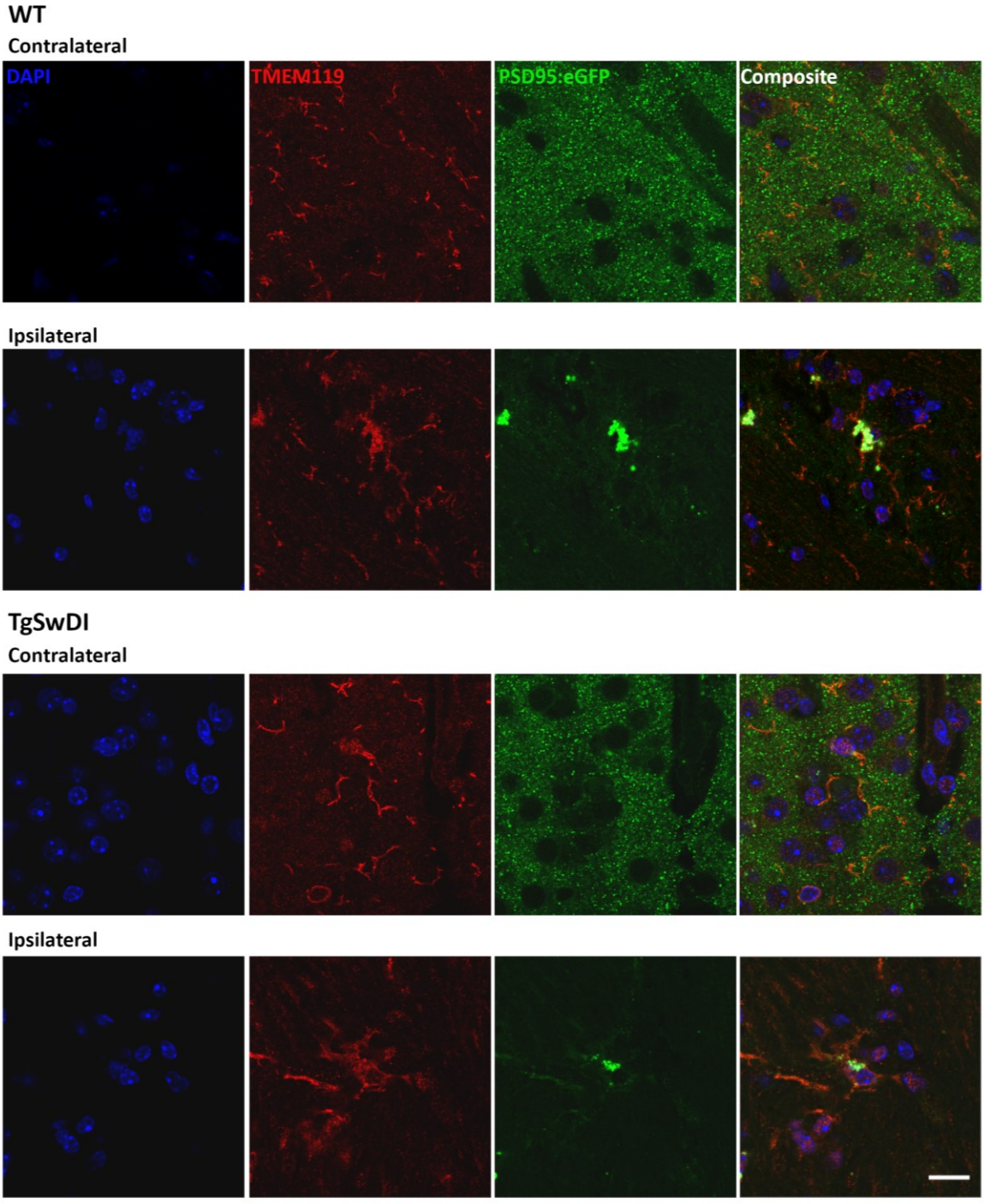

Figure 5.11 Preliminary analysis in which TMEM119+ microglia appear to colocalise with PSD95+ clusters in the striatal ischaemic lesion, more than in the contralateral striatum. Scale bar = 15µm.

microglia/macrophages and astrocyte protein levels. Western blot analysis was used on additional cohort of WT and TgSwDI mice, at 24 hours, 1 month and 3 months post-MCAO.

VGLUT1 protein levels were measured with western blotting and normalised to the levels of α-tubulin (Figure 5.12A). There were no significant differences in the VGLUT1 levels between the hemispheres and genotypes at any of the time-points (Figure 5.12B-C). The data was analysed with two-way ANOVAs and the results were: at 24 hours, surgery ($F(1,30) = 0.597$, $p = 0.446$), genotype ($F(1,30) = 2.743$, $p = 0.108$), and interaction ($F(1,30) = 0.320$, $p = 0.576$); at 1 month, surgery ($F(1,28) = 0.422$, $p = 0.521$), genotype ($F(1,28) = 2.479$, $p = 0.127$), and interaction ($F(1,28) = 0.240$, $p = 0.628$); and at 3 months, surgery ($F(1,32) = 0.445$, $p = 0.510$), genotype ($F(1,32) = 0.817$, $p = 0.373$), and interaction ($F(1,32) = 1.207$, $p = 0.280$). PSD95 protein levels were measured using the same approach and normalised to α-tubulin levels (Figure 5.13A). The PSD95 protein levels, however, were significantly reduced with surgery at 24 hours post-MCAO ($F(1,30) = 7.391$, $p = 0.0108$), whilst there was no effect of genotype ($F(1,30) = 0.119$, $p = 0.732$) and no interaction ($F(1,30) = 0.540$, $p = 0.468$) (Figure 5.13B). Post-hoc analysis revealed that PSD95 protein levels were only significantly reduced in the ipsilateral striatum of TgSwDI mice at 24 hours post-MCAO. At 1 month and 3 months, however, there were no significant differences in PSD95 protein levels between the contralateral and ipsilateral striatum, and no difference between WT and TgSwDI mice (Figure 5.13C,D). The two-way ANOVA results at 1 month and 3 months after MCAO were: at 1 month, surgery ($F(1,28) = 2.334$, $p = 0.138$), genotype ($F(1,28) = 0.0338$, $p = 0.855$), and interaction ($F(1,28) = 0.913$, $p = 0.348$); and at 3 months, surgery ($F(1,32) = 0.215$, $p = 0.646$), genotype ($F(1,32) = 1.128$, $p = 0.296$), and interaction ($F(1,32) = 0.0475$, $p = 0.829$). Overall, this analysis found a significant reduction in PSD95 protein levels in the ipsilateral striatum of TgSwDI mice at 24 hours after MCAO surgery,

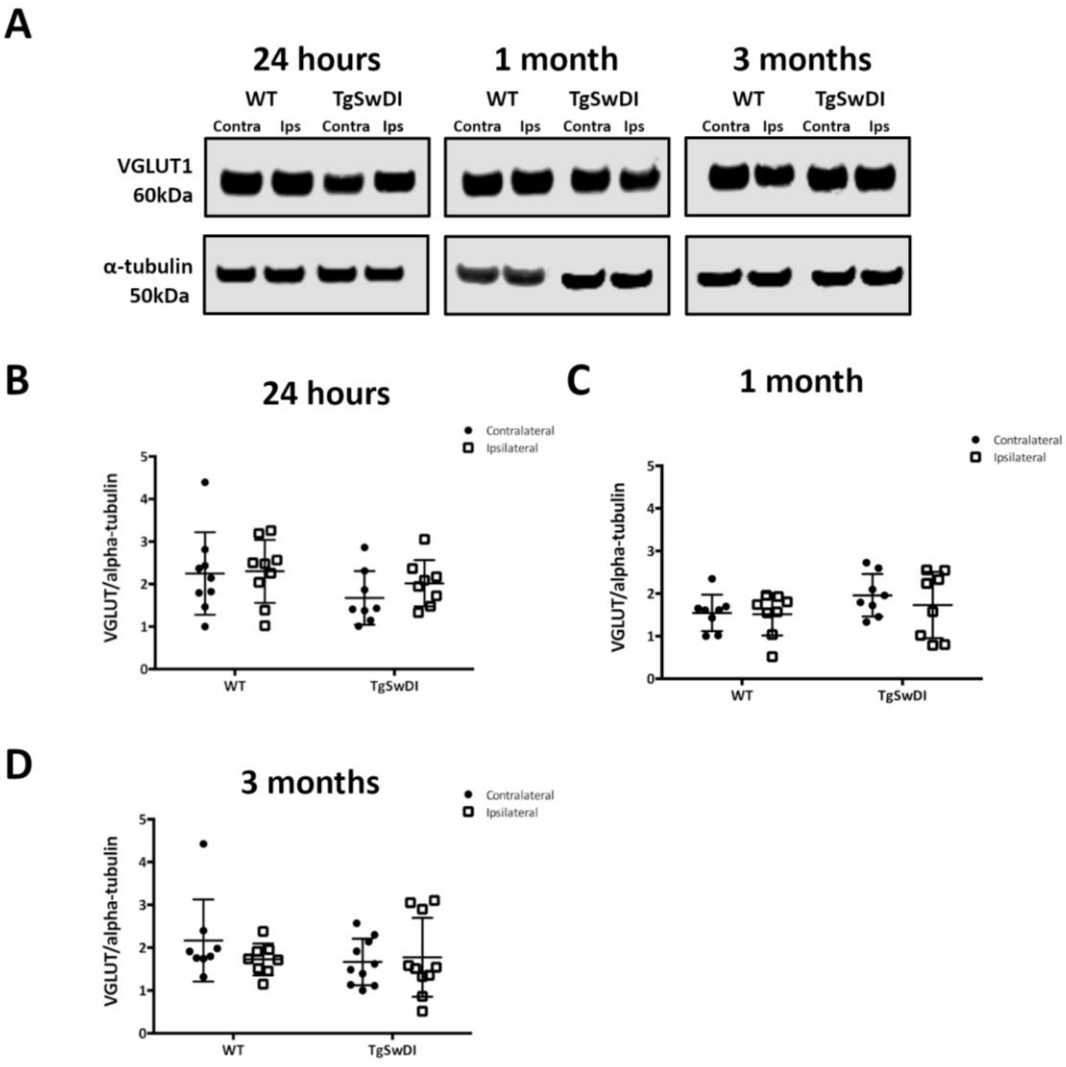

Figure 5.12 Western blot analysis found no significant differences in VGLUT1 protein levels, compared between the ipsilateral and contralateral striatum, and between WT and TgSwDI mice, at 24 hours, 1 month and 3 months after MCAO. (A) VGLUT1 protein levels measured in the contralateral and ipsilateral striatum at the different time points after MCAO, normalised to α-tubulin. There were no significant differences in the striatal VGLUT1 protein levels between the contralateral and ipsilateral stratum, and between WT and TgSwDI mice, at (B) 24 hours, (C) 1 month and (D) 3 months after MCAO. Data presented as mean ± SD, n = 8-10 per group. Two-way ANOVA.

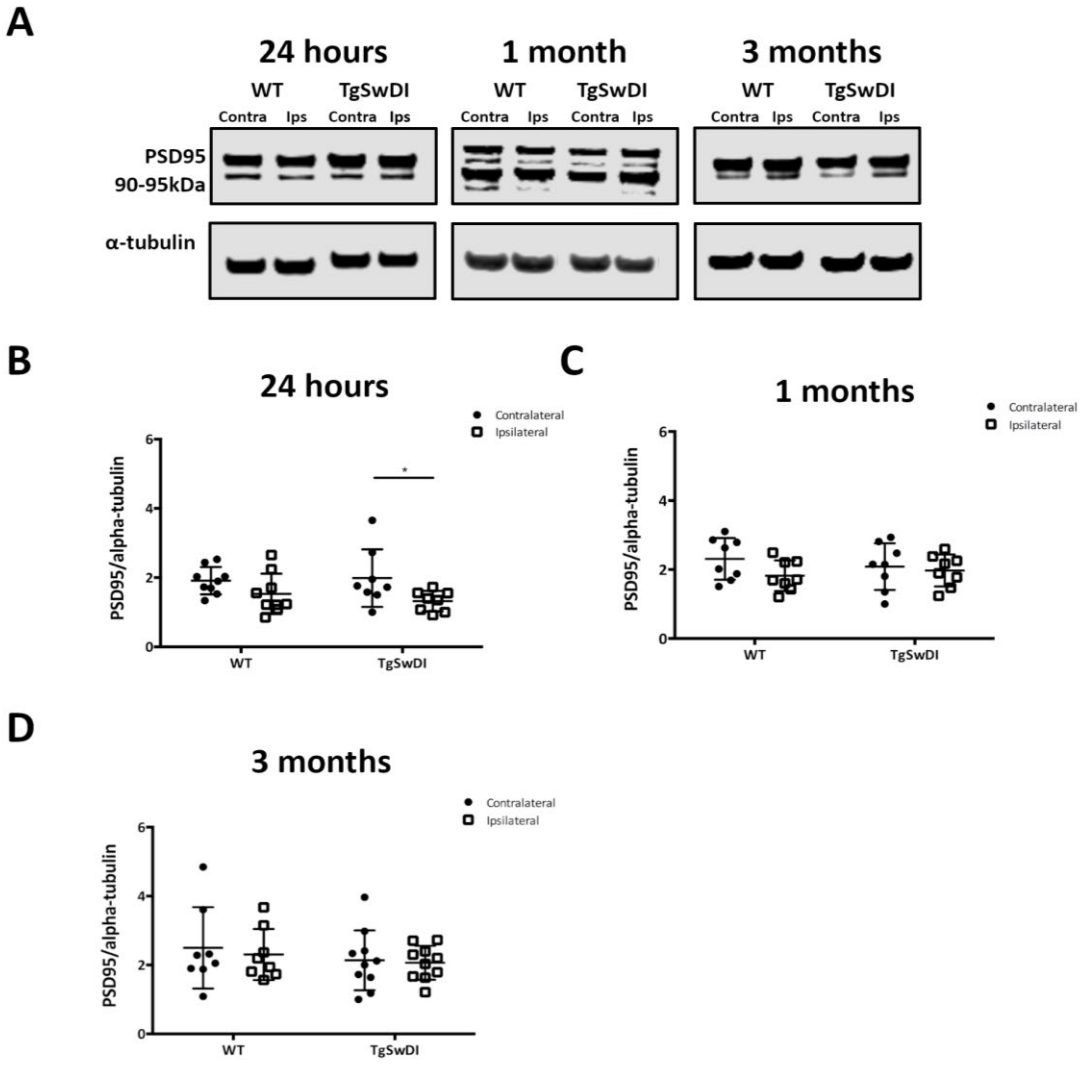

Figure 5.13 Western blot analysis found a significant reduction in TgSwDI ipsilateral striatal PSD95 levels at 24 hours after MCAO, but not in the WT. (A) PSD95 protein levels measured in the contralateral and ipsilateral striatum at the different time points after MCAO, normalised to α-tubulin. (B) PSD95 levels were reduced in the ipsilateral striatum of TgSwDI mice at 24 hours, however, there was no significant surgery effect in WT mice, and no overall genotype effect. There were no significant differences in the striatal PSD95 protein levels at (C) 1 month and (D) 3 months after MCAO, compared between the contralateral and ipsilateral striatum, and between WT and TgSwDI mice. Data presented as mean ± SD, n = 8-10 per group. Two-way ANOVA with Bonferroni's multiple comparisons test *p<0.05.

but otherwise no other significant effects of surgery or genotype on VGLUT1 and PSD95 protein levels.

5.3.7 Western blot analysis: temporal glial profile

The next stage of the investigation was to determine the temporal glial profile following MCAO. In the same tissue samples taken from WT and TgSwDI mice 24 hours, 1 month and 3 months after MCAO, the protein levels of Iba1 (Figure 5.14A) were measured with western blotting and normalised to the levels of α-tubulin. At 24 hours, there were no significant differences in normalised Iba1 protein levels between the ipsilateral and contralateral striatum ($F(1,30) = 1.824$, $p = 0.187$), no genotype effect ($F(1,28) = 0.304$, $p = 0.586$) and no interaction ($F(1,28) = 0.500$, $p = 0.485$) (Figure 5.14B). Statistical comparison of Iba1 measured at 1 after MCAO found that there was a significant surgery effect ($F(1,28) = 18.73$, $p = 0.0002$) and a significant genotype effect ($F(1,28) = 4.504$, $p = 0.0428$), with no interaction ($F(1,28) = 3.154$, $p = 0.0866$) (Figure 5.14C). Bonferroni's multiple comparison test found a significant increase in Iba1 protein levels in ipsilateral striatum of WT mice compared to the contralateral striatum, however, there was not a significant effect in the TgSwDI mice. Furthermore, it revealed that the Iba1 protein levels were significantly higher in the ipsilateral striatum of the WT mice, compared to the ipsilateral striatum of TgSwDI mice. At 3 months, there was an overall significant effect of surgery on the Iba1 protein levels ($F(1,32) = 7.825$, $p = 0.0087$), although there was no genotype effect ($F(1,32) = 1.297$, $p = 0.263$) and no interaction ($F(1,32) = 0.0110$, $p = 0.917$) (Figure 5.14D). Bonferroni's multiple comparisons test, however, did not find a significant difference between the Iba1 protein levels in contralateral and ipsilateral hemisphere in either the WT or TgSwDI mice,

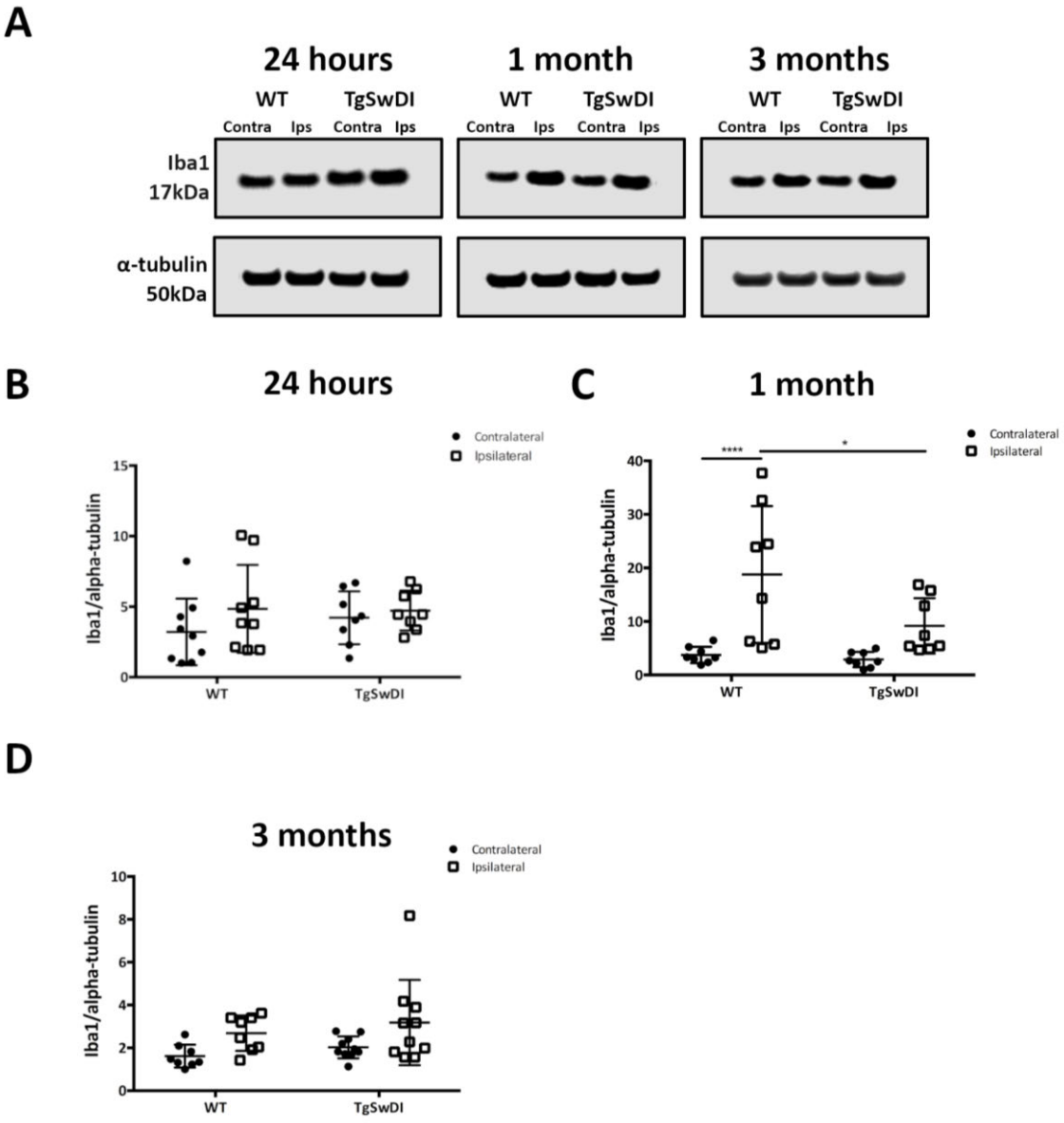

Figure 5.14 Iba1 protein levels were increased in the WT ipsilateral striatum 1 month after MCAO, compared to the contralateral striatum and the TgSwDI striatum. There was a trend towards an Iba1 elevation in the ipsilateral striatum at 3 months. (A) Iba1 protein levels measured in the contralateral and ipsilateral striatum at the different time points after MCAO, normalised to α-tubulin. (B) There were no significant differences in the Iba1 protein levels at 24 hours after MCAO, compared between the contralateral and ipsilateral striatum, in WT and TgSwDI mice. (C) Iba1 protein levels were increased in the ipsilateral striatum in WT at 1 month compared to the contralateral striatum, and significantly greater than TgSwDI ipsilateral Iba1 levels. (D) At 3 months, there was an overall significant surgery effect on the Iba1 protein levels and a trend towards an increase in the ipsilateral striatum, although post-hoc analysis found no significant changes between the groups. Data presented as mean ± SD, n = 8-10 per group. Two-way ANOVA with Bonferroni's multiple comparisons test. ***/*p<0.05.

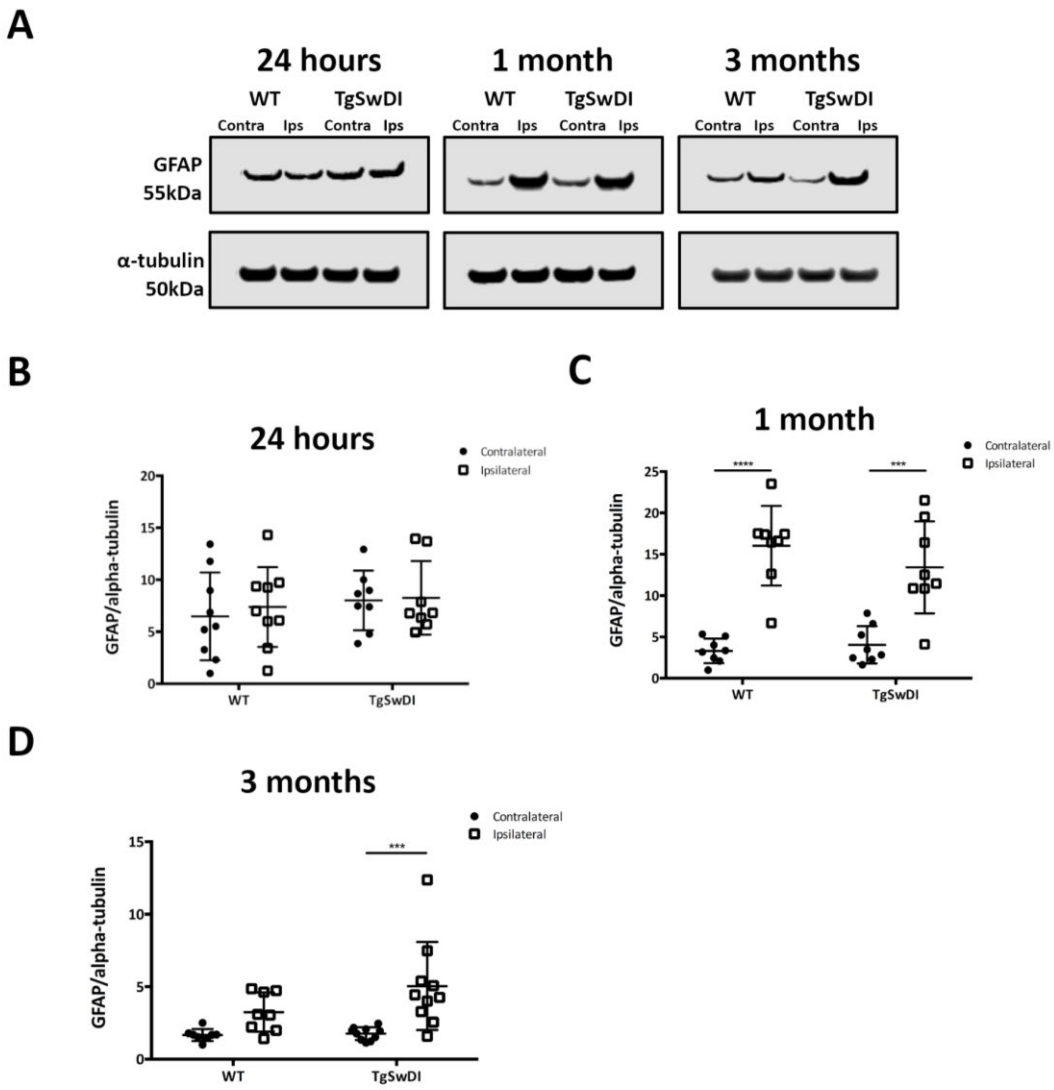

Figure 5.15 GFAP protein levels were increased in the ipsilateral striatum 1 month after MCAO compared to the contralateral, of both WT and TgSwDI mice. And in the TgSwDI ipsilateral striatum at 3 months. (A) GFAP protein levels measured in the contralateral and ipsilateral striatum at the different time points after MCAO, normalised to α-tubulin. (B) There were no significant differences in the GFAP protein levels at 24 hours after MCAO. (C) GFAP protein levels were increased in the ipsilateral striatum compared to the contralateral, in WT and TgSwDI at 1 month. (D) Ipsilateral striatal GFAP protein levels were increased in ipsilateral striatum compared to the contralateral in TgSwDI mice, at 3 months after MCAO. Data presented as mean ± SD, n = 8-10 per group. Two-way ANOVA with Bonferroni's multiple comparisons; ****/***p<0.0001. ***p = 0.0002.

indicating that there is a trend towards an increase in Iba1 in the lesioned striatum.

The GFAP protein levels were also measured by western blotting in the same tissue and normalised to α-tubulin levels (Figure 5.15A). At 24 hours, there were no significant differences in the GFAP levels between the contralateral and ipsilateral striatum ($F(1,30) = 0.209$, $p = 0.651$), no genotype effect ($F(1,30) = 0.910$, $p = 0.348$) and no interaction ($F(1,30) = 0.0648$, $p = 0.801$) (Figure 5.15B). By 1 month after MCAO, however, there was a significant increase in GFAP protein as a result of surgery ($F(1,28) = 63.62$, $p < 0.0001$), which post-hoc analysis showed to occur in both WT and TgSwDI mice, although there was no genotype effect ($F(1,28) = 0.467$, $p = 0.500$) or interaction ($F(1,28) = 1.470$, $p = 0.236$) (Figure 5.15C). Finally, in the 3 month groups, there was an effect of surgery ($F(1,32) = 17.01$, $p = 0.0002$), but no effect of genotype ($F(1,32) = 2.562$, $p = 0.119$) or an interaction ($F(1,32) = 2.090$, $p = 0.158$) (Figure 5.15D). Post-hoc analysis revealed that MCAO surgery resulted in a significant increase in GFAP protein levels in the ipsilateral striatum of TgSwDI mice, whereas it did not reach significance in the WT mice.

Taken together, the western blot analysis indicates that at 24 hours after MCAO the microglia/macrophage and astrocyte levels are unchanged, whereas at 1 month there is an elevation in the ipsilateral striatum compared to the contralateral hemisphere. At 3 months, there was a trend towards an increase in neuroinflammation in the ipsilateral striatum, which appeared to be greater in TgSwDI mice.

5.4 Discussion

The current study demonstrated that glutamatergic pre- and post-synaptic loss is evident months after the initial focal ischaemic insult, which coincided with chronic increase in glial cell density. Contrary to the hypothesis, the study did not find an overt effect of

TgSWDIAPP expression on neuronal, synaptic or glial changes. There was, however, an indication that greater degeneration of glutamatergic presynaptic terminals occurred in the peri-lesion of TgSwDI mice compared to WT. Furthermore, there is a trend towards greater levels of microglia/macrophages and astrocytes in the lesioned striatum of TgSwDI mice at 3 months, as measured by western blotting.

5.4.1 Focal ischaemia resulted in acute motor impairment and long-term ischaemic neuronal and axonal pathology, with no effect of genotype

5.4.1.1 Behaviour impairment

The striatum is a key brain region for motor function and damage to it in human stroke is associated with motor deficits (Corbetta et al. 2015). Impairment in motor function following stroke includes deficits in muscle control and limited mobility, usually in the contralateral upper limb and affects about 80% of patients (Cramer et al. 1997). These motor deficits are usually experienced transiently, as a degree of recovery can occur over time (Jorgensen et al. 1995; Cramer et al. 1997). In the present study, focal ischaemia induced acute motor impairment in the contralateral fore- and hindlimbs of mice 3 days post-MCAO, as measured by the ladder-rung test. At 6 weeks, however, there was no deficit in the MCAO animals, implying functional recovery by this time-point. Previous publications have demonstrated that focal ischaemia in rodent models leads to acute motor deficits with recovery over time. An example of this is the paper by Bouët et al., who found that 60 minutes of MCAO caused motor deficits on the accelerating rotarod at 3 days post-surgery, which was alleviated by 6 weeks (Bouët et al. 2007).

The version of the ladder-rung test used in the present study was adapted from (Farr et al. 2006). The test is designed to give a score based on the locomotion, grip strength, and

balance of the mice, by calculating the percentage of limb placement errors (partial placements and slips) the mice make with their contralateral limbs, out of the total number of limb placements they make. Farr et al. did not count 'partial placements' as an error in their version of the test, however, the protocol was adapted for the present study to make the test sensitive enough to distinguish between the sham and MCAO mice, as very few of the lesioned mice slipped on the rungs. Moreover, the variation in the sham data was quite high, as many of these mice were also making a lot of 'partial placements'. This may be because some were running across the ladder. Another reason could be that as the sham surgery involves permanent occlusion of the external carotid artery (ECA) (Section 2.2.2), therefore, it could cause some motor decline in these animals. This is a caveat for the study, and an improvement would be to include a trial of the ladder-rung test prior to surgery or to have additional naïve control groups that do not receive surgery. Furthermore, the test could be made more challenging, such as using an inclined ladder (Pin-Barre et al. 2014), which should improve the sensitivity of distinguishing between sham and MCAO mice, and reduce the variation. Another potential caveat of this test could be that the ladder was elevated to enable space for the camcorder to be placed underneath, however, this may have caused an anxiety response in the mice. Previous studies using the elevated plus maze have shown that MCAO causes greater anxiety in rodents (Winter et al. 2005; Zhang et al. 2017), therefore, this may have affected the performance of the test in the present study.

There were no differences in the contralateral limb placement %errors between WT and TgSwDI mice after MCAO surgery. Alzheimer's disease is not typically associated with motor impairment, although changes in posture and gait can be present (Pettersson et al. 2002). Moreover, deficits in balance, motor coordination and locomotion have been found

in some mouse lines expressing human mutated APP as reviewed by (Lalonde et al. 2012). However, to date no motor impairment in TgSwDI mice has been reported. This study showed that TgSwDIAPP expression did not affect the motor abilities of mice after either sham or MCAO surgery. Previous publications have found a significant correlation between lesion volume and motor impairment after MCAO in rats (Rogers et al. 1997). As there was no difference in the size of the ischaemic lesion between WT and TgSwDI mice, therefore, it may be expected that there was also no difference in the motor deficit between the genotypes.

An important consideration when interpreting behavioural data from mouse models of unilateral lesions is that the right and left brain hemispheres may play different roles in motor control, therefore, the results may change depending on which hemisphere the lesion is in. Research of stroke patients has revealed that contralesional arms perform different depending on which hemisphere is damaged (Mani et al. 2013). In the study investigating anxiety and hyperactivity in mice, they found that mice with MCAO in the right hemisphere had increased spontaneous locomotor activity, while mice with left MCAO had increased anxiety (Winter et al. 2005). In addition, right MCAO in rats has been shown to result in worsened neurological score, more limb faults on a balance beams, and longer latency in a Morris water maze (Zhai & Feng 2018; Gao & Zhang 2008). In the current study, MCAO was performed in the right hemisphere, therefore, we can predict that the motor deficits would have been even more modest if the vessel occlusion had been on the left. Another factor that is expected to influence the motor outcome after focal ischaemia is age. A recent paper showed that DH stroke mice of 3 months old recovered from motor impairment on the ladder rung test by week 4, whilst mice of 18 months of mice were still impaired by the final measurement at 6 weeks (Nguyen et al.

2018). The mice used in the current study were 4-5 months old at the time of surgery, and if we had used older mice they would be expected to have delayed motor recovery.

The present study confirmed the MCAO surgery induces acute motor impairment, however, it did not investigate whether cognition was affected. The development of cognitive decline and dementia occurs in around 30% of stroke patients (Bruno et al. 1996; Pohjasvaara et al. 1997; Pohjasvaara et al. 1998; Desmond et al. 2000). Deterioration of specific cognitive domains depend on the type of lesion, volume, numbers, location and severity (Kalaria et al. 2016). Functions relating to the frontal lobe are the most commonly affected in post-stroke dementia, such as working memory, processing speed and executive function (Chen et al. 2016). A number of studies have investigated whether focal ischaemia in rodents is sufficient to induce cognitive impairment, however, the results have been conflicting. Maze tests with visuospatial cues, such as the 8-arm radial arm maze (RAM) and Morris water maze (MWM), have been used to find working and spatial memory impairment, respectively, in rats after MCAO surgery (Okada et al. 1995; Yonemori et al. 1996; Markgraf et al. 1992). These mazes, however, require the rats to have good motor abilities to perform, which is confounding for this model. Bingham et al. used a modified protocol of the MWM to minimise the impact of sensory and motor impairments, and found only minimal deficits in spatial memory deficits after permanent MCAO in rats (Bingham et al. 2012). Alternative tests that have been used to probe for memory impairment are the passive avoidance test, and novel object recognition or relocation tests. Bouët et al. found that transient 60 minutes of MCAO in mice resulted contextual memory impairment, at 9 and 15 days post-surgery (Bouët et al. 2007). Contextual memory may be affected after MCAO surgery if the cingulate cortex is subject to remote changes (Popp et al. 2009), as the brain region has been shown to be involved in

contextual memory functions (Maren et al. 2013). Impairment in recognition memory has been found using the novel recognition test, 60 days after permanent MCAO in mice (Fréchou et al. 2019). Furthermore, Nguyen et al. demonstrated that young DH stroke mice experienced cognitive dysfunction in object relocation task by 7 weeks post-surgery, whereas older mice experienced impairment earlier at 4 weeks post-surgery (Nguyen et al. 2018). Recognition memory involves the function of the perirhinal cortex (Barker & Warburton 2011), which is part of the ischaemic lesion in MCAO models with long or permanent occlusion (Bingham et al. 2012; Fréchou et al. 2019). A development of the present study could be to investigate long-term affect of MCAO on cognition with novel object recognition or relocation. Although 15 minutes of MCAO did not result in ischaemic lesions that included the perirhinal cortex, it may still induce activity changes in this region and result in recognition memory deficits.

5.4.1.2 Ischaemic neuronal pathology

The next aim of the study was to investigate the long-term impact of focal ischaemia and TgSwDIAPP expression on ischaemic neuron damage. The areas and the total volume of ischaemic neuron pathology were compared between WT and TgSwDI mice at 3 months post-MCAO, and found to be indistinct between the genotypes. This pathology was observed as diffuse selective neuron loss, predominantly in the striatum. The middle cerebral artery supplies blood to the striatum via the lenticulostriate arteries, which branch off from the MCA and penetrate the basal ganglia (see Figure 1.1). These vessels are 'end arteries' with poor collateral blood supply in this part of the brain, making this territory susceptible to ischaemic damage and a common location of strokes (Feekes et al. 2005; Feekes & Cassell 2006).

The model chosen for the current study was 15 minutes of intraluminal MCAO. We know that the extent of ischaemic damage depends on the occlusion time and type of MCAO surgery. Heiss and Rosner first demonstrated that neuronal death or recovery is dependent on the degree and duration of blood flow reduction, indicating that a 30% reduction of CBF for 45 minutes results in ischaemic damage to cortical neurons with unlikely chances of recovery (Heiss & Rosner 1983). Popp et al. quantitatively showed that longer MCAO (120 minutes) in rats leads to larger and quicker forming ischaemic lesions, whereas 30 minutes of MCAO resulted in a smaller and delayed lesion development (Popp et al. 2009). Pedrono et al. used T2-weighted MRI to determine that 15 minutes of MCAO in mice was the shortest occlusion time needed to result in a striatal lesion 24 hours after surgery (Pedrono et al. 2010). The current investigation aimed to understand chronic changes following focal ischaemia; therefore, brief occlusion was needed to ensure the mice would survive for 3 months after surgery. To this end, 15 minutes of MCAO was used for this study.

In the present study, MCAO lead to long-term diffuse lesions of selective neuronal loss in the striatum. This type of neuropathology is also known as partial/incomplete infarction, which describes lesions in where the extracellular matrix and the tissue structure remains largely remains intact, yet there is death of single neurons within this area (Lassen 1982; Baron et al. 2014). The neuropathology was not confined to the striatum, however, as all mice had changes in the ipsilateral substantia nigra pars reticulata (SN_R), as seen by a loss of large neurons and many smaller cell bodies, presumably neuroinflammatory cells. The substantia nigra is not a region that is directly fed by the MCA, however, it does connect to the striatum by a number of pathways which are crucial for motor function (Kravitz & Kreitzer 2012). Damage to brain regions that have neuronal connectivity with the site of

primary brain injury is known as secondary neurodegeneration, which is investigated further in Chapter 6 (Figure 1.7).

Early neuronal damage after vessel occlusion occurs from the ischaemic cascade, as described in Section 1.4.1.1. In cases of short occlusion durations, the process of ischaemic neuronal damage may be delayed and more selective. This is supported by observations that after 15 minutes of MCAO in rats, neuron death is first detected at 7 days afterwards and the levels of surviving neurons in the striatum gradually decreased until the final measurement at 16 weeks (Fujioka et al. 2003). Another important theory is that in cases of transient occlusion models, reperfusion causes neuronal injury rather than or in addition to ischaemia (Baron et al. 2014). Reperfusion injury can occur due to an increase in reactive oxygen species when blood flow is restored, as anti-oxidants are depleted during ischaemia. Increased reactive oxygen species results in oxidative stress, cell damage and promoting further neuroinflammation (reviewed by Wu et al. 2018).

The present study found no significant difference between the areas and volumes of ischaemic neuronal pathology between WT and TgSwDI mice. This was unexpected, as previous studies had found that the volume of ischaemic neuron pathology was increased in mouse models with β-amyloid. Mice expressing APP_{695}SWE were shown to have larger infarcts than WT mice, 24 hours after permanent distal MCAO (Zhang et al. 1997). Furthermore, in young and old Tg2576 mice, 45 minutes of MCAO resulted in larger infarct volumes compared to their WT littermates, 3 days following surgery (Milner et al. 2014). The discrepancy between our data and the papers referenced here could be a result of using different TgAPP models. Milner et al. showed that β-amyloid deposits were present in penetrating arteries in the cortex in Tg2576 mice, therefore, they predict that vessel constriction from cerebral amyloid angiopathy (CAA) worsened the effect of MCAO (Milner

et al. 2014). TgSwDI mice do not get CAA in the cortex, although they do get some vascular β-amyloid deposition in the thalamus (Salvadores et al. 2017), which may not affect the vessels in the MCA territory. Moreover, laser speckle analysis in the present study determined that there was no difference in ipsilateral cortical CBF between WT and TgSwDI mice after MCAO surgery.

As described in Section 5.2.5, the areas of ischaemic neuronal pathology were detected with cresyl violet stain and were manually mapped out from eight coronal sections throughout the brain. This method is widely used in the pre-clinical stroke field, developed by Osborne et al. (Osborne et al. 1987). The approach overcomes issues with atrophy, which is prominent in chronic stroke models due to the resolution of the injured area. The ischaemic lesions were quite challenging to map, however, as areas of damage were quite diffuse and cresyl violet is not a neuron-specific stain. An improved approach would be to use immunohistochemistry for NeuN to detect neuronal cell bodies and more sensitively show regions of neuronal loss. Another limitation of this approach could be that the tissue sections were thick at 30μm; although this was needed to ensure good tissue quality for slidescanner imaging, it may have masked smaller ischaemic lesions. Despite these limitations, there was no evidence of a genotype effect on ischaemic neuronal pathology after MCAO surgery.

5.4.1.3 Axonal pathology

Axons are vulnerable to degeneration with ischaemia. In 'Time is Brain – Quantified', the author states that for every minute an ischaemic stroke goes untreated, 7 miles of axons are lost (Saver 2006). Axonal pathology has been observed in patients with brain infarctions (Ohgami et al. 1992) and in rodent models of focal ischemia in regions of neuron damage and nearby white matter tracts (Yam et al. 1998; Stephenson et al 1992).

In the current study the areas of ipsilateral axon pathology were analysed at the different coronal levels and the volumes of pathology calculated. There was no significant difference in the areas or volumes of axon pathology between WT and TgSwDI, indicating that β-amyloid in TgSwDI mice did not cause greater vulnerability to axon degeneration. The area of axon pathology was largest in the striatum at level -0.10mm from bregma, however, axonal bulbs were consistently present in the ipsilateral internal capsule and substantia nigra. Previous studies have shown that APP+ axon bulbs can occur in the lesioned striatum within 24 hours after occlusion in rodents (Yam 1998; Gresle et al. 2006). Furthermore, Zhang et al. showed that 30 minutes of MCAO in rats lead to the formation of axon bulbs by 6 hours afterwards in the striatum, cortex and hippocampus (Zhang et al. 2012). The present study demonstrated that axon pathology spreads to brain regions connected to the striatum, the ipsilateral internal capsule and SN_R, by 3 months after MCAO.

Axon damage may be an outcome of the degeneration of neuron cell bodies, however, there is also evidence that disconnected axons can survive for days to weeks after the neuronal cell body has apoptosed (Mack et al. 2001). This indicates that neuron death and axon degeneration could occur by distinct pathways. Axon degeneration may occur through pathways initiated by large calcium influx, as part of extracellular glutamate release and excitotoxicity. Under physiological conditions, oligodendrocytes in the myelin sheath provide metabolic support to axons by transporting lactate to them (Lee et al. 2012). The release of glutamate into the peri-axonal space and activation of glutamate receptors on the myelin sheath stimulates glycolysis, which produces lactate to transport to axons (Saab et al. 2016). This fuel enables axonal mitochondria to synthesise ATP and maintain the ion balance within the axons with Na+/K+-ATPase. During ischaemia when the local glucose supplies become depleted, the production of lactate and ATP is reduced,

therefore, the ion balance in the axon cannot be maintained and the axons and synapses experience an overload in Ca^{2+} ions. This can lead to the activation of calcium-sensitive proteases, calpains, which cause the disassembly of the axonal cytoskeleton (Vargas & Barres 2007). In addition, there is evidence that activation of NMDA-receptors in the myelin sheath contribute to the propagation of axon degeneration. A recent study demonstrated that when isolated mouse optic nerves were subjected to oxygen-glucose deprivation, they had increased release of vesicular glutamate into the peri-axonal space under the myelin sheath, which coincided with more axon injury (Doyle et al. 2018). Furthermore, they found that the pre-treatment of mice with QNZ-46, which specifically blocks the activity of GluN2C/D subunits of extrasynaptic NMDA-receptors, lead to a smaller lesion volume and fewer signs of white matter pathology 24 hours after transient MCAO. Slow debris clearance has been proposed as another major contributor to axon degeneration. Microglia and macrophages mop up myelin debris, however, this function may become impaired in injury, if the phagocytic phenotypes of these cells are repressed (Lloyd et al. 2017).

Amyloid precursor peptide (APP) is often used to detect the bulbs of degenerating axons. APP is normally transported along axons, however, it aggregates when axons are disrupted in injury such as stroke (Imai et al. 2002). Although this is a widely used method of analysing axon pathology, particularly in acute stroke, it is important to note that this approach shows the end-stage of the degeneration process. Using this method of detection, therefore, is likely to result in an underestimated view of the extent of axon degeneration particularly in chronic stroke, as in this study (Hinman 2014). Another method for analysing degenerating axons is to detect non-phosphorylated neurofilament epitopes with the SMI-32 antibody. Neurofilaments in axons are normally highly

phosphorylated and become dephosphorylated when damaged (Trapp et al. 1998; Leifer & Kowall 1993). SMI-32 is useful for studying axon injury within the core of a lesion and may have revealed a larger area of axonal pathology if it had been used in the current study. Antibodies for APP and SMI-32 were both used to investigate the axon pathology up to 72 hours following distal ET-1 MCAO (Gresle et al. 2006). The results showed different immunostaining patterns, with SMI-32 predominantly in the cortical ischaemic core, whereas APP bulbs were present in remote areas of the striatum and corpus callosum on both the contralateral and ipsilateral hemisphere.

As previously described, the areas of axonal pathology were manually mapped out and then measured. This approach was useful for quantifying the volume of pathology for each brain, however, it is limited in that the densities of axon bulbs would not be consistent throughout. The concentration of axon bulbs in a given brain region could be more sensitively analysed by counting, image analysis or using a grading system. Fluoro-Jade stains are commonly used to detect degenerating neurons (Schmued & Hopkins 2000; Schmued et al. 2005). They have been used in focal ischaemia models to detect degenerating neurons in the ipsilateral hemisphere (Liu et al. 2009). Although the exact mechanism by which it works is not understood, it seems to be a good method for identifying damaged neurons, axons and dendrites; as immunostaining for APP+ axon bulbs shows axons that have degenerated, whilst Fluoro-Jade may reveal axons and neurons that are in the process of degenerating.

It was surprising not to find an exaggerated affect on axonal pathology in TgSwDI mice in this study, as there is evidence indicating that β-amyloid is neurotoxic (Walsh et al. 2002) and axon swellings have been shown to be an early feature of Alzheimer's disease (Stokin et al. 2005). This might be because TgSwDI mice have quite diffuse β-amyloid deposits,

which may not be sufficient to damage axons. In a study of TgCRND8 mice expressing YFP-H in cortical neurons, they found that many axons could transverse the amyloid plaques without swelling, or have small local swellings without disintegrating (Adalbert et al. 2009). This study highlighted how resilient axons can be to β-amyloid pathology.

5.4.2 Focal ischaemia resulted in long-term synaptic degeneration in the striatum.

Synapses have a large metabolic demand needed to support their function, with postsynaptic activity and propagation of action potentials being the most energetically expensive processes (Attwell & Laughlin 2001). With this, synaptic transmission is highly susceptible to glucose shortage during ischaemia. Electrophysiology studies have shown that synaptic silencing is an early effect of ischaemia or hypoxia (Bolay & Dalkara 1998; Sun 2003; Mittmann et al. 1998), and more recently multiphoton imaging studies have revealed that dendritic spines, which postsynaptic densities project from, are rapidly lost in the ischaemic region, starting at 10 minutes after occlusion (Zhang et al. 2005; Zhang & Timothy H. Murphy 2007). These studies also demonstrated that if there is restoration of blood flow, dendrites and spines may be able to recover. This would suggest that synapses are the first neuronal structures to be damaged during ischaemia, which can be reversed with timely reperfusion (Zhu, Wang, Ju, Ran, et al. 2017). Less attention, however, has been given to the long-term impact of focal ischaemia on synapses.

The results in the present study showed that brief focal ischaemia resulted in long-term reductions of glutamatergic pre- and postsynaptic terminals within the ischaemic lesion; whilst in the peri-lesion there was significant loss of glutamatergic postsynaptic terminals in both genotypes, there was only significant loss of presynaptic terminals in TgSwDI animals. As previously described in Section 1.4.1.1, vessel occlusion initiates the ischaemic

cascade which causes energy depletion, ion imbalance and depolarisation for a focal population of neurons, and initiating degenerative processes. Excessive glutamate release and activation of AMPA- and NMDA-receptors of neighbouring neurons causes this wave of depolarization to spread, in so-called spreading depolarisation (Hartings et al. 2003; Lai et al. 2014). In the present study, the loss of synaptic terminals was found to often cover most of the striatum at anatomical level -0.10mm from Bregma, which may result from spreading depolarisation throughout this brain region. This is consistent with a recent study that captured striatal spreading depolarisation occurring in a rat corticostriatal slice, using intrinsic optical signal imaging (de Lure et al. 2019).

The current study demonstrated that glutamatergic pre- and postsynaptic terminals are vulnerable to ischaemic damage. There is evidence that presynaptic failure occurs through different mechanisms to postsynaptic failure. A study investigating the electrical activity of neurons in the peri-lesion, hours after transient MCAO (1 hour) in rats, found results which suggested that presynaptic mechanisms had become impaired whilst postsynaptic excitability was preserved (Bolay et al. 2002). Their results showed a decrease in phosphorylated synapsin-1, which they predict will cause a dysfunction in vesicle docking and transmitter release in the presynaptic terminal. A later study found that endocytosis and exocytosis were both impaired in hypoxic conditions in cortical neuron cultures (Fedorovich et al. 2017), which is consistent with the theory that presynaptic failure occurs through dysfunction of vesicle recycling. In the present study, VGLUT1 was used as a marker for glutamatergic presynaptic terminals, which has previously been shown to be reduced in the striatum and cortex at 7 days after 90 minutes MCAO in rats (Sánchez-Mendoza et al. 2010). The function of this protein is to load glutamate into the presynaptic vesicles (Kaneko et al. 2002; Kaneko & Fujiyama 2002; Smith & Bolam 1990), therefore, its

loss may be part of the disruption in vesicle recycling. VGLUT1 interacts with endophilin in clathrin-dependent endocytosis for quick glutamate uptake, and when the stimulation is larger and prolonged the machinery does not interact with endophilin and VGLUT1 recycles glutamate more slowly (Voglmaier et al. 2006). This suggests that the reduction of VGLUT1+ terminals in the lesions may be a consequence of a decreased density of presynaptic terminals that recruit VGLUT1 to the endocytic vesicles for glutamate uptake, as the system has been slowed due to extracellular glutamate overload. Another mechanism by which the glutamatergic neurotransmission may be impaired is by VGLUT1 nitrosylation by NO radicals. This process has been shown to occur in the frontal cortex and hippocampus in a mouse model with β-amyloid pathology, APP/PS1 mice (Wang et al. 2017). The same authors had previously found that a nitric oxide donor was able to increase the level of nitrosylated VGLUT1 and reduce the uptake of glutamate (Wang et al. 2015). Considering that the generation of reactive oxygen and nitrogen species is a downstream event of focal ischaemia, this mechanism could be involved in the reduction of glutamate endocytosis and synaptic vesicle recycling following focal ischaemia.

Another mechanism that may be involved in ischaemia-induced synaptic degeneration is the activation of a family of proteases, known as calpains. These enzymes are calcium sensitive, therefore, they can become activated as a result of calcium influxes through stimulated NMDA- and AMPA-receptors during the ischaemic cascade. Calpain activation has been proposed to be a key player in both pre- and postsynaptic degeneration in ischaemia, as they can cleave important synaptic proteins (Curcio et al. 2016; Yamashima 2016). SNAP-25 is an important presynaptic protein needed for vesicle fusion and exocytosis (Rizo & Xu 2015), and has been shown to be cleaved by calpains in cell culture (Ando et al. 2005). Furthermore, SNAP-25 protein levels were found to be reduced in post-

mortem tissue from vascular dementia patients, indicating that this protein is vulnerable to ischemic damage (Sinclair et al. 2015). Calpains have been shown to work selectively on synaptic proteins, however, as calpain-I resulted in reduced protein levels of VGLUT2, whilst VGLUT1 and synaptophysin appeared to be unchanged (Lobo et al. 2011). These studies indicate that specific synaptic proteins can degenerate through different mechanisms, even though they are present in the same or similar types synaptic structures. Analysis of one synaptic protein, therefore, may be insufficient to fully determine the impact of ischaemia on whole synaptic structures.

The results in the present study indicated that brief focal ischaemia also leads to long-term degeneration of excitatory postsynaptic terminals. Postsynaptic failure is likely to occur through pathways stimulated by over-activation of AMPA- and NMDA-receptors. There is a growing body of evidence that the PSD95-NMDAR-nNOS mechanism is a key process in synaptic failure during ischaemia, and that blocking this process may have therapeutic potential. GluN2B subunits of synaptic NMDA-receptors bind to PSD95, which in turn interacts with neuronal nitric oxide synthase (nNOS). Simultaneous binding of GluN2B and nNOS to PSD95 tethers them together and ensures the activation of nNOS during calcium influxes, thus generating reactive oxygen and nitrogen species which trigger mechanisms of neuronal injury (Lai et al. 2014). A recent study demonstrated that blocking the NMDAR GluN2B-PSD95 interaction actually protected against secondary injury in a model of haemorrhagic stroke; reducing the number apoptotic and necrotic cell death in the peri-lesion cortex, and increased the association with Neuoligin-1 and Neurexin-1, which is predicted to be neuroprotective (Wang et al. 2018). Conversely, PSD95 may also have neuroprotective functions during ischaemia if it forms pro-survival interactions with other NMDA-receptor subunits. Recently it has been proposed that NMDAR GluN2A subunits

interact with PSD95 and promote neuronal and synaptic survival through γ-enolase/PI3K/Akt signalling pathway, by blocking cleavage of synaptic proteins by calpains (Shah et al. 2019). They found that treating rats with the antioxidant melatonin enhanced this pathway after permanent MCAO and lead to increased synaptophsyin immunoreactivity in the cortex and striatum compared to vehicle treated rats, 24 hours after surgery. NMDA-receptors are not the only glutamate receptors that have been shown to be involved in ischaemic damage in focal ischaemia. A recent study demonstrated that an AMPA-receptor antagonist, perampanel, reduced the lesion volume, neuroinflammatory response and functional impaired 7 days after 90 minutes of MCAO in rats (Nakajima et al. 2018). Calcium-dependent calpains also degrade postsynaptic proteins, such as NMDA-receptor subunits (Curcio et al. 2016). Taken together, the literature indicates that focal ischaemia can initiate a number of downstream mechanisms leading to glutamatergic pre- and postsynaptic loss within the lesion.

In the present study, there was a differential effect in the loss of VGLUT1+ and PSD95+ synaptic terminals in the peri-lesion. Whilst PSD95 %densities were significantly reduced in both WT and TgSwDI mice, there was only a significant reduction of VGLUT1 %density in TgSwDI mice. This result may indicate that in the WT animals, glutamatergic presynaptic terminals are more resilient to degeneration than postsynaptic terminals. Moreover, this could highlight a selective vulnerability of these specific proteins to calpain degradation, as VGLUT1 has been found to be resilient to this (Lobo et al. 2011), whereas PSD95 is not (Gascon et al. 2008). The finding also implies that glutamatergic presynaptic terminals in the peri-lesion are more vulnerable to degeneration in mice expressing TgSwDIAPP. This is consistent with evidence that VGLUT1 protein levels are reduced in the prefrontal cortex of Alzheimer's disease brains (Kashani et al. 2008), and a progressive decrease of VGLUT1

immunoreactivity in the cortices of Tg2576 mice with age (Giuliani et al. 2019). Furthermore, in Alzheimer's brains, punctate β-amyloid colocalises with VGLUT1 (Sokolow et al. 2012) and there is an inverse relationship between VGLUT1 and Aβ42 levels (Rodriguez-Perdigon et al. 2016).

The present study did not find any evidence that TgSwDIAPP expression worsened degeneration of glutamatergic postsynaptic terminals. There is conflicting evidence as to whether or not PSD95 is vulnerable to β-amyloid, as investigations of its protein levels in human Alzheimer's brain tissue have found increases (Gong et al. 2009) and decreases (Gylys et al. 2004). The inconsistencies in these studies, however, may result from the differences in the brain regions analysed and different stages of the disease (Savioz et al. 2014). The evidence indicating that β-amyloid does contribute to PSD95 loss, and that the levels of PSD95 positively correlated with the levels of Aβ42 from fractions taken from sporadic and familial Alzheimer's brains (Shinohara et al. 2014). Moreover, in a mouse models of β-amyloid pathology, Koffie et al. demonstrated that the density of PSD95 terminals progressively decrease around the core of amyloid plaques (Koffie et al. 2009). Conversely, research conducted during my MSc project found is no difference in the density of PSD95+ terminals in cortex and thalamus of heterozygous TgSwDIxPSD95:eGFP mice. This is supported by the findings in the sham mice in the current study, as there was no difference in PSD95 %densities between the genotypes. The β-amyloid deposition in TgSwDI mice is diffuse, which can be seen with 6E10 immunostaining in Figure 6.8. Masliah et al. reported that diffuse amyloid plaques in Alzheimer's brain do not cause synaptic loss (Masliah et al. 1990). Instead, soluble oligomeric β-amyloid has been shown to be the species which causes inhibition of long-term potentiation (Walsh et al. 2002). TgSwDI mice do not produce much soluble β-amyloid (Xu et al. 2007), which may underpin the lack of

genotype effect on synapses in this study. A future development of this study, therefore, could be to investigate the effect of concurrent focal ischaemia and β-amyloid on synapses with a different TgAPP line, such as APP E693Δ, which produces β-amyloid oligomers without plaques, and causes synaptic loss (Tomiyama et al. 2010). In addition, the study could be expanded to investigate whether other glutamatergic postsynaptic proteins are affected, as PSD95 may be selectively resilient. There is evidence that the function of NMDAR-GluN2B subunits are vulnerable to β-amyloid leading to inhibition of long-term potentiation and calpain activation (Hu et al. 2009; Ferreira 2012). GluN2B, therefore, may be a more sensitive target for detecting β-amyloid – induced synapotoxicity.

The peri-lesion may also be a site of synaptic recovery, as ischaemic injury can promote synaptogenesis, axonal sprouting, activation and migration of neural progenitor cells, which tend to occur from days to weeks/months after the initial injury (Sandvig, Augestad, et al. 2018). By 3 months after MCAO there may have been some synaptic recovery, especially as there was no overall significant motor deficits in the animals at 6 and 11 weeks post-surgery. Previous studies have found that synaptic recovery occurs in the peri-lesion region; such as an observation of progressive reconstruction in YFP+ dendritic spines in the cortical peri-lesion in mice after distal MCAO with *in vivo* two-photon microscopy (Mostany et al 2010). Their results showed rapid spine density reductions after surgery, but the spines started to gradually increase again between 16 and 90 days afterwards. Another study demonstrated that spine loss in the peri-lesion of a photothrombotic occlusion lesion was restored by 6 weeks after surgery (Brown et al. 2007). In the present study, therefore, there may have been a degree of synaptic recovery overtime. This possibility is further supported by a recent study which demonstrated that the number of VGLUT1+ terminals was increased in the cortical peri-lesion compared to the density of the contralateral

hemisphere, at 21 days after cortical photothrombosis (Stokowska et al. 2017). Their results also showed an increase in GAP43 in the same region, which is a marker for axonal sprouting and rewiring. The studies described here found evidence of synaptogenesis in the cortex, which is known to be a more neural plastic brain region. There are a limited number publications that have investigated synaptogenesis in peri-lesion striatum after focal ischaemia, however, there is evidence that new neurons can form in the striatum in adult rodents, either through migration of neural progenitor cells from the subventricular zone or by a distinct mechanism (Dayer et al. 2005; Luzzati et al. 2006). An ischaemic lesion in the striatum could initiate neural progenitor migration and synaptic/neuronal recovery in the peri-lesion. A development of the current study could be to investigate neuronal recovery in the striatum 3 months after MCAO, by probing for synaptogenesis and neurogenesis could be probed for with immunohistochemistry detection of GAP43, and doublecortin (DCX) with BrdU treatment (Rao & Shetty 2004). This data would demonstrate whether 15 minutes of MCAO initiates long-term synaptic recovery in the peri-lesion, and whether this is affected by concurrent β-amyloid.

There was an indication from the present study that synaptic plasticity occurs in the contralateral striatum after MCAO, as there was a small increase in the PSD95 %density in the WT animals and a trend towards an increase in VGLUT1 %density as well, in comparison to the sham levels. Focal ischaemia may stimulate contralateral synaptic plasticity to compensate for ipsilateral injury and help functional recovery. Takatsuru et al. found evidence of contralateral synaptic plasticity in the somatosensory cortex, as the %gain of dendritic spines in this region had increased between 3 days and 1 week after photothrombotic thrombosis (Takatsuru et al. 2009). This process may have occurred in the contralateral striatum in the present study. As previously stated, GAP43 could be used

as a marker to detect regions of synaptic plasticity within the current study, to determine whether there is any evidence of these restoration mechanisms after brief MCAO. This analysis showed that the synaptic density was not totally stable in the contralateral striatum after MCAO surgery, which is a caveat for using the contralateral striatum as the control for the ipsilateral synapse measurements. The contralateral striatum was kept as the control, however, as the difference between the shams was small; there was no genotype effect between the contralateral synapse densities; and this enabled the approach of using the specific, delineated lesion and peri-lesion regions of interest for each mouse.

Western blotting was used to access the temporal profile of VGLUT1 and PSD95 protein levels, to determine at what time-point after MCAO the synapse degeneration occurs. As previously described, a number of studies have demonstrated that longer or permanent focal ischaemia leads to rapid dendritic blebbing and loss of synaptic structures (Zhang & Murphy 2007; Enright et al. 2007; Zhang et al. 2005), however, it is unclear whether brief focal ischaemia causes rapid synaptic loss or progressive synaptic degeneration over time. The western blot results from the present study showed no significant differences in the VGLUT1 protein levels in the ipsilateral striatum compared to the contralateral in WT and TgSwDI, at 24 hours, 1 month or 3 months after 15 minutes of MCAO. This is a perplexing result, as the histological analysis at 3 months showed that VGLUT1 %density was reduced in the lesion, and peri-lesion of TgSwDI mice. Similarly, there were no significant differences in PSD95 protein levels apart from a decrease in the ipsilateral striatum of TgSwDI mice at 24 hours post MCAO. This result was consistent with previous reports that postsynaptic proteins are vulnerable at acute stages after MCAO (Murotomi et al. 2012).

Although there were no significant differences in the VGLUT1 protein levels between the hemispheres, there may be a slight trend towards an increase in protein levels in the ipsilateral striatum of the TgSwDI mice at 24 hours after MCAO, which would be consistent with the results by Sánchez-Mendoza et al. (Sánchez-Mendoza et al. 2010). The data was highly variable and difficult to interpret, which may result from issues with sampling. As described in Section 2.5.2, the striatum was dissected from the thawed brain slices just before homogenisation. Although great care was taken to remove just the striatum from these sections, tissue from other brain regions may have contaminated the samples and introduced variation in the synaptic protein levels. Another issue could be that synaptic proteins were too dilute in the sample and required further enrichment to increase sensitivity. Enriching for synaptoneurosomes in the striatal homoegenates could be an approach for improving the sensitivity of synaptic protein detection (Bai & Witzmann 2007).

Another concern could be that the western blots lack specificity for VGLUT1. There are three isoforms of VGLUT(1-3), therefore, antibodies raised against one isoform could potentially interact with the others. The VGLUT1 antibody used for the present study, however, was chosen based on the high quality of staining and colocalisation with other presynaptic markers (Micheva et al. 2015; Melone et al. 2005). Another concern was that VGLUT proteins could be expressed in astrocytes, as well as by glutamatergic presynaptic terminals, although there is no strong evidence to support this. Sánchez-Mendoza et al. published confocal microscopy images from their MCAO study which show overlapping signals for VGLUT2 and VGLUT3, but not VGLUT1, with GFAP within the ipsilateral corpus callosum (Sánchez-Mendoza et al. 2010). This paper, however, lacks sufficient quantitative analysis for this data. In another study, observations were made of VGLUT1+ terminals

being closely associated with astrocyte processes in the frontal cortex, striatum and hippocampus, using immunofluorescent microscopy and immunogold electron microscopy (Ormel et al. 2012). Yet, the images taken using both methods appear to show VGLUT1 clusters around astrocyte processes rather than within them, which supports the concept of the tripartite synapse and astrocytic processes being entwined with synapses (Araque et al. 1999). Finally, Li et al. investigated the expression VGLUT isoforms in cultured mouse astrocytes and found no evidence to support it (Li et al. 2013). Taken together, these studies indicate that VGLUT1 is not expressed by astrocytes and that the antibody used for VGLUT1 detection is specific, although we did not check the specificity ourselves. The specificity of the PSD95 antibody was checked during protocol optimisation, by comparing the PSD95 immunostaining on a western blot with samples from PSD95KO and WT mice, and seeing no staining for the KO samples.

Another caveat of the study was that, due to the availability of mice, the 1 month cohort were from the xPSD95:eGFP line, whilst the 24 hour and 3 month cohorts were not. This can be observed in the PSD95 western blots, as the 1 month groups have two bands for PSD95 and PSD95:eGFP. Statistical analysis, therefore, was performed with a two-way ANOVA at each time-point, rather than comparing between time-points, as the 1 month group is a different line compared to the others.

Overall, the present study demonstrated that brief focal ischaemia leads to long-term degeneration of glutamatergic pre- and postsynaptic terminals in the lesion, with greater vulnerability to postsynaptic terminals in the peri-lesion. There was also indication of TgSwDIAPP expression causing greater degeneration of presynaptic terminals in the peri-lesion.

5.4.3 Focal ischaemia results in chronic glial responses within the lesion.

Chronic post-ischaemic neuroinflammation is known to be a contributor or consequence of delayed neuronal damage after ischaemia. There is a large body of literature focused on the acute inflammatory response to focal ischaemia, whilst less is known about the chronic effect. The present study focused on quantifying the density of glial cells, Iba1+ microglia/macrophages and GFAP+ astrocytes, which are known to be sensitive to environmental changes. Although these cells are involved in neuroinflammatory responses (Section 1.4.4), the breath of the analysis performed in these studies was insufficient to determine whether these cells are in an activated, neuroinflammatory state. This would require an investigation into the expression of specific inflammatory markers, to indicate whether these cells are in an activated pro-inflammatory or anti-inflammatory state (see Chapter 7).

In the present study, elevated levels of microglia/macrophages and astrocytes were present within the ischaemic lesion, 3 months after surgery. This is consistent with histological analysis of post-mortem stroke tissue has revealed that chronic elevation of glial and immune cells is still present in weeks to months after the initial injury (Mena et al. 2004). Furthermore, Kristian Doyle and colleagues, who showed that markers for microglia/macrophages, phagocytes, antigen presentation, B cells and T cells were present in ischaemic lesions, 7 weeks after distal MCAO with hypoxia surgery in mice (Doyle et al. 2015). In the present study, western blot analysis indicated that at 24 hours after MCAO there was only a trend towards increased microglia/macrophage and astrocytes levels in the leisoned striatum, whereas this was largely increased by 1 month, and the had reduced somewhat by 3 months. Although there was no overt genotype effects, there was indication that the levels of glial cells are slightly exaggerated in TgSwDI mice.

5.4.3.1 Microglia/macrophages

Activated microglia/macrophages within ischemic lesions and the surrounding tissue are expected to play key roles in the pathophysiology (Mabuchi et al. 2000). In injured tissue these cells take on an 'amoeboid' morphology with larger cell bodies and thicker processes, which is associated with their activation state (Schilling et al. 2003). This type of morphology was observed in Iba1+ cells in the ischaemic lesions in the current study. Iba1 is expressed by both microglia and macrophages, which is involved in phagocytosis (Ohsawa et al. 2000). Recent publications, however, have presented data indicating that microglia and macrophages have distinct roles in the ischaemic brain. By analysing other cell-specific markers, progress is being made in understanding the relative contribution of microglia and macrophages following focal ischaemia, especially at acute time-points. A previous study using flow cytometry to investigate neuroinflammation in rats after thromboembolic MCAO, differentiated between microglia and macrophages by their expression of $CD11b^{medium}/CD45^{low}$ and $CD11b^{medium}/CD45^{high}$, respectively (Lehmann et al. 2014). They found that at 24 hours post-surgery, there was an increase of infiltrated macrophages into the lesioned hemisphere, however, there was no difference in the number of microglia compared to the contralateral hemisphere. Microglial increase in the ipsilateral hemisphere may be delayed compared to the increase in macrophages. Rajan et al. found an increase in ipsilateral microglial numbers between 1 and 3 days, with an even greater elevation at 7 days post-MCAO in the ipsilateral hemisphere (Rajan et al. 2018). Additional studies agree that there is a large increase in microglial numbers in the ischaemic hemisphere between 3 and 7 days post-MCAO; whilst infiltrated macrophage numbers increase but the levels are still much lower than microglia (Wattananit et al. 2016; Zarruk et al. 2017; Yoon et al. 2018). The present study did not find a significant

difference in Iba1 protein levels between the ipsilateral and contralateral striatum, however, there does appear to be a slight increase in the group average for the lesioned hemispsheres. This could indicate that a small increase in the microglia/macrophage levels has occurred in the lesioned striatum at 24 hours, and may have been further elevated over the following week, which would be consistent with the studies described (Rajan et al. 2018; Yoon et al. 2018; Zarruk et al. 2017; Wattananit et al. 2016).

There is a growing body of research indicating that microglia and macrophages have complex, injury-specific activation states, rather than expressing either M1 or M2 activation states. A study using single-cell RNA sequencing analysis found at least nine transcriptionally distinct microglial states (Hammond et al. 2019). Moreover, these states can express pro-inflammatory and anti-inflammatory proteins, and change with injury progression. Zarruk and colleagues showed that mRNA levels for the pro-inflammatory cytokine TNF-α was highly expressed in ipsilateral microglia at 3 and 7 days after permanent MCAO, whereas its expression in macrophages was very low by comparison (Zarruk et al. 2017). A number of studies propose that whilst microglia have a pro-inflammatory phenotype following focal ischaemia, infiltrating macrophages are expressing anti-inflammatory and wound-healing properties (Rajan et al. 2018; Benakis et al. 2015). This theory is supported by observations that at 3 days post-MCAO, ipsilateral macrophages expressed significantly higher levels of Arg-1 and YkI40 genes, which code for Arginase-1 and Chitinase-3-like protein 1 (CHI3L1), compared to microglia (Rajan et al. 2018). Arginiase-1 is an enzyme needed in the process of catalysing L-arginine into polyamines and L-proline, which are needed for cell growth, especially smooth muscle cells, and for collagen synthesis (Durante et al. 2007). CHI3L1 is thought to have anti-inflammatory effects, as when its knocked-out the mice had greater levels of microgliosis

and astrogliosis in a traumatic brain injury model (Wiley et al. 2015). In another study, however, analysis of the total RNA extracted from FACs- sorted cells taken 7 days after MCAO (30 minutes) in mice, showed that the distinction between pro-inflammatory and anti-inflammation function of microglia and macrophages was not clear-cut (Kronenberg et al. 2018). Although there was a trend towards microglia expressing genes with a pro-inflammatory phenotype, and anti-inflammatory phenotype for macrophages, it did not show a dichotomous pattern and both cell types expressed genes involved in similar functions. Similarly, Rajan and colleagues found that infiltrated macrophages expressed higher levels of *Nos2* gene than in microglia, indicating that they too can have some pro-inflammatory function (Rajan et al. 2018).

In the present study, Iba1 protein levels were significantly increased in the ipsilateral striatum at 1 month after MCAO in WT mice. Other studies that have found long-term elevation of microglia/macrophages after focal ischaemia, in the peri-lesional cortex at 14 days (Kluge et al. 2017) and at 28 days (Jones et al. 2015), following photothrombotic occlusion. Whereas in another study, they showed an initial increase in macrophage numbers, which had decreased again by day 14 after MCAO (Wattananit et al. 2016). Taken together, these results may indicate that the levels of different glial and inflammatory cells peak at different times after ischaemia. Furthermore, variations in the surgical procedure used to induce ischaemia will impact the glial and inflammatory response; as shown by Zhou et al., who found higher levels of Iba1+ cells in permanent MCAO, compared to 30 and 90 minutes of MCAO in mice (Zhou et al. 2013). Kluge et al. demonstrated that at 14 days after photothrombotic occlusion, microglia-expressing Cx3R1-GFP in the peri-lesion were responsive to laser stimulation and colocalised with CD68 immunofluorescence, indicating that the cells were functional and were phagocytic (Kluge et al. 2017). CD68 was

also elevated at 1 month after photothrombotic occlusion in the peri-lesion cortices in another study (Jones et al. 2015). These studies indicate that microglia are phagocytic at sub-acute or chronic stage within the lesioned hemisphere. The evidence that microglia are involved in the removal of neural tissue and synapses through phagocytosis is discussed later on in this section. The current study used Iba1 as a marker of microglia and macrophages. Immunostaining with TMEM119, which is exclusively expressed by microglia, could be used to make the distinction between these cells types (Bennett et al. 2016; Satoh et al. 2016). Furthermore, in the present study the Iba1+ cells in lesion and peri-lesion the phenotypic state of the Iba1+ cells in the lesion and peri-lesion could be further characterised, to determine if they are phagocytic cells and have roles in clearing cellular debris (Kluge et al. 2017). Future developments of this work could be to use single-cell RNA sequencing to determine the activation state of Iba1+ cells in the lesion at acute, sub-acute and chronic time-points after focal ischaemia, and whether their phenotypes indicate detrimental or protective roles.

The data from the current study showed a significant inverse correlation between PSD95 %density and Iba1 %density in the lesion, indicating that a loss of excitatory postsynaptic terminals relates to an increase in microglia/macrophages. This result may demonstrate that the microglia/macrophage are a contributor to synaptic loss in the ischaemic lesion. Recently, there has been a recent growing body of literature focused on the interface between neuroinflammation and synapse function in heath and disease, and from this the term ‘synaptoimmunology’ has been coined (Nisticò et al. 2017). For example, pro-inflammatory cytokines released during CNS injury have been shown to have an effect on synaptic function. TNFα was found to reduce synaptic excitability in rat hippocampal slices (Tancredi et al. 1992) and promote a decrease in surface AMPA-receptor units in the

striatum (Lewitus et al. 2014). Release of pro-inflammatory cytokines after ischaemic injury may contribute to further synapse silencing in nearby brain regions.

Another theory that has been gaining more attention is that activated microglia/macrophages engulf synaptic terminals in disease conditions, known as 'synaptic pruning or stripping'. Work by Beth Stevens and colleagues have indicated that this happens during development to refine neural networks (Stevens et al. 2007; Schafer et al. 2012). More recently other groups have investigated synapse stripping in disease models. Hong et al. published a study showing high-resolution confocal imaging data showing Homer+ postsynaptic terminals colocalising with Iba1, in a way which it appears to be within the cell body, after intravenous injections of β-amyloid (Soyon Hong et al. 2016). Furthermore, this group and others have proposed that complement components are the inflammatory markers that mediate synaptic pruning by microglia. This is supported by observations by Hong et al. that complement component 1q (C1q) colocalised with PSD95+ terminals in mice with Aβ pathology (Hong et al. 2016). Deficits in complement component 3 (C3) and C1q lead to less synapse loss after nerve injuries and faster recovery (Berg et al. 2012; Norris et al. 2018). Furthermore, blocking C3 pathways in models of focal ischaemia and traumatic brain injury lead to a decrease of microgliosis and astrogliosis and an increase in neuronal/synaptic structures (Alawieh et al. 2015; Alawieh et al. 2018). Preliminary data from the present study indicated that PSD95:eGFP+ terminals were co-localised with TMEM119+ microglia within the ischaemia lesion, which would support the theory of synaptic stripping in disease (Rajendran & Paolicelli 2018) Colocalisation of microglia and synaptic terminals may also represent engulfment of debris rather then stripping active synaptic terminals. A recent study demonstrated that high-resolution microscopy was needed to sensitively show if pruning occurs. The authors proposed that

microglia do not engulf postsynaptic terminals, but rather 'nibble' them (Weinhard et al. 2018). To further investigate whether synaptic pruning occurs in an ischaemic lesion, high-resolution microscopy techniques are needed to determine whether the synaptic terminals are within the microglial cells.

The present study did not find a significant effect of TgSwDIAPP expression on the densities of Iba1+ cells in the lesion or peri-lesion, nor was there significant differences in the Iba1 protein levels. This was an unexpected finding, as previous research has shown an exaggerated immune response in the primary lesion of animals with both focal ischaemia and β-amyloid pathology compared to ischaemia alone (Amtul et al. 2015). We predicted that TgSwDIAPP expression would prime the microglia/macrophages, and so caused an exaggerated glial response after MCAO surgery, as described in Section 6.4.2. However, the analysis of Iba1 %density in the sham animals showed that there was no difference in the levels of microglia/macrophages WT and TgSwDI mice without MCAO surgery. This indicated that heterozygous TgSwDIAPP expression does not stimulate increased microglia/macrophage density in the striatum, in 9-month-old animals. It is known that β-amyloid stimulates activation of glial and immune cells (Section 1.4.4), however, previous analysis by Xu et al. showed that the striatum of both heterozygous and homozygous TgSwDI mice is largely spared of β-amyloid deposition (Xu et al. 2007). Therefore, TgSwDIAPP expression may not impact the density of Iba1+ cells in either sham or MCAO mice, as β-amyloid deposition in the striatum in limited.

5.4.3.2 Astrocytes

Astrocytes are also known to respond quickly to ischaemia and hypoxia (Angelova et al. 2015). During normal physiological conditions, they have small cell bodies with many fine processes and occupy their own distinct space within the tissue. On activation, however,

their morphology becomes hypertrophic, with thickened processes and increased expression of intermediate filament proteins, such GFAP and Vimentin. The degree of astrocyte activation is dependent on the severity of the stimulus, therefore, large injuries will result in glial scar formed from overlapping astrocytes with microglia and pericytes (Sofroniew 2009; Pekny et al. 2018). The GFAP+ astrocytes in the lesions and peri-lesions had a morphology that may indicate an activated state, compared to the cells in the contralateral striatum with faint processes.

The current study found no significant differences in GFAP proteins levels between ipsilateral and contralateral striatum at 24 hours after MCAO. This result is consistent with a recent publication showing no activated astrocytes in the striatum at 24 hours after MCAO (30 minutes), whilst there clear clustering of GFAP+ cells at 48 hours (Buscemi et al. 2019). In the present study, the protein levels of GFAP were greatly increased in the ipsilateral striatum at 1 month after MCAO. Similar results were published by Yoon et al., who found a large elevation of astrocytes in the lesioned hemisphere at 1 month after MCAO (2 hours) in rats; whilst the astrocytic levels were low at the other time point measured, between 0 hours and 7 days after surgery (Yoon et al. 2018). At 3 months after MCAO, the GFAP protein levels had appeared to decrease again, and there was only a significant increase in the ipsilateral striatum of TgSwDI mice, although there was also a trend towards an increase in WT mice as well. The histological analysis also shows that an astrocytic response remains prominent in the ipsilateral striatum at 3 months after surgery. This result indicates that whilst the reactive astrocyte levels in the ipsilateral striatum have decreased between 1 and 3 months, there is still a long-lasting response in the lesion and peri-lesion.

An interesting finding in our histological cohort was that whilst Iba1+ cells were only elevated within the lesion, GFAP+ cells were increased in the lesion and peri-lesion. Previously, research has indicated that reactive astrocytes are more prominent in the peri-lesion than microglia/macrophages. A histological study investigating spatio-temporal glial responses following 30 minutes MCAO in mice, found that by 1 week GFAP+ cells clustered in the peri-lesion, but were largely absent from the lesion, whereas the Iba1+ cells were elevated throughout the lesion (Buscemi et al. 2019). Another study, by Yoon et al. showed a delayed increase in astrocytes in the border of an infarct, 1 month after 2 hours MCAO (Yoon et al. 2018). In the current study, the astrocytes were overlapping throughout the lesion rather than clustering around the edge. These discrepancies may be explained by the fact that the lesions in the present study were not infarcts, but were lesions of diffuse and selective neuronal loss. The heighted levels of astrocytes in the present study may act like a glial scar to protect the surrounding healthy tissue (Sofroniew 2015).

There is evidence that astrocytes play different roles at the different stages after focal ischaemia. As previously mentioned, upregulation of intermediate filament proteins, GFAP and Vimentin, is a hallmark of reactive astrocytes. In a model of neurotrauma, knock out mice $GFAP^{-/-}Vim^{-/-}$ had significantly less synaptic complexes after injury compared to WT mice at 4 days after injury, whereas at 14 days they had more synapse complexes (Wilhelmsson 2004). In that model, astrogliosis had neuroprotective effects at the acute stages after injury, whilst being detrimental later on. $GFAP^{-/-}Vim^{-/-}$ mice were more recently used in a study of focal ischaemia with cortical photothrombosis (Liu et al. 2014), which showed an impairment in motor function 3-28 days after surgery, and shorter corticospinal tract axons in the spinal cord, compared to WT mice. In this study, therefore, astrogliosis appeared to protect neuronal recovery throughout the disease process. The authors

proposed that GFAP$^{-/-}$Vim$^{-/-}$ mice had attenuated glial scar formation, preventing containment of neurotoxic compounds from diffusing into healthy tissue.

Reactive astrocytes may have other neuroprotective activities following focal ischaemia. Lin et al. propose that astrocytes mediate long-term post-ischaemic neuronal survival and repair (Lin et al. 2016). This study demonstrated that blocking the action of IL-17A, either with a knock out mouse or a specific antibody, lead to a reduction in new neuronal cells and in levels for presynaptic proteins, SNAP25 and synaptophysin, in the ischaemic striatum, 35 days after 60 minutes MCAO. They also showed that mRNA and protein levels of IL-17A have two peaks after ischaemia, one at 3 days and another smaller one at 28 days. When using an antibody to neutralise IL-17A activity, they treated the mice with it from 14 days after MCAO in order to inhibit the second peak. This demonstrated that delayed IL-17A increase had neuroprotective function, which they suggest occurs though promoting the migration and survival of neural progenitor cells (Lin et al. 2016). They found that astrocytes cultured from the damaged brains colocalise with IL-17A immunoreactivity on activation, although other inflammatory cells in the brain may release IL-17A. γδ-T cells have been shown to contribute to acute tissue damage by IL-17A release after ischaemia, likely by promoting the recruitment of neutrophils (Gelderblom et al. 2012).

Another method by which astrocytes may promote neuronal recovery after ischaemia is through the secretion of thrombospondins. Knock out mice of thrombospondin 1 and 2 have been found to have reduced synaptophsyin and PSD95 levels, and reduced axon sprouting, in the peri-lesion at 28 days after focal ischaemia (Liauw et al. 2008). These results support that hypothesis that thrombospondins facilitate axon sprouting and synaptogenesis by interactions with the extracellular matrix (Christopherson et al. 2005).

Furthermore, peri-synaptic astrocyte processes have been found to physically contact synaptic terminals, where they may promote stability of synapses (Bernardinelli et al. 2014; Carmona et al. 2009). In the present study, the large increase in GFAP protein levels in the ipsilateral striatum could be involved in promoting neuronal recovery at this time-point, although it did not coincide with an increase in VGLUT1 and PSD95 protein levels. The current study could be developed to investigate whether astrocytes are participate in synaptogenesis in the peri-lesion, 3 months after MCAO, with detected immunohistochemistry markers for axonal plasticity GAP43, astrocytes GFAP, and endogenous PSD95:eGFP. Additional exploration could be conducted into whether thrombospondins or epthrin signalling is involved, as previously suggested (Carmona et al. 2009; Overman et al. 2012; Liauw et al. 2008).

Recently there was been advancements in understanding the complexities of reactive astrocyte transcriptome in different injuries, similarly to microglia (Liddelow & Barres 2017). Rakers et al. used RiboTag to isolate and sequence astrocyte-specific mRNAs at 72 hours post-tMCAO, and found that the astrocytes were expressing genes associated with neuroprotection and neurotoxicity (Rakers et al. 2019). Among the genes upregulation was Stat3 (Signal transducer and actor of transcription 3), which is involved in IL-6/JAK/STAT3 pathway leading to cytokine production. The researchers made an astrocyte-specific conditional Stat3 knockout mouse, and found that this had smaller ischaemic lesions than WT mice following tMCAO (Rakers et al. 2019). Moreover, there is evidence that activated microglia may induce a neurotoxic phenotype in astrocytes (Liddelow et al. 2017), therefore, astrocytic transcriptome may be influenced by the chronic neuroinflammation following ischaemia. Future development of the present study would be to use techniques

to elucidate the astrocyte transcriptome at acute, sub-acute and chronic following MCAO, and to determine whether they have more neurotoxic or neuroprotective functions.

In the present study, there was an implication that the GFAP protein levels were increased in the ipsilateral striatum of TgSwDI mice, and not WT mice, although there was no overt genotype effect. As previously discussed, the expectation was that TgSwDIAPP expression would prime the glial cells, and MCAO surgery would lead to an exaggerated response of microglia/macrophages and astrocytes in these animals (discussed in Section 6.4.3). The evidence indicates that TgSwDIAPP expression did cause a small increase in astrocyte levels, therefore, a future development of this study could be to determine if there is a genotype-effect on the astrocytic transcriptomes. TgSwDIAPP expression may stimulate different post-ischemic phenotypes in astrocytes compared to in WT mice, which may affect their functions.

5.4.4 Conclusions

This study demonstrated that brief focal ischaemia lead to long-term neuronal and axonal pathology, degeneration of glutamatergic pre- and postsynaptic terminals, and chronic glial responses within the lesion territory. Moreover, the levels of microglia/macrophages were inversely related to postsynaptic loss, implying that these cells may have roles in synaptic degeneration post-ischaemia. Although there were no overt genotype effects, there was an indication the TgSwDIAPP expression caused greater presynaptic degeneration in the peri-lesion and higher astrocyte levels in the lesioned striatum. The implication of this study is that focal ischaemia causes more pathological changes than human mutated APP expression.

Chapter 6: The long-term impact of focal ischaemia and concurrent TgSwDIAPP expression on glutamatergic synapses and glial responses in connected brain regions

6.1 Introduction

The results in the previous chapter demonstrated that focal ischaemia leads to long-term degeneration of neurons, axons and glutamatergic synaptic terminals within the lesion territory, which coincided with elevated levels of microglia/macrophages and astrocytes. Contrary to the initial hypothesis, these changes were mostly unaffected by the expression of TgSwDIAPP, although there was indication of greater astrocyte elevation in TgSwDI mice. There is a growing appreciation for the impact of secondary neurodegenerative changes following a focal ischaemic injury. Evidence in humans and rodent models have revealed that neurodegeneration can occur spreading from the primary injury site to remote brain regions it connects with, known as diachisis (J. Zhang et al. 2012; Abe et al. 2003; Nakane et al. 1992; Winter et al. 2015). Neuroimaging of patients with lesions in the striatum have also shown development of neuropathology in the substantia nigra and thalamus at later stages (Nakane et al. 1992). Both of these brain regions are in circuits with the striatum, as part of the motor network. The schematic diagram in Figure 1.7 shows this network in a mouse brain: inhibitory neurons project from the striatum to the substantia nigra pars reticulata (SN_R) in the direct pathway, whilst inhibitory and excitatory projections connect the striatum, globus pallidus (GPe) and subthalamic nucleus (STN) and SN_R, which projects back to the thalamus (Benarroch 2016). These projections run through

the internal capsule white matter tract (Reinius et al. 2015). In the present study, secondary neurodegeneration and glial responses were investigated in the internal capsule, SN_R and thalamus.

There is a gap in the literature as to whether concurrent β-amyloid pathology worsens secondary neurodegeneration and glial responses after focal ischaemia. Nguyen et al. found that distal MCAO in WT mice lead to neuropathology in remote brain regions of just the ipsilateral hemisphere, whilst pathology changes were found in both hemispheres in a TgAβPP mouse (Nguyen et al. 2018). The present study sought to determine whether focal ischaemia resulted in neurodegeneration and glial responses in remote regions through diachisis, and whether these changes were exaggerated in TgSwDI mice.

6.1.1 Hypothesis

Focal ischaemia leads to long-term degeneration of glutamatergic synaptic terminals and axons in remote brain regions by diachisis, coinciding with chronic glial responses, culminating in progressive functional decline. In cases with concurrent β-amyloid, secondary neurodegeneration and glial responses is exacerbated, causing worsened functional decline.

6.1.2 Aims

The aim of this study was to determine whether transient MCAO causes long-term degeneration of axons and glutamatergic synaptic terminals in remote brain regions that connect with the striatum, and whether this is related to the extent of cellular inflammation. Further, we aimed to elucidate whether these changes are exaggerated in TgSwDI mice.

6.2 Materials and Methods

6.2.1 Animals, surgery and tissue collection

The tissue used in the present study was from the same mice used in Chapter 5. The animals, surgery and tissue collection procedures were all according to Sections 5.2.1, 5.2.2 and 5.2.4.

6.2.2 Detection of axonal pathology

Axonal bulbs were detected in the internal capsule and SN_R, in tissue sections from -2.06mm and -.2.92mm from bregma. Immunohistochemistry for APP was performed on this tissue as previously described Section 5.2.6.

6.2.2.1 Analysis in the internal capsule

The APP+ axon bulbs were counted in the ipsilateral and contralateral internal capsule and normalised to the area of this structure, using the cell counter plugin on ImageJ. The density of APP+ axon bulbs was compared between the hemispheres and genotypes using two-way ANOVA.

6.2.2.2 Analysis in the SN_R

The APP+ axon bulb density was very high in the SN_R, therefore, it was not possible to count the individual bulbs. Instead the %density of bulbs was measured using a threshold to cover the positive staining. The ipsilateral SN_R was delineated from the cresyl violet imaged and superimposed on to the images of APP immunostained sections. As the SN_R constantly appeared to be smaller on the ipsilateral side, likely due to atrophy, the ipsilateral ROI was used to measure the density on the contralateral side as well. The

%density of APP+ axon bulbs was compared between the hemispheres and genotypes using two-way ANOVA.

6.2.3 Detection of glutamatergic synaptic terminals in the SN_R and thalamus.

6.2.3.1 Analysis in the SN_R

Postsynaptic terminals were visualised by PSD95:eGFP signal in the SN_R using slide scanner microscopy, see Section 5.2.7. The %density was measured as previously described in Section 5.2.9.1, within a ROI delineated from the ipsilateral SN_R, as used in 6.2.2.2. The same ROI's were used to measure the signal on the ipsilateral and contralateral hemispheres.

6.2.3.2 Analysis in the thalamus

Glutamatergic pre- and postsynaptic terminals were detected in the thalamus using immunohistochemistry of VGLUT1 and slide scanner microscopy, see Section 5.2.7. As before, the %density of this signal was measured in ImageJ with a threshold. The regions of interest were the VPM and VPL thalamic nuclei, which had been delineated from images of the cresyl violet sections, similar to in Section 5.2.9.1. The %density of PSD95 and VGLUT1 was compared between the hemispheres and genotypes using two-way ANOVA.

6.2.4 Detection of microglia/macrophages and astrocytes

In additional sections taken from 2.06mm and -.2.92mm from bregma, immunohistochemistry was used to detect Iba1+ and GFAP+ cells, as in Section 5.2.8. The %density of these signals were analysed using the same method as in 5.2.9.1., within the ROIs: internal capsule, SN_R, VPM and VPL, which were delineated from slide scanner images of cresyl violet stained sections. The ROI's for the SN_R were taken from the

ipsilateral hemisphere and flipped for analysis on the contralateral hemisphere. For the other regions, the areas were delineated from both hemispheres in the cresyl violet images. The %densities of Iba1 and GFAP were compared between the hemispheres and genotypes using two-way ANOVA.

6.2.5 Detection of β-amyloid deposits

Sections from -2.06mm from bregma were taken from TgSwDI mice, 3 months after either MCAO or sham surgery. Detection of β-amyloid was undertaken with immunohistochemistry of 6E10, according to Section 2.6.3.1. As before, the %density of the stain was measured with a threshold, in the ROIs delineated from the contralateral and ipsilateral VPM and VPL from the cresyl violet sections of each mouse.

6.2.6 Statistical analysis

The density for each marker, in each brain, was compared between with two-way ANOVA, with surgery and genotype as factors. Post-hoc analysis was performed with Bonferroni's multiple comparison test. Spearman's rank correlation was used to determine relationships between the densities of the markers. For all analysis, $p < 0.05$ was considered to be statistically significant.

6.3 Results

The previous chapter had demonstrated that MCAO surgery induces long-term glutamatergic synaptic loss and chronic glial responses in the striatum. In this chapter sought to determine whether MCAO surgery results in secondary axon and glutamatergic synaptic loss, plus chronic glial responses, in these connected brain regions by diaschisis, and this is exacerbated by TgSwDIAPP expression. Therefore, pathological changes were

investigated in the regions that connect with the striatum: internal capsule, SN_R and thalamus.

6.3.1 MCAO lead to long-term secondary neurodegeneration in the internal capsule and substantia nigra, but not the thalamus, and with no genotype effect.

6.3.1.1 Internal capsule

The first aim of the study was to investigate the pathological changes in the internal capsule, the white matter tract which connects the striatum and substantia nigra. As before, APP immunohistochemistry was used to analyse the levels of axon degeneration in this region. The results in the previous chapter had shown that there is axon pathology in the internal capsule, however, this was done by measuring the volume of tissue containing axon bulbs. Here, the number of axon bulbs was counted and normalised to the area of the internal capsule, for a more sensitive measurement of axon pathology (Figure 6.1A). Statistical analysis with two-way ANOVA demonstrated that there was a significant surgery effect ($F(1,20) = 24.47$, $p < 0.0001$), with no genotype effect ($F(1,20) = 0.382$, $p = 0.544$) and no interaction ($F(1,20) = 0.0985$, $p = 0.757$) (Figure 6.1B). Post-hoc analysis revealed that there was an increase in the density of axonal bulbs in the ipsilateral internal capsule of both WT and TgSwDI mice. This finding indicated that a focal ischaemic lesion in the striatum caused secondary neurodegeneration leading to axon degeneration in the internal capsule, which was not exacerbated in TgSwDI mice.

6.3.1.2 Substantia nigra

The striatum projects to the substantia nigra through direct and indirect pathways (Figure 1.7). The axon bulb densities were measured in the ipsilateral and contralateral SN_R of WT

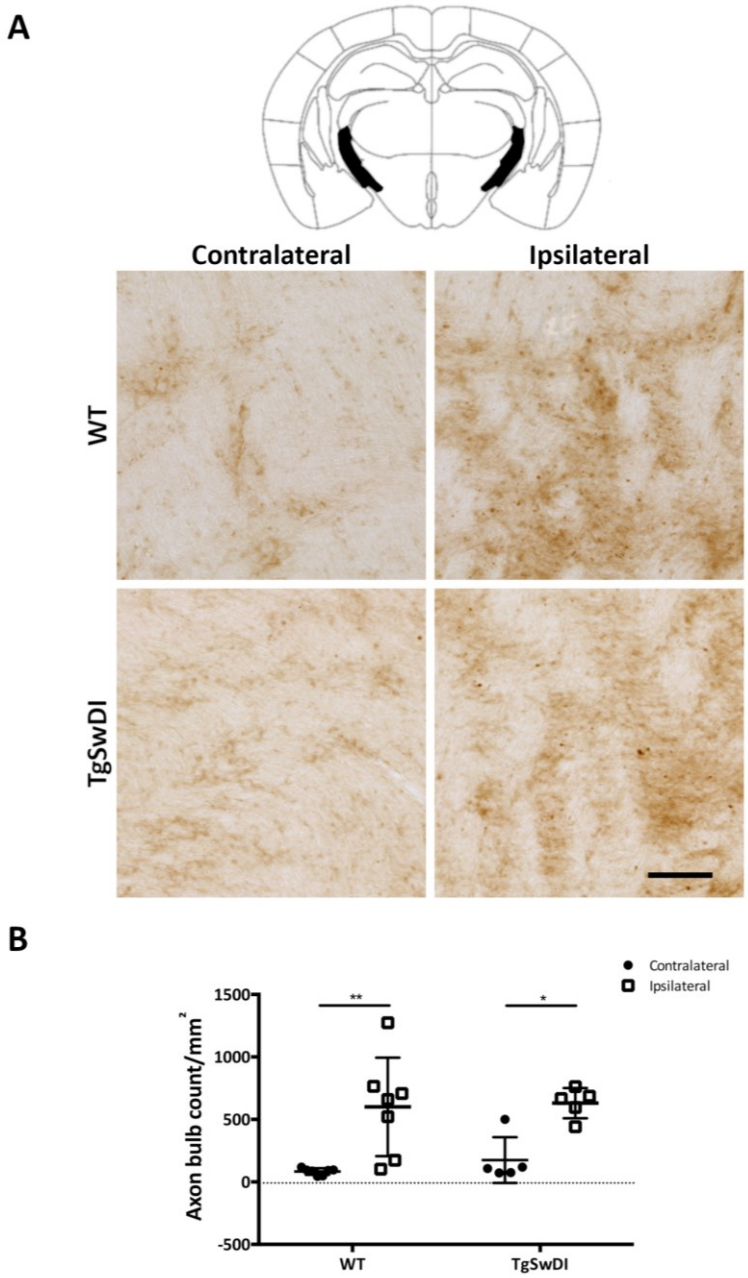

Figure 6.1 MCAO leads to long-term axonal degeneration in the ipsilateral internal capsule. (A) APP immunohistochemistry used to detect axonal bulbs in the internal capsule. (B) There was significantly higher density of axonal bulbs in the ipsilateral internal capsule compared to the contralateral, in both WT and TgSwDI mice. Data presented as mean ± SD, n = 5,7 per group. Two-way ANOVA with Bonferroni's multiple comparison test. **/ *p<0.05. Scale bar = 50µm.

and TgSwDI mice, 3 months after MCAO. There were many more axon bulbs in the ipsilateral SN_R compared to the internal capsule, and the bulbs often clustered together, making it difficult to count them individually. The %density of APP+ bulbs, therefore, was used to measure the level of axon degeneration in the SN_R. The region of the ipsilateral SN_R was delineated from the cresyl violet stained sections. As the ipsilateral SN_R consistently looked smaller than the contralateral SN_R, the region of interest for the ipsilateral side was also used for the contralateral side when the image was flipped horizontally. This method of analysis was also used for measuring the %density of PSD95, Iba1 and GFAP. There was a significant surgery effect on APP+ axon bulbs %density in the ipsilateral SN_R ($F(1,20) = 23.44$, $p < 0.0001$), but there was no genotype effect ($F(1,20) = 0.0059$, $p = 0.940$) and no interaction ($F(1,20) = 0.556$, $p = 0.465$) (Figure 6.2B). Post-hoc analysis showed that increase in axon bulb density was increased in both the WT and TgSwDI ipsilateral SN_R. Next, the density of postsynaptic terminals in the SN_R was analysed to determine whether there was an impact of MCAO surgery and TgAPP expression (Figure 6.3A). There was a significant surgery effect, reducing PSD95 %density in the ipsilateral SN_R ($F(1, 20) = 24.12$, $p < 0.0001$), with no genotype effect ($F(1, 20) = 1.346$, $p = 0.260$) and no interaction ($F(1, 20) = 0.0761$, $p = 0.786$) (Figure 6.3B). Bonferroni's multiple analysis showed that the significant reduction of PSD95 %density in the ipsilateral SN_R of WT and TgSwDI mice. Taken together, MCAO resulted in long-term axon and glutamateric postsynaptic terminals in the ipsilateral SN_R, however, there was no exaggeration in TgSwDI mice.

6.3.1.3 Thalamus

In the striatonigral pathway, glutamatergic transmission projects from the SN_R to the thalamus (Figure 1.7). Thalamic nuclei, the ventral posteromedial (VPM) nucleus and the ventral posterolateral (VPL) nucleus, have been shown to be vulnerable to secondary

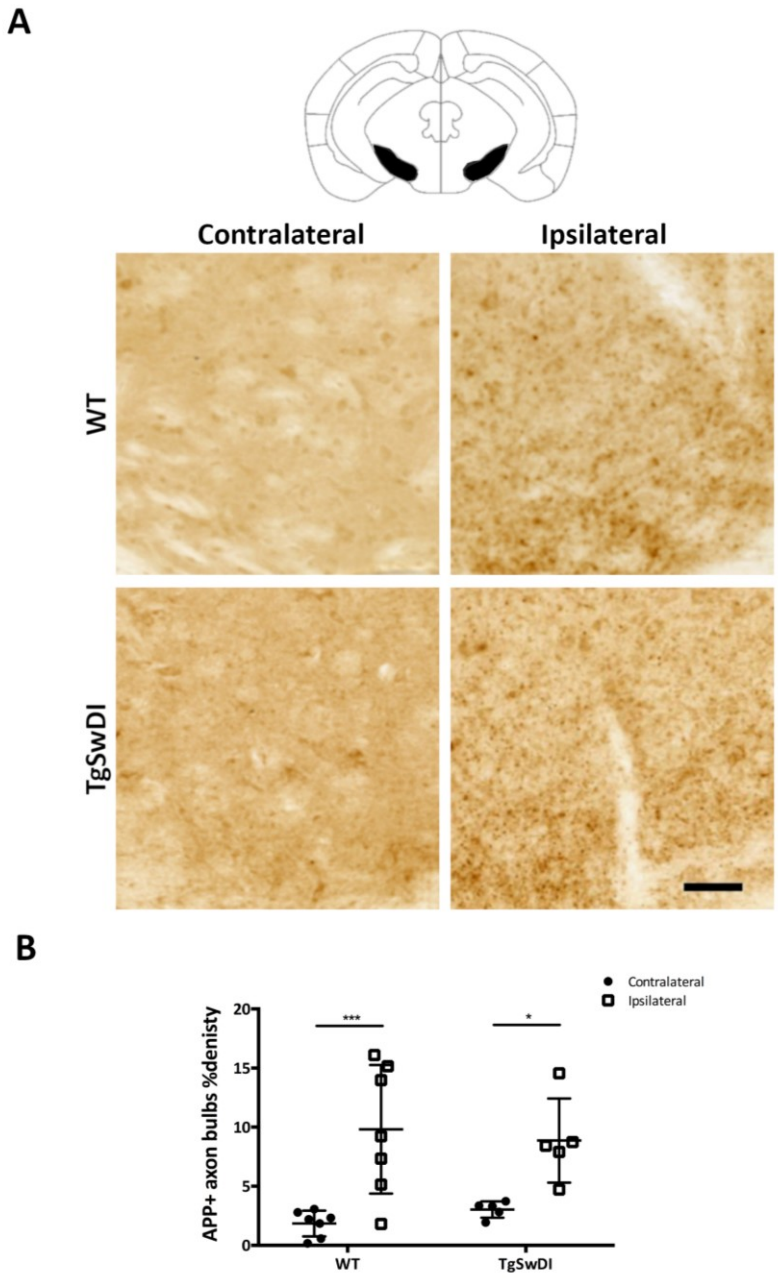

Figure 6.2 MCAO lead to long-term axonal degeneration in the ipsilateral SN_R. (A) APP immunohistochemistry used to detect axonal bulbs in the SN_R. (B) There was significantly higher density of axonal bulbs in the ipsilateral SN_R compared to the contralateral, in both WT and TgSwDI mice. Data presented as mean ± SD, n = 5,7 per group. Two-way ANOVA with Bonferroni's multiple comparison test. **/ *p<0.05. Scale bar = 50µm.

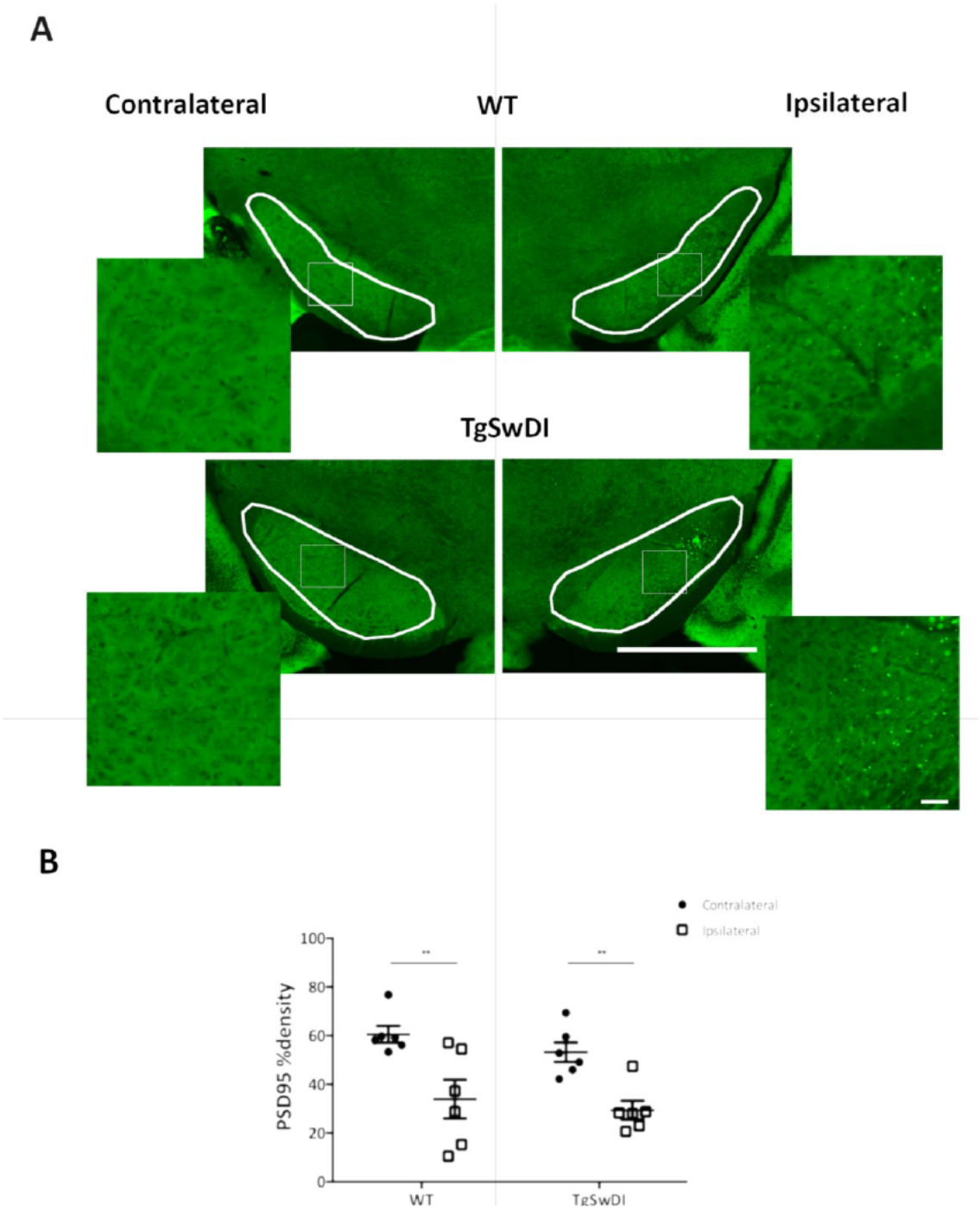

Figure 6.3 MCAO lead to to long-term PSD95+ synaptic terminal loss in the ipsilateral SN_R. (A) PSD95:eGFP %density measured in the ipsilateral and contralateral SN_R, 3 months after MCAO. (B) There was significantly lower density of PSD95 %density in the ipsilateral SN_R compared to the contralateral, in both WT and TgSwDI mice. Data presented as mean ± SD, n = 6,6 per group. Two-way ANOVA with Bonferroni's multiple comparison test. **p<0.05. Scale bar = 1mm, insert 50µm. Grey boxes = inserts.

neurodegeneration following permanent MCAO (Abe et al. 2003). The thalamus is also a prominent region for β-amyloid pathology in TgSwDI mice (Davis et al. 2004). Thus, the impact of focal ischaemia and TgSwDIAPP expression on pre- and postsynaptic terminals in the thalamus was investigated. As before, the cresyl violet stained sections were used to delineate the regions of the VPM and VPL on the ipsilateral and contralateral hemispheres, and the regions were superimposed onto the sections stained for VGLUT1 and PSD95 (Figure 6.4A).

VGLUT1 %density in the VPM was not affected by surgery ($F(1, 22) = 1.900$, $p = 0.182$) or genotype ($F(1, 22) = 0.944$, $p = 0.342$), and no there was no interaction between them ($F(1, 22) = 0.592$, $p = 0.450$) (Figure 6.4B). Similarly, there was no effect of surgery ($F(1, 22) = 1.747$, $p = 0.200$) or genotype ($F(1, 22) = 0.394$, $p = 0.537$) of VGLUT1 %density in VPL, and no interaction ($F(1, 22) = 0.295$, $p = 0.592$) (Figure 6.4C).

The %density of PSD95 was measured using the same method as for VGLUT1. This analysis revealed that there was a significant increase in PSD95 %density in the VPM with surgery ($F(1, 22) = 24.11$, $p < 0.0001$), however, there was no genotype effect ($F(1, 22) = 0.329$, $p = 0.572$) and no interaction ($F(1, 22) = 0.329$, $p = 0.572$) (Figure 6.4D). Post-hoc analysis showed that PSD95 %density was increased in the ipsilateral VPM of both WT and TgSwDI mice. In the VPL, the two-way ANOVA revealed that there was an overall surgery effect on the PSD95% density in the ipsilateral hemisphere ($F(1, 22) = 5.46$, $p = 0.0289$), but no genotype effect ($F(1, 22) = 0.543$, $p = 0.469$) and no interaction ($F(1, 22) = 0.215$, $p = 0.647$) (Figure 6.4E). Although there was an overall surgery effect, Bonferroni's multiple comparison test did not find a significant difference between the hemispheres of either WT or TgSwDI mice. Overall, there was no difference in the density of glutamatergic presynaptic terminals in either thalamic nuclei, however, there was evidence that focal

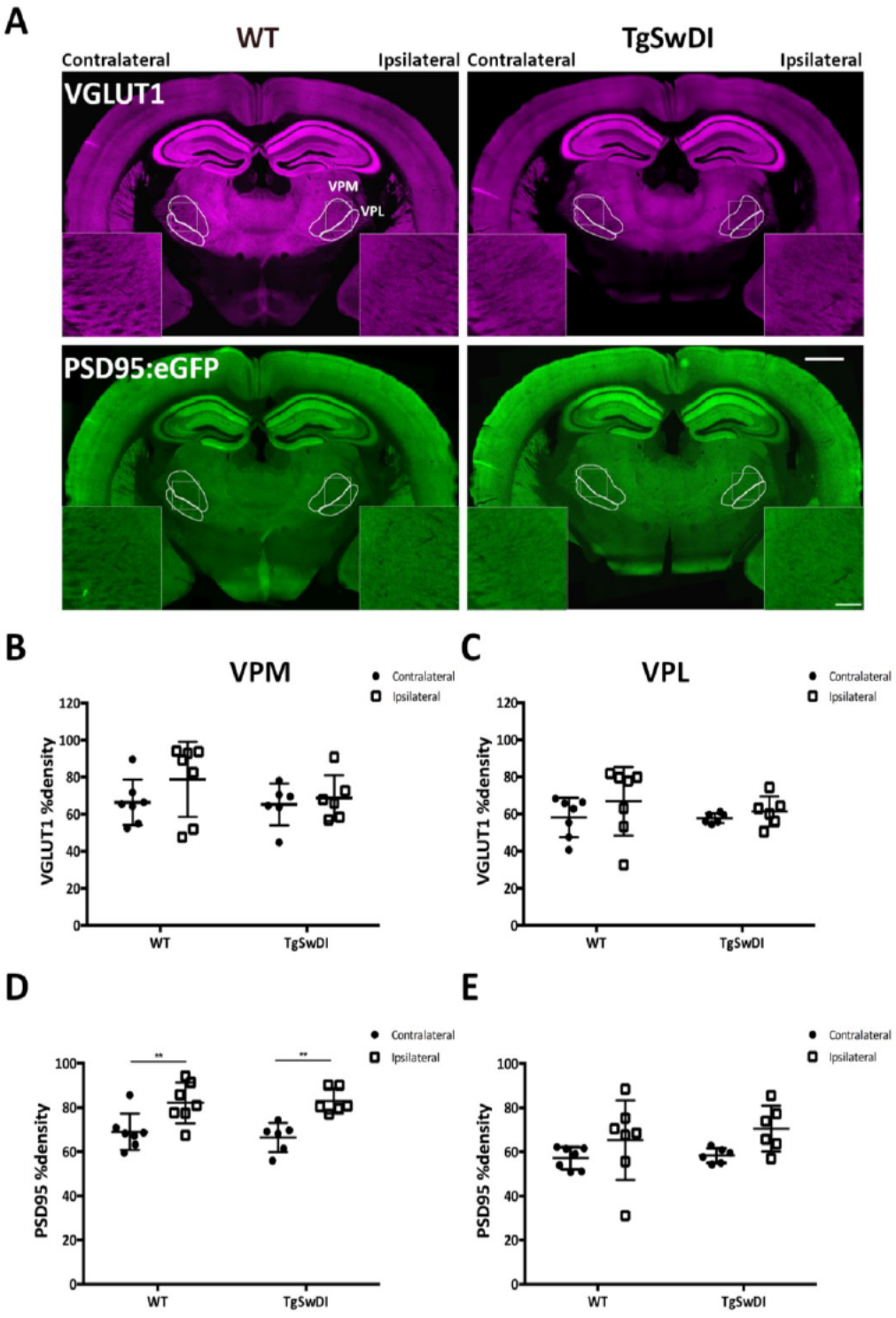

Figure 6.4 MCAO resulted in long-term increase of PSD95 %density in the ipsilateral VPM thalamic nuclei. (A) Density of VGLUT1 and PSD95:eGFP measured in the VPM and VPL thalamus. (B,C) VGLUT1 %density was not significantly changed between the ipsilateral and contralateral VPM and VPL, and no genotype effect. (D) PSD95 %density were increased in the ipsilateral VPM compared to the contralateral, however there were no changes in VPL (E). Data presented as mean ± SD, n = 6,7 per group. Two-way ANOVA with Bonferroni's multiple comparison test. **p<0.05. Scale bar = 1mm, insert 200µm. Grey boxes = inserts.

ischaemia stimulated an increase in postsynaptic terminals in the ipsilateral VPM thalamus, with no genotype effect.

6.3.2 MCAO leads to long-term glial responses in remote brain regions, with an exaggerated effect in the internal capsule and thalamus of TgSwDI mice

6.3.2.1 Internal capsule

Chronic glial responses have been linked with white matter disruption, as previously found in models of hypoperfusion from our lab (Kitamura et al. 2017; Coltman et al. 2011). The next question to address in this study, therefore, was whether chronic glial responses occurred in the internal capsule after focal ischaemia in the striatum, and whether there is a differential effect between WT and TgSwDI mice. The density of microglia/macrophages was detected with immunohistochemistry analysis for Iba1 (Figure 6.5A). The regions of the internal capsule were delineated from the cresyl violet stained sections and the Iba1 %density was measured in these regions. There was a significant surgery effect ($F(1, 22) = 119.8$, $p < 0.0001$) and genotype effect ($F(1, 22) = 10.42$, $p = 0.0039$) increasing Iba1 %density in the ipsilateral internal capsule, although there was no interaction ($F(1, 22) = 0.842$, $p = 0.369$) (Figure 6.5B). Bonferroni's multiple comparisons test showed that there was a significant Iba1% density increase in the ipsilateral internal capsule compared to the contralateral hemisphere; and a greater increase in the TgSwDI ipsilateral internal capsule compared to the WT.

The density of astrocytes was also analysed with GFAP immunohistochemistry in neighbouring coronal sections from the same mice (Figure 6.5C). There was a surgery effect ($F(1, 22) = 61.95$, $p < 0.0001$) and a genotype effect ($F(1, 22) = 14.31$, $p = 0.001$) on

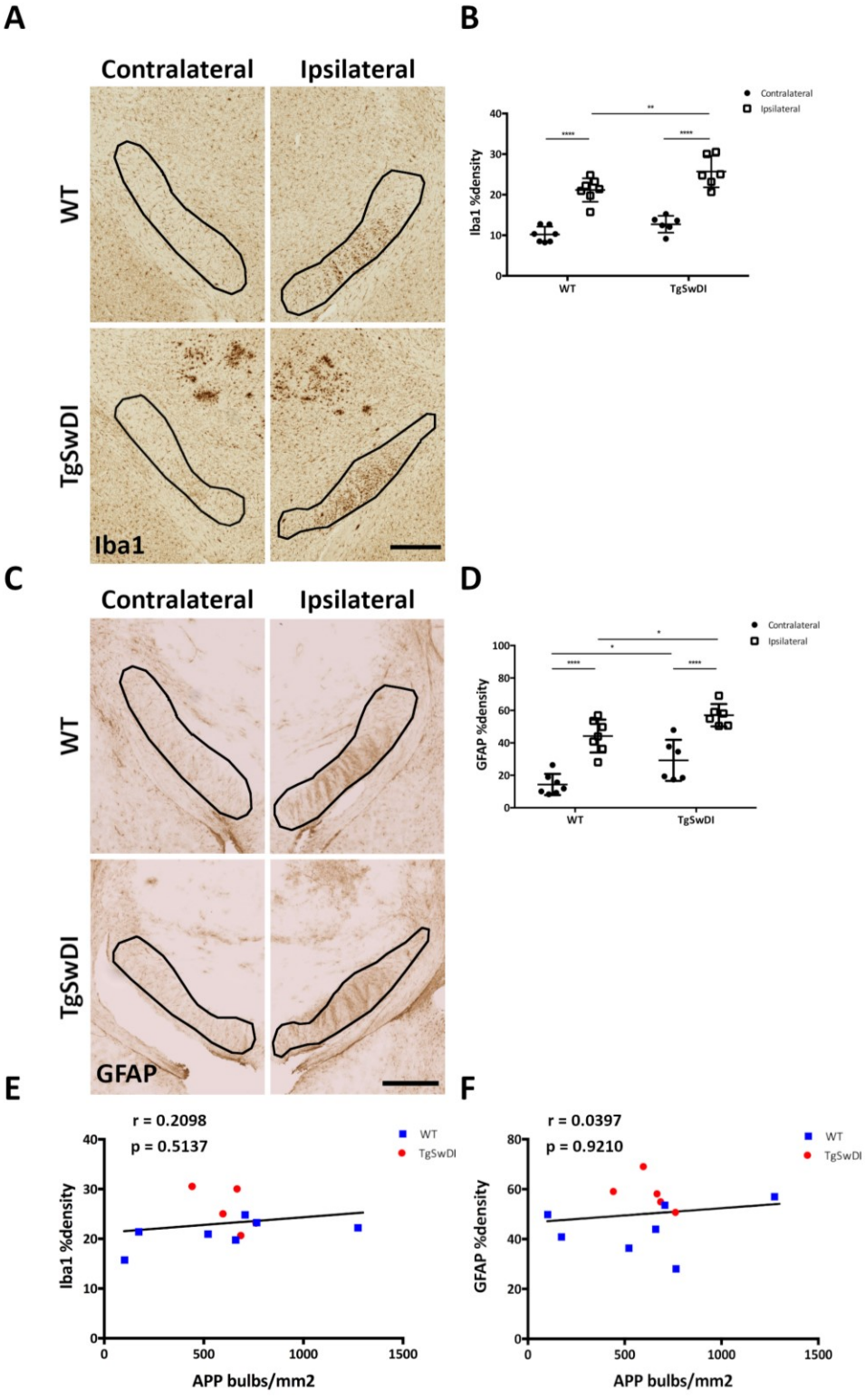
A
B
Contralateral
Ipsilateral
WT
TgSwDI
Iba1
Contralateral
Ipsilateral
Iba1 %density
WT
TgSwDI
C
D
Contralateral
Ipsilateral
WT
TgSwDI
GFAP
Contralateral
Ipsilateral
GFAP %density
WT
TgSwDI
E
F
r = 0.2098
p = 0.5137
WT
TgSwDI
Iba1 %density
APP bulbs/mm2
r = 0.0397
p = 0.9210
WT
TgSwDI
GFAP %density
APP bulbs/mm2

Figure 6.5 MCAO lead to chronic increases in microglia/macrophage and astrocyte levels in the ipsilateral internal capsule, which were exaggerated in TgSwDI mice. (A) Iba1 immunohistochemistry used to detect microglia/macrophages in the internal capsule. (B) There was an increase in Iba1 %density in the ipsilateral internal capsule compared to the contralateral, with an even greater increase in the TgSwDI mice. (C) GFAP immunohistochemistry used to detect astrocytes in the internal capsule. (D) There was an increase in GFAP %density in the ipsilateral internal capsule, with exaggerated GFAP %densities in both hemispheres of TgSwDI mice, compared to WT. (E) There was no relationship between the densities of axon bulbs and microglia/macrophages in the ipsilateral internal capsule. (F) Similarly, there was no relationship with the densities of axon bulbs and astrocytes in the ipsilateral internal capsule. Data presented as mean ± SD, n = 6,7 per group. Two-way ANOVA with Bonferroni's multiple comparison test.****p<0.0001. **/*p = 0.05. Scale bar = 200µm.

GFAP %density (Figure 6.5D), with an interaction between the factors ($F(1, 22) = 0.0766$, $p = 0.785$). Bonferroni's multiple comparison test revealed that GFAP %density is increased in the ipsilateral internal capsule in both WT and TgSwDI mice, plus there was a greater increase in both hemispheres of TgSwDI mice compared to the WT. Taken together, these results indicate that focal ischaemic injury in the striatum leads to long-term chronic elevation of microglia/macrophages and astrocytes in the internal capsule, and concurrent TgSwDIAPP expression causes a greater increase in neuroinflammation as compared to WT.

To determine whether there is a relationship between the density of degenerated axons and microglia/macrophages and astrocytes in the ipsilateral internal capsule, the densities of axon bulbs were plotted against Iba1 and GFAP %densities and analysed with Spearman rank. There was no correlation between axon bulb density with the densities of Iba1 ($r = 0.2098$, $p = 0.5137$) (Figure 6.5E), or GFAP ($r = 0.03497$, $p = 0.921$) (Figure 6.5F). The levels of microglia/macrophages and astrocytes do not directly relate to the density of degenerating axons in the internal capsule.

6.3.2.2 Substantia nigra

The next stage of this study was to determine whether chronic glial responses occurred within the SN_R following MCAO and whether it is exacerbated in TgSwDI mice. As before, microglia/macrophage were detected with Iba1 immunohistochemistry (Figure 6.6A). Iba1% density was significantly increased with surgery ($F(1,22) = 17.29$, $p = 0.0004$), although there was no genotype effect ($F(1,22) = 0.421$, $p = 0.523$) and no interaction ($F(1,22) = 2.122$, $P = 0.159$) (Figure 6.6B). Bonferroni's multiple comparisons test showed that there was an increase in Iba1% density in the ipsilateral SN_R in WT mice only. Next, the astrocyte levels were analysed in the SN_R (Figure 6.6C). There was an effect of surgery on the GFAP %densities in the SN_R ($F(1, 22) = 155.5$, $p < 0.0001$), but there was no effect of ($F(1, 22) = 1.055$, $p = 0.315$) and no interaction ($F(1, 22) = 0.113$, $p = 0.740$) (Figure 6.6D). There was a significant increase in the astrocyte levels in the ipsilateral SN_R in both WT and TgSwDI mice. Taken together, these results demonstrate that focal ischaemic injury in the striatum results in chronic neuroinflammation in the SN_R and concurrent TgSwDI expression does not cause an exaggerated response.

The density of axon bulbs was plotted against the densities of microglia/macrophage and astrocytes, to determine whether there is a relationship between axon degeneration and glial cells in the ipsilateral SN_R. APP+ axon bulb %density did not correlate with Iba1 %density ($r = 0.1189$, $P = 0.716$) or GFAP %density ($r = 0.5245$, $P = 0.0839$) (Figure 6.6E,F). This indicates that in the ipsilateral SN_R long-term axon degeneration is either a cause or consequence of astrogliosis in the same region.

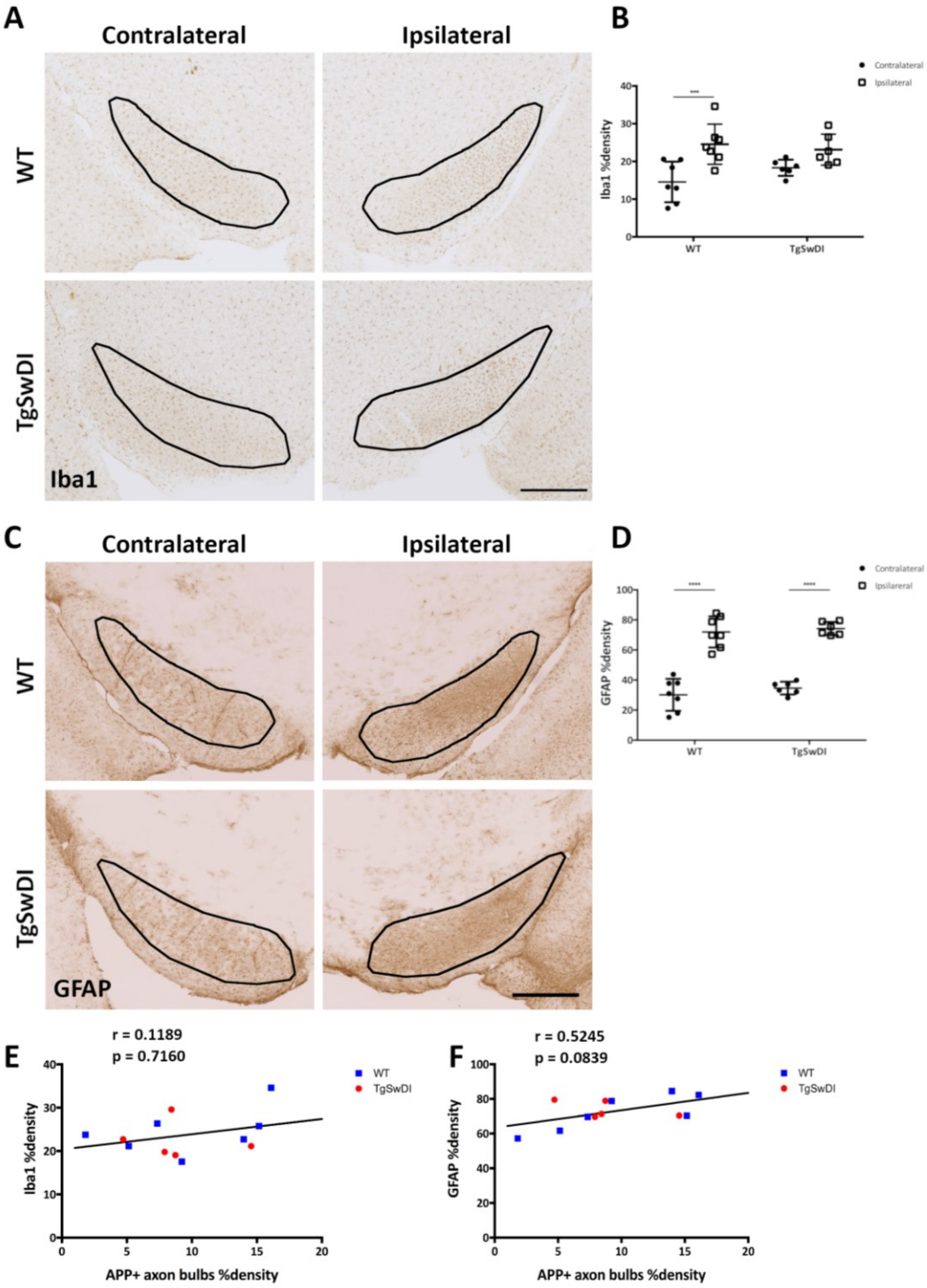
A
Contralateral
Ipsilateral
WT
TgSwDI
Iba1
B
Contralateral
Ipsilateral
Iba1 %density
WT
TgSwDI
C
Contralateral
Ipsilateral
WT
TgSwDI
GFAP
D
Contralateral
Ipsilareral
GFAP %density
WT
TgSwDI
E
r = 0.1189
p = 0.7160
WT
TgSwDI
Iba1 %density
APP+ axon bulbs %density
F
r = 0.5245
p = 0.0839
WT
TgSwDI
GFAP %density
APP+ axon bulbs %density

Figure 6.6 MCAO lead to chronic microglia/macrophage and astrocyte levels in the ipsilateral SN_R. (A) Iba1 immunohistochemistry used to detect microglia/macrophages. (B) Iba1 %density was significantly increased in the ipsilateral SN_R, compared to contralateral, in WT mice only. (C) GFAP immunohistochemistry to detect astrocytes. (D) GFAP %density was elevated in the ipsilateral SN_R, compared to contralateral, in both genotypes. (E) Iba1 %density did not correlate with the APPs+ axon bulbs %density in the ipsilateral SN_R. (F) Similarly, there was no relationship with the densities of axon bulbs and astrocytes in the ipsilateral SN_R. Data presented as mean ± SD, n = 6,7 per group. Two-way ANOVA with Bonferroni's multiple comparison test. ***/ *p<0.05. Scale bar = 500µm.

6.3.2.3 Thalamus

Next, the chronic glial responses were investigated in the VPM and VPL thalamic nuclei (Figure 6.7). There was a significant effect of genotype in the VPM Iba1 %density ($F(1, 22) = 10.51$, $p = 0.0037$), whilst there was a trend towards a surgery effect, although it did not reach significance ($F(1, 22) = 3.975$, $p = 0.0593$) and no interaction ($F(1, 22) = 0.166$, $p = 0.688$) (Figure 6.7B). Bonferroni's multiple comparison test showed that there was an increase in Iba1 %density in the ipsilateral VPM in TgSwDI mice, compared to the ipsilateral VPM of WT mice. In the VPL, there was a genotype effect on the Iba1 %densities ($F(1, 22) = 8.881$, $p = 0.0068$), whereas there was no effect of surgery ($F(1, 22) = 2.959$, $p = 0.0037$) and no interaction ($F(1, 22) = 0.853$, $p = 0.338$) (Figure 6.7C). Post-hoc analysis showed that there was an increase in Iba1 %density in the ipsilateral VPL of TgSwDI, compared to the ipsilateral VPL of WT mice. Taken together, this analysis revealed that there was a trend towards an increase in the microglia/macrophage levels in the thalamus of the lesioned hemisphere, however, there was an exaggerated increase in the TgSwDI mice.

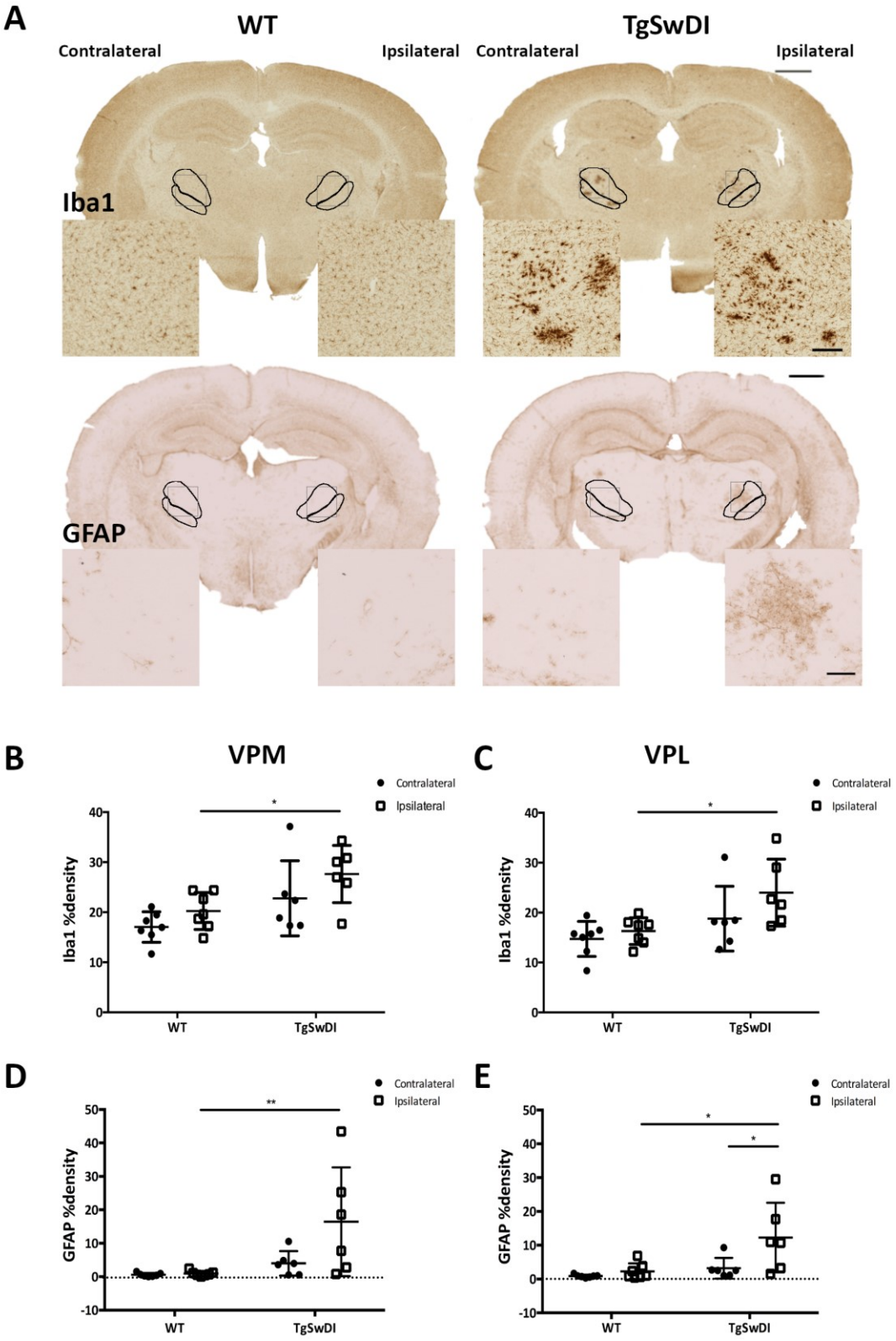
A
WT
TgSwDI
Contralateral
Ipsilateral
Contralateral
Ipsilateral
Iba1
GFAP
B
VPM
C
VPL
Contralateral
Ipsilateral
Iba1 %density
WT
TgSwDI
D
E
GFAP %density

Figure 6.7 Microglia/macrophage and astrocytes densities increased in the TgSwDI VPM and VPL, compared to WT mice. (A) Iba1 and GFAP immunohistochemistry. Iba1 %density increased in the TgSwDI ipsilateral (B) VPM and (C) VPL, compared to the ipsilateral VPM and VPL in WT mice, with no significant surgery effect. GFAP %density increased in the TgSwDI ipsilateral (D) VPM and (E) VPL, with greater GFAP %density in TgSwDI ipsilateral VPL compared to contralateral VPL. Data presented as mean ± SD, n = 6,7 per group. Scale bar = 1mm, insert 200µm. Two-way ANOVA with Bonferroni's multiple comparison test. **p<0.05. Scale bar = 1mm, insert 200µm.

Next, the levels of astrocytes were measured in the same thalamic regions and compared between the ipsilateral and contralateral hemispheres, and between the genotypes. In the VPM, there was a significant effect of genotype ($F(1, 22) = 9.128$, $p = 0.0063$) and almost a significant effect of surgery ($F(1, 22) = 4.177$, $p = 0.0531$), with no interaction ($F(1, 22) = 3.718$, $p = 0.0668$) (Figure 5.7D). Bonferroni's multiple comparison test showed that there was a greater GFAP %density in the ipsilateral VPM of TgSwDI mice, compared to the ipsilateral VPM of WT mice. Although it did not quite reach significance, there appears to be a trend towards an increase in GFAP %density in the ipsilateral VPM compared to the contralateral in TgSwDI. The GFAP %densities were also measured in the VPL. There was a significant genotype effect ($F(1, 22) = 8.852$, $p = 0.007$) and significant surgery effect ($F(1, 22) = 6.415$, $p = 0.0.019$), although there was no significant interaction ($F(1, 22) = 8.852$, $p = 0.007$) (Figure 5.7E). Bonferroni's multiple comparisons test found that there was a significant increase in the GFAP %densities between the ipsilateral VPL of TgSwDI mice and the WT; plus there was a significant increase between the ipsilateral and contralateral VPL of TgSwDI mice. Overall, this analysis showed that focal ischaemia leads to a trend of increased reactive astrocyte levels in the ipsilateral thalamus, which is exaggerated in TgSwDI mice.

Taken together, these results demonstrate that TgSwDI mice have chronic elevated levels glial cells in the ipsilateral thalamus, 3 months after MCAO surgery. Plus, there was a trend towards an increase in microglia/macrophages and astrocytes in the ipsilateral hemispheres compared to the contralateral, however, the changes were mostly too small to reach statistical significance. The densities of Iba1 or GFAP did not correlate with the densities of VGLUT1 or PSD95 (data not shown), indicating that the levels of these neuroinflammatory cells were not related to the small increases observed in the synaptic terminals levels.

6.3.3 β-amyloid levels in TgSwDI mice were unchanged with MCAO surgery

As there was a genotype effect on chronic neuroinflammation in the ipsilateral thalamus of TgSwDI, the next stage in the investigation was to determine whether there was a surgery effect on β-amyloid levels in TgSwDI mice after sham or MCAO surgery. β-amyloid burden was detected with 6E10 immunohistochemistry, which could be observed as small, diffuse deposits mainly in the thalamus (Figure 5.8A). The %density of the β-amyloid deposits was measured in the VPM and VPL of TgSwDI mice 3 months after either sham or MCAO surgery. The results showed that there were no significant differences between the VPM hemispheres ($F(1, 22) = 2.221$, $p = 0.154$); no significant differences between sham and MCAO mice ($F(1, 22) = 1.491$, $p = 0.238$); and no interaction ($F(1, 22) = 0.113$, $p = 0.741$) (Figure 5.8B,C). The results showed that the β-amyloid deposits in these animals was small and highly varied; plus MCAO did not cause an increase β-amyloid deposition in either the ipsilateral or contralateral hemispheres. β-amyloid %density did not correlate with the %density of Iba1 or GFAP (data not shown), indicating that the increase of microglia/macrophages and astrocytes in TgSwDI mice is not directly related to the burden of β-amyloid deposits.

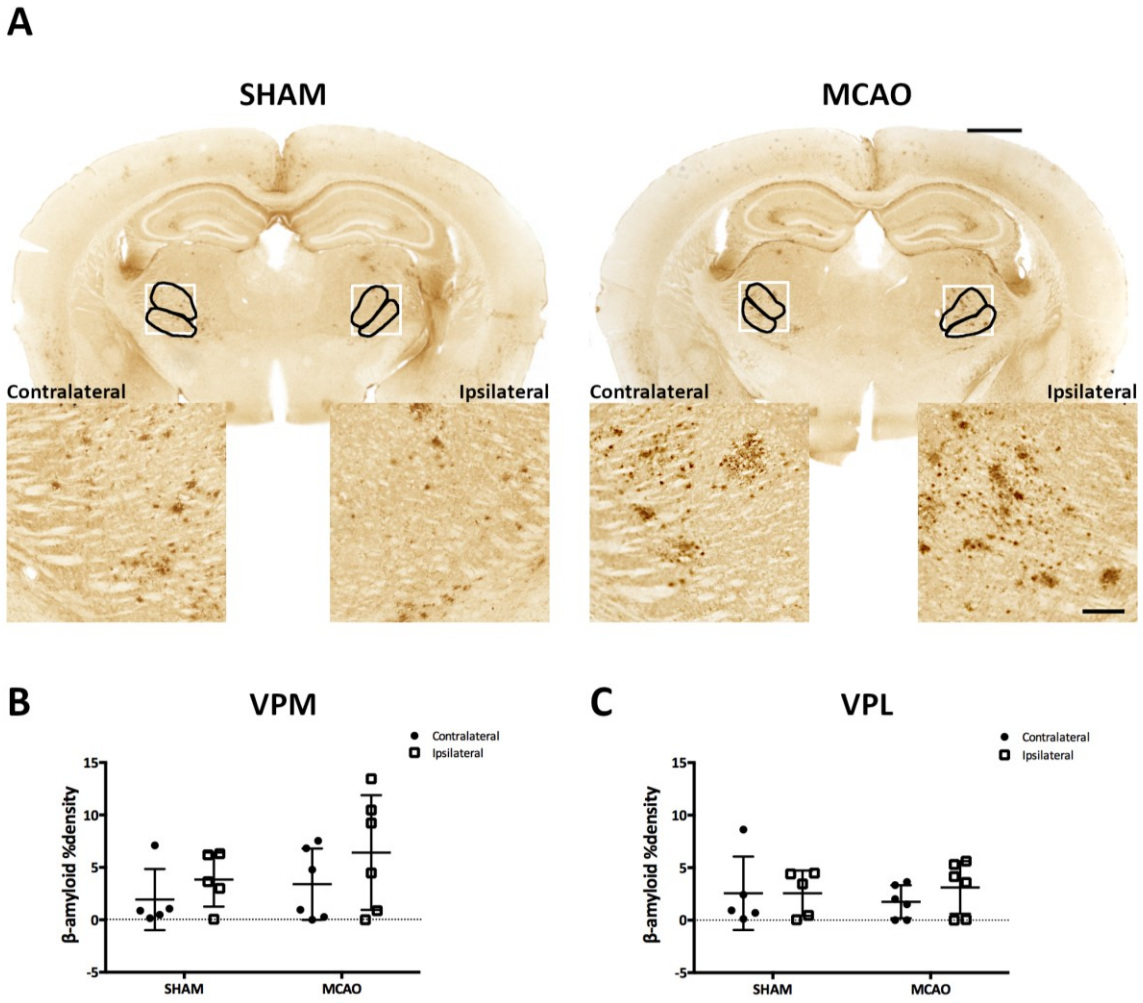

Figure 6.8 β-amyloid burden was unchanged in the VPM and VPL of TgSwDI mice after MCAO or sham surgery. (A) 6E10 immunohistochemistry detection of β-amyloid. No differences in β-amyloid burden in the (B) VPM or (C) VPL of either hemispheres after sham or MCAO surgery. Data presented as mean ± SD, n = 5,6 per group. Scale bar = 1mm, insert 200µm. Two-way ANOVA.

6.4 Discussion

Overall, this study demonstrated that focal ischaemia lead to secondary neurodegeneration and chronic glial responses in remote brain regions connected to the primary lesion site. There was evidence of increased axon degeneration in the ipsilateral internal capsule, plus axon and glutamatergic postsynaptic terminals in the ipsilateral SN_R. Plus, there was an increased density of PSD95+ postsynaptic terminals in the ipsilateral thalamus. These brain regions also had elevated levels of microglia/macrophages and reactive astrocytes. An important finding was that in TgSwDI mice there were higher levels of glial cell levels in the ipsilateral internal capsule and thalamus, compared to WT mice. Understanding secondary neurodegenerative changes following focal ischaemia is important, as it has been proposed that worsening of functional outcome after stroke is a consequence of delayed damage in these remote brain regions (Zhang et al. 2012). These brain regions are connected in the nigrostriatal pathway, which is part of the motor, limbic and cognitive systems (Groenewegen 2003), therefore, degeneration in this pathway would be expected to cause disruption of a number of brain functions.

6.4.1 Focal ischaemia resulted in long-term secondary neurodegeneration

The present study found a significant increase in axon bulbs in the ipsilateral internal capsule, which is the white matter tract that connects the striatum and the SN_R. White matter damage is a common pathological feature of stroke injury. On average, 95% of ischaemic stroke patients have white matter injury, and around 50% of the ischaemia processes involve the white matter (Ho et al. 2005). The present study focused on whether there was a greater density of axon bulbs in the ipsilateral internal capsule compared to the contralateral. There may, however, be other changes in the white matter, such as demyelination, loss of axon-glia integrity and reduced conductance of the tract, which will

affect the function of the nigrostriatal pathway. An interesting study by Weishaupt et al. showed that secondary neurodegeneration after prefrontal ischaemia resulted in Fluorojade-B+ axon degeneration and elevated numbers of Iba1+ cells in the internal capsule, however, there were no differences in the levels of myelin basic protein (MBP) in this region (Weishaupt et al. 2016). This study may indicate that secondary neurodegeneration occurs through the axons and demyelination is not a contributor to this process. A development of the current study could be to investigate whether there is a reduction in the myelin sheath in the ipsilateral internal capsule sheath, and whether this is exaggerated in TgSwDI mice; by immunohistochemistry detection of MBP, or myelin associated glycoprotein (MAG) which is normally expressed in the peri-axonal regions of oligodendrocytes and will only be expressed with white matter disruption, as previously shown by our group (Coltman et al. 2011). In the present study, there was no genotype effect on the density of axon bulbs in the internal capsule, which is surprising as evidence that β-amyloid can be damaging to axons (Lambert et al. 1998), and is toxic to oligodendrocytes (Xu et al. 2001). Plus, diffusion tensor imaging has shown disruption of white matter tracts in mice with injected β-amyloid (Sun et al. 2014). In the present study, there was a clear exaggeration of neuroinflammatory cells in the TgSwDI mice. It may be that whilst the density of axon bulbs is indistinguishable between WT and TgSwDI mice, the exacerbated neuroinflammatory response in TgSwDI mice may cause degeneration of oligodendrocytes, demyelination and worsened white matter conductance, as discussed later.

The present study showed neurodegenerative changes in the SN_R, as there was a significant increase in the density of axon bulbs and a significant loss in the density of glutamatergic postsynaptic terminals. Previous publications have found that secondary

changes occur in the SN_R after MCAO surgery in rodents. Permanent MCAO in rats resulted in neurodegeneration and gliosis in the ipsilateral SN_R at 14 days after surgery (Nakanishi et al. 1997; Tamura et al. 1990). Furthermore, significant losses of neurons have been found in the ipsilateral SN_R of mice starting at 7 days after 30 minutes of MCAO, whereas there was no significant loss of nigral neurons at 4 days post-surgery (Prinz et al. 2015). In the current study, neuronal and synaptic degeneration in the ipsilateral substantia nigra was observed after 3 months following 15 minutes of MCAO and although it is unclear when these changes occurred, results from other studies would suggest that nigral degeneration occurred at a time earlier than the three months endpoint.

The mechanism by which secondary neurodegeneration of the nigrostriatal pathway occurs remains unclear. A theory is that secondary neurodegeneration occurs via trans-synaptic retrograde degeneration, as neuronal damage occurs through neuronal networks, rather than spreading to adjacent brain regions. A recent *in vitro* study investigated how neurodegeneration can spread trans-synaptically between cortical and striatal neurons in a microfluidic chamber (Deleglise et al. 2018). They found that when the cortical neurons were damaged with either axotomy or chemical hypoxia, this resulted in blebbing of axons and dendrites. Furthermore, they demonstrated that blocking NMDA-receptor activity alleviated the damage (Deleglise et al. 2018). Evidence presented in previous studies has also shown that blocking NMDA-receptor activity can reduce the effects of secondary neurodegeneration (Prinz et al. 2015). The activity of NMDA-receptors appears to have a key role in secondary neurodegeneration of the substantia nigra after MCAO. At the site of the primary ischaemic injury, energy depletion leading to ion imbalance causes the neurons to become excitotoxic and to release excessive amounts of glutamate into the synaptic cleft. Glutamate then binds and over-activates the NMDA-receptors to the next

neuron in the circuit, causing the large influxes of calcium ions and stimulating degradative processes (Lai et al. 2014). Over time, this process may continue to progress from the primary ischaemic core, along the nigrostriatal pathway, resulting in axon degeneration in the internal capsule and SN_R. A number of studies have found that blocking NMDA-receptor activity alleviates secondary degeneration in rodent models. Prinz et al. demonstrated that treating mice with MK801 after MCAO alleviated long-term neuronal loss in the ipsilateral substantia nigra (Prinz et al. 2015).

The current study focused on investigating the loss of excitatory postsynaptic terminals and axon pathology in the substantia nigra. VGLUT1, which was used as a marker to detect glutamatergic presynaptic terminals in the striatum and thalamus, is not expressed in the substantia nigra, however, its isoform VGLUT2 is and could be used to further study the impact of focal ischaemia on presynaptic terminals in this region (Fremeau et al. 2001).

As discussed in the previous chapter, focal ischaemic injury can stimulate some neuronal recovery. There is evidence that recovery and rewiring can occur between brain regions that were previously disconnected. A study using confocal microscopy showed cells in the ipsilateral striatum that had colocalising signals for NeuN-immunoreactivity, BrdU for DNA synthesis and fluorogold which had been injected into the substantia nigra, 12 weeks after MCAO in rats (Sun et al. 2012). The authors suggest that this shows that at 12 weeks post-surgery, new striatal cells have formed in the ischaemic hemisphere, which have grown new projections with the cells in the substantia nigra. The paper shows images with these markers at 2 and 9 weeks post-MCAO, when these markers do not all colocalise (Sun et al. 2012). Although this study lacks numerical quantification of these changes, it does appear to show some neural rewiring between the striatum and substantia nigra after MCAO surgery. A development of the present study could be to determine the extent of neural

rewiring in the substantia nigra and striatum 3 months following MCAO in mice, and determine whether there is a differential effect between WT and TgSwDI mice. As previously discussed, GAP34 is a marker of axonal sprouting and is commonly used to determine regions of synaptic plasticity and rewiring following ischaemia (Frey et al. 2000). Conducting this analysis at multiple time-points would enable us to gain insight into the temporal progression of secondary neurodegeneration and recovery in this model.

The current study did not show a differential effect in synaptic degeneration in the substantia nigra between WT and TgSwDI mice. As previously discussed, there is a body of evidence indicating that β-amyloid is synaptotoxic (Section 1.7.2). The literature indicates that soluble oligomeric β-amyloid is the main toxic form, and the levels of soluble β-amyloid are very low in TgSwDI (Xu et al. 2007). The use of a mouse model with high levels of soluble oligomeric β-amyloid, such as APP E693Δ (Tomiyama et al. 2010), may have induced exaggerated synaptic loss following focal ischaemia.

The thalamus received GABAergic afferents from the SN_R and sends glutamatergic efferents to the striatum (Figure 1.7), therefore, it is another brain region that may undergo secondary changes following focal ischaemia in the striatum. The densities of glutamatergic VGLUT1+ pre- and PSD95+ postsynaptic terminals were analysed in the ventral posteromedial (VPM) and ventral posterolateral (VPL) thalamic nuclei, as these regions are important for sending motor and sensory function (Yamawaki & Shepherd 2015). Moreover, these are the regions where β-amyloid deposition occurs most prominently in TgSwDI mice (Xu et al. 2007). Despite this, there was no genotype effect on the %densities of VGLUT1 or PSD95 in the VPM or VPL, which further indicates that glutamatergic synaptic terminals are resilient to the expression of TgSwDIAPP. An interesting finding, however, was the increase of PSD95 %density in the ipsilateral VPM

compared to the contralateral for both genotypes. There also appeared to be a trend towards an increase in the PSD95 %density in the ipsilateral VPL, although these did not reach statistical significance. The thalamus has previously been shown to have the potential for synaptogenesis following focal ischaemia, as treadmill training after transient MCAO in rats resulted in increased synaptophysin protein levels in the ipsilateral thalamus, compared to the contralateral thalamus and the no exercise groups (Seo et al. 2010). As previously discussed, the present study could be developed to determine the extent of neural rewiring in brain regions connected to the striatum and to determine whether there is a differential effect between WT and TgSwDI mice, by investigating changes in GAP43 immunostaining, or the colocalisation of NeuN-immunoreactivity and BrdU signal.

Overall, this study showed that brief focal ischaemia leads to long-term secondary neurodegeneration, as there was significant axon degeneration in the ipsilateral internal capsule, plus axon degeneration and glutamatergic postsynaptic loss in the ipsilateral SN_R. In addition, there was evidence of synaptogenesis, with an increase in PSD95+ postsynaptic terminals in the ipsilateral thalamus. TgSwDIAPP expression did not exacerbate the changes caused by focal ischaemia, indicating that they are resilient to β-amyloid pathology associated with this transgenic model.

6.4.2 Focal ischaemia lead to chronic glial responses in remote brain regions, with exaggerated levels in the ipsilateral internal capsule and thalamus.

The present study showed that focal ischaemia induces a long-term elevation of microglia/macrophage and reactive astrocyte levels in the ipsilateral internal capsule, which was exaggerated in TgSwDI mice. This is consistent with previous findings that focal ischaemia can induce an increase in Iba1+ cells in the ipsilateral internal capsule (Weishaupt et al. 2016). Chronic glial and inflammatory responses are associated with

white matter injury in many CNS diseases. Previous work conducted by our group has demonstrated that the density of Iba1+ cells in the corpus callosum correlated with the extent of functional impairment of this white matter tract in a model of chronic cerebral hypoperfusion (Kitamura et al. 2017). Furthermore, treatment with anti-inflammatory drug, minocycline, reduced the functional impairment and microgliosis in the same model (Manso et al. 2018), and reduced white matter damage after transient MCAO in rats (Faheem et al. 2019). As previously discussed, microglia have roles in 'mopping-up' myelin debris, however, repressing the phagocytic activation state may lead to impairment in this function and promote further toxicity (Lloyd et al. 2017).

A particularly interesting result in this study was that the chronic neuroinflammatory was exaggerated in TgSwDI mice after focal ischaemia. Previous studies have found an association between Alzheimer's pathology and white matter neuroinflammation. Positron emission tomography (PET) neuroimaging has been used to show that the levels of activated microglia in the internal capsule is increased in Alzheimer's patients compared to control subjects (Suridjan et al. 2015). Moreover, there was indication that the levels of activated microglia inversely related to visuospatial function, which implies that glial activation in the white matter has a role in functional decline. This exaggerated immune response in the TgSwDI mice may be a result of 'primed' or 'sensitised' glia. Based on evidence described below, it has been proposed that chronic or repeated activation of microglia and astrocytes sensitises them and leads to an exaggerated immune response on subsequent stimulation. Research conducted by Cunningham and colleagues demonstrated that microglia and astrocytes are primed in the ME7 neurodegenerative prion disease model, and lead to exacerbated inflammation when subsequently challenged with LPS-induced systemic inflammation (Cunningham et al. 2005), or cytokine administration into

the brain (Hennessy et al. 2015). Furthermore, Krstic et al. demonstrated that when WT mice are subjected to a prenatal systemic immune challenge and an additional one during adulthood, it results in microglial and astrocytic activation with β-amyloid and tau pathology; which was comparable to the pathology in a TgAPP model (Krstic et al. 2012). There is also evidence that an exaggerated glial responses occurs in the brains of Tg2576 mice after LPS-induced systemic inflammation (Sly et al. 2001). In the present study, therefore, expression of TgSwDIAPP the resulting β-amyloid production may sensitise the microglia and astrocytes in the internal capsule, leading to an exaggerated neuroinflammatory response on focal ischaemia induction.

The present study found no relationship between the densities of glial cells and axon bulbs in the ipsilateral internal capsule. Furthermore, whilst there was increased neuroinflammation in the internal capsule of TgSwDI mice, there was no genotype effect on the density of axon bulbs in this region. Together, this indicates that glial responses in the internal capsule are not directly related to the axon degeneration in this region. Glial responses may contribute to white matter injury by different mechanisms, such as disruption of the axon-glia interface and loss of white matter integrity. Previous work conducted by our group found that global chronic hypoperfusion leads to disruption of axon-glia interface in the corpus callosum, which appears to coincide with an increase in Iba1+ cells (Manso et al. 2018). This axon-glia interface is the organisation of myelin fibres into separate domains (node of Ranvier, paranode and juxtaparanode), which are required for efficient action potentiation propagation (Babbs & Shi 2013). Loss of axon-glia integrity, therefore, may contribute to the propagation of secondary neuronal dysfunction and degeneration through the internal capsule after focal ischaemia. Manos et al. also showed that there was a complete overlap between Iba1+ cells and microglia-specific marker

TMEM119 in the hypoperfused corpus callosum (Manso et al. 2018), therefore, we can speculate that Iba1+ cells in the ipsilateral internal capsule are also microglia. The white matter microglia may be causing disruption of the axon-glial interface by adopting a pro-inflammatory activation state. Another group found that in a hypoperfusion model that the phagocyte marker, CD68, and other pro-inflammatory markers, were elevated in the white matter (Qin et al. 2017). Furthermore, CD68 expression was shown to be higher in white matter than grey matter of human stroke tissue (Zrzavy et al. 2017). The increased expression of CD68 may represent an activation of microglia to phagocytosis myelin debris. Reactive astrocytes may also partake in disruption of white matter integrity, through activation of the pro-inflammatory NF-κB pathway (Saggu et al. 2016a). As discussed in the previous chapter, the use of single-cell RNS sequencing has enabled huge advancements to be made in understanding the complex activation states of microglia/macrophages and astrocytes in injury. Future developments of the present study could be to use these techniques to elucidate the transcriptomes of these cells in the white matter, to determine whether they express neuroprotective or neurotoxic signals, and whether there is a phenotypic difference between those from WT and TgSwDI mice.

The present study showed that focal ischaemia induced chronic glial responses in the ipsilateral SN_R. Although the increase in Iba1 %density in the ipsilateral SN_R only reached significance in the WT mice, there was a trend towards a significant increase in the ipsilateral SN_R of TgSwDI mice. A recent neuroimaging study in humans used MRI to analyse the iron concentration (R* signal), which is rich in microglia and macrophages, and released from dying neurons. They found that the found higher R* signals in the ipsilateral substantia nigra at one year after the baseline recording, implying that chronic glial responses and dying neurons were present in this brain region long after the initial lesion

(Linck et al. 2019). Another study investigated the neuroinflammatory response in the SN_R following 45 minutes of MCAO in mice, and found that at 24 hours after reperfusion there was already significant increases in immunostaining for GFAP, CD45, ICAM1 and Iba1 in the ipsilateral striatum (Rodriguez-Grande et al. 2013). Importantly, there were no significant losses of neurons in the ipsilateral SN_R at this time-point, therefore, this study showed that elevated neuroinflammation had preceded neurodegeneration.

Other publications have found evidence of chronic glial responses in regions of diachisis, such as in the ipsilateral thalamus following photothrombosis in the cortex. In a study using the photothrombotic occlusion model, 28 days after surgery there were elevated levels of Iba1+ cells in the ipsilateral thalamus (Jones et al. 2015). More recently, the same group reported that microglia/macrophages in the ipsilateral thalamus have an activated morphology (Kluge et al. 2017). They went further to investigate the functionality of these cells, by characterising their motility and protein expression. Whilst microglia/macrophages in the peri-lesional cortex were motile and responded to laser stimulation from 3-56 days post-stroke, they were non-responsive in the thalamus, starting at day 7 (Kluge et al. 2018). Long-term increase in MHC-II and CD68, which are needed for antigen presentation and debris clearance, in the ipsilateral thalamus (Kluge et al. 2018), whilst they consistently found a chronic decrease of P2Y12 compared to the contralateral thalamus (Kluge et al. 2017; 2018; 2018). Microglial P2Y12 has been implicated to be involved in cell motility and synaptic plasticity (Sipe et al. 2016), therefore, its reduction here may be representative of a shift to debris clearance functions. They also found that protein levels of activated astrocytic GFAP and S100B are increased in the ipsilateral thalamus (Kluge et al. 2018). An interesting finding in this paper was that they compared the protein levels measured in the thalamus of young and old mice 28 days after

photothrombosis, and found that whilst glial and inflammatory protein changes occurred in young and old mice, the loss of synaptic proteins only occurred in old animals. These findings may indicate that the microglia/macrophages and astrocytes in the ipsilateral SN_R have a pro-inflammatory phenotype, and a development of the present study could be to characterise the functional state of these cells.

In the present study there was a trend towards a positive correlation between with the density of APP+ bulbs and GFAP immunostaining in the ipsilateral SN_R, although this did not reach statistical significance. This may suggest a relationship between the levels of astrocytes and the extent of axon degeneration in this region. Previous reports have found that elevated of GFAP+ astrocytes occurs in the ipsilateral $SN_{R,}$ which gradually increased from 1 to 4 weeks after surgery, whilst the density of intact neurons gradually decreased over the same time period after dMCAO (Wang et al. 2012). This paper also shows that axon sprouting marker GAP-43 and dendritic MAP2 are decreased in the ipsilateral SN_R. Interestingly, they found oligodendrocytic Nogo-A is associated with secondary neurodegeneration, as blocking it promoted neural recovery and reduced astrogliosis (Wang et al. 2012). This is supported by observations that blocking Nogo receptor 1 in a model of white matter stroke leads to improved oligodendrogenesis and white matter repair (Sozmen et al. 2016). Another proposed mechanism for secondary neurodegeneration after focal ischaemia is the disruption of neuronal lysosomes and release of proteases. A recent study found that CathB, which is released from perforated lysosomes, was increased in the ipsilateral SN_R as early at 1 week after distal MCAO (Zuo et al. 2018). They also show that blocking CathB reduces substantia nigral neurodegeneration and astrogliosis. Collectively, these studies may imply that reducing microgliosis and

astrocytosis in the substantia nigra may prevent secondary neurodegeneration in this region, and promote neural repair.

The present study showed that TgSwDIAPP expression exaggerated the glial responses in the internal capsule, whilst having no significant effect on glial responses in the SN_R. This may result from glial cells being more sensitive in the white matter than grey matter regions, based on evidence that there were more microglia and macrophages in the white matter than the grey matter in human stroke tissue (Zrzavy et al. 2017). Furthermore, white matter astrocytes have been shown to be more sensitive than their grey matter counterparts to oxygen-glucose deprivation, although this study was conducted in neonatal tissue and the relative sensitivity of these cells could be different in adulthood (Shannon et al. 2007). Taken together, the results imply microglia/macrophages and astrocytes in the internal capsule are particularly vulnerable to ischaemia and TgSwDIAPP expression.

The levels of glial cells were analysed in the thalamus to determine the impact of focal ischaemia and TgSwDIAPP expression in this region. There was a trend towards a surgery effect increasing the density of microglia/macrophages and reactive astrocytes in the VPM and VPL thalamic nuclei, which did reach a significant increase in reactive astrocyte levels in the ipsilateral VPL of TgSwDI mice compared to their contralateral hemispheres. Moreover, there was evidence for exaggerated levels of microglia/macrophages and reactive astrocytes in the ipsilateral thalamus of TgSwDI compared to that of the WT mice. This result may indicate that TgSwDIAPP expression caused glial priming, which is exacerbated in the ipsilateral thalamus following focal ischaemia, as discussed above.

Previous publications have shown that the thalamus is the main site of β-amyloid deposition in the TgSwDI line (Xu et al. 2007). Glial cells cluster around β-amyloid deposits,

in order to phagocytose them (Serrano-Pozo et al. 2011). The next stage of the study, therefore, was to investigate whether the elevated levels of glial cells in the ipsilateral thalamus of TgSwDI mice was the result of increase β-amyloid deposition after MCAO surgery.

6.4.3 Focal ischaemia did not result in increased thalamic β-amyloid burden in TgSwDI mice.

Contrary to previous publications, which have reported that focal ischaemia induces an increase in β-amyloid deposition (Groen et al. 2005; Mäkinen et al. 2008; Zhang et al. 2011; Garcia-Alloza et al. 2011; Nguyen et al. 2018; Kluge et al. 2018), no alterations in β-amyloid were found in the current study between TgSwDI mice after sham or MCAO surgery. These publications cited here may have found increased β-amyloid deposition with focal ischaemia as a result of severer surgical models or higher baseline β-amyloid production. Greon et al. found an increase in APP and β-amyloid immunoreactivity in the thalamus of Wistar rats 9 months after 2 hours of MCAO (Groen et al. 2005), whilst Zhang et al. showed that permanent distal MCAO lead to β-amyloid deposition in the ipsilateral thalamus of stroke-prone hypertensive rats (Zhang et al. 2011). These studies indicate that severe focal ischaemia in rats can induce production of β-amyloid, despite a lack of human mutated APP transgene expression. Moreover, Kluge et al. demonstrated that cortical photothrombosis resulted in elevated protein levels of β-amyloid oligomers in the thalamus of aged C57BL/6J mice, compared to sham control and young mice (Kluge et al. 2018), which indicates that age increases their vulnerability to β-amyloid production. APPSwe:PS1dE9 transgenic mouse model was used by Garcia-Alloza et al., who found an increase in the burden of dense-core amyloid plaques in the ipsilateral hemisphere 7 days after 1 hour of distal MCAO (Garcia-Alloza et al. 2011). Nguyen et al. demonstrated that

permanent distal MCAO plus hypoxia (DH stroke model), induced greater deposition of $A\beta_{42}$ and dense-core plaques in aged Thy1-hAPP$^{Lond/Swe}$ mice (Nguyen et al. 2018). Both of these transgenic mouse lines have more aggressive β-amyloid pathology than TgSwDI, as they produce amyloid dense core plaques (Rockenstein et al. 2001; Minkeviciene et al. 2008). Moreover, the focal ischaemia models used are more severe than in the present study as the duration of occlusion is longer. Taken together, the reason for a lack of surgery effect on the β-amyloid deposition is likely a result of brief occlusion time and relatively modest baseline β-amyloid production.

Another explanation could be that the method used for detecting β-amyloid changes lacks sensitivity. 6E10 immunostaining detects all types of insoluble β-amyloid and APP deposits (Portelius et al. 2009), however, there may have been changes in the soluble pools of β-amyloid. An improved method would be to use an ELISA to quantify the total levels of $A\beta_{40}$ and $A\beta_{42}$ in soluble and insoluble fractions in the ipsilateral thalamus of TgSwDI mice after either sham or MCAO surgery. This approach was previously used by our group to determine the effect of cerebral hypoperfusion on specific β-amyloid pools (Salvadores et al. 2017). Collectively, the results demonstrated that β-amyloid burden was low and unaffected by MCAO surgery, indicating that TgSwDIAPP expression and focal ischaemia resulted in exaggerated glial responses even in the absence of wide-spread plaque deposition.

6.4.4 Conclusions

The present study demonstrated that focal ischaemia lead to long-term neurodegeneration and glial responses in brain regions that are connected with the primary lesion site. Concurrent expression of TgSwDIAPP lead to exaggerated glial responses in the internal capsule and thalamus. The implications of this study are the focal ischaemia leads to long-

term global glial responses, which can be exacerbated by additional disease comorbidities. Future developments should focus on further characterising the chronic glial responses in WT and TgSwDI, and determine whether reducing this response will reduce neurodegeneration.

Chapter 7: Discussion and Conclusions

7.1 Summary

The studies presented in this thesis demonstrate that whilst modest chronic cerebral blood flow does not induce degeneration of glutamatergic synaptic terminals, brief focal ischaemia causes long-term glutamatergic synaptic loss in the primary lesion site and in distal, connected brain regions. These changes were found to coincide with chronic elevated levels of microglia/macrophages and astrocytes. These findings further confirm that focal brain lesions result in global pathological changes. Contrary to our predictions, the expression of TgSwDIAPP transgene did not result in overt worsening of synapse degeneration following focal ischaemia. It did, however, induce higher levels of microglia/macrophages and astrocytes in distal brain regions, which supports the prediction that multiple disease comorbidities can lead to exaggerated global glial responses.

7.2 Implications and future directions

Evidence presented in this thesis, and the publications discussed, demonstrate that focal ischaemic lesions can cause downstream secondary pathology in connected brain regions. Moreover, studies of patients with transient ischaemic attack and stroke have indicated that delayed atrophy in brain regions distal to the lesion sites are associated with cognitive deficits (Bivard et al. 2018; Diao et al. 2017). The implications of these studies are that secondary neurodegeneration following a focal ischaemic lesion are related to delayed cognitive decline, and preventing secondary neurodegeneration would be beneficial for alleviating cognitive impairment. Moreover, the data from this thesis and other rodent studies, showed that there are chronic glial responses in regions of secondary

neurodegeneration. Rodriguez-Grande et al. found that MCAO caused an increase in neuroinflammatory markers in the ipsilateral substantia nigra before neuronal loss occurred in this region (Rodriguez-Grande et al. 2013). Additionally, patient studies have revealed that elevated levels of several plasma inflammatory markers, such as IL-6, IL-12 and C-reactive protein, are associated with risk of post-stroke dementia (Rothenburg et al. 2010; Narasimhalu et al. 2015). Furthermore, a recent phase 2 trial investigated the therapeutic potential of a monoclonal antibody, called natalizumab, which binds to α-integrin and inhibits leukocyte transmigration into the brain (Elkins et al. 2017). Natalizumab was administered 9 hours after ischaemic stroke onset, resulting in improved cognition and other functions by 3 months, compared to the placebo group, although infarct size was unchanged. Taken together, these studies imply that therapeutic intervention targeted to prevent post-stroke global neuroinflammation will reduce secondary neurodegeneration and cognitive decline.

An important finding in the present studies was that expression of TgSwDIAPP exaggerated post-ischaemic glial cell levels in some brain regions. This supports the hypothesis that multiple disease comorbidities lead to worsened pathological changes. As discussed, the present studies focused on quantifying the density of glial cells, Iba+ microglia/macrophages and GFAP+ astrocytes. Future studies should elucidate the transcriptome of these cells to determine whether they are expressing pro-inflammatory or anti-inflammatory markers, and how additional comorbidities affect the post-ischaemic response. It may be that multiple comorbidities induce more neurotoxic phenotypes than ischaemia alone. The present study focused on the effect of concurrent TgSwDIAPP expression, however, there are many disease comorbidities associated with CVD and VCI. Old-age is associated with greater incidence of CVD and is the strongest risk factor for the

development of dementia. Moreover, rodent studies have revealed that focal ischaemia in aged animals results in exacerbated secondary synaptic and neurodegeneration (Kluge et al. 2018; Nguyen et al. 2018), and inflammatory signalling (Thammisetty et al. 2018). Future research should focus on interrogating the effect of different disease comorbidities with reduced CBF, to determine their effect on synaptic and neuronal degeneration, neuroinflammation and function outcome.

Collectively, the data presented in this thesis and the literature discussed confirms the damaging effects reduced CBF has on the brain, and supports the importance of cerebrovascular health. Moreover, it emphasises the need for understanding glial activation and chronic neuroinflammation in conditions of reduced CBF, and how it may contribute to synaptic degeneration and cognitive decline. Finally, this thesis shows the importance of further gaining insight into how activated microglia and astrocytes can support recovery processes after brain injuries, and whether therapeutic intervention targeted at reducing glial responses and neuroinflammation, and promoting synaptic and neuronal restoration can be achieved.

Chapter 8: Appendix

8.1 Presentations

- 3 Minute Thesis presentation, ARUK Scotland PhD student meeting, Oct 2015
- Presentation for CCACE PhD Student meeting, Edinburgh, Nov 2016
- Poster Presentation at ARUK conference, Aberdeen, March 2017
- 3 Minute Thesis presentation, ARUK Scotland network retreat, Sept 2017
- Poster Presentation at DRI launch event, Edinburgh, April 2018

8.2 Public engagement workshops

- 'Drawing the Mind' workshop on neuroanatomy for the ASCUS Lab, EISF, April 2017
- Featured scientist at ASCUS Lab Open Session, July 2017

Chapter 9: Bibliography

Abe, O. et al., 2003. MR imaging of postischemic neuronal death in the substantia nigra and thalamus following middle cerebral artery occlusion in rats. *NMR in Biomedicine*, 16(3), pp.152–159.

Abraham, H.M.A. et al., 2016. Cardiovascular risk factors and small vessel disease of the brain : Blood pressure , white matter lesions , and functional decline in older persons.

Adalbert, R. et al., 2009. Severely dystrophic axons at amyloid plaques remain continuous and connected to viable cell bodies. *Brain*, 132(2008), pp.402–416.

Alawieh, A. et al., 2018. Identifying the Role of Complement in Triggering Neuroinflammation after Traumatic Brain Injury. *The Journal of Neuroscience*, 38(10), pp.2519–2532.

Alawieh, A. et al., 2015. Modulation of post-stroke degenerative and regenerative processes and subacute protection by site-targeted inhibition of the alternative pathway of complement. *Journal of Neuroinflammation*, 12(1), pp.1–15.

Alosco, M.L. et al., 2013. Cerebral Perfusion is Associated With White Matter Hyperintensities in Older Adults With Heart Failure. *Congestive Heart Failure*, 19(4), pp.E29–E34.

Alsop, D.C. et al., 2010. Arterial spin labeling blood flow MRI: Its Role in the early characterization of Alzheimer's disease. *Journal of Alzheimer's Disease*, 20(3), pp.871–880.

Amtul, Z., Whitehead, S.N., et al., 2015. Comorbid rat model of ischemia and ??-Amyloid toxicity: Striatal and cortical degeneration. *Brain Pathology*, 25(1), pp.24–32.

Amtul, Z., Whitehead, S.N., et al., 2015. Comorbid Rat Model of Ischemia and β -Amyloid Toxicity : Striatal and Cortical Degeneration. , 25(45), pp.24–32.

Anderson, J.M. & Van Itallie, C.M., 2009. Molecular Structure and Function of the Tight Junction. *Cold Spring Harbor Perspectives in Biology*, 1(2).

Ando, K., Kudo, Y. & Takahashi, M., 2005. Negative regulation of neurotransmitter release by calpain: A possible involvement of specific SNAP-25 cleavage. *Journal of Neurochemistry*, 94(3), pp.651–658.

Angelova, P.R. et al., 2015. Functional oxygen sensitivity of astrocytes. *Journal of Neuroscience*, 35(29), pp.10460–10473.

Angulo, M.C. et al., 1997. Subunit Composition, Kinetic, and Permeation Properties of AMPA Receptors in Single Neocortical Nonpyramidal Cells. *The Journal of Neuroscience*, 17(17), pp.6685–6696.

Araque, A. et al., 1999. Tripartite Synapse Haydon 1999. *Trends in Neuroscience*, 22(5), pp.208–215.

Ashery, U. et al., 2014. *Synaptic Transmission : A View of the Presynaptic Terminal*,

Ashok, A. et al., 2016. Chronic cerebral hypoperfusion-induced impairment of Aβ clearance requires HB-EGF-dependent sequential activation of HIF1α and MMP9. *Neurobiology of disease*, 95, pp.179–193.

Attwell, D. & Laughlin, S.B., 2001. An energy budget for glutamatergic signalling in grey matter of the rat cerebral cortex. *Journal of Cerebral Blood Flow & Metabolism*, 21, pp.1133–1145.

Babbs, C.F. & Shi, R., 2013. Subtle Paranodal Injury Slows Impulse Conduction in a Mathematical Model of Myelinated Axons. *PLoS ONE*, 8(7).

Bai, F. & Witzmann, F.A., 2007. Synaptosome Proteomics. *Subcell Biochem.*, 43, pp.77–98.

Baleriola, J. et al., 2014. Axonally synthesized ATF4 transmits a neurodegenerative signal across brain regions. *Cell*, 158(5), pp.1159–1172.

Bamberger, M.E. et al., 2003. A cell surface receptor complex for fibrillar β-amyloid mediates microglial activation. *Journal of Neuroscience*, 23(7), pp.2665–2674.

Barker, G.R.I. & Warburton, E.C., 2011. When is the hippocampus involved in recognition memory? *Journal of Neuroscience*, 31(29), pp.10721–10731.

Barnes, C.A., 1979. Memory deficits associated with senescence: A neurophysiological and behavioral study in the rat. *Journal of Comparative and Physiological Psychology*, 93(1), pp.74–104.

Barnett, M.W. & Larkman, P.M., 2007. The action potential. *Journal of Neurology, Neurosurgery and Psychiatry*, 78(6), p.192.

Baron, J. et al., 2014. Selective neuronal loss in ischemic stroke and cerebrovascular disease. , (August 2013), pp.2–18.

Baron, J.C., 2001. Perfusion thresholds in human cerebral ischemia: historical perspective and therapeutic implications. *Cerebrovascular Diseases*, 11 Suppl 1(suppl 1), pp.2–8.

Bartsch, T. et al., 2015. Selective neuronal vulnerability of human hippocampal CA1 neurons: Lesion evolution, temporal course, and pattern of hippocampal damage in diffusion-weighted MR imaging. *Journal of Cerebral Blood Flow and Metabolism*, 35(11), pp.1836–1845.

Baumert, M. et al., 1989. Synaptobrevin: an integral membrane protein of 18,000 daltons present in small synaptic vesicles of rat brain. *The EMBO Journal*, 8(2), pp.379–384.

Bayés, Á. et al., 2011. Characterization of the proteome, diseases and evolution of the human postsynaptic density. *Nature Neuroscience*, 14(1), pp.19–21.

Bazargani, N. & Attwell, D., 2016. Astrocyte calcium signaling: the third wave. *Nature neuroscience*, 19(2), pp.182–9.

Bell, K.F.S. & Claudio Cuello, a., 2006. Altered synaptic function in Alzheimer's disease. *European Journal of Pharmacology*, 545(1), pp.11–21.

Benakis, C. et al., 2015. The role of microglia and myeloid immune cells in acute cerebral ischemia. *Frontiers in Cellular Neuroscience*, 8(January), pp.1–16.

Benarroch, E.E., 2016. Intrinsic circuits of the striatum Complexity and clinical correlations. *American Academy of Neurologyedua*.

Bennett, M.L. et al., 2016. New tools for studying microglia in the mouse and human CNS.

Bennett, S. a. L. et al., 1998. Chronic cerebral hypoperfusion elicits neuronal apoptosis and behavioral impairment. *NeuroReport*, 9(1), pp.161–166.

Berg, A. et al., 2012. Reduced removal of synaptic terminals from axotomized spinal motoneurons in the absence of complement C3. *Experimental Neurology*, 237(1), pp.8–17.

Bernardinelli, Y. et al., 2014. Activity-dependent structural plasticity of perisynaptic astrocytic domains promotes excitatory synapse stability. *Current Biology*, 24(15), pp.1679–1688.

Bernbaum, M. et al., 2015. Reduced blood flow in normal white matter predicts development of leukoaraiosis. *Journal of Cerebral Blood Flow and Metabolism*, 35(10), pp.1610–1615.

Bingham, D. et al., 2012. Watermaze performance after middle cerebral artery occlusion in the rat: The role of sensorimotor versus memory impairments. *Journal of Cerebral Blood Flow and Metabolism*, 32(6), pp.989–999.

Bittner, T. et al., 2012. Amyloid plaque formation precedes dendritic spine loss. *Acta Neuropathologica*, 124(6), pp.797–807.

Bivard, A. et al., 2018. Transient ischemic attack results in delayed brain atrophy and cognitive decline. *Stroke*, 49(2), pp.384–390.

Blair, G. et al., 2019. Intracranial functional haemodynamic relationships in patients with cerebral small vessel disease. *bioRxiv*, 32(0), pp.1–32.

Blair, G.W. et al., 2016. Magnetic resonance imaging for assessment of cerebrovascular reactivity in cerebral small vessel disease: A systematic review. *Journal of Cerebral Blood Flow & Metabolism*, 36(5), pp.833–841.

Boehme, A.K. et al., 2016. Inflammatory Markers and Outcomes after Lacunar Stroke: Levels of Inflammatory Markers in Treatment of Stroke Study. *Stroke*, 47(3), pp.659–667.

Bolay, H. et al., 2002. Persistent defect in transmitter release and synapsin phosphorylation in cerebral cortex after transient moderate ischemic injury. *Stroke*, 33(5), pp.1369–1375.

Bolay, H. & Dalkara, T., 1998. Mechanisms of motor dysfunction after transietn MCA occlusion. *Stroke*, 29, pp.1988–1994.

Bouët, V., Freret, T., Toutain, J., Divoux, D., Boulouard, M. & Schumann-Bard, P., 2007. Sensorimotor and cognitive deficits after transient middle cerebral artery occlusion in the mouse. *Experimental Neurology*, 203(2), pp.555–567.

Bouët, V., Freret, T., Toutain, J., Divoux, D., Boulouard, M. & Schumann-bard, P., 2007. Sensorimotor and cognitive deficits after transient middle cerebral artery occlusion in the mouse. , 203, pp.555–567.

Bouley, J., Fisher, M. & Henninger, N., 2007. Comparison between coated vs. uncoated suture middle cerebral artery occlusion in the rat as assessed by perfusion/diffusion weighted imaging. *Neuroscience Letters*, 412(3), pp.185–190.

Braak, H. & Braak, E., 1991. Neuropathological stageing of Alzheimer-related changes. *Acta neuropathologica*, 82(4), pp.239–59.

Bresler, T., 2004. Postsynaptic Density Assembly Is Fundamentally Different from Presynaptic Active Zone Assembly. *Journal of Neuroscience*, 24(6), pp.1507–1520.

Breteler, M.M.B. et al., 1994. Cerebral white matter lesions, vascular risk factors, and cognitive function in a population-based study: The Rotterdam Study. *Neurology*, 44(7), pp.1246–1246.

Brito-Moreira, J. et al., 2011. Aβ Oligomers Induce Glutamate Release from Hippocampal Neurons. *Current Alzheimer Research*, 8(5), pp.552–562.

Brown, C.E. et al., 2007. Extensive turnover of dendritic spines and vascular remodeling in cortical tissues recovering from stroke. *The Journal of neuroscience : the official journal of the Society for Neuroscience*, 27(15), pp.4101–4109.

Brown, W.R. & Thore, C.R., 2011. Review: Cerebral microvascular pathology in ageing and neurodegeneration. *Neuropathology and Applied Neurobiology*, 37(1), pp.56–74.

Brun, a & Englund, E., 1986. A white matter disorder in dementia of the Alzheimer type: a pathoanatomical study. *Annals of neurology*, 19(3), pp.253–262.

Bruno, C. et al., 1996. Dementia After First Stroke. *Stroke*, 27(7), pp.1205–1210.

Buscemi, L. et al., 2019. Spatio-temporal overview of neuroinflammation in an experimental mouse stroke model. *Scientific Reports*, 9(1), pp.1–13.

Busche, M.A. et al., 2012. Critical role of soluble amyloid-β for early hippocampal hyperactivity in a mouse model of Alzheimer's disease. *Proceedings of the National Academy of Sciences of the United States of America*, 109(22), pp.8740–8745.

Butler, T.R. et al., 2010. Selective vulnerability of hippocampal cornu ammonis 1 pyramidal cells to excitotoxic insult is associated with the expression of polyamine-sensitive N-methyl-d-asparate-type glutamate receptors. *Neuroscience*, 165(2), pp.525–534.

Cajal, S.R. y, 1928. Degeneration and regeneration of the nervous system. *Oxford Press*, (185), pp.799–802.

Cao, Y. et al., 2016. Glutamatergic and central cholinergic dysfunction in the CA1, CA2 and CA3 fields on spatial learning and memory in chronic cerebral ischemia-Induced vascular dementia of rats. *Neuroscience Letters*, 620, pp.169–176.

Carmichael, S.T. et al., 2017. Molecular, cellular and functional events in axonal sprouting after stroke. *Experimental Neurology*, 287, pp.384–394.

Carmichael, S.T., 2003. Plasticity of cortical projections after stroke. *The Neuroscientist : a review journal bringing neurobiology, neurology and psychiatry*, 9(1), pp.64–75.

Carmona, M. a. et al., 2009. Glial ephrin-A3 regulates hippocampal dendritic spine morphology and glutamate transport. *Proceedings of the National Academy of Sciences*, 106(30), pp.12524–12529.

Carrera, E. & Tononi, G., 2014. Diaschisis: Past, present, future. *Brain*, 137(9), pp.2408–2422.

Cassel, J.C. et al., 1998. Fimbria-fornix vs selective hippocampal lesions in rats: Effects on locomotor activity and spatial learning and memory. *Neurobiology of Learning and Memory*, 69(1), pp.22–45.

Catterall, W.A., 2011. Voltage-gated calcium channels. *Cold Spring Harbor perspectives in biology*, 3(8), p.a003947.

Chan, R.C.K. et al., 2008. Assessment of executive functions: Review of instruments and identification of critical issues. *Archives of Clinical Neuropsychology*, 23(2), pp.201–216.

Chandler, S. et al., 1995. Matrix metalloproteinases degrade myelin basic protein. *Neuroscience Letters*, 201(3), pp.223–226.

Chang, E.H. et al., 2006. AMPA receptor downscaling at the onset of Alzheimer's disease pathology in double knockin mice. *Proceedings of the National Academy of Sciences of the United States of America*, 103(9), pp.3410–3415.

Chao, L.L. et al., 2010. ASL Perfusion MRI Predicts Cognitive Decline and Conversion From MCI to Dementia. *Alzheimer Dis Assoc Disord*, 24(1), pp.1–9.

Charidimou, A. et al., 2016. Mapping the landscape of cerebral amyloid angiopathy research: An informetric analysis perspective. *Journal of Neurology, Neurosurgery and Psychiatry*, 87(3), pp.252–259.

Chen, A. et al., 2016. Frontal white matter hyperintensities , clasmatodendrosis and gliovascular abnormalities in ageing and post-stroke dementia. , (2015), pp.242–258.

Chen, Y., Fu, A.K.Y. & Ip, N.Y., 2019. Synaptic dysfunction in Alzheimer's disease: Mechanisms and therapeutic strategies. *Pharmacology and Therapeutics*, 195, pp.186–198.

Cho, K.-O. et al., 2006. Minocycline Attenuates White Matter Damage in a Rat Model of Chronic Cerebral Hypoperfusion. *Journal of Neuroscience Research*, 83, pp.285–291.

Choy, M. et al., 2006. The chronic vascular and haemodynamic response after permanent bilateral common carotid occlusion in newborn and adult rats. *Journal of Cerebral Blood Flow and Metabolism*, 26(8), pp.1066–1075.

Christopherson, K.S. et al., 2005. Thrombospondins are astrocyte-secreted proteins that promote CNS synaptogenesis. *Cell*, 120(3), pp.421–433.

Cipolla, M.J., 2009. *The Cerebral Circulation*,

Cipolla, M.J., 2016. *The Cerebral Circulation* Second Edi. D. N. Granger & J. P. Granger, eds., Morgan & Claypool Sciences.

Clare, R. et al., 2010. NIH Public Access. , 88(10), pp.2083–2090.

Clare, R. et al., 2011. Synapse Loss in Dementias. *J Neurosci Res*, 88(10), pp.2083–2090.

Cohen, R.A. et al., 2002. The relationship of subcortical MRI hyperintensities and brain volume to cognitive function in vascular dementia. , (8), pp.743–752.

Colonna, M. & Wang, Y., 2016. TREM2 variants: New keys to decipher Alzheimer disease pathogenesis. *Nature Reviews Neuroscience*, 17(4), pp.201–207.

Coltman, R. et al., 2011a. Selective white matter pathology induces a specific impairment in spatial working memory. *Neurobiology of Aging*, 32(12), pp.2324.e7–2324.e12.

Coltman, R. et al., 2011b. Selective white matter pathology induces a specific impairment in spatial working memory. *Neurobiology of Aging*, 32(12), pp.2324.e7–2324.e12.

Cooperrider, J. et al., 2014. Chronic Deep Cerebellar Stimulation Promotes Long-Term Potentiation, Microstructural Plasticity, and Reorganization of Perilesional Cortical Representation in a Rodent Model. *Journal of Neuroscience*, 34(27), pp.9040–9050.

Corbetta, M. et al., 2015. Case Study Common Behavioral Clusters and Subcortical Anatomy in Stroke Case Study Common Behavioral Clusters and Subcortical Anatomy in Stroke. *Neuron*, 85(5), pp.927–941.

Coultrap, S.J. et al., 2005. Differential expression of NMDA receptor subunits and splice variants among the CA1, CA3 and dentate gyrus of the adult rat. *Molecular Brain Research*, 135(1-2), pp.104–111.

Cull-Candy, S.G. & Leszkiewicz, D.N., 2004. Role of distinct NMDA receptor subtypes at central synapses. *Science's STKE : signal transduction knowledge environment*, 2004(255), pp.1–10.

Cunningham, C. et al., 2005. Central and systemic endotoxin challenges exacerbate the local inflammatory response and increase neuronal death during chronic neurodegeneration. *The Journal of neuroscience : the official journal of the Society for Neuroscience*, 25(40), pp.9275–9284.

Curcio, M. et al., 2016. Calpains and neuronal damage in the ischemic brain: the swiss knife in synaptic injury. *Progress in Neurobiology*.

D Filiou, M. et al., 2010. Profiling of mouse synaptosome proteome and phosphoproteome by IEF. *Electrophoresis*, 31(8), pp.1294–1301.

Davies, C. a et al., 1987. A quantitative morphometric analysis of the neuronal and synaptic content of the frontal and temporal cortex in patients with Alzheimer's disease. *Journal of the neurological sciences*, 78(2), pp.151–164.

Davis, J. et al., 2004. Early-onset and Robust Cerebral Microvascular Accumulation of Amyloid ??-Protein in Transgenic Mice Expressing Low Levels of a Vasculotropic Dutch/Iowa Mutant Form of Amyloid ??-Protein Precursor. *Journal of Biological Chemistry*, 279(19), pp.20296–20306.

Dawson, D. a. & Hallenbeck, J.M., 1996. Acute focal ischemia-induced alterations in MAP2 immunostaining: Description of temporal changes and utilization as a marker for volumetric assessment of acute brain injury. *Journal of Cerebral Blood Flow and Metabolism*, 16(1), pp.170–174.

Dawson, L.A. et al., 2001. Characterization of transient focal ischemia-induced increases in extracellular glutamate and aspartate in spontaneously hypertensive rats. , 53(6), pp.767–776.

Dayer, A.G. et al., 2005. New GABAergic interneurons in the adult neocortex and striatum are generated from different precursors. *Journal of Cell Biology*, 168(3), pp.415–427.

DeKosky, S.T. & Scheff, S.W., 1990. Synapse loss in frontal cortex biopsies in Alzheimer's disease: Correlation with cognitive severity. *Annals of Neurology*, 27(5), pp.457–464.

Deleglise, B. et al., 2018. Dysregulated Neurotransmission induces Trans-synaptic degeneration in reconstructed Neuronal Networks. *Scientific Reports*, 8(1), pp.1–12.

Desk, R., Williams, L. & Health, K., 1992. A new model of temporary focal neocortical ischemia in the rat AM Buchan, D Xue and A Slivka Stroke 1992;23;273-279.

Desmond, D.W. et al., 2000. Frequency and clinical determinants of dementia after ischemic stroke. *Neurology*, 54(5), pp.1124–1131.

Diao, Q. et al., 2017. Regional structural impairments outside lesions are associated with verbal short-term memory deficits in chronic subcortical stroke. *Oncotarget*, 8(19), pp.30900–30907.

Dichgans, M. & Leys, D., 2017. Vascular Cognitive Impairment. *Circulation Research*, 120(3), pp.573–591.

Dierksen, G. a et al., 2010. <Dierksen et al., 2010 CAA.pdf>. , pp.545–548.

Dietrich, W.D. et al., 1986. Photochemically induced cortical infarction in the rat. 1. Time course of hemodynamic consequences. *Journal of Cerebral Blood Flow and Metabolism*, 6(2), pp.184–194.

Dirnagl, U., Iadecola, C. & Moskowitz, M.A., 1999. Pathobiology of ischaemic stroke : an integrated view. , pp.391–397.

Dittmar, M. et al., 2003. External carotid artery territory ischemia impairs outcome in the endovascular filament model of middle cerebral artery occlusion in rats. *Stroke*, 34(9), pp.2252–2257.

Dos-anjos, S. et al., 2009. Global ischemia-induced modifications in the expression of AMPA receptors and inflammation in rat brain. *Brain Research*, 1287, pp.20–27.

Doussau, F. & Augustine, G.J., 2000. The actin cytoskeleton and neurotransmitter release: An overview. *Biochimie*, 82(4), pp.353–363.

Doyle, K.P. et al., 2015. B-Lymphocyte-Mediated Delayed Cognitive Impairment following Stroke. *Journal of Neuroscience*, 35(5), pp.2133–2145.

Doyle, K.P. et al., 2012. Distal hypoxic stroke: A new mouse model of stroke with high throughput, low variability and a quantifiable functional deficit. *Journal of Neuroscience Methods*, 207(1), pp.31–40.

Doyle, S. et al., 2018. Vesicular glutamate release from central axons contributes to myelin damage. *Nature Communications*, 9(1).

Drejer, J. et al., 1985. Cellular Origin of Ischemia-Induced Glutamate Release from Brain Tissue In Vivo and In Vitro.

Dresbach, T. et al., 2001. The presynaptic cytomatrix of brain synapses. *Cellular and Molecular Life Sciences*, 58(1), pp.94–116.

Du, a T. et al., 2002. Effects of subcortical ischemic vascular dementia and AD on entorhinal cortex and hippocampus. *Neurology*, 58(11), pp.1635–1641.

Duncombe, J. et al., 2017. Ageing causes prominent neurovascular dysfunction associated with loss of astrocytic contacts and gliosis. , pp.477–491.

Duncombe, J. et al., 2017. Chronic cerebral hypoperfusion: A key mechanism leading to vascular cognitive impairment and dementia. Closing the translational gap between rodent models and human vascular cognitive impairment and dementia. *Clinical Science*, 131(19), pp.2451–2468.

Durante, W., Johnson, F. & Johnson, R., 2007. Arginase: A critical regulator of nitric oxide synthesis and vascular function. *Clin Exp Pharmacol Physiol.*, 34(9), pp.906–911.

Efthymiou, A.G. & Goate, A.M., 2017. Late onset Alzheimer's disease genetics implicates microglial pathways in disease risk. *Molecular Neurodegeneration*, 12(1), pp.1–12.

Eguchi, M. & Yamaguchi, S., 2009. In vivo and in vitro visualization of gene expression dynamics over extensive areas of the brain. *NeuroImage*, 44(4), pp.1274–1283.

Elias, G.M. & Nicoll, R.A., 2007. Synaptic trafficking of glutamate receptors by MAGUK scaffolding proteins. *Trends in Cell Biology*, 17(7), pp.343–352.

Elkind, M.S.V. et al., 2014. C-Reactive protein as a prognostic marker after lacunar stroke levels of inflammatory markers in the treatment of stroke study. *Stroke*, 45(3), pp.707–716.

Elkins, J. et al., 2017. Safety and efficacy of natalizumab in patients with acute ischaemic stroke (ACTION): a randomised, placebo-controlled, double-blind phase 2 trial. *The Lancet Neurology*, 16(3), pp.217–226.

Eng, L.F. et al., 1971. An acidic protein isolated from fibrous astrocytes. *Brain Research*, 28(2), pp.351–354.

Enright, L.E., Zhang, S. & Murphy, T.H., 2007. Fine mapping of the spatial relationship between acute ischemia and dendritic structure indicates selective vulnerability of layer V neuron dendritic tufts within single neurons in vivo. *Journal of cerebral blood flow and metabolism : official journal of the International Society of Cerebral Blood Flow and Metabolism*, 27(6), pp.1185–200.

Faheem, H. et al., 2019. Neuroprotective effects of minocycline and progesterone on white matter injury after focal cerebral ischemia. *Journal of Clinical Neuroscience*, (xxxx), pp.8–15.

Farkas, E. et al., 2006. The effect of pre- and posttreatment with diazoxide on the early phase of chronic cerebral hypoperfusion in the rat. *Brain Research*, 1087(1), pp.168–174.

Farkas, E. & Luiten, P.G.M., 2001. *Cerebral microvascular pathology in aging and Alzheimer's disease*,

Farkas, E., Luiten, P.G.M. & Bari, F., 2007a. Permanent , bilateral common carotid artery occlusion in the rat : A model for chronic cerebral hypoperfusion-related neurodegenerative diseases. , 54.

Farkas, E., Luiten, P.G.M. & Bari, F., 2007b. Permanent, bilateral common carotid artery occlusion in the rat: A model for chronic cerebral hypoperfusion-related neurodegenerative diseases. *Brain Research Reviews*, 54(1), pp.162–180.

Farr, T.D. et al., 2006. Bilateral alteration in stepping pattern after unilateral motor cortex injury : A new test strategy for analysis of skilled limb movements in neurological mouse models. , 153, pp.104–113.

Fedorovich, S. et al., 2017. Reduced Synaptic Vesicle Recycling during Hypoxia in Cultured Cortical Neurons. *Frontiers in Cellular Neuroscience*, 11(February), pp.1–8.

Feekes, J. a. et al., 2005. Tertiary microvascular territories define lacunar infarcts in the basal ganglia. *Annals of Neurology*, 58(1), pp.18–30.

Feekes, J. a. & Cassell, M.D., 2006. The vascular supply of the functional compartments of the human striatum. *Brain*, 129(8), pp.2189–2201.

Fernández, E. et al., 2017. Arc Requires PSD95 for Assembly into Postsynaptic Complexes Involved with Neural Dysfunction and Intelligence. *Cell Reports*, 21(3), pp.679–691.

Ferreira, A., 2012. Calpain Dysregulation in Alzheimer's Disease. *ISRN Biochemistry*, 2012, pp.1–12.

Ferreira, A. et al., 2000. Synapsin III: developmental expression, subcellular localization, and role in axon formation. *The Journal of neuroscience : the official journal of the Society for Neuroscience*, 20(10), p.3736.

Filomeni, G., De Zio, D. & Cecconi, F., 2015. Oxidative stress and autophagy: The clash between damage and metabolic needs. *Cell Death and Differentiation*, 22(3), pp.377–388.

Finnema, S.J. et al., 2016. Imaging synaptic density in the living human brain. , pp.1–10.

Fluri, F., 2015. Animal models of ischemic stroke and their application in clinical research. , pp.3445–3454.

Fog, M., 1938. Fog Blood Pressure and Cat Pial Arteries. *J Neurol Psychiatry*, 3, pp.187–197.

Fogel, H. et al., 2014. APP homodimers transduce an amyloid-β-mediated increase in release probability at excitatory synapses. *Cell Reports*, 7(5), pp.1560–1576.

Fowler, J.H. et al., 2018. Dimethyl fumarate improves white matter function following severe hypoperfusion: Involvement of microglia/macrophages and inflammatory mediators. *Journal of Cerebral Blood Flow and Metabolism*, 38(8), pp.1354–1370.

Fréchou, M. et al., 2019. Behavioral tests that reveal long-term deficits after permanent focal cerebral ischemia in mouse. *Behavioural Brain Research*, 360(November), pp.69–80.

Freeman, L.R. & Keller, J.N., 2012. Oxidative stress and cerebral endothelial cells: Regulation of the blood-brain-barrier and antioxidant based interventions. *Biochimica et Biophysica Acta - Molecular Basis of Disease*, 1822(5), pp.822–829.

Fremeau, R.T. et al., 2001. The Expression of Vesicular Glutamate Transports Define Two Classes of Excitatory Synapse. *Neuron*, 31, pp.247–260.

Frey, D. et al., 2000. Shared and unique roles of CAP23 and GAP43 in actin regulation, neurite outrgowth, and anatomical plasticity. *Journal of Cell Biology*, 149(7), pp.1443–1453.

Friedrich, P. & Aszódi, a., 1991. MAP2: a sensitive cross-linker and adjustable spacer in dendritic architecture. *FEBS Letters*, 295(1-3), pp.5–9.

Fujioka, M. et al., 2003. Magnetic Resonance Imaging Shows Delayed Ischemic Striatal Neurodegeneration.

Fujiyama, F., Furuta, T. & Kaneko, T., 2001. Immunocytochemical localization of candidates for vesicular glutamate transporters in the rat cerebral cortex. *The Journal of comparative neurology*, 435(3), pp.379–87.

Gaberel, T. et al., 2014. Impaired glymphatic perfusion after strokes revealed by contrast-enhanced MRI: A new target for fibrinolysis? *Stroke*, 45(10), pp.3092–3096.

Games, D. et al., 1995. Alzheimer-type neuropathology in transgenic mice overexpressing V717F β-amyloid precursor protein. *Nature*, 373(6514), pp.523–527.

Gan, K.J. & Silverman, M. a., 2015. Dendritic and axonal mechanisms of Ca2+ elevation impair BDNF transport in Aβ oligomer-treated hippocampal neurons. *Molecular Biology of the Cell*, 26(6), pp.1058–1071.

Gao, H. & Zhang, M., 2008. Asymmetry in the brain influenced the neurological deficits and infarction volume following the middle cerebral artery occlusion in rats. *Behavioral and Brain Functions*, 4, pp.1–5.

Garcia-Alloza, M. et al., 2011. Cerebrovascular lesions induce transient ??-amyloid deposition. *Brain*, 134(12), pp.3694–3704.

Garcia-alloza, M. et al., 2011. Cerebrovascular lesions induce transient b -amyloid deposition.

Garde, E. et al., 2000. Relation between age-related decline in intelligence and cerebral white-matter hyperintensities in healthy octogenarians : a longitudinal study. *Lancet*, 356(9230), pp.628–634.

Gascon, S. et al., 2008. Excitotoxicity and focal cerebral ischemia induce truncation of the NR2A and NR2B subunits of the NMDA receptor and cleavage of the scaffolding protein PSD-95. *Molecular psychiatry*, 13, pp.99–114.

Gauberti, M. et al., 2013. Ultra-sensitive molecular MRI of vascular cell adhesion molecule-1 reveals a dynamic inflammatory penumbra after strokes. *Stroke*, 44(7), pp.1988–1996.

Gelderblom, M. et al., 2012. Neutralisation of the IL-17 axis deminishes neutrophil invasion and protects from ischemic stroke. *Blood*, 120(18), pp.3793–3802.

St. George-Hyslop, P.H. et al., 1987. The genetic defect causing familial Alzheimer's disease maps on chromosome 21. *Science*, 235(4791), pp.885–890.

Giraud, M. et al., 2015. Early Blood Brain Barrier Changes in Acute Ischemic Stroke: A Sequential MRI Study. *Journal of Neuroimaging*, 25(6), pp.959–963.

Giuliani, A. et al., 2019. Age-Related Changes of the Neurovascular Unit in the Cerebral Cortex of Alzheimer Disease Mouse Models : A Neuroanatomical and Molecular Study. , 78(2), pp.101–112.

Glenner, G.G. & Wong, C.W., 1984. Alzheimer's Disease: Initial report of the purification and characterisation. , 120(3), pp.885–890.

De Gois, S. et al., 2006. Identification of endophilins 1 and 3 as selective binding partners for VGLUT1 and their co-localization in neocortical glutamatergic synapses: Implications for vesicular glutamate transporter trafficking and excitatory vesicle formation. *Cellular and Molecular Neurobiology*, 26(4-6), pp.679–693.

Gong, S. et al., 2003. A gene expression atlas of the central nervous system based on bacterial artificial chromosomes. *Nature*, 425(6961), pp.917–925.

Gong, Y. et al., 2009. Disruption of glutamate receptors at Shank-postsynaptic platform in Alzheimer's disease. *Brain Research*, 1292, pp.191–198.

Gordon, M.N. et al., 2002. Time course of the development of Alzheimer-like pathology in the doubly transgenic PS1+APP mouse. *Experimental Neurology*, 173(2), pp.183–195.

Gordon, S., 2003. Alternative activation of macrophages_Nature Review. , 3(January).

Gorelick, P.B. et al., 2011. Vascular contributions to cognitive impairment and dementia: A statement for healthcare professionals from the American Heart Association/American Stroke Association. *Stroke*, 42(9), pp.2672–2713.

Grabowski, T.J. et al., 2001. Novel amyloid precursor protein mutation in an Iowa family with dementia and severe cerebral amyloid angiopathy. *Annals of Neurology*, 49(6), pp.697–705.

Gresle, M.M. et al., 2006. Injury to axons and oligodendrocytes following endothelin-1-induced middle cerebral artery occlusion in conscious rats. *Brain Research*, 1110(1), pp.13–22.

Gris, P. et al., 2007. Transcriptomal Regulation of Scar Gene Expression in Primary Astrocytes. *Glia*, 55, pp.1145–1155.

Groen, T. Van, Puurunen, K. & Ma, H., 2005. Transformation of Diffuse NL -Amyloid Precursor Protein and NL -Amyloid Deposits to Plaques in the Thalamus After Transient Occlusion of the Middle Cerebral Artery in Rats. , pp.1551–1557.

Groenewegen, H.J., 2003. The Basal Ganglia and Motor Control. *Neural Plasticity*, 10(1-2), pp.107–120.

Gundelfinger, E.D. & Tom Dieck, S., 2000. Molecular organization of excitatory chemical synapses in the mammalian brain. *Naturwissenschaften*, 87(12), pp.513–523.

Guntupalli, S., Widagdo, J. & Anggono, V., 2016. Amyloid- β -Induced Dysregulation of AMPA Receptor Trafficking. *Neural Plasticity*, 2016.

Guo, H. et al., 2011. Capillary Remodeling and Collateral Growth Without Angiogenesis After Unilateral Common Carotid Artery Occlusion in Mice. *Microcirculation*, 18(3), pp.221–227.

Gurol, M.E. et al., 2006. Plasma β-amyloid and white matter lesions in AD, MCI, and cerebral amyloid angiopathy. *Neurology*, 66(1), pp.23–29.

Gurol, M.E. et al., 2012. Predicting sites of new hemorrhage with amyloid imaging in cerebral amyloid angiopathy. *Neurology*, 79(4), pp.320–326.

Gylys, K.H. et al., 2004. Synaptic changes in Alzheimer's disease: increased amyloid-beta and gliosis in surviving terminals is accompanied by decreased PSD-95 fluorescence. *The American journal of pathology*, 165(5), pp.1809–1817.

Hachinski, V.C. & Bowler, J. V, 1993. Vascular Dementia. *Neurology*, 43(10), pp.2159–60.

Hachinski, V.C., Lassen, N. a. & Marshall, J., 1974. Multi-Infarct Dementia. a Cause of Mental Deterioration in the Elderly. *The Lancet*, 304(7874), pp.207–209.

Hall, A.M. & Roberson, E.D., 2012. Mouse models of Alzheimer's disease. *Brain research bulletin*, 88(1), pp.3–12.

Hallock, H.L., Wang, a. & Griffin, a. L., 2016. Ventral Midline Thalamus Is Critical for Hippocampal-Prefrontal Synchrony and Spatial Working Memory. *Journal of Neuroscience*, 36(32), pp.8372–8389.

Hamel, E., 2006. Perivascular nerves and the regulation of cerebrovascular tone. *Journal of Applied Physiology*, 100(3), pp.1059–1064.

Hammond, T.R. et al., 2019. Single-Cell RNA Sequencing of Microglia throughout the Mouse Lifespan and in the Injured Brain Reveals Complex Cell-State Changes. *Immunity*, 50(1), pp.253–271.e6.

Han, X.-J. et al., 2016. Changes in synaptic plasticity and expression of glutamate receptor subunits in the CA1 and CA3 areas of the hippocampus after transient global ischemia. *Neuroscience*, 327, pp.64–78.

Hanse, E., Seth, H. & Riebe, I., 2013. AMPA-silent synapses in brain development and pathology. *Nature reviews. Neuroscience*, 14(12), pp.839–50.

Hanson, P.I. et al., 1997. Structure and conformational changes in NSF and its membrane receptor complexes visualized by quick-freeze/deep-etch electron microscopy. *Cell*, 90(3), pp.523–535.

Hardy, J. a. & Higgins, G. a., 1992. Alzheimer's disease: The amyloid cascade hypothesis. *Science*, 256(5054), pp.184–185.

Hartings, J. a et al., 2003. Delayed Hartings 2003 Secondary Phase of Peri-Infarct Depolarizations.pdf. , 23(37), pp.11602–11610.

Hase, Y. et al., 2017. The effects of environmental enrichment on white matter pathology in a mouse model of chronic cerebral hypoperfusion. *Journal of Cerebral Blood Flow and Metabolism*, 14(81), pp.151–165.

Haseloff, R.F. et al., 2015. Transmembrane proteins of the tight junctions at the blood-brain barrier: Structural and functional aspects. *Seminars in Cell and Developmental Biology*, 38, pp.16–25.

Hata, R. et al., 1998. A Reproducible Model of Middle Cerebral Artery Occlusion in Mice: Hemodynamic, Biochemical, and Magnetic Resonance Imaging. *Journal of Cerebral Blood Flow & Metabolism*, 18(4), pp.367–375.

Hatakeyama, T. et al., 1988. Immunohistochemical investigation of ischemic and postischemic damage after bilateral carotid occlusion in gerbils. *Stroke*, 19(12), pp.1526–1534.

Hattori, Y., Kitamura, A., Nagatsuka, K., et al., 2014. A Novel Mouse Model of Ischemic Carotid Artery Disease. , 9(6), pp.1–7.

Hattori, Y. et al., 2015. A Novel Mouse Model of Subcortical Infarcts with Dementia. *Journal of Neuroscience*, 35(9), pp.3915–3928.

Hattori, Y., Kitamura, A., Tsuji, M., et al., 2014. Motor and cognitive impairment in a mouse model of ischemic carotid artery disease. *Neuroscience Letters*, 581, pp.1–6.

Hattori, Y. et al., 2016. Substantial Reduction of Parenchymal Cerebral Blood Flow in Mice with Bilateral Common Carotid Artery Stenosis. *Scientific Reports*, 6(August), p.32179.

Hawkes, C. a. et al., 2014. Failure of perivascular drainage of β-amyloid in cerebral amyloid angiopathy. *Brain Pathology*, 24(4), pp.396–403.

Hawkes, C. a. et al., 2011. Perivascular drainage of solutes is impaired in the ageing mouse brain and in the presence of cerebral amyloid angiopathy. *Acta Neuropathologica*, 121(4), pp.431–443.

Heiss, W. -D & Rosner, G., 1983. Functional recovery of cortical neurons as related to degree and duration of ischemia. *Annals of Neurology*, 14(3), pp.294–301.

Heneka, M.T. et al., 2015. Review Neuroinfl ammation in Alzheimer ' s disease. , 14(April), p.Cryan, John F., and Timothy G. Dinan. 2012. "Mind–.

Hennessy, E., Griffin, E.W. & Cunningham, C., 2015. Astrocytes Are Primed by Chronic Neurodegeneration to Produce Exaggerated Chemokine and Cell Infiltration Responses to Acute Stimulation with the Cytokines IL-1 and TNF- . *Journal of Neuroscience*, 35(22), pp.8411–8422.

Heo, C. et al., 2016. A soft, transparent, freely accessible cranial window for chronic imaging and electrophysiology. *Scientific Reports*, 6, pp.1–11.

Hertz, L. & Zielke, H.R., 2004. Astrocytic control of glutamatergic activity: astrocytes as stars of the show. *Trends in Neurosciences*, 27(12), pp.735–743.

Hill, R. a. et al., 2015. Regional Blood Flow in the Normal and Ischemic Brain Is Controlled by Arteriolar Smooth Muscle Cell Contractility and Not by Capillary Pericytes. *Neuron*, 87(1), pp.95–110.

Hinman, J.D., 2014. The back and forth of axonal injury and repair after stroke. *Curr Opin Neurol*, 27(6), pp.615–623.

Ho, P.W. et al., 2005. Is White Matter Involved in Patients Entered into Typical Trials of Neuroprotection ? , pp.2742–2744.

Hofman, A. et al., 1997. Atherosclerosis , apolipoprotein E , and prevalence of dementia and Alzheimer ' s disease in the Rotterdam Study. , 349.

Holcomb, L. et al., 1998. Accelerated Alzheimer-type phentype in transgenic mice carrying both mutant amyloid precursor protein and presenilin 1 transgenes. *Nature Medicine*, 4(1), pp.97–100.

Holland, P.R. et al., 2015. Gliovascular disruption and cognitive deficits in a mouse model with features of small vessel disease. *Journal of Cerebral Blood Flow & Metabolism*, (October 2014), pp.1–10.

Holland, P.R., Searcy, J.L.L., et al., 2015. Gliovascular disruption and cognitive deficits in a mouse model with features of small vessel disease. *Journal of cerebral blood flow and metabolism : official journal of the International Society of Cerebral Blood Flow and Metabolism*, 35(October 2014), pp.1–10.

Holland, P.R., Pannozzo, M. a, et al., 2015. Hypertension fails to disrupt white matter integrity in young or aged Fisher (F44) Cyp1a1Ren2 transgenic rats. *J Cereb Blood Flow Metab*, 35(2), pp.188–192.

Holland, P.R. et al., 2011. MRI is a sensitive marker of subtle white matter pathology in hypoperfused mice. *Neurobiology of Aging*, 32(12), pp.2325.e1–2325.e6.

Hong, S. et al., 2016. Complement and microglia mediate early synapse loss in Alzheimer mouse models. *Science*, 8373, pp.1–10.

Hong, S. et al., 2016. Complement and microglia mediate early synapse loss in Alzheimer mouse models. *Science (New York, N.Y.)*, 352(6286), pp.712–6.

Hsiao, K. et al., 1996. Amyloid Plaques in Transgenic Mice. *Science*, 274(October), pp.99–102.

Hsieh, C.L. et al., 2009. A role for TREM2 ligands in the phagocytosis of apoptotic neuronal cells by microglia. *Journal of Neurochemistry*, 109(4), pp.1144–1156.

Hsieh, H. et al., 2006. AMPAR Removal Underlies Aβ-Induced Synaptic Depression and Dendritic Spine Loss. *Neuron*, 52, pp.831–843.

Hu, H. et al., 2009. Calpain-1 induces apoptosis in pulmonary microvascular endothelial cells under septic conditions. *Microvascular Research*, 78(1), pp.33–39.

Hu, Y. et al., 2019. Postoperative intermittent fasting prevents hippocampal oxidative stress and memory deficits in a rat model of chronic cerebral hypoperfusion. *European Journal of Nutrition*, 58(1), pp.423–432.

Huang, C. et al., 2002. Cingulate cortex hypoperfusion predicts Alzheimer's disease in mild cognitive impairment. *BMC neurology*, 2, p.9.

Hudson, L.C. et al., 2005. Astrocytes and microglia differentially regulate trafficking of lymphocyte subsets across brain endothelial cells. *Brain Research*, 1058(1-2), pp.148–160.

Huneau, C. et al., 2018. Altered dynamics of neurovascular coupling in CADASIL. *Annals of Clinical and Translational Neurology*, 5(7), pp.788–802.

Hyman, B. et al., 1984. Alzheimer ' s Disease : Cell-Specific Pathology Isolates the Hippocampal Formation Alzheimer ' s Disease : Cell-Specific Pathology Isolates the Hippocampal Formation. *Advancement Of Science*, 225(4667), pp.1168–1170.

Iadecola, C., 2004. Neurovascular regulation in the normal brain and in Alzheimer's disease. *Nature Reviews Neuroscience*, 5(5), pp.347–360.

Iadecola, C. & Nedergaard, M., 2007. Glial regulation of the cerebral microvasculature. *Nature Neuroscience*, 10(11), pp.1369–1376.

Ibrahim, H.M. et al., 2000. Nucleus-specific expression of ionotropic glutamate receptor subunit mRNAs and binding sites in primate thalamus. *Molecular Brain Research*, 79(1-2), pp.1–17.

Iliff, J.J. et al., 2012. A paravascular pathway facilitates CSF flow through the brain parenchyma and the clearance of interstitial solutes, including amyloid β. *Science Translational Medicine*, 4(147).

Imai, H. et al., 2002. New Method for the Quantitative Assessment of Axonal Damage in Focal Cerebral Ischemia. , pp.1080–1089.

Isaac, J.T.R., Ashby, M. & McBain, C.J., 2007. The Role of the GluR2 Subunit in AMPA Receptor Function and Synaptic Plasticity. *Neuron*, 54(6), pp.859–871.

De Iure, A. et al., 2019. Striatal spreading depolarization: Possible implication in levodopa-induced dyskinetic-like behavior. *Movement Disorders*, (January), pp.1–13.

Jellinger, K.A., 2008. Morphologic diagnosis of " vascular dementia " — A critical update. , 270, pp.1–12.

Jessen, N.A. et al., 2015. The Glymphatic System: A Beginner's Guide. *Neurochemical Research*, 40(12), pp.2583–2599.

Jia, H. et al., 2012. Dendritic morphology of neurons in medial prefrontal cortex and hippocampus in 2VO rats. *Neurol Sci*, 33(5), pp.1063–1070.

Jiang, Q. et al., 2008. ApoE Promotes the Proteolytic Degradation of Aβ. *Neuron*, 58(5), pp.681–693.

Jin, W.N. et al., 2017. Depletion of microglia exacerbates postischemic inflammation and brain injury. *Journal of Cerebral Blood Flow and Metabolism*, 37(6), pp.2224–2236.

Johnson, J., 2013. Vulnerable subjects? The case of nonhuman animals in experimentation. *Journal of bioethical inquiry*, 10(4), pp.497–504.

Jones, K. a. et al., 2015. Chronic stress exacerbates neuronal loss associated with secondary neurodegeneration and suppresses microglial-like cells following focal motor cortex ischemia in the mouse. *Brain, Behavior, and Immunity*, 48, pp.57–67.

Jones, K.A. et al., 2018. Peripheral immune cells infiltrate into sites of secondary neurodegeneration after ischemic stroke. *Brain Behavior and Immunity*, 67, pp.299–307.

Jorgensen, H.S. et al., 1995. Recovery of Walking Function in Stroke Patients : The Copenhagen Stroke Study. , 76, pp.27–32.

Justin, B.N., Turek, M. & Hakim, A.M., 2013. Heart disease as a risk factor for dementia. *Clinical epidemiology*, 5(1), p.135.

Kageyama, G.H. & Wong-Riley, M.T.T., 1982. Histochemical localization of cytochrome oxidase in the hippocampus: Correlation with specific neuronal types and afferent pathways. *Neuroscience*, 7(10), pp.2337–2361.

Kalaria, R.N., Akinyemi, R. & Ihara, M., 2016. Stroke injury , cognitive impairment and vascular dementia ☆. *Biochimica et Biophysica Acta (BBA)*, 1862(5), pp.915–925.

Kalaria, R.N. & Hedera, P., 1996. β-amyloid vasoactivity in Alzheimer's disease. *Lancet*, 347(9013), pp.1492–1493.

Kaneko, T. & Fujiyama, F., 2002. Complementary distribution of vesicular glutamate transporters in the central nervous system. *Neuroscience Research*, 42(4), pp.243–250.

Kaneko, T., Fujiyama, F. & Hioki, H., 2002. Immunohistochemical localization of candidates for vesicular glutamate transporters in the rat brain. *Journal of Comparative Neurology*, 444(1), pp.39–62.

Kantarci, K. et al., 2017. White-matter integrity on DTI and the pathologic staging of Alzheimer's disease. *Neurobiology of Aging*, 56, pp.172–179.

Kashani, A. et al., 2008. Loss of VGLUT1 and VGLUT2 in the prefrontal cortex is correlated with cognitive decline in Alzheimer disease. *Neurobiology of Aging*, 29, pp.1619–1630.

Khan, S. et al., 2018. Tau pathology and neurochemical changes associated with memory dysfunction in an optimised murine model of global cerebral ischaemia - A potential model for vascular dementia? *Neurochemistry International*, 118(April), pp.134–144.

Kimbrough, I.F. et al., 2015. Vascular amyloidosis impairs the gliovascular unit in a mouse model of Alzheimer's disease. *Brain*, 138(12), pp.3716–3733.

Kirvell, S.L., Elliott, M.S., Kalaria, R., et al., 2010. Vesicular glutamate transporter and cognition in stroke. *Neurology*, pp.1803–1809.

Kirvell, S.L., Elliott, M.S., Kalaria, R.N., et al., 2010. Vesicular glutamate transporter and cognition in stroke A case-control autopsy study. , pp.1803–1809.

Kitamura, A. et al., 2017. Long-term cilostazol treatment reduces gliovascular damage and memory impairment in a mouse model of chronic cerebral hypoperfusion. , (February), pp.1–11.

Kitamura, A. et al., 2012. Selective white matter abnormalities in a novel rat model of vascular dementia. *NBA*, 33(5), pp.1012.e25–1012.e35.

Klann, E. et al., 1998. A role for superoxide in protein kinase C activation and induction of long-term potentiation. *Journal of Biological Chemistry*, 273(8), pp.4516–4522.

Klein, B. et al., 1986. Interdependency of local capillary density, blood flow, and metabolism in rat brains. *American Journal of Physiology*, 251(6 Pt 2), pp.H1333–40.

Kluge, M.G., Jones, K., et al., 2018. Age-dependent Disturbances of Neuronal and Glial Protein Expression Profiles in Areas of Secondary Neurodegeneration Post-stroke. *Neuroscience*, (August).

Kluge, M.G. et al., 2018. Age-dependent Disturbances of Neuronal and Glial Protein Expression Profiles in Areas of Secondary Neurodegeneration Post-stroke. *Neuroscience*, (August).

Kluge, M.G. et al., 2017. Impaired microglia process dynamics post-stroke are specific to sites of secondary neurodegeneration. , (February), pp.1–15.

Kluge, M.G., Abdolhoseini, M., et al., 2018. Spatiotemporal analysis of impaired microglia process movement at sites of secondary neurodegeneration post-stroke. *Journal of Cerebral Blood Flow and Metabolism*.

Knopman, D. et al., 2001. Cardiovascular risk factors and cognitive decline in middle-aged adults.

Koffie, R.M. et al., 2012. Apolipoprotein E4 effects in Alzheimer's disease are mediated by synaptotoxic oligomeric amyloid-β. *Brain*, 135(7), pp.2155–2168.

Koffie, R.M. et al., 2009. Oligomeric amyloid beta associates with postsynaptic densities and correlates with excitatory synapse loss near senile plaques. *Proceedings of the National Academy of Sciences of the United States of America*, 106(10), pp.4012–7.

Koizumi, J. et al., 1986. Experimental studies of ischemic brain edema. 1. A new experimental model of cerebral embolism in rats in which recirculation can be introduced in the ischemia area. *Jpn. J. Stroke*, 8(1), pp.1–8.

Kravitz, A. V & Kreitzer, A.C., 2012. Striatal mechanisms underlying movement, reinforcement and punishment. , 27(3).

Kril, J.J. et al., 2002. Patients with vascular dementia due to microvascular pathology have significant hippocampal neuronal loss. *Journal of neurology, neurosurgery, and psychiatry*, 72(6), pp.747–751.

Kronenberg, G. et al., 2018. Distinguishing features of microglia- and monocyte-derived macrophages after stroke. *Acta Neuropathologica*, 135(4), pp.551–568.

Krstic, D. et al., 2012. Systemic immune challenges trigger and drive Alzheimer-like neuropathology in mice. *Journal of Neuroinflammation*, 9(1), p.151.

Kusano, K., Miledi, R. & Stinnakre, J., 1975. Postsynaptic Entry of Calcium Induced by Transmitter Action. *Proceedings of the Royal Society of London. Series B, Biological Sciences*, 189(1094), pp.49–56.

Lai, T.W., Zhang, S. & Wang, Y.T., 2014. Excitotoxicity and stroke: Identifying novel targets for neuroprotection. *Progress in Neurobiology*, 115, pp.157–188.

Lalonde, R., Fukuchi, K.I. & Strazielle, C., 2012. Neurologic and motor dysfunctions in APP transgenic mice. *Reviews in the Neurosciences*, 23(4), pp.363–379.

Lambert, M.P. et al., 1998. Diffusible, nonfibrillar ligands derived from Abeta1-42 are potent central nervous system neurotoxins. *Proceedings of the National Academy of Sciences of the United States of America*, 95(11), pp.6448–53.

Landis, D.M.D. et al., 1988. The organization of cytoplasm at the presynaptic active zone of a central nervous system synapse. *Neuron*, 1(3), pp.201–209.

Lanz, T. a., Carter, D.B. & Merchant, K.M., 2003. Dendritic spine loss in the hippocampus of young PDAPP and Tg2576 mice and its prevention by the ApoE2 genotype. *Neurobiology of Disease*, 13, pp.246–253.

Larson, J. et al., 1999. Alterations in synaptic transmission and long-term potentiation in hippocampal slices from young and aged PDAPP mice. *Brain Research*, 840(1-2), pp.23–35.

Lassen, N.A., 1982. Comments and Opinions Incomplete Cerebral Infarction — Focal Incomplete Ischemic Tissue Necrosis Not Leading To Emollision. , pp.522–523.

Lee, C.Y.D. & Landreth, G.E., 2010. The role of microglia in amyloid clearance from the AD brain. *Journal of Neural Transmission*, 117(8), pp.949–960.

Lee, Y. et al., 2012. Oligodendroglia metabolically support axons and contribute to neurodegeneration. *Nature*, 487(7408), pp.443–448.

De Leeuw, F. et al., 2006. White Matter Lesions Are Associated With Progression of Medial Temporal Lobe Atrophy in Alzheimer Disease. , pp.2248–2253.

Lehmann, J. et al., 2014. Inflammatory cell recruitment after experimental thromboembolic stroke in rats. *Neuroscience*, 279, pp.139–154.

Leifer, D. & Kowall, N.W., 1993. Immunohistochemical patterns of selective cellular vulnerability in human cerebral ischemia. *Journal of the Neurological Sciences*, 119(2), pp.217–228.

Lein, E.S. et al., 2007. Genome-wide atlas of gene expression in the adult mouse brain. *Nature*, 445(7124), pp.168–176.

Levy, E. et al., 1990. Mutation of the Alzheimer's disease amyloid gene in hereditary cerebral hemorrhage, Dutch type. *Science*, 248(4559), pp.1124–6.

Lewitus, G.M. et al., 2014. An Adaptive Role of TNF in the Regulation of Striatal Synapses. *Journal of Neuroscience*, 34(18), pp.6146–6155.

Li, C. et al., 2014. Activation of GABA B Receptors Ameliorates Cognitive Impairment via Restoring the Balance of HCN1 / HCN2 Surface Expression in the Hippocampal CA1 Area in Rats With Chronic Cerebral Hypoperfusion. , pp.704–720.

Li, D. et al., 2013. Lack of Evidence for Vesicular Glutamate Transporter Expression in Mouse Astrocytes. *Journal of Neuroscience*, 33(10), pp.4434–4455.

Li, M. et al., 2017. Astrocyte-derived interleukin-15 exacerbates ischemic brain injury via propagation of cellular immunity. *Proceedings of the National Academy of Sciences of the United States of America*, 114(3), pp.E396–E405.

Li, P. & Murphy, T.H., 2008. Two-Photon Imaging during Prolonged Middle Cerebral Artery Occlusion in Mice Reveals Recovery of Dendritic Structure after Reperfusion. *Journal of Neuroscience*, 28(46), pp.11970–11979.

Li, S. et al., 2009. Soluble Oligomers of Amyloid β Protein Facilitate Hippocampal Long-Term Depression by Disrupting Neuronal Glutamate Uptake. *Neuron*, 62(6), pp.788–801.

Liauw, J. et al., 2008. Thrombospondins 1 and 2 are necessary for synaptic plasticity and functional recovery after stroke. *Journal of Cerebral Blood Flow and Metabolism*, 28(10), pp.1722–1732.

Lichtenwalner, R.J. & Parent, J.M., 2006. Adult neurogenesis and the ischemic forebrain. , pp.1–20.

Liddelow, S. a. & Barres, B. a., 2017. Reactive Astrocytes: Production, Function, and Therapeutic Potential. *Immunity*, 46(6), pp.957–967.

Liddelow, S.A. et al., 2017. Neurotoxic reactive astrocytes are induced by activated microglia. *Nature Publishing Group*.

Liesz, A. et al., 2015. DAMP signaling is a key pathway inducing immune modulation after brain injury. *Journal of Neuroscience*, 35(2), pp.583–598.

Lin, R.C. & Scheller, R.H., 1997. Structural Organization of the Synaptic Exocytosis Core Complex. *Neuron*, 19(5), pp.1087–1094.

Lin, Y. et al., 2016. Critical role of astrocytic interleukin-17 A in post-stroke survival and neuronal differentiation of neural precursor cells in adult mice. , pp.1–14.

Linck, P.A. et al., 2019. Neurodegeneration of the Substantia Nigra after Ipsilateral Infarct: MRI R2* Mapping and Relationship to Clinical Outcome. *Radiology*, (9), p.182126.

Linden, D.E.J., 2007. The working memory networks of the human brain. *The Neuroscientist : a review journal bringing neurobiology, neurology and psychiatry*, 13(3), pp.257–267.

Link, W. et al., 1995. Somatodendritic expression of an immediate early gene is regulated by synaptic activity. *Proceedings of the National Academy of Sciences of the United States of America*, 92(12), pp.5734–5738.

Liu, B. et al., 2006. Ischemic Insults Direct Glutamate Receptor Subunit 2-Lacking AMPA Receptors to Synaptic Sites. *Journal of Neuroscience*, 26(20), pp.5309–5319.

Liu, B., 2006. Ischemic Insults Direct Glutamate Receptor Subunit 2-Lacking AMPA Receptors to Synaptic Sites. *Journal of Neuroscience*, 26(20), pp.5309–5319.

Liu, C. et al., 2018. Emerging Roles of Astrocytes in Neuro-Vascular Unit and the Tripartite Synapse With Emphasis on Reactive Gliosis in the Context of Alzheimer ' s Disease. , 12(July), pp.1–12.

Liu, C.C. et al., 2017. Astrocytic LRP1 mediates brain Aβ clearance and impacts amyloid deposition. *Journal of Neuroscience*, 37(15), pp.4023–4031.

Liu, F., Schafer, D.P. & McCullough, L.D., 2009. TTC, Fluoro-Jade B and NeuN staining confirm evolving phases of infarction induced by middle cerebral artery occlusion. *Journal of Neuroscience Methods*, 179(1), pp.1–8.

Liu, H.-X. et al., 2005. Altered expression of MAP-2, GAP-43, and synaptophysin in the hippocampus of rats with chronic cerebral hypoperfusion correlates with cognitive impairment. *Brain research. Molecular brain research*, 139(1), pp.169–177.

Liu, J. et al., 2006. Paeoniflorin attenuates chronic cerebral hypoperfusion-induced learning dysfunction and brain damage in rats. *Brain Research*, 1089(1), pp.162–170.

Liu, S. et al., 2009. Rodent Stroke Model Guidelines for Preclinical Stroke Trials (1St Edition). *Journal of experimental stroke & translational medicine*, 2(2), pp.2–27.

Liu, Z. et al., 2014. Beneficial effects of gfap/vimentin reactive astrocytes for axonal remodeling and motor behavioral recovery in mice after stroke. *Glia*, 62(12), pp.2022–2033.

Liu, Z. & Chopp, M., 2016a. Astrocytes, therapeutic targets for neuroprotection and neurorestoration in ischemic stroke. *Progress in Neurobiology*, 144, pp.103–120.

Liu, Z. & Chopp, M., 2016b. Progress in Neurobiology Astrocytes , therapeutic targets for neuroprotection and neurorestoration in ischemic stroke. *Progress in Neurobiology*, 144, pp.103–120.

Lloyd, A.F., Davies, C.L. & Miron, V.E., 2017. Microglia: origins, homeostasis, and roles in myelin repair. *Current Opinion in Neurobiology*, 47, pp.113–120.

Lobo, A.C. et al., 2011. Neurobiology of Disease Cleavage of the vesicular glutamate transporters under excitotoxic conditions. *Neurobiology of Disease*, 44(3), pp.292–303.

Love, S. & Miners, J.S., 2016. Cerebral Hypoperfusion and the Energy Deficit in Alzheimer's Disease. *Brain Pathology*, 26(5), pp.607–617.

Lu, W. et al., 2009. Subunit Composition of Synaptic AMPA Receptors Revealed by a Single-Cell Genetic Approach. *Neuron*, 62(2), pp.254–268.

Lu, Y. et al., 2016. Activation of GABAB2 subunits alleviates chronic cerebral hypoperfusion-induced anxiety-like behaviours : A role for BDNF signalling and Kir3 channels. *Neuropharmacology*, 110, pp.308–321.

Luo, P. et al., 2016. Baclofen ameliorates spatial working memory impairments induced by chronic cerebral hypoperfusion via up-regulation of HCN2 expression in the PFC in rats. *Behavioural Brain Research*, 308, pp.6–13.

Luo, P. et al., 2015. Long-lasting spatial learning and memory impairments caused by chronic cerebral hypoperfusion associate with a dynamic change of HCN1/HCN2 expression in hippocampal CA1 region. *Neurobiology of Learning and Memory*, 123, pp.72–83.

Luzzati, F. et al., 2006. Neurogenesis in the Caudate Nucleus of the Adult Rabbit. *Journal of Neuroscience*, 26(2), pp.609–621.

Mabuchi, T., Kitagawa, K. & Ohtsuki, T., 2000. Contribution of Microglia / Macrophages to Expansion of Infarction and Response of Oligodendrocytes After Focal Cerebral Ischemia in Rats.

Mack, T.G. a. et al., 2001. Wallerian degeneration of injured axons and synapses is delayed by a Ube4b/Nmnat chimeric gene. *Nature Neuroscience*, 4(12), pp.1199–1206.

Madinier, a. et al., 2013. Ipsilateral versus contralateral spontaneous post-stroke neuroplastic changes: Involvement of BDNF? *Neuroscience*, 231, pp.169–181.

Maeda, K., Hata, R. & Hossmann, K., 1999. Regional Metabolic Disturbances and Cerebrovascular Anatomy after Text Permanent Middle Cerebral Artery Occlusion in C57Black / 6 and SV129 Mice. , 108, pp.101–108.

Mahapatra, S. et al., 2012. Calcium channel types contributing to chromaffin cell excitability, exocytosis and endocytosis. *Cell Calcium*, 51(3-4), pp.321–330.

Mahmoud, S. et al., 2019. Astrocytes Maintain Glutamate Homeostasis in the CNS by Controlling the Balance between Glutamate Uptake and Release. *Cells*, 8(2), p.184.

Mäkinen, S. et al., 2008. Coaccumulation of calcium and β-amyloid in the thalamus after transient middle cerebral artery occlusion in rats. *Journal of Cerebral Blood Flow and Metabolism*, 28(2), pp.263–268.

Mani, S. et al., 2013. Contralesional motor deficits after unilateral stroke reflect hemisphere-specific control mechanisms. , pp.1288–1303.

Manso, Y. et al., 2018. Minocycline reduces microgliosis and improves subcortical white matter function in a model of cerebral vascular disease. , (April 2016), pp.34–46.

Maren, S., Phan, K.L. & Liberzon, I., 2013. The contextual brain: implications for fear conditioning, extinction and psychopathology. *Nat Rev Neurosci*, 14(6), pp.417–428.

Markgraf, C.G. et al., 1992. Sensorimotor and cognitive consequences of middle cerebral artery occlusion in rats. *Brain Research*, 575(2), pp.238–246.

Masliah, E. et al., 1990. Diffuse plaques do not accentuate synapse loss in Alzheimer's disease. *The American journal of pathology*, 137(6), pp.1293–1297.

Masliah, E. et al., 1991. Immunoelectron microscopic study of synaptic pathology in Alzheimer's disease. *Acta neuropathologica*, 81(4), pp.428–433.

Masliah, E. et al., 1989. Immunohistochemical quantification of the synapse-related protein synaptophysin in Alzheimer disease. *Neuroscience letters*, 103(2), pp.234–9.

Mattiasson, G. et al., 2003. Flow cytometric analysis of mitochondria from CA1 and CA3 regions of rat hippocampus reveals differences in permeability transition pore activation. *Journal of Neurochemistry*, 87(2), pp.532–544.

Mayor, D. & Tymianski, M., 2017. Neurotransmitters in the mediation of cerebral ischemic injury. *Neuropharmacology*, 134, pp.178–188.

McColl, B.W. et al., 2004. Extension of cerebral hypoperfusion and ischaemic pathology beyond MCA territory after intraluminal filament occlusion in C57Bl/6J mice. *Brain Research*, 997(1), pp.15–23.

McQueen, J. et al., 2014. Restoration of oligodendrocyte pools in a mouse model of chronic cerebral hypoperfusion. *PLoS ONE*, 9(2).

Mehta, D. et al., 2017. Why do trials for Alzheimer's disease drugs keep failing? A discontinued drug perspective for 2010-2015. *Expert Opinion on Investigational Drugs*, 26(6), pp.735–739.

Melone, M., Burette, A. & Weinberg, R.J., 2005. Light microscopic identification and immunocytochemical characterization of glutamatergic synapses in brain sections. *Journal of Comparative Neurology*, 492(4), pp.495–509.

Mena, H., Cadavid, D. & Rushing, E.J., 2004. Human cerebral infarct: A proposed histopathologic classification based on 137 cases. *Acta Neuropathologica*, 108(6), pp.524–530.

De Meyer, S.F. et al., 2016. Thromboinflammation in stroke brain damage. *Stroke*, 47(4), pp.1165–1172.

Miao, J. et al., 2005. Cerebral microvascular amyloid beta protein deposition induces vascular degeneration and neuroinflammation in transgenic mice expressing human vasculotropic mutant amyloid beta precursor protein. *The American journal of pathology*, 167(2), pp.505–515.

Michael-Titus, A., Revest, P. & Shortland, P., 2010. 2 - ELEMENTS OF CELLULAR AND MOLECULAR NEUROSCIENCE. In A. Michael-Titus, P. Revest, & P. B. T.-T. N. S. (Second E. Shortland, eds. Churchill Livingstone, pp. 31–46.

Micheva, K.D. et al., 2015. Array Tomography : High-Resolution Three-Dimensional Immunofluorescence. , pp.1214–1219.

Migaud, M. et al., 1998. Enhanced long-term potentiation and impairedlearninginmicewithmutant postsynaptic density-95 protein. *Nature*, pp.433–439.

Milner, E. et al., 2014. Cerebral amyloid angiopathy increases susceptibility to infarction after focal cerebral ischemia in Tg2576 mice. *Stroke*, 45(10), pp.3064–3069.

Minkeviciene, R. et al., 2008. Age-related decrease in stimulated glutamate release and vesicular glutamate transporters in APP/PS1 transgenic and wild-type mice. *Journal of Neurochemistry*, 105(3), pp.584–594.

Mittmann, T. et al., 1998. Long-term cellular dysfunction after focal cerebral ischemia: In vitro analyses. *Neuroscience*, 85(1), pp.15–27.

Mölders, A. et al., 2018. Heterogeneity of the astrocytic AMPA-receptor transcriptome. *Glia*, 66(12), pp.2604–2616.

Monici, M., 2005. Cell and tissue autofluorescence research and diagnostic applications. *Biotechnology Annual Review*, 11(SUPPL.), pp.227–256.

Montana, V., 2004. Vesicular Glutamate Transporter-Dependent Glutamate Release from Astrocytes. *Journal of Neuroscience*, 24(11), pp.2633–2642.

Moolman, D.L. et al., 2004. Dendrite and dendritic spine alterations in Alzheimer models. *Journal of Neurocytology*, 33, pp.377–387.

Morris, G.P. et al., 2016. A comparative study of variables influencing ischemic injury in the longa and koizumi methods of intraluminal filament middle cerebral artery occlusion in mice. *PLoS ONE*, 11(2), pp.1–34.

Morris, R.G.M. et al., 1982. Place navigation impaired in rats with hippocampal lesions. *Nature*, 297(5868), p.681.

Morris, R.S. et al., 2018. Relationships between selective neuronal loss and microglial activation after ischaemic stroke in man. *Brain*, 141(7), pp.2098–2111.

Mucke, L. et al., 2000. High-level neuronal expression of abeta 1-42 in wild-type human amyloid protein precursor transgenic mice: synaptotoxicity without plaque formation. *The Journal of neuroscience : the official journal of the Society for Neuroscience*, 20(11), pp.4050–4058.

Mungas, D. et al., 2001. MRI predictors of cognition in subcortical ischemic vascular disease and Alzheimer ' s disease. , pp.2229–2236.

Murakami, Y. et al., 2000. Ameliorative effect of tacrine on spatial memory deficit in chronic two-vessel occluded rats is reversible and mediated by muscarinic M1 receptor stimulation. *Behavioural Brain Research*, 109(1), pp.83–90.

Murotomi, K. et al., 2012. Neuroscience Letters Transient focal cerebral ischemia differentially decreases Homer1a and 1b / c contents in the postsynaptic density. *Neuroscience Letters*, 515(1), pp.92–96.

Nakajima, M. et al., 2018. AMPA Receptor Antagonist Perampanel Ameliorates Post-Stroke Functional and Cognitive Impairments. *Neuroscience*, 386, pp.256–264.

Nakane, M. et al., 1992. Degeneration of the ipsilateral substantia nigra following cerebral infarction in the striatum. *Stroke; a journal of cerebral circulation*, 23(Figure 3), pp.328–332.

Nakanishi, H. et al., 1997. Electrophysiological Studies of Rat Substantia Nigra Neurons in an in Vitro Slice Preparation After Middle Cerebral Artery Occlusion. , 77(4), pp.1021–1028.

Narasimhalu, K. et al., 2015. Inflammatory markers and their association with post stroke cognitive decline. *International Journal of Stroke*, 10(4), pp.513–518.

Neumann, J. et al., 2006. Microglia provide neuroprotection after ischemia. *FASEB Journal*, 20(6), pp.714–716.

Neumann, J. et al., 2015. Very-late-antigen-4 (VLA-4)-mediated brain invasion by neutrophils leads to interactions with microglia, increased ischemic injury and impaired behavior in experimental stroke. *Acta Neuropathologica*, 129(2), pp.259–277.

Nguyen, T. V et al., 2018. Alzheimer ' s associated amyloid and tau deposition co-localizes with a homeostatic myelin repair pathway in two mouse models of post-stroke mixed dementia. , pp.1–25.

Ni, J.W. et al., 1994. Progressive cognitive impairment following chronic cerebral hypoperfusion induced by permanent occlusion of bilateral carotid arteries in rats. *Brain Research*, 653(1-2), pp.231–236.

Nichols, E. et al., 2019. Global, regional, and national burden of Alzheimer's disease and other dementias, 1990–2016: a systematic analysis for the Global Burden of Disease Study 2016. *The Lancet Neurology*, 18(1), pp.88–106.

Nie, C. et al., 2016. Betaine reverses the memory impairments in a chronic cerebral hypoperfusion rat model. *Neuroscience Letters*, 615, pp.9–14.

Nishino, A. et al., 2016. Long-term effects of cerebral hypoperfusion on neural density and function using misery perfusion animal model. *Scientific Reports*, 6(April), pp.10–17.

Nishio, K. et al., 2010. A mouse model characterizing features of vascular dementia with hippocampal atrophy. *Stroke*, 41(6), pp.1278–1284.

Nishio, K. et al., 2010. A Mouse Model Characterizing Features of Vascular Dementia With Hippocampal Atrophy * Supplemental Methods. *Stroke*, 41(6), pp.1278–1284.

Nisticò, R. et al., 2017. Synaptoimmunology - roles in health and disease. , pp.1–12.

Niwa, K. et al., 2001. Aβ-peptides enhance vasoconstriction in cerebral circulation. *American Journal of Physiology - Heart and Circulatory Physiology*, 281(6 50-6), pp.2417–2424.

Norris, G.T. et al., 2018. Neuronal integrity and complement control synaptic material clearance by microglia after CNS injury. , pp.1–13.

O'Brien, J.T. et al., 2003. Vascular cognitive impairment. , 2(February), pp.89–98.

O'Rourke, N.A. et al., 2013. Deep Molecular Diversity of Mammalian Synapses: Why It Matters and How to Measure It. *Nature Reviews Neurology*, 13(6), pp.365–379.

Ohsawa, K. et al., 2000. Involvement of Iba1 in membrane ruffling and phagocytosis of macrophages/microglia. *Journal of cell science*, 113 (Pt 1, pp.3073–84.

Ohtaki, H. et al., 2006. Progressive expression of vascular endothelial growth factor (VEGF) and angiogenesis after chronic ischemic hypoperfusion in rat. *Acta Neurochirurgica, Supplementum*, (96), pp.283–287.

Okada, M. et al., 1995. Long-term spatial cognitive impairment following middle cerebral artery occlusion in rats. A behavioral study. *Journal of Cerebral Blood Flow and Metabolism*, 15(3), pp.505–512.

Olton, D.S., Becker, J.T. & Handelmann, G.E., 1980. Hippocampal function: Working memory or cognitive mapping? *Physiological Psychology*, 8(2), pp.239–246.

Olton, D.S. & Samuelson, R.J., 1976. Remembrance of places passed: Spatial memory in rats. *Journal of Experimental Psychology: Animal Behavior Processes*, 2(2), pp.97–116.

Ordy, J.M. et al., 1993. Selective vulnerability and early progression of hippocampal CA1 pyramidal cell degeneration and GFAP-postivie astrocyte reactivity in the rat four-vessel occlusion model of transient global ischemia. *Experimental Neurobiology*, 119, pp.128–139.

Ormel, L. et al., 2012. VGLUT1 is localized in astrocytic processes in several brain regions. *Glia*, 60(2), pp.229–238.

Osborne, K. a et al., 1987. Quantitative assessment of early brain damage in a rat model of focal cerebral ischaemia. *J.Neurol.Neurosurg.Psychiatry*, 50(4), pp.402–410.

Østergaard, L. et al., 2016. Cerebral small vessel disease: Capillary pathways to stroke and cognitive decline. *Journal of Cerebral Blood Flow and Metabolism*, 36(2), pp.302–325.

Otori, T. et al., 2003. LONG-TERM MEASUREMENT OF CEREBRAL BLOOD FLOW AND METABOLISM IN A RAT CHRONIC HYPOPERFUSION MODEL. , (September 2002), pp.266–272.

Ouyang, Y.-B. et al., 2007. Selective Dysfunction of Hippocampal CA1 Astrocytes Contributes to Delayed Neuronal Damage after Transient Forebrain Ischemia. *Journal of Neuroscience*, 27(16), pp.4253–4260.

Overman, J.J. et al., 2012. A role for ephrin-A5 in axonal sprouting, recovery, and activity-dependent plasticity after stroke. *Proceedings of the National Academy of Sciences*, 109(33), pp.E2230–E2239.

Palop, J.J. & Mucke, L., 2016. Network abnormalities and interneuron dysfunction in Alzheimer disease. *Nature Reviews Neuroscience*, 17(12), pp.777–792.

Pantoni, L., 2010. Cerebral small vessel disease: from pathogenesis and clinical characteristics to therapeutic challenges. *The Lancet. Neurology*, 9(7), pp.689–701.

Papadakis, M. et al., 2013. Tsc1 (hamartin) confers neuroprotection against ischemia by inducing autophagy. *Nature Medicine*, 19(3), pp.351–357.

Paresce, D.M., Ghosh, R.N. & Maxfield, F.R., 1996. Microglial cells internalize aggregates of the Alzheimer's disease amyloid β-protein via a scavenger receptor. *Neuron*, 17(3), pp.553–565.

Pedrono, E. et al., 2010. An Optimized Mouse Model for Transient Ischemic Attack. , 69(2), pp.188–195.

Pekny, M. et al., 2018. Astrocyte activation and reactive gliosis—A new target in stroke? *Neuroscience Letters*, (May), pp.0–1.

Percie du Sert, N. et al., 2017. The IMPROVE Guidelines (Ischaemia Models: Procedural Refinements Of in Vivo Experiments). *Journal of Cerebral Blood Flow and Metabolism*, 37(11), pp.3488–3517.

Perdahl, E. et al., 1984. Synapsin I (Protein I) in Different Brain Regions in Senile Dementia of Alzheimer Type and in Multiinfarct Dementia. , 141, pp.133–141.

Pettersson, A.F., Engardt, M. & Wahlund, L.-O., 2002. Activity level and balance in subjects with mild Alzheimer's disease. *Dementia and Geriatric Cognitive Disorders*, 13(4), pp.213–216.

Phillips, S.J. & Whisnant, J.P., 1992. Hypertension and the Brain. *Archives of Internal Medicine*, 152(5), pp.938–945.

Pimentel-coelho, P.M., Michaud, J. & Rivest, S., 2013. Effects of mild chronic cerebral hypoperfusion and early amyloid pathology on spatial learning and the cellular innate immune response in mice. *NBA*, 34(3), pp.679–693.

Pin-Barre, C. et al., 2014. Acute Neuromuscular Adaptation at the Spinal Level Following Middle Cerebral Artery Occlusion-Reperfusion in the Rat. , 9(2), pp.10–12.

Pohjasvaara, T. et al., 1998. Clinical determinants of poststroke dementia. *Stroke*, 29(1), pp.75–81.

Pohjasvaara, T. et al., 1997. Dementia Three Months After Stroke. *Stroke*, 28(4), pp.785–792.

Popp, A. et al., 2009. Identification of Ischemic Regions in a Rat Model of Stroke. , 4(3).

Porritt, M.J. et al., 2012. Photothrombosis-induced infarction of the mouse cerebral cortex is not affected by the Nrf2-activator sulforaphane. *PLoS ONE*, 7(7), pp.17–19.

Portelius, E. et al., 2009. Identification of novel APP/Aβ isoforms in human cerebrospinal fluid. *Neurodegenerative Diseases*, 6(3), pp.87–94.

Powers, W.J. et al., 2015. 2015 American Heart Association/American Stroke Association Focused Update of the 2013 Guidelines for the Early Management of Patients With Acute Ischemic Stroke Regarding Endovascular Treatment. *Stroke*, 46(10), pp.3020–3035.

Prinz, V. et al., 2015. MRI heralds secondary nigral lesion after brain ischemia in mice: A secondary time window for neuroprotection. *Journal of Cerebral Blood Flow and Metabolism*, 35(12), pp.1903–1909.

Promjunyakul Nutta-On, H. et al., 2018. Baseline NAWM structural integrity and CBF predict periventricular WMH expansion over time. *Neurology*, 90(24).

Qin, C. et al., 2017. Fingolimod protects against ischemic white matter damage by modulating microglia toward M2 polarization via STAT3 pathway. *Stroke*, 48(12), pp.3336–3346.

Qiu, C. et al., 2006. Heart Failure and Risk of Dementia and Alzheimer Disease: A Population-Based Cohort Study. *Archives of Internal Medicine*, 166(9), pp.1003–1008.

Radde, R. et al., 2006. Aβ42-driven cerebral amyloidosis in transgenic mice reveals early and robust pathology. *EMBO Reports*, 7(9), pp.940–946.

Rajan, W.D. et al., 2018. Dissecting functional phenotypes of microglia and macrophages in the rat brain after transient cerebral ischemia. , (July), pp.1–14.

Rajan, W.D. et al., 2019. Dissecting functional phenotypes of microglia and macrophages in the rat brain after transient cerebral ischemia. *Glia*, 67(2), pp.232–245.

Rajendran, L. & Paolicelli, R.C., 2018. Microglia-Mediated Synapse Loss in Alzheimer ' s Disease. , 38(12), pp.2911–2919.

Rakers, C. et al., 2019. Stroke target identification guided by astrocyte transcriptome analysis. *Glia*, 67(4), pp.619–633.

Rao, M.S. & Shetty, A.K., 2004. Efficacy of doublecortin as a marker to analyse the absolute number and dendritic growth of newly generated neurons in the adult dentate gyrus. *European Journal of Neuroscience*, 19, pp.234–246.

Reijmer, Y.D. et al., 2016. Small Vessel Disease and Cognitive Impairment : The Relevance of Central Network Connections. , 2454(November 2015), pp.2446–2454.

Reimer, M.M. et al., 2011. Rapid disruption of axon-glial integrity in response to mild cerebral hypoperfusion. *The Journal of neuroscience : the official journal of the Society for Neuroscience*, 31(49), pp.18185–94.

Reimer, M.M. et al., 2011. Rapid disruption of axon-glial integrity in response to mild cerebral hypoperfusion. *The Journal of neuroscience : the official journal of the Society for Neuroscience*, 31(49), pp.18185–94.

Reinders, N.R. et al., 2016. Amyloid-β effects on synapses and memory require AMPA receptor subunit GluA3. *Proceedings of the National Academy of Sciences*, p.201614249.

Reinius, B. et al., 2015. Conditional targeting of medium spiny neurons in the striatal matrix. *Frontiers in Behavioral Neuroscience*, 9(March), pp.1–14.

Rizo, J. & Xu, J., 2015. The Synaptic Vesicle Release Machinery. *Annual Review of Biophysics*, 44(1), pp.339–367.

Rockenstein, E. et al., 2001. Early formation of mature amyloid-β protein deposits in a mutant APP transgenic model depends on levels of Aβ1-42. *Journal of Neuroscience Research*, 66(4), pp.573–582.

Rodriguez-Grande, B. et al., 2013. Loss of substance P and inflammation precede delayed neurodegeneration in the substantia nigra after cerebral ischemia. *Brain, Behavior, and Immunity*, 29, pp.51–61.

Rogers, D.C. et al., 1997. Correlation Between Motor Impairment and Infarct Volume After Permenant and Transient Middle Cerebral Artery Occlusion in the Rat. *Stroke*, 28, pp.2060–2066.

Rossi, D.J., Brady, J.D. & Mohr, C., 2007. Astrocyte metabolism and signaling during brain ischemia. *Nature Neuroscience*, 10(11), pp.1377–1386.

Rothenburg, L.S. et al., 2010. The relationship between inflammatory markers and post stroke cognitive impairment. *Journal of Geriatric Psychiatry and Neurology*, 23(3), pp.199–205.

Rothstein, J.D. et al., 1993. Chronic inhibition of glutamate uptake produces a model of slow neurotoxicity. , 90(July), pp.6591–6595.

Ruan, Y.W. et al., 2012. Remodeling of synapses in the CA1 area of the hippocampus after transient global ischemia. *Neuroscience*, 218, pp.268–277.

Rudinskiy, N. et al., 2012. Orchestrated experience-driven Arc responses are disrupted in a mouse model of Alzheimer's disease. *Nature neuroscience*, 15(10), pp.1422–9.

Ruitenberg, A. et al., 2005. Cerebral hypoperfusion and clinical onset of dementia: The Rotterdam Study. *Annals of Neurology*, 57(6), pp.789–794.

Rusnakova, V. et al., 2013. Heterogeneity of Astrocytes: From Development to Injury - Single Cell Gene Expression. *PLoS ONE*, 8(8).

Saab, A.S. et al., 2016. Oligodendroglial NMDA Receptors Regulate Glucose Import and Axonal Energy Metabolism. *Neuron*, 91(1), pp.119–132.

Sadigh-Eteghad, S. et al., 2018. Intranasal cerebrolysin improves cognitive function and structural synaptic plasticity in photothrombotic mouse model of medial prefrontal cortex ischemia. *Neuropeptides*, 71(February), pp.61–69.

Saggu, R. et al., 2016a. Astroglial NF-kB contributes to white matter damage and cognitive impairment in a mouse model of vascular dementia. *Acta Neuropathologica Communications*, pp.1–10.

Saggu, R. et al., 2016b. Astroglial NF-kB contributes to white matter damage and cognitive impairment in a mouse model of vascular dementia. *Acta neuropathologica communications*, 4(1), p.76.

Salminen, A., Kauppinen, A. & Kaarniranta, K., 2017. Hypoxia/ischemia activate processing of Amyloid Precursor Protein: impact of vascular dysfunction in the pathogenesis of Alzheimer's disease. *Journal of Neurochemistry*, 140(4), pp.536–549.

Salter, M.W. & Stevens, B., 2017. Microglia emerge as central players in brain disease. *Nature Medicine*, 23(9), pp.1018–1027.

Salvadores, N. et al., 2017. Chronic cerebral hypoperfusion alters amyloid-β peptide pools leading to cerebral amyloid angiopathy, microinfarcts and haemorrhages in Tg-SwDI mice. *Clinical Science*, 131(16), pp.2109–2123.

Sam, K. et al., 2016. Development of White Matter Hyperintensity Is Preceded by Reduced Cerebrovascular Reactivity. *Annals of Neurology*, 80(2), pp.277–285.

Sánchez-Mendoza, E. et al., 2010. Transient focal cerebral ischemia significantly alters not only EAATs but also VGLUTs expression in rats: Relevance of changes in reactive astroglia. *Journal of Neurochemistry*, 113(5), pp.1343–1355.

Sandvig, I., Sandvig, A., et al., 2018. Neuroplasticity in stroke recovery . The role of microglia in engaging and modifying synapses and networks. , (April), pp.1–15.

Sandvig, I., Augestad, I.L., et al., 2018. Neuroplasticity in stroke recovery. The role of microglia in engaging and modifying synapses and networks. *European Journal of Neuroscience*, 47(12), pp.1414–1428.

Sankaranarayanan, S. & Ryan, T. a., 2000. Real-time measurements of vesicle-SNARE recycling in synapses of the central nervous system. *Nature Cell Biology*, 2(4), pp.197–204.

Sarti, C. et al., 2002. Persistent impairment of gait performances and working memory after bilateral common carotid artery occlusion in the adult Wistar rat. *Behavioural Brain Research*, 136(1), pp.13–20.

Sasaguri, H. et al., 2017. APP mouse models for Alzheimer's disease preclinical studies. *The EMBO Journal*, 36(17), p.e201797397.

Satoh, J. et al., 2016. TMEM119 marks a subset of microglia in the human brain. , (August 2015), pp.39–49.

Saver, J.L., 2006. Time is brain - Quantified. *Stroke*, 37(1), pp.263–266.

Savioz, A., Leuba, G. & Vallet, P.G., 2014. A framework to understand the variations of PSD-95 expression in brain aging and in Alzheimer's disease. *Ageing Research Reviews*, 18, pp.86–94.

Schafer, D.P. et al., 2012. Microglia Sculpt Postnatal Neural Circuits in an Activity and Complement-Dependent Manner. *Neuron*, 74(4), pp.691–705.

Scheff, S.W. et al., 2006. Hippocampal synaptic loss in early Alzheimer's disease and mild cognitive impairment. *Neurobiology of Aging*, 27(10), pp.1372–1384.

Schilling, M. et al., 2003. Microglial activation precedes and predominates over macrophage infiltration in transient focal cerebral ischemia: A study in green

fluorescent protein transgenic bone marrow chimeric mice. *Experimental Neurology*, 183(1), pp.25–33.

Schmid-Elsaesser, R., Zausinger, S. & Hungerhuber, E., 1998. A Critical Reevaluation of the Intraluminal Thread Model of Focal Cerebral Ischemia Evidence of Inadvertent Premature Reperfusion and Subarachnoid. , pp.2162–2171.

Schmidt-Kastner, R. et al., 2001. Transient changes of brain-derived neurotrophic factor (BDNF) mRNA expression in hippocampus during moderate ischemia induced by chronic bilateral common carotid artery occlusions in the rat. *Molecular Brain Research*, 92(1-2), pp.157–166.

Schmued, L.C. et al., 2005. Fluoro-Jade C results in ultra high resolution and contrast labeling of degenerating neurons. *Brain Research*, 1035(1), pp.24–31.

Schmued, L.C. & Hopkins, K.J., 2000. Fluoro-Jade B: A high affinity fluorescent marker for the localization of neuronal degeneration. *Brain Research*, 874(2), pp.123–130.

Schneider, J.A. et al., 2003. Relation of cerebral infarctions to dementia and cognitive function in older persons.

Schrimpf, S.P. et al., 2005. Proteomic analysis of synaptosomes using isotope-coded affinity tags and mass spectrometry. *Proteomics*, 5(10), pp.2531–2541.

Schwartz-Bloom, R.D. & Sah, R., 2001. g-Aminobutyric AcidA neurotransmission and cerebral ischemia. *Journal of Neurochemistry*, 77, pp.353–371.

Selkoe, B.D.J., 2018. Early network dysfunction in Alzheimer's disease.

Selkoe, D.J., 2002. Alzheimer's disease is a synaptic failure. *Science (New York, N.Y.)*, 298(October), pp.789–791.

Sengillo, J.D. et al., 2013. Deficiency in mural vascular cells coincides with blood-brain barrier disruption in alzheimer's disease. *Brain Pathology*, 23(3), pp.303–310.

Seo, H.G. et al., 2010. Early motor balance and coordination training increased synaptophysin in subcortical regions of the ischemic rat brain. *Journal of Korean Medical Science*, 25(11), pp.1638–1645.

Seo, J.H. et al., 2013. OPCs induce early blood-brain barrier opening. , 123(2), pp.2–6.

Serrano-Pozo, A. et al., 2011. Reactive glia not only associates with plaques but also parallels tangles in Alzheimer's disease. *American Journal of Pathology*, 179(3), pp.1373–1384.

Shah, F.A. et al., 2019. Melatonin Protects MCAO-Induced Neuronal Loss via NR2A Mediated Prosurvival Pathways. *Frontiers in Pharmacology*, 10(March), pp.1–11.

Shankar, G.M. et al., 2008. Amyloid-beta protein dimers isolated directly from Alzheimer's brains impair synaptic plasticity and memory. *Nature medicine*, 14(8), pp.837–842.

Shankar, G.M. et al., 2007. Natural oligomers of the Alzheimer amyloid-beta protein induce reversible synapse loss by modulating an NMDA-type glutamate receptor-dependent signaling pathway. *The Journal of neuroscience : the official journal of the Society for Neuroscience*, 27(11), pp.2866–2875.

Shannon, C., Salter, M. & Fern, R., 2007. GFP imaging of live astrocytes: Regional differences in the effects of ischaemia upon astrocytes. *Journal of Anatomy*, 210(6), pp.684–692.

Sheng, M. & Sala, C., 2001. Pdz D Omains and the O Rganization of S Upramolecular C Omplexes. *Annual review of neuroscience*, 24(1), pp.1–29.

Shi, K. et al., 2019. Global brain inflammation in stroke. *The Lancet Neurology*, 18(November).

Shi, S.-H. et al., 2001. Subunit-Specific Rules Governing AMPA Receptor Trafficking to Synapses in Hippocampal Pyramidal Neurons. *Cell*, 105, pp.331–343.

Shi, Y. et al., 2016. Cerebral blood flow in small vessel disease: A systematic review and meta-analysis. *Journal of Cerebral Blood Flow & Metabolism*, p.0271678X16662891.

Shi, Y. et al., 2020. Small vessel disease is associated with altered cerebrovascular pulsatility but not resting cerebral blood flow. *Journal of Cerebral Blood Flow & Metabolism*, 40(1), pp.85–99.

Shibata, M. et al., 2004. White matter lesions and glial activation in a novel mouse model of chronic cerebral hypoperfusion. *Stroke*, 35(11), pp.2598–2603.

Shibata, M., Yamasaki, N. & Miyakawa, T., 2007. Selective Impairment of Working Memory in a Mouse Model of Chronic Cerebral Hypoperfusion. , pp.2826–2833.

Shigeri, Y., Seal, R.P. & Shimamoto, K., 2004. Molecular pharmacology of glutamate transporters, EAATs and VGLUTs. *Brain Research Reviews*, 45(3), pp.250–265.

Shinohara, M. et al., 2014. Regional distribution of synaptic markers and APP correlate with distinct clinicopathological features in sporadic and familial Alzheimer's disease. *Brain : a journal of neurology*, 137(Pt 5), pp.1533–49.

Sibarita, J.B., 2005. Deconvolution microscopy. *Advances in Biochemical Engineering/Biotechnology*, 95, pp.201–243.

Sigfridsson, E. et al., 2018. Astrocyte-specific overexpression of Nrf2 protects against optic tract damage and behavioural alterations in a mouse model of cerebral hypoperfusion. *Scientific Reports*, 8(1), pp.1–14.

Sims, N.R. & Yew, W.P., 2017. Reactive astrogliosis in stroke: Contributions of astrocytes to recovery of neurological function. *Neurochemistry International*, 107, pp.88–103.

Sinclair, L.I., Tayler, H.M. & Love, S., 2015. Synaptic protein levels altered in vascular dementia. *Neuropathology and Applied Neurobiology*, 41(4), pp.533–543.

Sinha, R. et al., 2011. Two synaptobrevin molecules are sufficient for vesicle fusion in central nervous system synapses. *Proceedings of the National Academy of Sciences of the United States of America*, 108(34), pp.14318–14323.

Sipe, G.O. et al., 2016. Microglial P2Y12 is necessary for synaptic plasticity in mouse visual cortex. *Nature Communications*, 7.

Sly, L.M. et al., 2001. Endogenous brain cytokine mRNA and inflammatory responses to lipopolysaccharide are elevated in the Tg2576 transgenic mouse model of Alzheimer's disease. *Brain Research Bulletin*, 56(6), pp.581–588.

Smith, a D. & Bolam, J.P., 1990. Study of Synaptic Connections of Identified Neurones. , (7), pp.259–265.

Snowdon, D.A. et al., 1997. Brain Infarction and the Clinical Expression of Alzheimer Disease Study. *JAMA*, 277(10), pp.813–817.

Sofroniew, M. V., 2015. Astrocyte barriers to neurotoxic inflammation. *Nature Reviews Neuroscience*, 16(5), pp.249–263.

Sofroniew, M. V., 2009. Molecular dissection of reactive astrogliosis and glial scar formation. *Trends in Neurosciences*, 32(12), pp.638–647.

Sokolow, S. et al., 2012. Preferential accumulation of amyloid-beta in presynaptic glutamatergic terminals (VGLUT1 and VGLUT2) in Alzheimer's disease cortex. *Neurobiol Dis.*, 45(1), pp.381–387.

Söllner, T. et al., 1993. A protein assembly-disassembly pathway in vitro that may correspond to sequential steps of synaptic vesicle docking, activation, and fusion. *Cell*, 75(3), pp.409–418.

Sopala, M. et al., 2000. Middle cerebral artery occlusion produces secondary , remote impairment in hippocampal plasticity of rats ± involvement of N -methyl- D -aspartate receptors ? , 281, pp.143–146.

Sozmen, E.G. et al., 2016. Nogo receptor blockade overcomes remyelination failure after white matter stroke and stimulates functional recovery in aged mice. *Proceedings of the National Academy of Sciences*, 113(52), pp.E8453–E8462.

Spratt, N.J. et al., 2006. Modification of the method of thread manufacture improves stroke induction rate and reduces mortality after thread-occlusion of the middle cerebral artery in young or aged rats. *Journal of Neuroscience Methods*, 155(2), pp.285–290.

Stackman, R.W. et al., 2016. Temporary inactivation reveals that the CA1 region of the mouse dorsal hippocampus plays an equivalent role in the retrieval of long-term object memory and spatial memory. *Neurobiology of Learning and Memory*, 133, pp.118–128.

Stefansdottir Hrafnhildur, O. et al., 2013. Atrial Fibrillation is Associated With Reduced Brain Volume and Cognitive Function Independent of Cerebral Infarcts. *Stroke*, 44(4), pp.1020–1025.

Stephenson, D.T., Rash, K. & Clemens, J. a, 1992. Amyloid precursor protein accumulates in regions of neurodegeneration following focal cerebral ischemia in the rat. *Brain Research*, 593(1), pp.128–135.

Stevens, B. et al., 2007. The Classical Complement Cascade Mediates CNS Synapse Elimination. *Cell*, 131(6), pp.1164–1178.

Stewart, C.R. et al., 2010. CD36 ligands promote sterile inflammation through assembly of a Toll-like receptor 4 and 6 heterodimer. *Nature Immunology*, 11(2), pp.155–161.

Stewart, M.G. et al., 2013. Structure and Complexity of the Synapse and Dendritic Spine. *The Synapse: Structure and Function*, pp.1–20.

Stokin, G.B. et al., 2005. Axonopathy and Transport Deficits Early in the Pathogenesis of Alzheimer ' s Disease. *Science*, 307(February), pp.1282–1288.

Stokowska, A. et al., 2016. Complement peptide C3a stimulates neural plasticity after experimental brain ischaemia. *Brain*, p.aww314.

Stokowska, A. et al., 2017. Complement peptide C3a stimulates neural plasticity after experimental brain ischaemia. *Brain*, 140(2), pp.353–369.

Storck, S.E. & Pietrzik, C.U., 2017. Endothelial LRP1 – A Potential Target for the Treatment of Alzheimer's Disease: Theme: Drug Discovery, Development and Delivery in Alzheimer's Disease Guest Editor: Davide Brambilla. *Pharmaceutical Research*, 34(12), pp.2637–2651.

Sun, B.L. et al., 2018. Lymphatic drainage system of the brain: A novel target for intervention of neurological diseases. *Progress in Neurobiology*, 163-164, pp.118–143.

Sun, M.-K., 2003. Pharmacological Protection of Synaptic Function, Spatial Learning, and Memory from Transient Hypoxia in Rats. *Journal of Pharmacology and Experimental Therapeutics*, 300(2), pp.408–416.

Sun, S.W. et al., 2014. In vivo diffusion tensor imaging of amyloid-β-induced white matter damage in mice. *Journal of Alzheimer's Disease*, 38(1), pp.93–101.

Sun, X. et al., 2012. New striatal neurons form projections to substantia nigra in adult rat brain after stroke. *Neurobiology of Disease*, 45(1), pp.601–609.

Sun, Z.Y. et al., 2013. Magnetoencephalography assessment of evoked magnetic fields and cognitive function in subcortical ischemic vascular dementia patients. *Neuroscience Letters*, 532(1), pp.17–22.

Suridjan, I. et al., 2015. In-vivo imaging of grey and white matter neuroinflammation in Alzheimer's disease: A positron emission tomography study with a novel radioligand, " 18 F"-FEPPA. *Molecular Psychiatry*, 20(12), pp.1579–1587.

Szirmai, I. et al., 2002. Strategic infarcts of the thalamus in vascular dementia. *Journal of the neurological sciences*, 204, pp.91–97.

Takagi, K. et al., 1995. Local hemodynamic changes during transient middle cerebral artery occlusion and recirculation in the rat: a [14 C]iodoantipyrine autoradiographic study. *Brain Research*, 691(1-2), pp.160–168.

Takatsuru, Y. et al., 2009. Neuronal Circuit Remodeling in the Contralateral Cortical Hemisphere during Functional Recovery from Cerebral Infarction. *Journal of Neuroscience*, 29(32), pp.10081–10086.

Talma, N. et al., 2016. Neuroprotective hypothermia – Why keep your head cool during ischemia and reperfusion. *Biochimica et Biophysica Acta - General Subjects*, 1860(11), pp.2521–2528.

Tamura, A. et al., 1990. Atrophy of the i lateral substantia nigra followir occlusion in the rat middle a ery. , 9, pp.154–157.

Tamura, A. & Teasdale, M., 1981. Focal Cerebral Ischaemia in the Rat : 1 . Description of Technique and Early Neuropathological Consequences Following Middle Cerebral Artery Occlusion. , pp.53–60.

Tancredi, V. et al., 1992. Tumor necrosis factor alters synaptic transmission in rat hippocampal slices. *Neuroscience Letters*, 146(2), pp.176–178.

Tanzi, R.E. et al., 1987. Amyloid beta Protein Gene: cDNA, mRNA Distribution, and Genetic Linkage Near the Alzheimer Locus. *Science*, 235.

Tennant, K.A. et al., 2017. Optigenetic rewiring of thalamocortical cicuirts to restore function in the stroke injured brain. *Nature Communications*, 8(15879), pp.1–14.

Terry, R.D. et al., 1991. Physical basis of cognitive alterations in Alzheimer's disease: Synapse loss is the major correlate of cognitive impairment. *Annals of Neurology*, 30(4), pp.572–580.

Terry, R.D. et al., 1991. Physical Basis of Cognitive Alterations in Alzheimers-Disease - Synapse Loss Is the Major Correlate of Cognitive Impairment. *Ann Neurol*, 30(4), pp.572–580.

Thal, D.R. et al., 2003. Vascular Pathology in Alzheimer Disease: Correlation of Cerebral Amyloid Angiopathy and Arteriosclerosis/Lipohyalinosis with Cognitive Decline. *Journal of Neuropathology and Experimental Neurology*, 62(12), pp.1287–1301.

Thammisetty, S.S. et al., 2018. Age-related deregulation of TDP-43 after stroke enhances NF-κB-mediated inflammation and neuronal damage. *Journal of neuroinflammation*, 15(1), p.312.

Thomas, T. et al., 1996. β-Amyloid-mediated vasoactivity and vascular endothelial damage. *Nature*, 380(6570), pp.168–171.

Thrippleton, M.J. et al., 2018. Cerebrovascular reactivity measurement in cerebral small vessel disease: Rationale and reproducibility of a protocol for MRI acquisition and image processing. *International Journal of Stroke*, 13(2), pp.195–206.

Tomiyama, T. et al., 2010. A mouse model of amyloid β oligomers: Their contribution to synaptic alteration, abnormal tau phosphorylation, glial activation, and neuronal loss in vivo. *Journal of Neuroscience*, 30(14), pp.4845–4856.

Trapp, B.D. et al., 1998. Axonal transection in the lesions of multiple sclerosis. *The New England journal of medicine*, 338(5), pp.278–85.

Tsai, J. et al., 2004. Fibrillar amyloid deposition leads to local synaptic abnormalities and breakage of neuronal branches. *Nature neuroscience*, 7(11), pp.1181–1183.

Tsien, J.Z., Huerta, P.T. & Tonegawa, S., 1996. The essential role of hippocampal CA1 NMDA receptor-dependent synaptic plasticity in spatial memory. *Cell*, 87(7), pp.1327–1338.

Tsuchiya, D. et al., 2003. Effect of suture size and carotid clip application upon blood flow and infarct volume after permanent and temporary middle cerebral artery occlusion in mice. *Brain Research*, 970(1-2), pp.131–139.

Tzingounis, A. V & Wadiche, J.I., 2007. Glutamate transporters: confining runaway excitation by shaping synaptic transmission. *Nature Reviews Neuroscience*, 8(12), p.935.

Uchino, S. et al., 2001. Induced Glutamate Release From Hippocampal Slices. *Brain*, 13(July 2000), pp.670–678.

Vargas, M.E. & Barres, B. a., 2007. Why Is Wallerian Degeneration in the CNS So Slow? *Annual Review of Neuroscience*, 30(1), pp.153–179.

Verpelli, C., Heise, C. & Sala, C., 2013. *Structural and Functional Organization of the Postsynaptic Density*, Elsevier.

Vigneault, É. et al., 2015. Distribution of vesicular glutamate transporters in the human brain. *Frontiers in Neuroantomy*, 9, pp.1–13.

Villegas-Llerena, C. et al., 2016. Microglial genes regulating neuroinflammation in the progression of Alzheimer's disease. *Current Opinion in Neurobiology*, 36, pp.74–81.

Voglmaier, S.M. et al., 2006. Distinct Endocytic Pathways Control the Rate and Extent of Synaptic Vesicle Protein Recycling. *Neuron*, 51(1), pp.71–84.

Völgyi, K. et al., 2017. Chronic Cerebral Hypoperfusion Induced Synaptic Proteome Changes in the rat Cerebral Cortex.

Walsh, D.M. et al., 2002. Naturally secreted oligomers of amyloid beta protein potently inhibit hippocampal long-term potentiation in vivo. *Nature*, 416(6880), pp.535–539.

Wang, F. et al., 2012. Nogo-A is associated with secondary degeneration of substantia nigra in hypertensive rats with focal cortical infarction. *Brain Research*, 1469, pp.153–163.

Wang, L. et al., 2016. Chronic cerebral hypoperfusion induces memory de fi cits and facilitates A β generation in C57BL / 6J mice. , 283, pp.353–364.

Wang, W.Y. et al., 2015. Role of pro-inflammatory cytokines released from microglia in Alzheimer's disease. *Annals of Translational Medicine*, 3(10), pp.1–15.

Wang, X. et al., 2016. Enriched environment improves post-stroke cognitive impairment in mice by potential regulation of acetylation homeostasis in cholinergic circuits. *Brain Research*, 1650, pp.232–242.

Wang, X. et al., 2007. Genome-wide transcriptome profiling of region-specific vulnerability to oxidative stress in the hippocampus. *Genomics*, 90(2), pp.201–212.

Wang, X. et al., 2009. Genomic and biochemical approaches in the discovery of mechanisms for selective neuronal vulnerability to oxidative stress. *BMC Neuroscience*, 10, pp.1–20.

Wang, X. et al., 2005. High intrinsic oxidative stress may underlie selective vulnerability of the hippocampal CA1 region. *Molecular Brain Research*, 140(1-2), pp.120–126.

Wang, X. & Michaelis, E.K., 2010. Selective neuronal vulnerability to oxidative stress in the brain. *Frontiers in Aging Neuroscience*, 2(MAR), pp.1–13.

Wang, Y. et al., 2017. Nitrosylation of Vesicular Transporters in Brain of Amyloid Precursor Protein/Presenilin 1 Double Transgenic Mice. *Journal of Alzheimer's Disease*, 55(4), pp.1683–1692.

Wang, Y. et al., 2015. Protein cysteine S-nitrosylation inhibits vesicular uptake of neurotransmitters. *Neuroscience*, 311, pp.374–381.

Wang, Z. et al., 2016. Chronic cerebral hypoperfusion induces long-lasting cognitive deficits accompanied by long-term hippocampal silent synapses increase in rats. *Behavioural Brain Research*, 301, pp.243–252.

Wang, Z. et al., 2018. Treatment of secondary brain injury by perturbing postsynaptic density protein-95-NMDA receptor interaction after intracerebral hemorrhage in rats. *Journal of Cerebral Blood Flow and Metabolism*.

Warburton, E.C. et al., 2000. Disconnecting hippocampal projections to the anterior thalamus produces deficits on tests of spatial memory in rats. *European Journal of Neuroscience*, 12(5), pp.1714–1726.

Wardlaw, J.M., Smith, C. & Dichgans, M., 2019a. Small vessel disease: mechanisms and clinical implications. *The Lancet Neurology*, 18(7), pp.684–696.

Wardlaw, J.M., Smith, C. & Dichgans, M., 2019b. Small vessel disease: mechanisms and clinical implications. *The Lancet Neurology*, 18(7), pp.684–696.

Wattananit, S. et al., 2016. Monocyte-Derived Macrophages Contribute to Spontaneous Long-Term Functional Recovery after Stroke in Mice. *Journal of Neuroscience*, 36(15), pp.4182–4195.

Weinhard, L. et al., 2018. Microglia remodel synapses by presynaptic trogocytosis and spine head spine head filopodia induction. *Nature Communications*, 9(1228).

Weishaupt, N. et al., 2016. Prefrontal ischemia in the rat leads to secondary damage and inflammation in remote gray and white matter regions. *Frontiers in Neuroscience*, 10, pp.1–9.

Wen, Y., Zhai, R.G. & Kim, M.D., 2013. The role of autophagy in Nmnat-mediated protection against hypoxia-induced dendrite degeneration. *Molecular and Cellular Neuroscience*, 52, pp.140–151.

Wiley, C. a. et al., 2015. Role for mammalian chitinase 3-like protein 1 in traumatic brain injury. *Neuropathology*, 35(2), pp.95–106.

Wilhelmsson, U., 2004. Absence of Glial Fibrillary Acidic Protein and Vimentin Prevents Hypertrophy of Astrocytic Processes and Improves Post-Traumatic Regeneration. *Journal of Neuroscience*, 24(21), pp.5016–5021.

Winter, B. et al., 2005. Anxious and hyperactive phenotype following brief ischemic episodes in mice. *Biological Psychiatry*, 57(10), pp.1166–1175.

Winter, B. et al., 2015. Striatal Infarction Elicits Secondary Extrafocal MRI Changes in Ipsilateral Substantia Nigra. , pp.1–11.

De Wit, H. et al., 2009. Synaptotagmin-1 Docks Secretory Vesicles to Syntaxin-1/SNAP-25 Acceptor Complexes. *Cell*, 138(5), pp.935–946.

Wolfe, N. et al., 1990. Multiple Lacunar Infarcts. , (n 1), pp.1–4.

Won, S.J. et al., 2018. Cofilin-Actin rod formation in neuronal processes after brain ischemia. *PLoS ONE*, 13(10), pp.1–17.

Wortmann, M., 2012. Dementia : a global health priority – highlights from an ADI and World Health Organization report. , pp.4–6.

Wu, M.Y. et al., 2018. Current Mechanistic Concepts in Ischemia and Reperfusion Injury. *Cellular Physiology and Biochemistry*, 46(4), pp.1650–1667.

Wyss-Coray, T. et al., 2003. Adult mouse astrocytes degrade amyloid-β in vitro and in situ. *Nature Medicine*, 9(4), pp.453–457.

Xu, F. et al., 2007. Early-onset subicular microvascular amyloid and neuroinflammation correlate with behavioral deficits in vasculotropic mutant amyloid ??-protein precursor transgenic mice. *Neuroscience*, 146, pp.98–107.

Xu, J. et al., 2001. Amyloid-β Peptides Are Cytotoxic to Oligodendrocytes. *The Journal of Neuroscience*, 21(1), pp.RC118–RC118.

Xu, X. et al., 2012. DECREASE OF SYNAPTIC PLASTICITY ASSOCIATED WITH ALTERATION OF INFORMATION FLOW IN A RAT MODEL OF VASCULAR DEMENTIA. , 206, pp.136–143.

Yam, P.S., 1998. Topographical and quantitative assessment of white matter injury following a focal ischaemic lesion in the rat brain. , pp.315–322.

Yamashima, T., 2016. Can “calpain-cathepsin hypothesis” explain Alzheimer neuronal death? *Ageing Research Reviews*, 32, pp.169–179.

Yamawaki, N. & Shepherd, G.M.G., 2015. Synaptic Circuit Organization of Motor Corticothalamic Neurons. *Journal of Neuroscience*, 35(5), pp.2293–2307.

Yanamoto, H. et al., 2003. Evaluation of MCAO stroke models in normotensive rats: Standardized neocortical infarction by the 3VO technique. *Experimental Neurology*, 182(2), pp.261–274.

Yang, C. et al., 2017. Arginine vasopressin ameliorates spatial learning impairments in chronic cerebral hypoperfusion via V1a receptor and autophagy signaling partially. *Nature Publishing Group*, (October 2016).

Yang, Y. et al., 2013. Autophagy in axonal and dendritic degeneration. *Trends in Neurosciences*, 36(7), pp.418–428.

Ye, X. et al., 2017. Regulation of Synaptic Aβ Generation Through BACE1 Retrograde Transport in a Mouse Model of Alzheimer ’ s Disease Regulation of Synaptic A β

Generation Through BACE1 Retrograde Transport in a Mouse Model of Alzheimer ' s Disease Department of Cell Biology.

Yonemori, F. et al., 1996. Spatial memory disturbance after focal cerebral ischemia in rats. *Journal of Cerebral Blood Flow and Metabolism*, 16(5), pp.973–980.

Yoon, J.S. et al., 2018. Spatiotemporal Protein Atlas of Cell Death-Related Molecules in the Rat MCAO Stroke Model. *Experimental Neurobiology*, 27(4), p.287.

Zarruk, J.G., Greenhalgh, A.D. & David, S., 2017. Microglia and macrophages di ff er in their in fl ammatory pro fi le after permanent brain ischemia. , (August).

Zhai, Z. & Feng, J., 2018. Left-right asymmetry influenced the infarct volume and neurological dysfunction following focal middle cerebral artery occlusion in rats. *Brain and Behavior*, 8(12), pp.1–6.

Zhang, F. et al., 1997. Increased susceptibility to ischemic brain damage in transgenic mice overexpressing the amyloid precursor protein. *Journal of Neuroscience*, 17(20), pp.7655–7661.

Zhang, F.X. et al., 2018. Vesicular glutamate transporter isoforms: The essential players in the somatosensory systems. *Progress in Neurobiology*, 171(August), pp.72–89.

Zhang, J., Zhang, Y. & Xing, S., 2012. Secondary Neurodegeneration in Remote Regions After Focal Cerebral Infarction A New Target for Stroke Management ? , (58), pp.1700–1705.

Zhang, Q. et al., 2017. Proinflammatory cytokines correlate with early exercise attenuating anxiety-like behavior after cerebral ischemia. *Brain and Behavior*, 7(11), pp.1–7.

Zhang, Q. et al., 2012. Transient focal cerebral ischemia/reperfusion induces early and chronic axonal changes in rats: Its importance for the risk of Alzheimer's disease. *PLoS ONE*, 7(3), pp.1–7.

Zhang, S. et al., 2005. Rapid Reversible Changes in Dendritic Spine Structure. *Neuroscience*, 25(22), pp.5333–5338.

Zhang, S. & Murphy, T.H., 2007. Imaging the impact of cortical microcirculation on synaptic structure and sensory-evoked hemodynamic responses in vivo. *PLoS Biology*, 5(5), pp.1152–1167.

Zhang, S. & Murphy, T.H., 2007. Imaging the Impact of Cortical Microcirculation on Synaptic Structure and Sensory-Evoked Hemodynamic Responses In Vivo. , 5(5).

Zhang, Y. et al., 2014. An RNA-Sequencing Transcriptome and Splicing Database of Glia, Neurons, and Vascular Cells of the Cerebral Cortex. *Journal of Neuroscience*, 34(36), pp.11929–11947.

Zhang, Y., Xing, S., Zhang, J., Li, J., Li, C. & Pei, Z., 2011. Reduction of b -amyloid deposits by c -secretase inhibitor is associated with the attenuation of secondary damage in the ipsilateral thalamus and sensory functional improvement after focal cortical infarction in hypertensive rats. , pp.572–579.

Zhang, Y., Xing, S., Zhang, J., Li, J., Li, C., Pei, Z., et al., 2011. Reduction of B-amyloid deposits by γ-secretase inhibitor is associated with the attenuation of secondary damage in the ipsilateral thalamus and sensory functional improvement after focal cortical infarction in hypertensive rats. *Journal of Cerebral Blood Flow and Metabolism*, 31(2), pp.572–579.

Zhao, Y. et al., 2014. Chronic cerebral hypoperfusion causes decrease of O-GlcNAcylation, hyperphosphorylation of tau and behavioral deficits in mice. *Frontiers in Aging Neuroscience*, 6(10), pp.1–16.

Zhou, W. et al., 2013. Postischemic brain infiltration of leukocyte subpopulations differs among murine permanent and transient focal cerebral ischemia models. *Brain Pathology*, 23(1), pp.34–44.

Zhu, F. et al., 2018. Architecture of the Mouse Brain Synaptome. *Neuron*, 99(4), pp.781–799.e10.

Zhu, L., Wang, L., Ju, F., Khan, A., et al., 2017. Reversible recovery of neuronal structures depends on the degree of neuronal damage after global cerebral ischemia in mice. *Experimental Neurology*, 289, pp.1–8.

Zhu, L., Wang, L., Ju, F., Ran, Y., et al., 2017. Transient global cerebral ischemia induces rapid and sustained reorganization of synaptic structures. , (222).

Zlokovic, B. V., 2008. The Blood-Brain Barrier in Health and Chronic Neurodegenerative Disorders. *Neuron*, 57(2), pp.178–201.

Zola-Morgan, S. et al., 1992. Enduring memory impairment in monkeys after ischemic damage to the hippocampus. *The Journal of Neuroscience*, 12(7), pp.2582–2596.

Zott, B. et al., 2019. A vicious cycle of β amyloid–dependent neuronal hyperactivation. *Science*, 365(6453), pp.559–565.

Zrzavy, T. et al., 2017. Dominant role of microglial and macrophage innate immune responses in human ischemic infarcts.

Zuo, X. et al., 2018. Inhibition of cathepsins B induces neuroprotection against secondary degeneration in ipsilateral substantia nigra after focal cortical infarction in adult male rats. *Frontiers in Aging Neuroscience*, 10(MAY), pp.1–17.